



UNIVERSITAT
POLITÈCNICA
DE VALÈNCIA

– **TELECOM** ESCUELA
TÉCNICA **VLC** SUPERIOR
DE INGENIERÍA DE
TELECOMUNICACIÓN

UNIVERSITAT POLITÈCNICA DE VALÈNCIA

School of Telecommunications Engineering

Development of error models and tools for space-based
multilateration systems performance assessment

Master's Thesis

Master's Degree in Telecommunication Engineering

AUTHOR: Ganau Sánchez, Álex

Tutor: Balbastre Tejedor, Juan Vicente

External cotutor: CHUQUITARCO JIMENEZ, CARLOS ALEXANDER

ACADEMIC YEAR: 2022/2023

Abstract

Space-based Communications, Navigation, and Surveillance (CNS) systems have played a crucial role in enhancing the safety of air operations and expanding airspace capacity. Among these systems, space-based Automatic Dependent Surveillance-Broadcast (ADS-B) technology stands at the forefront of aeronautical surveillance advancements. The next evolutionary leap for space-based CNS systems lies in the development of ADS-B+MLAT composite surveillance systems. These systems combine aircraft's ADS-B data, which are broadcasted on the 1090 MHz carrier and received by satellite-based receiving stations belonging to a globally deployed Low Earth Orbit (LEO) constellation, with data obtained through multilateration (MLAT) systems. These MLAT receiving stations are also present on the same satellites as the ADS-B receivers. The primary objective of this Master's Thesis is to develop tools that can estimate the theoretical error associated with a space-based multilateration system. By doing so, it becomes possible to design a satellite constellation that provides position data with acceptable errors, as defined in specific standards like EUROCAE ED-142A. To achieve this goal, appropriate error indicators will be defined, error models for the receivers onboard the satellites will be developed, and an interface will be co-designed with a LEO constellation propagation tool. This interface will facilitate the provision of dynamic satellite position information. Leveraging this information, performance evaluations of a particular system can be conducted and the results can be displayed through a graphical interface. Furthermore, the graphical interface will enable the configuration of evaluation parameters, empowering the user to tailor the analysis to their specific needs.

Resumen

Los sistemas de Comunicaciones, Navegación y Vigilancia (CNS) basados en el espacio han desempeñado un papel crucial en el mejoramiento de la seguridad de las operaciones aéreas y en la expansión de la capacidad del espacio aéreo. Entre estos sistemas, la tecnología de Vigilancia y Difusión Dependiente Automática (ADS-B, por sus siglas en inglés) basada en el espacio se encuentra a la vanguardia de los avances en vigilancia aeronáutica. El siguiente salto evolutivo para los sistemas CNS basados en el espacio radica en el desarrollo de sistemas de vigilancia compuestos ADS-B+MLAT. Estos sistemas combinan los datos ADS-B de las aeronaves, que se transmiten en la portadora de 1090 MHz y se reciben en estaciones de recepción basadas en satélites pertenecientes a una constelación de órbita terrestre baja (LEO, por sus siglas en inglés) desplegada a nivel global, con los datos obtenidos a través de sistemas de multilateración (MLAT). Estas estaciones de recepción MLAT también se encuentran presentes en los mismos satélites que los receptores ADS-B. El objetivo principal de esta tesis de maestría es desarrollar herramientas que puedan estimar el error teórico asociado con un sistema de multilateración basado en el espacio. Al hacerlo, se vuelve posible diseñar una constelación de satélites que proporcione datos de posición con errores aceptables, según se definen en estándares específicos como el EUROCAE ED-142A. Para lograr este objetivo, se definirán indicadores de error apropiados, se desarrollarán modelos de error para los receptores a bordo de los satélites y se co-diseñará una interfaz con una herramienta de propagación de constelación LEO. Esta interfaz facilitará la provisión de información dinámica de posición de los satélites. Aprovechando esta información, se podrán realizar evaluaciones de rendimiento de un sistema específico y los resultados podrán visualizarse a través de una interfaz gráfica. Además, la interfaz gráfica permitirá la configuración de parámetros de evaluación, brindando al usuario la capacidad de adaptar el análisis a sus necesidades específicas.

Resum

Els sistemes de Comunicacions, Navegació i Vigilància (CNS) basats en l'espai han exercit un paper crucial en el millorament de la seguretat de les operacions aèries i en l'expansió de la capacitat de l'espai aeri. Entre aquests sistemes, la tecnologia de Vigilància i Difusió Dependent Automàtica (ADS-B, per les seues sigles en anglés) basada en l'espai es troba a l'avantguarda dels avanços en vigilància aeronàutica. El següent salt evolutiu per als sistemes CNS basats en l'espai radica en el desenvolupament de sistemes de vigilància compostos ADS-B+MLAT. Aquests sistemes combinen les dades ADS-B de les aeronaus, que es transmeten en la portadora de 1090 MHz i es reben en estacions de recepció basades en satèl·lits pertanyents a una constel·lació d'òrbita terrestre baixa (LEO, per les seues sigles en anglés) desplegada a nivell global, amb les dades obtingudes a través de sistemes de multilateració (MLAT). Aquestes estacions de recepció MLAT també es troben presents en els mateixos satèl·lits que els receptors ADS-B. L'objectiu principal d'aquesta tesi de mestratge és desenvolupar eines que puguin estimar l'error teòric associat amb un sistema de multilateració basat en l'espai. En fer-ho, es torna possible dissenyar una constel·lació de satèl·lits que proporcione dades de posició amb errors acceptables, segons es defineixen en estàndards específics com el EUROCAE ED-142A. Per a aconseguir aquest objectiu, es definiran indicadors d'error apropiats, es desenvoluparan models d'error per als receptors a bord dels satèl·lits i es co-dissenyarà una interfície amb una eina de propagació de constel·lació LEO. Aquesta interfície facilitarà la provisió d'informació dinàmica de posició dels satèl·lits. Aprofitant aquesta informació, es podran realitzar avaluacions de rendiment d'un sistema específic i els resultats podran visualitzar-se a través d'una interfície gràfica. A més, la interfície gràfica permetrà la configuració de paràmetres d'avaluació, brindant a l'usuari la capacitat d'adaptar l'anàlisi a les seues necessitats específiques.

Contents

I Introduction

1	General Information	1
1.1	Framework	1
1.1.1	Automatic Dependent Surveillance (ADS)	4
1.1.2	Multilateration (MLAT)	6
1.1.3	Space-based Multilateration (SBM)	7
1.2	Motivation	8
1.3	Objectives	10
2	MLAT Systems	13
2.1	Definition and Operating Principles	13
2.2	Theoretical Horizontal and Vertical Position Accuracies	16
2.3	MLAT Systems based on TDOA, AOA, and FDOA	18
2.3.1	Time Difference of Arrival (TDOA)	18
2.3.2	Angle of Arrival (AOA)	20
2.3.3	Frequency Difference of Arrival (FDOA)	20
2.3.4	Hybrid MLAT Systems: Error Models	20

II MLAT Systems Design and Deployment

1	Particularities of MLAT Systems	24
1.1	System Design Parameters	25
1.2	System Performance Parameters	31
1.3	System Design vs Performance Parameters	38
1.4	Coordinate Systems: LLA and ECEF	39
1.5	Solutions for MLAT Systems Design	39
2	Satellite Constellation	40
2.1	Orbital Parameters	40
2.2	Kepler's Laws of Planetary Motion	42
2.3	Newton's Laws of Motion	42
2.4	Satellite Dynamics	43
2.4.1	Keplerian Elements	43
2.4.2	Satellite's Motion	44
2.4.3	Orbit Perturbations	44
2.5	Iridium constellation	46
2.6	Proposed constellation	46

III Algorithms for Mode S MLAT

1	Localization Problem	48
2	The Inverse Problem	49
3	Singular Value Decomposition	50
3.1	The Ordinary SVD (OSVD)	50
3.2	Null Space and Range of a Matrix	51
3.3	The Generalized SVD (GSVD)	51
3.4	Ill-Conditioned Problems	52
3.5	Regularization Methods for solving ICPs	53
3.6	Classification of the ICPs	54
3.7	Analysis Parameters of ICPs	54
3.7.1	The Condition Number	55
3.7.2	The Rank of a Matrix	55
3.7.3	The Numerical Rank	55
3.8	Least Squares and the Pseudoinverse	56
4	Localization Algorithms	57
4.1	Basic concepts	57
4.1.1	Data Model	58
4.1.2	Numerical Algorithm	59
4.1.3	Classification of Localization Algorithms	59
4.2	Closed Form Localization Algorithms	60
4.2.1	Smith and Abel	60
4.2.2	Friedlander	62
4.2.3	Schau and Robinson	64
4.2.4	Chan and Ho	66
4.2.5	Bancroft	70
4.3	Open Form Localization Algorithms	72
4.3.1	Taylor-Series Expansion	72
4.4	Review of the Localization Algorithms	75
5	Regularization Algorithms	76
5.1	Basic Concepts	77
5.1.1	Classification of Regularization Algorithms	78
5.2	Direct Regularization Methods	79
5.2.1	Tikhonov Regularization	79
5.2.1.1	Solving Regularized MLE by SVD	81
5.2.1.2	Effect of the Tikhonov Regularization	82
5.2.1.3	Regularization Error of the Tikhonov Regularization	83
5.2.1.4	Estimation of the Regularization Parameter	84
5.2.2	SVD-based Methods	87

5.2.2.1	Solution by Truncated SVD (T-SVD)	88
5.2.2.2	T-SVD with Sub-set Selection	90
5.2.3	TLS-based methods	90
5.2.3.1	Solution by Truncated TLS (T-TLS)	91
5.3	Indirect Regularization Methods	92
5.4	Localization strategy for SBM systems	92

IV Examples

1	Graphical User Interface (GUI)	94
2	Iridium constellation	96
2.1	North Atlantic	98
2.2	South Atlantic	101
2.3	Key points	105
3	Proposed constellation	106
3.1	Case 1: TOA error = $1 \mu\text{s}$ SAT position error = 2200 m	108
3.1.1	North Atlantic	108
3.1.2	South Atlantic	110
3.1.3	Key points	113
3.2	Case 2: TOA error = $1 \mu\text{s}$ SAT position error = 550 m	114
3.3	Case 3: TOA error = $1 \mu\text{s}$ SAT position error = 100 m	116
3.4	Case 4: TOA error = $1 \mu\text{s}$ SAT position error = 50 m	119
3.5	Case 5: TOA error = $1 \mu\text{s}$ SAT position error = 25 m	121
3.6	Case 6: SAT position error = 50 m TOA error = 100 ns	124
3.7	Case 7: SAT position error = 50 m TOA error = 10 ns	126
3.8	Case 8: SAT position error = 50 m TOA error = 1 ns	129
3.9	Key points	131
3.10	Trajectory-based	133
3.10.1	Trajectory I: North Atlantic	138
3.10.2	Trajectory II: South Atlantic	154

V Conclusions

1	Overall Findings	161
2	Future Work	164
3	Acknowledgments	165
	Bibliography	166

VI Sustainable Development Goals (SDGs)

List of Figures

1.2.1	Hyperbolic audio location system.	14
1.2.2	Hyperbolic navigation system principle.	14
1.2.3	Section of a hyperboloid for a pair of receiving stations.	15
1.2.4	Intersection of three hyperboloids.	15
1.2.5	Hyperbolas for four stations and a target located in an arbitrary position.	16
1.2.6	CRLB vs Taylor + Pseudoinverse.	17
3.3.1	Regularization strategy for turning ICP into WCP.	53
4.1.1	Matlab GUI.	94
4.2.1	Iridium constellation: Satellite distribution.	96
4.2.2	Iridium constellation: Satellite sensors.	97
4.2.3	Region I: North Atlantic airspace.	98
4.2.4	North Atlantic: Simultaneous connections.	98
4.2.5	Iridium North Atlantic TOA: 17:30h.	99
4.2.6	Iridium North Atlantic TOA: 17:50h.	99
4.2.7	Iridium North Atlantic TOA: 18:10h.	100
4.2.8	Iridium North Atlantic TOA: 18:30h.	100
4.2.9	Iridium North Atlantic TOA: 18:50h.	101
4.2.10	Region II: South Atlantic airspace.	101
4.2.11	South Atlantic: Simultaneous connections.	102
4.2.12	Iridium South Atlantic TOA: 17:30h.	102
4.2.13	Iridium South Atlantic TOA: 17:50h.	103
4.2.14	Iridium South Atlantic TOA: 18:10h.	103
4.2.15	Iridium South Atlantic TOA: 18:30h.	104
4.2.16	Iridium South Atlantic TOA: 18:50h.	104
4.3.1	Proposed constellation: Satellites distribution.	106
4.3.2	Proposed constellation: Satellites sensors.	107
4.3.3	Case 1 North Atlantic TDOA THPA + HDOP 17:30h.	108
4.3.4	Case 1 North Atlantic TDOA THPA + HDOP 17:50h.	108
4.3.5	Case 1 North Atlantic TDOA THPA + HDOP 18:10h.	109
4.3.6	Case 1 North Atlantic TDOA THPA + HDOP 18:30h.	109
4.3.7	Case 1 North Atlantic TDOA THPA + HDOP 18:50h.	110
4.3.8	Case 1 South Atlantic TDOA THPA + HDOP 17:30h.	110
4.3.9	Case 1 South Atlantic TDOA THPA + HDOP 17:50h.	111
4.3.10	Case 1 South Atlantic TDOA THPA + HDOP 18:10h.	111
4.3.11	Case 1 South Atlantic TDOA THPA + HDOP 18:30h.	112
4.3.12	Case 1 South Atlantic TDOA THPA + HDOP 18:50h.	112
4.3.13	Case 2 TDOA THPA 17:30h.	114
4.3.14	Case 2 TDOA THPA 17:50h.	114
4.3.15	Case 2 TDOA THPA 18:10h.	115
4.3.16	Case 2 TDOA THPA 18:30h.	115
4.3.17	Case 2 TDOA THPA 18:50h.	116
4.3.18	Case 3 TDOA THPA 17:30h.	116
4.3.19	Case 3 TDOA THPA 17:50h.	117

4.3.20	Case 3 TDOA THPA 18:10h.	117
4.3.21	Case 3 TDOA THPA 18:30h.	118
4.3.22	Case 3 TDOA THPA 18:50h.	118
4.3.23	Case 4 TDOA THPA 17:30h.	119
4.3.24	Case 4 TDOA THPA 17:50h.	119
4.3.25	Case 4 TDOA THPA 18:10h.	120
4.3.26	Case 4 TDOA THPA 18:30h.	120
4.3.27	Case 4 TDOA THPA 18:50h.	121
4.3.28	Case 5 TDOA THPA 17:30h.	121
4.3.29	Case 5 TDOA THPA 17:50h.	122
4.3.30	Case 5 TDOA THPA 18:10h.	122
4.3.31	Case 5 TDOA THPA 18:30h.	123
4.3.32	Case 5 TDOA THPA 18:50h.	123
4.3.33	Case 6 TDOA THPA 17:30h.	124
4.3.34	Case 6 TDOA THPA 17:50h.	124
4.3.35	Case 6 TDOA THPA 18:10h.	125
4.3.36	Case 6 TDOA THPA 18:30h.	125
4.3.37	Case 6 TDOA THPA 18:50h.	126
4.3.38	Case 7 TDOA THPA 17:30h.	126
4.3.39	Case 7 TDOA THPA 17:50h.	127
4.3.40	Case 7 TDOA THPA 18:10h.	127
4.3.41	Case 7 TDOA THPA 18:30h.	128
4.3.42	Case 7 TDOA THPA 18:50h.	128
4.3.43	Case 8 TDOA THPA 17:30h.	129
4.3.44	Case 8 TDOA THPA 17:50h.	129
4.3.45	Case 8 TDOA THPA 18:10h.	130
4.3.46	Case 8 TDOA THPA 18:30h.	130
4.3.47	Case 8 TDOA THPA 18:50h.	131
4.3.48	Trajectory I - North Atlantic Region.	133
4.3.49	Trajectory II - South Atlantic Region.	134
4.3.50	North Atlantic Tracks westbound crossing.	135
4.3.51	Chan & Ho: Estimated positions	135
4.3.52	Tikhonov: Regularized positions	136
4.3.53	Bancroft: Estimated positions	136
4.3.54	T-SVD: Regularized positions	137
4.3.55	North Atlantic Smith & Abel + Pseudoinverse: Graph.	138
4.3.56	North Atlantic Smith & Abel + Pseudoinverse: Statistics.	138
4.3.57	North Atlantic Smith & Abel + Tikhonov: Graph.	139
4.3.58	North Atlantic Smith & Abel + Tikhonov: Statistics.	139
4.3.59	North Atlantic Smith & Abel + T-SVD: Graph.	140
4.3.60	North Atlantic Smith & Abel + T-SVD: Statistics.	140
4.3.61	North Atlantic Friedlander + Pseudoinverse: Graph.	141
4.3.62	North Atlantic Friedlander + Pseudoinverse: Statistics.	141
4.3.63	North Atlantic Friedlander + Tikhonov: Graph.	142
4.3.64	North Atlantic Friedlander + Tikhonov: Statistics.	142
4.3.65	North Atlantic Friedlander + T-SVD: Graph.	143
4.3.66	North Atlantic Friedlander + T-SVD: Statistics.	143
4.3.67	North Atlantic Schau & Robinson + Pseudoinverse: Graph.	144
4.3.68	North Atlantic Schau & Robinson + Pseudoinverse: Statistics.	144
4.3.69	North Atlantic Schau & Robinson + Tikhonov: Graph.	145

4.3.70 North Atlantic Schau & Robinson + Tikhonov: Statistics.	145
4.3.71 North Atlantic Schau & Robinson + T-SVD: Graph.	146
4.3.72 North Atlantic Schau & Robinson + T-SVD: Statistics.	146
4.3.73 North Atlantic Chan & Ho + Pseudoinverse: Graph.	147
4.3.74 North Atlantic Chan & Ho + Pseudoinverse: Statistics.	147
4.3.75 North Atlantic Chan & Ho + Tikhonov: Graph.	148
4.3.76 North Atlantic Chan & Ho + Tikhonov: Statistics.	148
4.3.77 North Atlantic Chan & Ho + T-SVD: Graph.	149
4.3.78 North Atlantic Chan & Ho + T-SVD: Statistics.	149
4.3.79 North Atlantic Bancroft + Pseudoinverse: Graph.	150
4.3.80 North Atlantic Bancroft + Pseudoinverse: Statistics.	150
4.3.81 North Atlantic Bancroft + Tikhonov: Graph.	151
4.3.82 North Atlantic Bancroft + Tikhonov: Statistics.	151
4.3.83 North Atlantic Bancroft + T-SVD: Graph.	152
4.3.84 North Atlantic Bancroft + T-SVD: Statistics.	152
4.3.85 South Atlantic Chan & Ho + Pseudoinverse: Graph.	154
4.3.86 South Atlantic Chan & Ho + Pseudoinverse: Statistics.	154
4.3.87 South Atlantic Chan & Ho + Tikhonov: Graph.	155
4.3.88 South Atlantic Chan & Ho + Tikhonov: Statistics.	155
4.3.89 South Atlantic Chan & Ho + T-SVD: Graph.	156
4.3.90 South Atlantic Chan & Ho + T-SVD: Statistics.	156
4.3.91 South Atlantic Bancroft + Pseudoinverse: Graph.	157
4.3.92 South Atlantic Bancroft + Pseudoinverse: Statistics.	157
4.3.93 South Atlantic Bancroft + Tikhonov: Graph.	158
4.3.94 South Atlantic Bancroft + Tikhonov: Statistics.	158
4.3.95 South Atlantic Bancroft + T-SVD: Graph.	159
4.3.96 South Atlantic Bancroft + T-SVD: Statistics.	159

List of Tables

1.2.1 Possibilities of hybrid MLAT systems	21
2.1.1 Qualitative scale for the DOP values	27
2.2.1 Main parameters of the proposed constellation	46
3.4.1 Characteristics of the localization algorithms	75
4.3.1 Error models for the different use cases.	107
4.3.2 Trajectory I - North Atlantic Region	133
4.3.3 Trajectory II - South Atlantic Region	134
6.0.1 Sustainable Development Goals (SDGs)	171

Acronyms

A-CDM Airport CDM.

ADS Automatic Dependent Surveillance.

ADS-B ADS-Broadcast.

ADS-C ADS-Contract.

ANSP Air Navigation Service Provider.

AOA Angle of Arrival.

ARTAS ATM Surveillance Tracker and Server.

ATC Air Traffic Control.

ATCS Air Traffic Control Specialist.

ATFM Air Traffic Flow Management.

ATM Air Traffic Management.

CDM Collaborative Decision Making.

CNS Communication, Navigation and Surveillance.

CPS Central Processing Station.

CRLB Cramér-Rao Lower Bound.

DF Doppler Frequency.

DIPP Discrete Ill-Posed Problems.

DOP Dilution of Precision.

DRM Direct Regularization Method.

E-MLAT Enhanced MLAT.

ECEF Earth-centered, Earth-fixed coordinate system.

EM Electromagnetic.

ES Extended Squitter.

EUROCAE European Organisation for Civil Aviation Equipment.

EUROCONTROL European Organisation for the Safety of Air Navigation.

FAA Federal Aviation Administration.

FDOA Frequency Difference of Arrival.

FIM Fisher Information Matrix.

FL Flight Level.

GCV Generalized Cross Validation.

GDOP Geometric Dilution of Precision.

GEO Geosynchronous Equatorial Orbit.

GNSS Global Navigation Satellite System.

GPS Global Positioning System.

GS Ground Station.

GSVD Generalized SVD.

GUI Graphical User Interface.

HDOP Horizontal Dilution of Precision.

ICAO International Civil Aviation Organization.

ICP Ill-Conditioned Problem.

IRM Indirect Regularization Method.

ISL Inter-Satellite Link.

ISS International Space Station.

LA Localization Algorithm.

LAM Local Area Multilateration.

LEO Low Earth Orbit.

LLA Latitude, Longitude, Altitude.

LOS Line of Sight.

LS Least Squares.

MEO Medium Earth Orbit.

MLAT Multilateration.

MLE Maximum Likelihood Estimator.

MOPS Minimum Operational Performance Specification.

MTOW Maximum Take-Off Weight.

NAT North Atlantic Tracks.

NAT-OTS North Atlantic Organized Track System.

NLOS Non-Line-of-Sight.

NM Nautical Mile.

NSA National Supervisory Authority.

OSVD Ordinary SVD.

PBN Performance-based Navigation.

PDOP Position (3D) Dilution of Precision.

PoD Probability of Detection.

PoFD Probability of False Detection.

PoFID Probability of False Identification.

PoID Probability of Identification.

PSR Primary Surveillance Radar.

RA Regularization Algorithm.

RAAN Right Ascension of the Ascending Node.

RAIM Receiver Autonomous Integrity Monitoring.

RDP Rank-Deficient Problem.

RF Radio Frequency.

RMS Root Mean Square.

ROI Region of Interest.

RS Receiving Station.

RSS Root Sum Square.

RTD Round-Trip Delay.

SASS-C Surveillance Analysis Support System for ATC-Centre.

SBM Space-based Multilateration.

SDG Sustainable Development Goal.

SDP System Design Parameters.

SES Single European Sky.

SMS Safety Management Systems.

SNR Signal-to-Noise Ratio.

SPP System Performance Parameters.

SSR Secondary Surveillance Radar.

SVD Singular Value Decomposition.

T-SVD Truncated SVD.

T-SVD-SS T-SVD with Sub-set Selection.

T-TLS Truncated TLS.

TBO Trajectory-based Operation.

TCAS Traffic and Collision Avoidance System.

TDOA Time Difference of Arrival.

TDOP Time Dilution of Precision.

THPA Theoretical Horizontal Position Accuracy.

TLS Total Least Squares.

TOA Time of Arrival.

TPA Theoretical Position Accuracy.

TV Total Variation.

TVPA Theoretical Vertical Position Accuracy.

UAT Universal Access Transceiver.

UPS Uninterruptible Power Supply.

VDL VHF Data Link.

VDOP Vertical Dilution of Precision.

WAM Wide Area MLAT.

WCP Well-Conditioned Problem.

WW-I World War I.

WW-II World War II.

Part I

Introduction

Chapter 1

General Information

1.1 Framework

Air traffic is one of the major contributors to green-house gas emissions. That raises the need of reducing the environmental impact of aviation operations. Among others, one possible way to achieve this goal is by using Trajectory-based Operation (TBO)s leading to less fuel consumption. These operations are enabled by new generation aviation surveillance systems deployed in the mainland, especially in areas with high traffic density. New generation surveillance systems have also contributed to increase the airspace capacity as well as the air operations' level of safety. However, most of these surveillance systems are ground-based by nature. That means that operations in the airspace over oceanic and uninhabited areas cannot benefit from them. However, the air traffic density is quite high in some of these areas, thus posing environmental and safety concerns that may not be ignored. Extending the coverage of new generation surveillance systems to oceanic and uninhabited continental areas will help tackle these issues, as it has been done over continental populated areas. Traditionally, the provision of air navigation services (such as the Air Traffic Control (ATC) service) has been based on Secondary Surveillance Radar (SSR) [1].

The state-of-the-art SSR technology is the Mode S, which enables aircraft to send a variety of data obtained from different on-board sensors in the replies elicited by Mode S interrogations from ground-based radar stations. Although they represent a significant improvement over older SSR Mode A/C technologies, they still have some shortcomings common to radar technology: due to the limited rotation speed of large radar antennas, Mode S SSR typically take between 5 and 12 s to refresh aircraft position data and, although the positioning error in range is quite fair (less than 14 m bias plus a maximum random $1-\sigma$ error of 15 m), the figures in azimuth are not so good: bias between 0.022° and 0.033° , depending on the elevation angle, plus a maximum random $1-\sigma$ error of 0.068° (that means a bias between 180 and 273 m and a random $1-\sigma$ error of 563 m at 256 Nautical Mile (NM) away from the ground station, which is the border of the usual SSR Ground Station (GS) coverage) [2].

ADS-Broadcast (ADS-B) is a Mode S based surveillance technology in which electronic airborne equipment automatically broadcasts aircraft location (obtained from an onboard global navigation satellite system – Global Navigation Satellite System (GNSS) – receiver with around 12 m $1-\sigma$ random error in x-y directions [3]), along with identity, altitude, velocity, and other data at 1,090 MHz using a Mode S format known as Extended Squitter (ES) (ES1090).

In conventional ADS-B systems, dedicated ground stations within the aircraft transmitter coverage receive the broadcasted data and relay the information to air traffic control units, providing air traffic controllers with updated aircraft information almost every second, much faster and more precise than any radar (including Mode S ones). This fast update of highly accurate ADS-B data enhances the Air Traffic Control Specialist (ATCS)' awareness of aircraft in the airspace, helping them identify and resolve potentially hazardous situations quickly and effectively. As a result, separation between aircraft (commonly known as separation minima) may be reduced without compromising safety. Implementing ADS-B in modern ATC systems enhances airspace capacity and enables more efficient operations (TBO) that reduce fuel emissions. However, ADS-B relies on GNSS data for surveillance, which is susceptible to jamming and spoofing attacks. These vulnerabilities directly impact the situational awareness of ATC systems. To address this, a secondary independent surveillance system is often necessary. One affordable and practical solution is the use of Multilateration (MLAT) for passive aircraft localization. MLAT systems consist of strategically deployed Receiving Station (RS) and a Central Processing Station (CPS). RS detect radiofrequency signals emitted by aircraft, measure their Time of Arrival (TOA), and digitize the signals. The CPS computes the Time Difference of Arrival (TDOA) based on the measured TOA, forming a system of non-linear equations. Solving these equations provides an independent estimation of the aircraft's position. Proper synchronization of multiple clocks used for time-stamping TOA measurements is crucial in MLAT systems. By incorporating MLAT alongside ADS-B, a more resilient air traffic surveillance network can be established, addressing the limitations associated with GNSS-based surveillance alone.

ADS-B and MLAT systems may be used in a combined way known as Wide Area MLAT (WAM) with composite ADS-B surveillance functionality (referred to as ADS-B+WAM hereinafter). Hence, composite surveillance provides some advantages over the ADS-B or MLAT stand-alone surveillance (beyond the obvious one of providing two independent streams of surveillance data):

1. Comparing ADS-B and MLAT horizontal position data allows to define an ADS-B/MLAT integrity category (also known as AWIC) additional to the Receiver Autonomous Integrity Monitoring (RAIM) NIC-p.
2. MLAT data may be used to estimate and compensate the bias in aircraft positions contained in ADS-B messages due to uncompensated latency caused by the airborne ADS-B equipment.
3. MLAT data may be used to monitor the ADS-B performance, as required by performance-based surveillance specifications (especially when no other surveillance source is available).
4. MLAT data can be used to enhance ADS-B security by detecting GNSS jamming and spoofing attacks.
5. ADS-B data may be used to detect malfunctions of MLAT systems.
6. MLAT can be used to locate aircraft not already equipped with ADS-B or more in general locate the aircraft exploiting also the no-ADS-B signals, such as Mode S replies or Traffic and Collision Avoidance System (TCAS) messages.

In light of the benefits expected from all these new-generation surveillance technologies, the International Civil Aviation Organization (ICAO) set out a plan to modernize the surveillance systems worldwide, fostering since the early 2000s the transition from SSR Mode A/C to SSR Mode S technology, the implementation of MLAT systems and ADS-B, as well as the use of state-of-the-art surveillance data processing and evaluation systems [4].

In Europe, the European Organisation for the Safety of Air Navigation (EUROCONTROL) coordinated and supported this process since the beginning with relevant activities such as the Mode S program [5], the CASCADE program (ADS-B and MLAT) [6], and the development of ATM Surveillance Tracker and Server (ARTAS) and Surveillance Analysis Support System for ATC-Centre (SASS-C) [7], [8]. As a result, Mode S and ADS-B became the pillars of the Single European Sky (SES). As a matter of fact, in Europe, aircraft with more than 5,700 kg Maximum Take-Off Weight (MTOW) have to be equipped with ADS-B capable Mode S transponders and Air Navigation Service Provider (ANSP)s have to exploit enhanced surveillance data provided by them.

Hence, about the 90% of the fleet is currently equipped with ADS-B V2 transponders and more than 1,000 ADS-B ground stations have been deployed by European ANSPs over the last years [9], encompassing composite ADS-B+WAM systems, Mode S radars with ADS-B functionality, and standalone ADS-B systems. This network provides a very extensive and steadily expanding ADS-B coverage. However, despite the effort to upgrade the surveillance infrastructure underpinning these new, optimized operations, long-haul flights over oceanic areas or over almost uninhabited regions cannot benefit from it. The former, because existing surveillance systems are ground-based, the latter due to the cost of installing and maintaining surveillance infrastructures on them. Therefore, although aircraft may broadcast ADS-B data, there is no receiving station within the transmitter range to receive and inject them into the surveillance chain, which encompasses all the systems used to capture surveillance data and make them available to the ATCS, directly or by means of supporting tools.

Hence, large separation minima must be applied therein [10], and no optimized aircraft operations are feasible even though the traffic levels may be significant (for instance, more than 1,700 operations per day over the North Atlantic Tracks (NAT) region in 2019 [11]). Therefore, there is a need to extend the coverage of new generation performance-based surveillance systems, especially over oceanic and remote areas, in view of operating with optimal and safer routes and attain the consequent reduction in fuel consumption to contribute to the reduction of greenhouse gas emissions.

Space-based ADS-B systems are an especially well-suited way to provide surveillance in oceanic and uninhabited areas [12], because in these systems the receiving stations are on board of a Low Earth Orbit (LEO) satellite constellation within the range of the aircraft's transmitters (i.e., no receiving stations on the ground are needed). The data gathered by a particular satellite are routed through the constellation by means of an Inter-Satellite Link (ISL) network until they reach a satellite from which they can be downloaded to the ground and relayed to the appropriate ATC unit, where they are used in the same way as those received from ADS-B GS. Space-based ADS-B systems are cutting-edge surveillance systems that are being deployed to provide the position of aircraft in real time in places where traditional surveillance and navigation systems are not able to provide coverage.

Examples of space-based ADS-B surveillance systems have been developed (or are being developed) by Startical [13] and Aireon [14]. Nonetheless, as mentioned before, ADS-B (no matter where the receiving station is located) is intrinsically dependent because aircraft position data are obtained by processing the signals transmitted from a satellite constellation by a third-party GNSS such as the Global Positioning System (GPS) and/or GALILEO; thus, an integrity check supported by some kind of non-dependent measurements may be used to validate ADS-B data [15]. Nowadays, ground-based MLAT systems and radars, where available, are used to this purpose, but they have the same issues as ground-based ADS-B systems and they rarely cover oceanic and remote areas.

Space-based Multilateration (SBM) systems leveraging ADS-B LEO constellations arise as the natural way to provide this non-dependent cross-reference for space-based ADS-B integrity assessment, since they do not need ground stations either. Unfortunately, the extension of conventional MLAT techniques to the space environment is not straightforward. As mentioned before, MLAT systems consist of a set of remote stations deployed on the coverage area which receive an electromagnetic wave emitted by an aircraft flying over there.

Each remote station measures one parameter of the received signal and sends it to a central station which processes all the received data to get the aircraft's position. Conventional ground-based MLAT systems are mostly based on TOA measurements, sometimes complemented by Angle of Arrival (AOA) ones. TOA-based MLAT systems need the precise knowledge of the positions of the receivers, some kind of synchronization mechanism between the receiving stations, and a proper receiver distribution in space to reduce the so-called Dilution of Precision (DOP). Therefore, in case of SBM, the fundamental technical open points are:

- The effect of the satellite position accuracy, i.e., the capability to carry out a robust satellite orbit determination with high accuracy.
- The effect of satellite synchronization error, that is the need to have satellite synchronization architectures.
- Classical MLAT localization must be performed with a minimum number of satellites, and this also introduces some problems in the position estimation, that could be ill-conditioned or numerically unstable, enhancing the localization system with other measurements (e.g., more accurate AOA or Frequency Difference of Arrival (FDOA)) could be necessary.
- The measurement done on board the satellites of a signal emitted by an aircraft must reach the central processing station within a time window of a few milliseconds. Therefore, latencies in the satellite communication may cause issues that must be addressed with ad-hoc network solution that may exploit also inter-satellite links.

All these aspects need to be addressed and assessed by means of Enhanced MLAT (E-MLAT) systems in order to get the aircraft position with a limited satellite coverage overlap. Finally, based on the feasibility of new or adapted MLAT techniques, it is necessary to propose and validate relevant ADS-B data integrity indicators for optimized air operations.

Summarizing, there is a need for an enhanced space-based MLAT system leveraging constellations that provide space-based ADS-B surveillance to provide composite ADS-B + E-MLAT from the space. In this way, the ADS-B will be hardened by providing a complementary stream of GNSS independent surveillance data enabling the definition of integrity parameters for space-based ADS-B data down-linked to ground systems.

1.1.1 Automatic Dependent Surveillance (ADS)

Automatic Dependent Surveillance (ADS) is a technology used in aviation for tracking and broadcasting the position and other information of aircraft. There are two main types of ADS:

- **ADS-B:**

It is a surveillance technology that allows aircraft to automatically broadcast their own position, altitude, velocity, and other information to ground-based ADS-B receivers and other nearby aircraft equipped with ADS-B receivers. ADS-B is a global standard and operates on two different frequencies: 1090 MHz (1090ES) for air-to-air and air-to-ground communication, and 978 MHz (Universal Access Transceiver (UAT)) for air-to-ground communication only. ADS-B is a key technology for modernizing ATM systems and enabling more efficient and environmentally friendly operations in aviation. Here are some key characteristics of ADS-B:

1. **Broadcast of position and other data:**

ADS-B allows aircraft to automatically broadcast their own position, altitude, velocity, heading, and other information to nearby aircraft and ground-based ADS-B receivers. This enables real-time and accurate tracking of aircraft positions, providing enhanced situational awareness for pilots, ATCS, and other stakeholders.

2. **Frequency and message formats:**

ADS-B operates on two different frequencies: 1090 MHz (1090ES) for air-to-air and air-to-ground communication, and 978 MHz (UAT) for air-to-ground communication only. ADS-B messages are transmitted in a standard format called ADS-B ES or UAT, which include various information such as position, altitude, velocity, and identification of the aircraft.

3. **Compliance with regulatory requirements:**

ADS-B is mandated or recommended by aviation authorities in many regions around the world as part of the modernization of air traffic management systems. For example, in the United States, ADS-B Out is required for most aircraft operating in controlled airspace by the Federal Aviation Administration (FAA) since January 1, 2020.

4. **Surveillance accuracy and integrity:**

ADS-B provides accurate position information with horizontal and vertical accuracy of about 7.5 meters (25 feet) or better. ADS-B messages also include integrity information to indicate the quality and reliability of the position data, helping to ensure the accuracy and integrity of the surveillance information.

5. **Continuous and automatic broadcasting:**

ADS-B operates continuously and automatically broadcasts position and other information from the aircraft without any intervention from the pilots or air traffic controllers. This enables real-time and continuous tracking of aircraft positions, providing timely and accurate information for ATM and other applications.

6. **Enhanced situational awareness:**

ADS-B improves situational awareness for pilots by allowing them to see the position and trajectory of nearby aircraft equipped with ADS-B receivers on their cockpit displays. This enhances collision avoidance capabilities and enables more efficient route planning and traffic coordination.

7. **Integration with other surveillance technologies:**

ADS-B can be integrated with other surveillance technologies, such as radar and ADS-Contract (ADS-C), to provide a comprehensive and integrated picture of aircraft positions and movements. This allows for redundancy and improved accuracy in aircraft surveillance.

8. Data sharing and applications:

ADS-B data can be shared with other aircraft, air traffic controllers, and other stakeholders, allowing for collaborative decision-making and improved operational efficiency. ADS-B data can also be used for various applications, such as ATM, flight tracking, weather observation, and aviation safety.

- **ADS-C:**

It consists of a surveillance technology that uses communication contracts between aircraft and air traffic control (ATC) to periodically report the aircraft's position and other information. ADS-C is typically used in oceanic and remote areas where radar coverage is limited or unavailable. With ADS-C, aircraft send position reports to ATC via satellite communication links, allowing for more accurate and updated tracking of aircraft positions. ADS-C is used for long-range surveillance and is often used in conjunction with ADS-B in regions where both technologies are implemented.

ADS-C is a surveillance and communication system that offers several key characteristics. Firstly, it operates through pre-defined communication contracts between aircraft and air traffic control (ATC). These contracts establish the frequency, format, and content of position reports, which can be sent periodically or based on event-triggered conditions. Additionally, ADS-C relies on satellite communication links, enabling long-range surveillance and overcoming limitations of radar coverage, particularly in remote or oceanic areas. Various technologies like VHF Data Link (VDL), SATCOM, or other data link services can be employed for satellite communication.

The position reports generated by ADS-C include essential information such as latitude, longitude, altitude, velocity, and heading derived from onboard navigation systems. Moreover, ADS-C can be event-triggered, automatically transmitting reports when specific events like altitude or route deviations occur. The system offers flexibility and adaptability through dynamic updates of communication contracts during flight, allowing adjustments to operational requirements or ATC instructions. Integration with other surveillance technologies, such as ADS-B and radar, is common, providing a comprehensive and redundant picture of aircraft positions and movements. Lastly, ADS-C is subject to regulatory requirements defined by organizations like the ICAO, playing a vital role in the global standard for air traffic management systems.

Both ADS-B and ADS-C are important technologies for enhancing the accuracy, efficiency, and safety of aircraft surveillance in modern aviation. They provide real-time and accurate tracking of aircraft positions, which enables more effective ATC, flight tracking, and other applications, leading to improved situational awareness and operational benefits in aviation.

1.1.2 Multilateration (MLAT)

A MLAT system, also known as a hyperbolic positioning system, utilizes receiver/interrogator stations and algorithms to calculate the position of a target. These systems rely on measured parameters from a transponder device, either actively requested or emitted passively, to compute the target's position at each receiving station. MLAT systems are valuable for ATC surveillance, extracting and displaying the position and identification of aircraft or vehicles equipped with an SSR transponder. Ground receiving stations, connected to a CPS, measure signal characteristics such as TOA, AOA, or Round-Trip Delay (RTD) to detect and identify targets.

Enhanced or hybrid MLAT systems incorporate additional measurements alongside TOA. The system's hardware includes GSs, the CPS, communication data links, and auxiliary electronic devices, while the software consists of procedures performing specific functions in both GS and CPS. Designing and setting up an adequate number of receiving stations across the coverage area is crucial for effective implementation, tailored to specific requirements and restrictions.

1.1.3 Space-based Multilateration (SBM)

SBM is a surveillance technique used to determine the location of aircraft or other objects in three-dimensional space using signals received from satellites. SBM relies on the measurement of the TOA or TDOA of signals transmitted by an aircraft to multiple satellites in space, and then using these measurements to compute the aircraft's precise location.

SBM relies on signals received from satellites in space, typically those in LEO constellations. These satellites are equipped with receivers that can detect and measure signals transmitted by aircraft, allowing for global coverage and continuous surveillance of aircraft positions. This surveillance technique uses the MLAT technique, already described in the previous section. By measuring the time it takes for signals transmitted by an aircraft to reach multiple satellites, SBM can determine the aircraft's precise location in three-dimensional space.

SBM could provide high accuracy and integrity in determining aircraft positions, typically with horizontal and vertical accuracies of a few meters. It can also provide integrity information to indicate the quality and reliability of the position data obtained by means of ADS-B, ensuring the overall integrity of the surveillance information. One of the key advantages of SBM is its ability to provide continuous surveillance of aircraft positions, regardless of their location around the globe. This makes SBM particularly useful for remote and oceanic regions where traditional surveillance technologies such as radar or ADS-B may be limited or unavailable.

SBM can be used in conjunction with other surveillance technologies, such as radar, ADS-B, and ADS-C (where available), to provide a multilayer and integrated picture of aircraft positions and movements. This allows for redundancy and increased safety levels in aircraft surveillance. In the field of Air Traffic Management (ATM), SBM has various applications. It can be used for aircraft tracking, collision avoidance, route optimization, and traffic coordination. SBM data can be shared with other aircraft, ATCS, and other stakeholders, allowing for collaborative decision-making and improved operational efficiency.

Overall, SBM is a satellite-based surveillance technique used to determine the accurate location of aircraft. It offers high accuracy, global coverage, and does not rely on ground infrastructure, making it valuable for ATM and aviation. A MLAT system carries out essential functions including TOA-related measurements, target tracking, identification, position estimation, integrity analysis, and system synchronization. However, noise can negatively impact measurement accuracy, particularly in scenarios with long distances. To enhance accuracy and reliability, a data fusion function combines estimated positions with data from other surveillance systems like Primary Surveillance Radar (PSR), SSR, MLAT, and ADS-B (where available). The overall performance of MLAT depends on system layout design, measurement quality and accuracy, and the localization process, which involves target position estimation and tracking.

To achieve optimal system coverage and performance within constraints and regulatory standards, deploying receiving stations with specific locations and sensor-antenna characteristics is crucial. This ad-hoc design process involves multiple iterations to achieve satisfactory station distribution. Key design parameters, including error contributions and radioelectric coverage, significantly influence the system's overall design. Despite uncontrollable and subjective parameters that may result in sub-optimal designs, an acceptable configuration will suffice for the required analysis. Subsequent optimization efforts can focus on satellite constellation configuration, studied mechanisms, and parameters to improve accuracy and reduce measurement uncertainty. Performance parameters, including aircraft Probability of Detection (PoD), Probability of False Detection (PoFD), and system capacity, will be analyzed. This project uses a well-known tool, the Cramér-Rao Lower Bound (CRLB), widely used in the design of ground-based MLAT systems, to thoroughly explore and analyze the effect on the system performance of different system parameters and errors, as well as the radioelectric coverage to improve the system's structure and achieve accurate results with reduced uncertainty.

Two categories of algorithms are used to calculate the aircraft's position: closed form and open form. Both types involve solving a system of highly nonlinear equations. Factors influencing the accuracy of position estimation include the spatial distribution of receiving stations (system geometry), Signal-to-Noise Ratio (SNR), measurement accuracy (TOA, TDOA, AOA, and FDOA), system transient performance, and the effectiveness of the localization algorithm in solving the equation system.

System synchronization, especially between receiving stations on-board the satellites, introduces persistent and uncontrolled errors and will be studied in relation to target localization. Although the SBM system integration will not be addressed in this project, acceptable error bounds will be identified. As limited research exists on this topic, the project aims to propose innovative strategies for aircraft tracking and identification using satellites. It will encompass system design and a comprehensive performance study for ATM operations.

1.2 Motivation

EUROCONTROL is a pan-European intergovernmental organization that plays a crucial role in coordinating and promoting ATM across Europe. Its main objective is to ensure the safe, efficient, and environmentally sustainable movement of aircraft. EUROCONTROL undertakes various activities in the field of ATM to achieve this goal. One of its key activities is Air Traffic Flow Management (ATFM). It coordinates the flow of air traffic across the European airspace, aiming to optimize airspace capacity utilization and minimize delays. This involves monitoring air traffic demand, capacity, and other factors that can impact the flow of aircraft. Based on this information, measures such as rerouting, ground holding, and slot allocation are implemented to optimize the flow of traffic. Another important area of focus is airspace design and management. It works on designing and managing European airspace in a manner that ensures efficient and safe handling of air traffic. This includes developing airspace management plans, defining airspace boundaries, and coordinating the use of airspace among different states and ANSPs, whose goal is to optimize the capacity and safety of the airspace.

EUROCONTROL collaborates with its member states and partners to develop and implement common ATM systems and technologies. This includes establishing standards and guidelines for ATM systems, supporting the implementation of new technologies such as Performance-based Navigation (PBN) and data link communication, and promoting the harmonization and interoperability of ATM systems across Europe. Safety management is another crucial aspect of EUROCONTROL's activities in ATM. It works towards enhancing safety in ATM through the development and implementation of Safety Management Systems (SMS) and safety regulations.

This involves conducting safety assessments, providing safety guidance, and promoting a safety culture among aviation stakeholders. By ensuring safe operations in European airspace, EUROCONTROL contributes to maintaining a high level of safety in air traffic. Additionally, Collaborative Decision Making (CDM) processes among stakeholders are facilitated in ATM. It promotes cooperation, information sharing, and joint decision-making among airlines, ANSPs, airports, and other aviation entities. The objective of CDM is to improve the efficiency of ATM by optimizing operational planning and reducing delays. Furthermore, it closely collaborates with its member states, ANSPs, international organizations, and industry stakeholders to harmonize and optimize air traffic management across Europe. Through its activities in ATM, EUROCONTROL contributes to enhancing the safety, efficiency, and environmental sustainability of air traffic operations in the European airspace. On the other hand, the European Organisation for Civil Aviation Equipment (EUROCAE) is a non-profit organization that plays a significant role in the aviation industry by developing and publishing standards and guidelines. Its focus lies in the field of Communication, Navigation and Surveillance (CNS) services. By creating technical standards and guidelines, it ensures interoperability, safety, and efficiency in aviation operations.

Airport CDM (A-CDM) aims to improve the efficiency and resilience of airport operations by optimizing the use of resources and improving the predictability of air traffic. One major advantage of integrating SBM systems with A-CDM elements is enhanced flight efficiency. With precise aircraft positioning data available in real-time, ATCS could optimize routing and sequencing, leading to more direct flight paths, reduced holding patterns, and minimized ground delays. This not only saves valuable time for airlines and passengers but also reduces fuel consumption and environmental impact. Moreover, the accurate surveillance data provided by space-based MLAT systems allows for improved airspace management. ATCS can proactively manage traffic flow and capacity, ensuring optimal utilization of airspace and airport resources. By sharing this information with stakeholders through CDM tools, such as the CDM Portal, all parties can make informed decisions regarding flight planning, ground handling, and airport resource allocation. This coordination leads to smoother operations, minimized congestion, and increased overall capacity.

Additionally, the integration of SBM systems with CDM elements could enhance safety and situational awareness. Real-time aircraft position data enables controllers to quickly detect and resolve potential conflicts, preventing airspace infringements and maintaining safe separation between aircraft. This shared information also enhances collaborative decision-making among stakeholders, fostering a proactive and cooperative approach to mitigating operational challenges and unforeseen events. Existing A-CDM airports have already experienced many real operational benefits. Implementing A-CDM may not be an easy task but more and more airports are opting for it.

Some example benefits can be seen below:

- Reduce environmental nuisance.
- Optimize the use of available capacity and the turn-round time.
- Improve safety by reducing apron and taxiway congestion.
- Improve the usage of infrastructure and public information data quality.
- Reduce late aircraft stand and gate changes to adhere to airport slot.
- Improve predictability of operations and resource management.
- Minimize the impact of delays due to late arrival of inbound flight.
- Improve ground handler resource management.

1.3 Objectives

The primary objective of this project is to pave the way to the development of a SBM system to be used in ATC operations by developing design strategies and tools as well as algorithms to provide efficient and reliable real-time flights data. The operational strategies focus on the adaptation of localization algorithms used in ground-based MLAT addressing the challenges of position uncertainty and low accuracy inherent to space environment. These new strategies could be applied across various ATC domains, including airport surface surveillance, takeoff-landing, approach, and en-route control, being the latter the most relevant, specially in transatlantic regions. To accomplish the overarching objective, the following specific objectives are proposed:

1. To investigate the potential benefits and feasibility of implementing a SBM system within the aviation industry. Such a system could provide valuable data and insights for improving aviation operations, enhancing fuel efficiency, optimizing flight routes, and minimizing environmental impact. By addressing the Sustainable Development Goal (SDG)s through the research findings, this study aims to contribute to sustainable development by promoting cleaner and more efficient energy use, fostering innovation in the aviation industry, and taking actionable steps towards mitigating climate change. By promoting sustainability in aviation operations, the research aims to drive positive environmental change, support economic growth, and enhance social well-being on a global scale. The proposed implementation of a SBM system plays a crucial role in aligning with several SDGs, whose description and explanation is available in *Part VI - Sustainable Development Goals (SDGs)*.
2. To develop advanced tools capable of estimating the theoretical error associated with SBM systems following the CRLB. These tools will play a pivotal role in designing satellite constellations that could deliver positioning accuracy within acceptable limits, as defined by industry standards such as the EUROCAE ED-142A. By accurately assessing the theoretical error of the SBM system, this research seeks to achieve a significant milestone in evaluating space-based systems and improving existing positioning technologies. The ultimate goal is to provide the ATCS with the most precise and reliable real-time data.

The developed tools will encompass sophisticated algorithms and mathematical models that consider various factors affecting the positioning accuracy, including satellite geometry, atmospheric conditions, and potential sources of error. These tools will provide valuable insights into the expected performance and limitations of the SBM system under different operational scenarios. Moreover, the research will focus on adjusting the design of the satellite constellation to ensure the best possible positioning accuracy while meeting the predefined standards.

This will involve determining the number, distribution, and orbital parameters of satellites to minimize the overall error and enhance system performance. By providing accurate estimates of the theoretical error and offering valuable guidance for satellite constellation design, this research contributes to improving the current state of positioning systems. The research outcomes will enable the ATCS to access the most reliable and precise real-time data, facilitating enhanced situational awareness and decision-making capabilities. The implications of this research extend beyond the ATCS domain, as accurate positioning systems have widespread applications in fields such as transportation, logistics, surveying, and emergency services. The developed tools will not only support the design of SBM systems but also drive advancements in positioning technology, benefiting industries and society as a whole.

3. To tackle the challenges posed by ill-conditioned systems of equations and minimize errors resulting from various sources of measurement noise. To achieve this, the study will focus on defining appropriate error indicators that accurately reflect the quality and reliability of satellite measurements. These indicators will serve as crucial metrics for assessing the magnitude and impact of errors in positioning and navigation. By addressing the ill-conditioning of the system of equations, the research aims to enhance the robustness and accuracy of satellite-based positioning and navigation systems. This includes the development of methodologies to reduce the amplification of errors and improve the overall reliability of the computed results.

The effectiveness of the proposed error indicators and estimators will be validated through extensive numerical experimentation and testing. Real-world scenarios and synthetic data sets will be employed to simulate various challenging conditions and accurately assess the performance of the error mitigation strategies. The outcomes of this research endeavor have significant implications for a wide range of applications reliant on satellite-based positioning and navigation systems. By reducing and mitigating errors due to measurement noise sources, the research contributes to enhancing the accuracy, precision, and reliability of satellite-based positioning technologies across sectors such as transportation, surveying, agriculture, and disaster management.

4. To develop, implement, and evaluate a comprehensive set of localization and regularization algorithms that effectively address the location problem by employing an inverse problem approach. The primary objective is to determine the best-performing algorithms that yield improved and more reliable estimations for the positions of aircraft. Through rigorous simulations and extensive numerical testing, this study aims to compare and analyze the performance of various localization and regularization algorithms, as well as to assess their sensitivity against different error sources, such as starting points uncertainty and measurement errors. The research will involve the utilization of advanced computational models and sophisticated statistical techniques to evaluate the efficacy of the algorithms. The simulations will incorporate diverse scenarios to replicate real-world situations.

The outcomes of this research will provide valuable insights into the strengths and limitations of different localization/regularization algorithms. By identifying the algorithms that offer superior performance and more reliable estimations, this study seeks to contribute to the enhancement of aircraft positioning systems and ATC operations. Furthermore, the findings will support the development of more efficient and accurate localization methodologies, which can have significant implications for air transportation, including improved safety, enhanced operational efficiency, and reduced environmental impact.

5. The effectiveness of the implemented strategies will be rigorously assessed through comprehensive simulation tests involving potential flight plans in highly congested airspace regions, with a particular emphasis on the North Atlantic area, known for its intense air traffic. The simulation tests will involve the utilization of sophisticated modeling techniques and state-of-the-art simulation tools to replicate real-world conditions accurately.

By subjecting the implemented strategies to these demanding simulation tests, their performance and impact on studying airspace utilization and minimizing congestion will be thoroughly analyzed. The evaluation will include assessing key metrics such as flight delays, airspace capacity, fuel efficiency, and overall operational effectiveness. Moreover, the simulation tests will provide insights into potential challenges and limitations of the strategies when deployed in complex and congested airspace regions.

6. To develop a user-friendly graphical interface that enables users to configure and customize evaluation parameters effectively. This interface aims to provide a simple yet powerful tool for analyzing and assessing the performance of the MLAT system comprehensively. By obtaining the highest levels of accuracy, this research aims to facilitate substantial cost savings through the deployment of precise satellite constellations for ATC/ATM operations. The designed graphical interface will offer intuitive controls and visual representations, allowing users to adjust and fine-tune evaluation parameters effortlessly. Through this interface, users will have the flexibility to define and customize various performance metrics, criteria, and thresholds according to specific operational requirements and industry standards.

The comprehensive analysis conducted using the graphical interface will encompass the entire MLAT system, considering crucial factors such as satellite positioning, data transmission, signal processing, and integration with existing ATC/ATM infrastructure. By evaluating the system's performance across these key areas, the research aims to identify opportunities for enhancement. The primary focus will be on achieving the highest possible accuracy levels in MLAT-based positioning. By fine-tuning the system parameters and configuration, it becomes possible to achieve precise and reliable aircraft tracking, contributing to improved safety, efficiency, and operational effectiveness.

The successful deployment of accurate satellite constellations for ATC/ATM operations could carry significant financial implications. By ensuring superior accuracy levels, substantial cost savings could be realized. Accurate aircraft tracking would allow for optimal flight routing, reduced fuel consumption, minimized delays, and enhanced airspace capacity, leading to potential savings amounting to millions of euros.

Chapter 2

MLAT Systems

MLAT systems refer to hyperbolic localization systems used to determine the position of cooperative aeronautical targets. This is achieved by analyzing responses obtained from secondary radar interrogations in Mode A/C or Mode S, as well as through interrogations of secondary radars in Mode A/C or Mode S. Additionally, positions can be derived from messages emitted spontaneously by ADS-B transmitters, known as squitters. The MLAT system comprises a network of N receiving stations strategically deployed across the coverage area.

These stations are synchronized with each other, allowing for precise measurement of the time instant at which they receive signals transmitted by the target. This synchronization ensures that all stations share a common time base, enabling accurate TOA measurements. By analyzing the TOA information collected from multiple receiving stations, the MLAT system calculates the hyperbolic curves that intersect at the location of the target. These intersections provide valuable data for determining the precise position of the cooperative aeronautical target. The utilization of MLAT systems enhances the surveillance capabilities in ATM by enabling the tracking and localization of aircraft even in areas where primary radar coverage may be limited.

These systems play a crucial role in improving situational awareness, enhancing airspace safety, and supporting efficient air traffic operations. By leveraging the synchronized network of receiving stations and the analysis of radar responses and ADS-B messages, MLAT systems provide a robust and reliable solution for accurately determining the positions of cooperative aeronautical targets.

2.1 Definition and Operating Principles

The concept of the MLAT system originated during World War I (WW-I). It was during this time that the first localization application utilizing the hyperbolic positioning principle emerged, known as the Hyperbolic Audio Location System. This system relied on measuring the relative time of arrival of sound signals and played a crucial role in determining the locations of concealed war cannons on the battlefields. The original scheme of this system is reproduced in Figure 1.2.1.

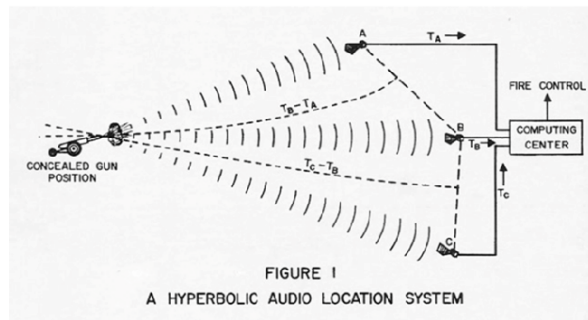


Fig. 1.2.1: Hyperbolic audio location system.

The initial system described above relied on measuring the TOA of explosion sounds at receiving stations A, B, and C. These measurements were made using a chronograph installed in the computing center. By manually determining the distances between stations A and B, and B and C based on TOA measurements, two hyperbolas ($T_B - T_A$ and $T_C - T_B$) were drawn (see Figure 1.2.1). The intersection of these hyperbolas was taken as the location of the cannon. However, the system had limitations due to the short range of sound waves, resulting in low accuracy of time measurements. Subsequent developments in air navigation tools began during World War II (WW-II).

Radio Frequency (RF) generators capable of delivering kilowatt-level signals and devices with the ability to measure TOA with an accuracy of one millionth of a second were developed. These advancements led to the creation of the first hyperbolic navigation systems within the category of radio navigation systems [16]. These systems can be considered as an evolution from the previous system shown in Figure 1.2.1. In the new scheme, hyperbolic navigation systems utilize a network of GSs deployed in known locations, which are synchronized in time and phase. These GS transmit Electromagnetic (EM) signals that are received by aircraft. The aircraft's onboard navigation equipment measures a physical parameter such as TOA or phase. Using these measurements and appropriate navigation algorithms, the aircraft's position relative to a reference site can be calculated. This is illustrated in Figure 1.2.2.

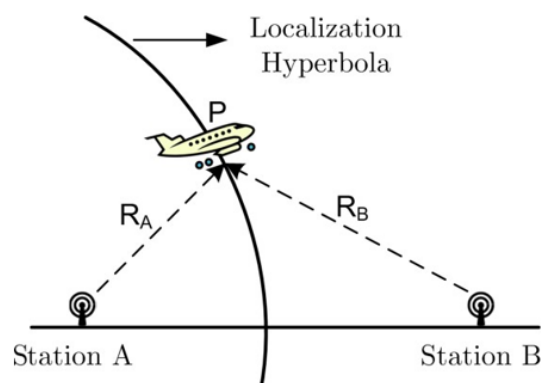


Fig. 1.2.2: Hyperbolic navigation system principle.

The development of hyperbolic navigation systems represented a significant advancement in air navigation, providing more accurate and reliable positioning capabilities compared to the earlier audio location system. These systems played a crucial role in improving navigation during WW-II and continue to be used in various forms in modern aviation.

In contrast, Figure 1.2.3 illustrates a hyperboloid with its foci located at the positions of the receiving stations. In the ideal case without any noise, the target is located precisely on this hyperboloid. Figure 1.2.4 demonstrates the intersection of three hyperboloids following the same principle. Since the objective is to determine a specific position rather than a surface or volume, obtaining more than one hyperboloid is necessary, which requires more than two receiving stations. Mathematically, a minimum of three stations (equivalent to two hyperbolic equations) is needed to calculate a position in a two-dimensional spatial reference frame (2D localization), while at least four stations (equivalent to three hyperbolic equations) are required for three-dimensional localization (3D localization). However, due to measurement errors, the intersection of hyperboloids represents a dynamic area or volume rather than a precise point.

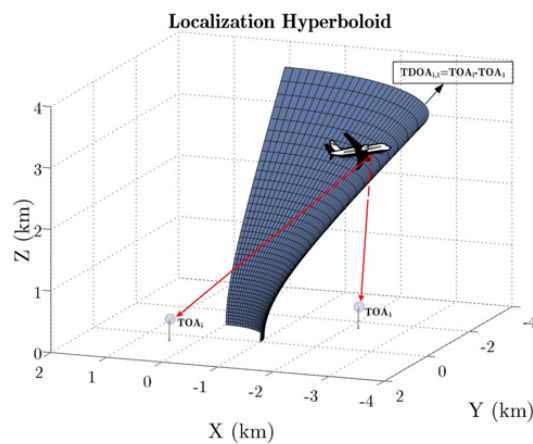


Fig. 1.2.3: Section of a hyperboloid for a pair of receiving stations.

It is important to consider these measurement errors when interpreting the results, as they introduce uncertainties in the determined position. The size of the intersection area or volume provides an indication of the potential error associated with the calculated position. Techniques for estimating and mitigating these errors will be discussed in subsequent chapters, aiming to improve the accuracy and reliability of the MLAT system.

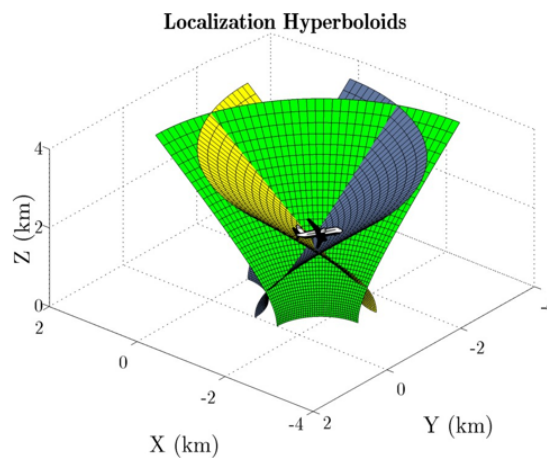


Fig. 1.2.4: Intersection of three hyperboloids.

Figure 1.2.5 provides an example of a 2D localization scenario where the target's possible positions are represented by hyperbolas rather than hyperboloids. In this case, considering the TDOA measurement obtained from stations 4 and 1, the target can only be situated along the green hyperbola. However, when multiple hyperbolas are mathematically combined, the potential target location can be narrowed down to a single spatial point in most cases, as depicted in Figure 1.2.5.

The presence of multiple intersecting areas depends on the system's geometry, the placement of receiving stations, and the actual position of the target. It is essential to eliminate false intersections or unwanted analysis areas by identifying and disregarding redundant information. This information may originate from additional or external sources or systems. When a larger number of stations receive the transponder emitted signal, the resulting solution becomes more accurate and reliable compared to scenarios with fewer stations.

To enhance the accuracy and reliability of the localization process, it is important to consider factors such as the geometry of the system, the distribution of receiving stations, and the quality of measurements. The incorporation of additional stations and the optimization of their placement can contribute to improved localization performance, minimizing errors and uncertainties in the final results.

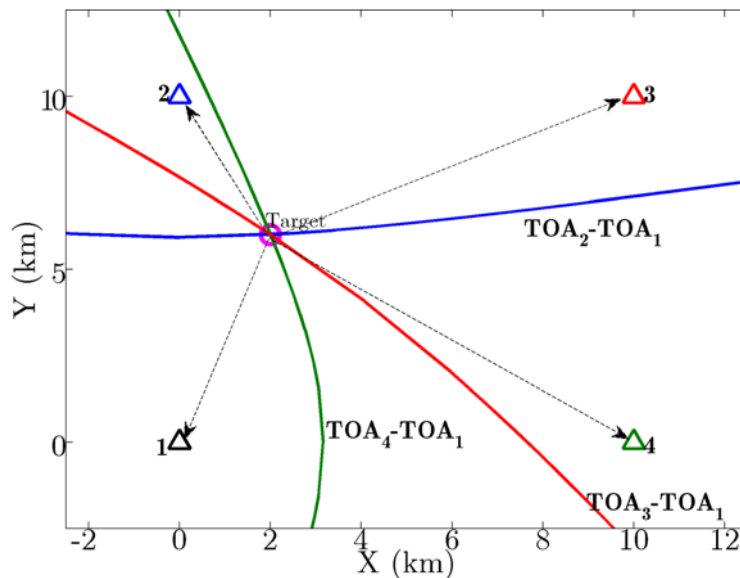


Fig. 1.2.5: Hyperbolas for four stations and a target located in an arbitrary position.

2.2 Theoretical Horizontal and Vertical Position Accuracies

Let θ be the position of the target in rectangular coordinates at the instant t_e at which the signal to be used as the basis for its localization is transmitted. Let $\hat{m} = [\hat{m}_1, \hat{m}_2, \dots, \hat{m}_N]^T$ be a vector containing N observations of a radio-frequency signal emitted by the target at instant t_e from position θ , measured in a set of N_s receiving stations located at positions defined by θ_i in the same rectangular coordinate system used to reference the position of the target. In general, $N_s \neq N$. It is assumed that the measured magnitude depends on the position of the target, i. e. $\hat{m} = \hat{m}(\theta)$.

The objective of the positioning system is to know the target position, θ , at the instant t_e from the measurements $\hat{m}(\theta)$. The relationship between the measured magnitude and the target position, $m(\theta)$, is assumed to be known, so it would be sufficient to invert this relationship to know the exact target position, θ . However, due to measurement error, $m(\theta) \neq \hat{m}(\theta)$ (it is generally assumed that $\hat{m}(\theta) = m(\theta) + m_{\Delta}(\theta)$), being $m_{\Delta}(\theta)$ the measurement error vector, which is considered to be of type Gaussian with zero mean and with a known covariance matrix $N(\theta)$). The positioning system will obtain a position estimator that depends on the measurements made at the receiving stations, $\hat{\theta}(\hat{m})$. Therefore, the error in the position estimator is $\theta_{\Delta} = \theta - \hat{\theta}(\hat{m})$. Considering the estimator is unbiased, $E[\theta_{\Delta}] = 0$, the covariance matrix of the error will satisfy Cramér-Rao's inequality presented in 2.1:

$$N_{\Delta}(\theta) = E[\theta_{\Delta}\theta_{\Delta}^T] \geq [J(\theta)]^{-1} = C(\theta) \quad (2.1)$$

where $J(\theta)$ is the Fisher Information Matrix (FIM) (see 2.2). Ignoring higher order terms:

$$J(\theta) = \frac{\partial m^T}{\partial \theta} [N(\theta)]^{-1} \frac{\partial m}{\partial \theta} \quad (2.2)$$

where $\frac{\partial m}{\partial \theta}|_{i,j} = \frac{\partial m_i}{\partial \theta_j}$ stands for the Jacobian of the transformation $m(\theta)$. From 2.1, metrics for the position error are defined, more specifically the Theoretical Horizontal Position Accuracy (THPA) and Theoretical Vertical Position Accuracy (TVPA), both defined in 2.3 and 2.4:

$$THPA = \sqrt{C(\theta)_{1,1} + C(\theta)_{2,2}} \quad (2.3)$$

$$TVPA = \sqrt{C(\theta)_{3,3}} \quad (2.4)$$

In general, THPA is indicated in meters, and TVPA, in feet (1 ft = 30,38 cm). From [17], a practical example of how CRLB defines the limits of the minimum error values is shown in Figure 1.2.6.

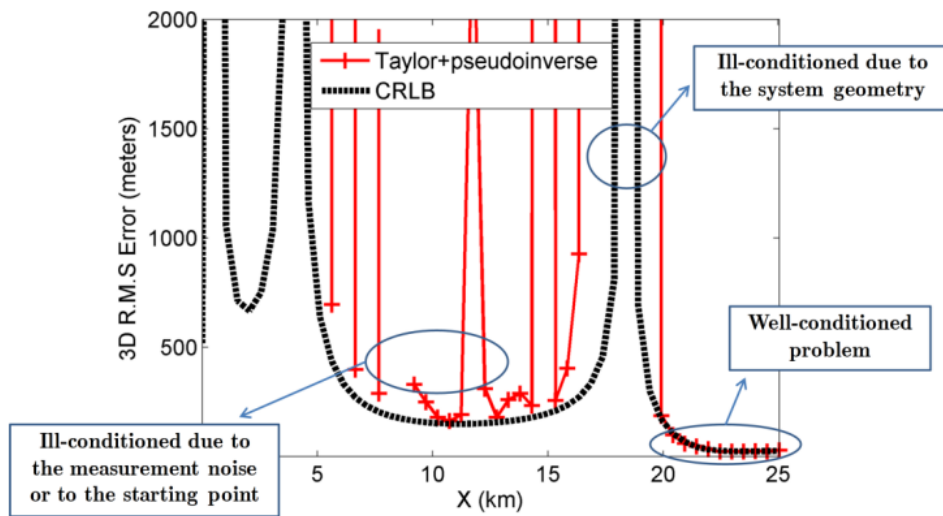


Fig. 1.2.6: CRLB vs Taylor + Pseudoinverse.

2.3 MLAT Systems based on TDOA, AOA, and FDOA

This section is oriented to propose some SBM system designs by establishing a set of techniques used for accurate and precise positioning. MLAT systems with TDOA-based multilateration systems utilize the differences in arrival times of signals at multiple receiving stations to estimate the position of a target. By measuring the time delays between the arrival of signals at different stations, the system can determine the target's location by intersecting hyperboloids or hyperbolas. Moreover, AOA-based MLAT systems rely on measuring the angles at which signals from a target arrive at multiple receiving stations. By comparing the angles of arrival, the system can determine the target's location through triangulation or other geometric methods. Finally, FDOA-based MLAT systems exploit the differences in the frequency of signals received at different stations. These frequency differences can be caused by the Doppler effect or other factors. By analyzing the frequency variations, the system can estimate the target's position.

Combining these three techniques in a MLAT system provides enhanced accuracy and reliability in target localization and tracking. By integrating multiple sources of information, such as time, angles, and frequencies, these systems can mitigate the effects of measurement errors, environmental factors, and interference, resulting in improved positioning accuracy and robustness. MLAT systems based on TDOA, AOA, and FDOA have diverse applications, including ATC/ATM, surveillance, military operations, and wireless communication networks. They offer valuable capabilities for precise positioning, navigation, and tracking, contributing to the safety, efficiency, and performance of various systems and industries.

2.3.1 Time Difference of Arrival (TDOA)

The MLAT system is composed of a set of N receiving stations deployed in the coverage area. All of them are synchronized with each other, so that they can measure the instant of time at which they receive a signal emitted by the target TOA in the same time base. Thus, the TOA depends both on the position of the target and the N stations in the system, as stated in 2.5:

$$TOA_i = t_e + \frac{\sqrt{(x - x_i)^2 + (y - y_i)^2 + (z - z_i)^2}}{c} + n_i = t_e + \frac{\|\theta - \theta_i\|}{c} + n_i \quad (2.5)$$

with $i = 1, 2, \dots, N_s$, where c is the speed of light in free space, t_e is the instant of time (unknown to the system) at which the target emitted the signal, $\theta = [x, y, z]$ is the position vector of the target, $\theta_i = [x_i, y_i, z_i]$ are the Cartesian coordinates of the i -th receiving station in the same coordinate system used to reference the target, $\|\cdot\|$ is the Euclidean norm in \mathbb{R}^3 , and n_i is the error in the measurement of the TOA at the i -th station.

TDOA is a technique that relies on measuring the difference in arrival time of a signal at multiple receivers. By knowing the speed of signal propagation, which is typically the speed of light, the difference in arrival times can be converted into differences in distance. The intersection of these distance differences can then be used to determine the source's location. Considering one of the N_s receiving stations as the reference station (hereafter and without loss of generality, the reference station will be the number 1), a set of N_s-1 TDOA is obtained, as 2.6 indicates:

$$TDOA_{i,1} = \frac{1}{c} \|\theta - \theta_1\| - \frac{1}{c} \|\theta - \theta_i\| + n_1 - n_i = m(\theta) + n_{i,1}, \quad i = 2, \dots, N_s \quad (2.6)$$

By subtracting the TOA, the emission time t_e disappears from the equations, and with it the bias due to the drift of the reference clocks at the different stations. 2.6 defines a set of N_s-1 hyperboloids whose foci are located at the reference station and the i -th station. The intersection of these hyperboloids provides the position of the target, as shown in Figure 1.2.5. Such is the case that four receiving stations would be sufficient to generate a system of three equations whose solution would provide the estimated position of the target, because a hyperboloid with a certain thickness is defined due to the error term. Therefore, the intersection of these geometrical figures will not define a point in \mathbb{R}^3 but a volume of uncertainty $V_\epsilon \subset \mathbb{R}^3$, within which the target will be found with a given probability. The more hyperboloids used, the smaller the volume of uncertainty.

Due to the error in the TOA measurement, the MLAT system does not provide the target position, θ , but rather an estimation, $\hat{\theta}$. Assuming that the measurement error of the TOA has zero mean, the estimator $\hat{\theta}$ turns out to be unbiased, that is $E[\hat{\theta} - \theta] = 0$, so the variance of the error in the estimation of the position is $\sigma^2 = E[(\hat{\theta} - \theta)(\hat{\theta} - \theta)^T]$. Since the estimator is unbiased, there is a lower limit to this error, known as CRLB. This limit is considered the Theoretical Position Accuracy (TPA) of the system. In general, the CRLB provides bounds on the Root Mean Square (RMS) error, or standard deviation of the error in each direction of the space $(\sigma_x, \sigma_y, \sigma_z)$, which can be combined to define different quality parameters of the system. The required accuracy values are obtained from the Minimum Operational Performance Specification (MOPS) defined in the EUROCAE-ED 142 standard.

In the case of MLAT systems based on TDOA, the receiving stations measure the TOA of the signal emitted by the target, which is given by 2.5 and 2.6, thanks to which it is possible to obtain the elements of the measurement vector $\hat{m}(\theta) : \hat{m}_i(\theta) = c \cdot TDOA_i$, for $N = N_s - 1$ number of measurements. Assume N_s receiving stations capable of measuring the arrival time of the emitted signal exist, and that the error of the TOA measurements of the i -th station is n_i , for $1 \leq i \leq N_s$, so the error in the elements of the measurements vector is $m_{\Delta,i} = c(n_{i+1} - n_1)$, for $1 \leq i \leq N$. Assuming that $E[n_i] = 0$, for $1 \leq i \leq N_s$, and $E[n_i n_j] = \delta_{i,j} \sigma_{TOA_i}^2$, for $1 \leq i, j \leq N_s$, the covariance matrix of the error is given by 2.7:

$$N_{TDOA} = E[m_{\Delta} m_{\Delta}^T] \quad (2.7)$$

Considering $E[m_{\Delta,i}] = E[cn_{i+1} - cn_1] = cE[n_{i+1}] - cE[n_1] = 0$, for $1 \leq i \leq N$, and applying the $E[n_i n_j]$ assumptions, the corresponding i,j -th element of the covariance matrix is given by 2.8:

$$N_{TDOA_{i,j}} = E[m_{\Delta,i} m_{\Delta,j}] = E[(cn_{i+1} - cn_1)(cn_{j+1} - cn_1)] = c^2(\sigma_{TOA_1}^2 + \delta_{i,j} \sigma_{TOA_{i+1}}^2) \quad (2.8)$$

For TDOA-based MLAT systems, the transformation between the target coordinates and the elements of the measurement vector, regardless of the TOA error, is given by 2.9, and the elements of the Jacobian of the transformation appear in 2.10:

$$\begin{aligned} m_i(\theta) &= \|\theta - \theta_{i+1}\| - \|\theta - \theta_1\| = \\ &= [(\theta_1 - \theta_{i+1,1})^2 + (\theta_2 - \theta_{i+1,2})^2 + (\theta_3 - \theta_{i+1,3})^2]^{\frac{1}{2}} \\ &\quad - [(\theta_1 - \theta_{1,1})^2 + (\theta_2 - \theta_{1,2})^2 + (\theta_3 - \theta_{1,3})^2]^{\frac{1}{2}} \end{aligned} \quad (2.9)$$

$$\left. \frac{\partial m}{\partial \theta} \right|_{i,j} = \frac{\partial m_i}{\partial \theta_j} = \frac{(\theta_j - \theta_{i+1,j})}{\|\theta - \theta_{i+1}\|} - \frac{(\theta_j - \theta_{1,j})}{\|\theta - \theta_1\|}, \quad 1 \leq i \leq N, 1 \leq j \leq 3 \quad (2.10)$$

2.3.2 Angle of Arrival (AOA)

Other MLAT systems use clusters of antennas capable of estimating the AOA, the direction from which the signal emitted by the target arrives. This second approach of geolocation system is therefore based on the AOA. This can be achieved using antenna arrays or by comparing the signal strength at multiple antennas. By measuring the AOA at multiple receivers, it is possible to triangulate the source's location. However, only the implementation of an AOA-dependent system is not possible because of the non-linear equations generated from it.

In order to determine the angles of signal arrival accurately, non-linear transformations must be applied. These transformations enable the derivation of the respective partial derivatives, which are used to compute the FIMs. These matrices, in turn, are crucial for obtaining the covariance matrices required to estimate the horizontal and vertical errors. This approach has been successfully employed in the case of TDOA measurements.

The focus of this project does not encompass the utilization of such non-linear transformations. However, a potential future direction would involve exploring and incorporating additional signal sources. By doing so, a more resilient hybrid model could be constructed, thereby enhancing the system's overall capabilities.

2.3.3 Frequency Difference of Arrival (FDOA)

As a third approximation, an additional measure is set to improve the performance of the MLAT system, based on the Doppler effect, so the system relies on the FDOA. It consists of a technique that utilizes the difference in frequency between a transmitted signal and the received signal. This difference is caused by the Doppler effect, which occurs when the source or receiver is in motion relative to each other. By measuring the frequency difference at multiple receivers, the source's location can be estimated. Just like in the case of AOA analysis, the study of Doppler signals also involves the presence of non-linear transformations. The objectives of this project do not currently include their utilization.

2.3.4 Hybrid MLAT Systems: Error Models

Hybrid SBM systems combine multiple techniques, such as TDOA, AOA, and FDOA, to accurately determine the location of a signal source in space. These systems are commonly used in applications such as satellite communications, radar systems, and navigation systems. Hybrid SBM systems combine these techniques to improve the accuracy and robustness of the location estimation. By integrating TDOA, AOA, and FDOA measurements from multiple receivers, the system can compensate for the limitations and errors inherent in each technique. The fusion of these measurements can provide a more precise and reliable determination of the signal source's position in space. As mentioned, the AOA does not work by itself, but serves as a complement to either the TDOA or the FDOA, or even to both jointly, resulting the latter combination in the most hybrid system. The different cases appear listed in Table 1.2.1:

Case	TDOA	AOA	FDOA
1	✓		
2		∃!	
3			✓
4	✓	✓	
5	✓		✓
6		✓	✓
7	✓	✓	✓

Table 1.2.1: Possibilities of hybrid MLAT systems

Probably, apart from the system geometry (i.e., the satellites distribution), the most important, or determining, aspect in a MLAT system is the error measurement sources. For the proposed system, there is a set of three potential associated error sources, for time, angle, and frequency. These errors contribute significantly to the accuracy of the overall system, and the effectiveness and robustness against eventualities, or high-demanding traffic between satellites. A common factor of them is the SNR, which is obtained as:

$$SNR = \frac{P_T G_T G_R \lambda^2}{4\pi R^2 k T_0 B_R F_R L_T} \quad (2.11)$$

The following outlines the time-associated measurements, and the influence the SNR has on it, making the SNR-dependent factors the most dominating error conforming the standard deviation [18]. The measurement accuracy is characterized by the RMS measurement error, σ_T , given by the Root Sum Square (RSS) of the three error components:

$$\sigma_T^2 = \sigma_{TN}^2 + \sigma_{TF}^2 + \sigma_{TB}^2 \quad (2.12)$$

The components are:

- σ_{TN} : Random time measurement error, dependent on the SNR.
- σ_{TF} : Fixed random error, quantification and clock noises.
- σ_{TB} : Bias error, synchronization error.

The standard deviation of the SNR-dependent random time measurement error is given by:

$$\sigma_{TN} = \frac{\Delta R}{\sqrt{2SNR}} = \frac{c}{2B\sqrt{2SNR}} \quad (2.13)$$

On the other hand, the contribution of σ_{TF} and σ_{TB} can be considered, as done for this application, as a common error factor, hereby known as σ_{TOA} , which represents the Graphical User Interface (GUI) input parameter *TOA error* (*s*).

There is a second contributor as error model, corresponding to the satellite position error. This value, referred to as *SAT position error* (m) in the interface, plays a pivotal role in determining the horizontal errors, and represents the deviation introduced when estimating the true satellites positions. These two error measurement sources define the covariance matrix of the errors that, along with the Jacobian of the transformations, conform the FIMs of each measurement. With these matrices, the corresponding covariance matrices are obtained as the inverse of the FIMs. However, it is of high importance to perform a translation of coordinates to find the horizontal errors in a two-dimensional plane, placed at the point of interest. This translation is made using a rotation matrix, which is defined in 2.14:

$$RM = \begin{bmatrix} -\sin(\beta) & \cos(\beta) & 0 \\ -\cos(\beta)\sin(\alpha) & -\sin(\beta)\sin(\alpha) & \cos(\alpha) \\ \cos(\beta)\cos(\alpha) & \sin(\beta)\cos(\alpha) & \sin(\alpha) \end{bmatrix} \quad (2.14)$$

In 2.14, α and β are the latitude and longitude of the point of interest, respectively. This translation allows finding the horizontal and vertical errors.

Imagine the CRLB using only TDOA is being analyzed. With the measurement error accuracy contributions listed above (σ_T), the covariance matrix of the error is obtained (N_{TDOA}). Using the Jacobian of the transformation (J_{TDOA}), the FIM associated to the TDOA is given by 2.15:

$$FIM_{TDOA} = J'_{TDOA}/N_{TDOA} * J_{TDOA} \quad (2.15)$$

The corresponding matrix through which the CRLB limits are obtained, denoted as CT_{TDOA} (also referred to as covariance matrix) is the inverse of 2.15. Applying the translation with 2.14, the covariance matrix translated CT_{TDOA}^t is properly obtained, also of size 3×3 , and therefore, used to find the horizontal and vertical errors, THPA and TVPA. Their expressions appear in 2.16 and 2.17:

$$THPA = \sqrt{|C_{TDOA}^t(1,1) + C_{TDOA}^t(2,2)|} \quad (2.16)$$

$$TVPA = \sqrt{|C_{TDOA}^t(3,3)|} \quad (2.17)$$

In parallel, the Horizontal Dilution of Precision (HDOP) and Vertical Dilution of Precision (VDOP) are given by 2.18 and 2.19:

$$HDOP = \sqrt{|C_{TDOA}^{0,t}(1,1) + C_{TDOA}^{0,t}(2,2)|} \quad (2.18)$$

$$VDOP = \sqrt{|C_{TDOA}^{0,t}(3,3)|} \quad (2.19)$$

The difference here is the covariance matrix of the error used, now relying only on the system geometry not in the error sources, denoted as N_{TDOA}^0 , and used to find FIM_{TDOA}^0 , and $C_{TDOA}^{0,t}$ with the translation. However, when several measurements are used (TDOA and/or AOA and/or FDOA), their corresponding FIMs need to be obtained separately, and then find the common information matrix as their sum [19].

Part II

MLAT Systems Design and Deployment

Chapter 1

Particularities of MLAT Systems

The design of a MLAT system involves meeting various restrictions, requirements, and regulations while enhancing system performance with limited resources. International bodies like the ICAO and national regulatory bodies such as the National Supervisory Authority (NSA) impose safety and security requirements that must be satisfied. Additionally, the ANSP defines navigation rules for effective air traffic services management.

System accuracy, redundancy, radioelectric coverage, connectivity, and minimum probabilities of detection and identification are among the requirements that need to be fulfilled. A clear distinction can be made between System Design Parameters (SDP) and System Performance Parameters (SPP) in MLAT system design. SPP depends on how the MLAT system is designed, while SDP refers to specific aspects related to system accuracy, functionality, and configuration. The objective of MLAT system design is to maximize compliance with requirements while minimizing resource usage and satisfying restrictions.

Specific functions within the MLAT system, such as synchronization, identification, integrity, and tracking, can be individually designed, calibrated, and optimized. Some functions can be implemented on both the receiving stations and the CPS, while others are exclusive to the CPS. Localization algorithms can be easily implemented and modified as needed. However, determining the ideal system geometry and structure is a complex task. As the number of receiving stations increases, so does the complexity of the system and the design process. The coverage area size, or surveillance volume, is another aspect that affects system design.

Synchronization functions can be adjusted by modifying communication links, such as the ISL distribution. However, changing the geometry of a SBM system, which uses satellites in LEO, is challenging compared to MLAT systems based on GSs used in existing 3G, 4G, and 5G deployments. Therefore, the design process for SBM systems focuses on improving performance based on system geometry, including the number and position of receiving stations and the Region of Interest (ROI) for surveillance. Multiple parameters are used to evaluate the MLAT system's performance, known as SPP, most of which depend on the positioning function, the core function of MLAT systems. However, SPP are influenced by another set of parameters known as SDP.

1.1 System Design Parameters

This section aims to provide a comprehensive description of the SDP in MLAT systems, emphasizing their key characteristics, peculiarities, and their interrelationship with the overall system design process. Implementing these parameters correctly is crucial as SPP heavily rely on them. It is essential to understand the following significant parameters when designing a SBM system: Line of Sight (LOS), radioelectric coverage, Doppler Frequency (DF), DOP, TPA, error balance, and system connectivity and redundancy. Each parameter is described in detail below:

- **Line of Sight (LOS):**

In SBM, LOS refers to the unobstructed path between the satellite and the transmitting object, typically an aircraft equipped with ADS-B or other transponder systems. LOS is a crucial factor in the successful reception and processing of signals by the satellite-based surveillance system. For effective communication and signal reception, the satellite needs to have a direct line of sight to the transmitting object. This means there should be no physical obstacles, such as terrain, buildings, or other objects, blocking the path between the satellite and the aircraft. The LOS concept is essential because radio waves, including the signals transmitted by ADS-B transponders, generally travel in straight lines. When a satellite has a clear line of sight to an aircraft, it can receive the signals directly, allowing for accurate measurement and processing of the signals.

However, obstacles or obstructions between the satellite and the transmitting object can cause signal attenuation or complete signal loss. This can result in reduced or no coverage for the affected areas. For instance, mountain ranges or tall buildings can obstruct the LOS and prevent the satellite from receiving the signals from aircraft in the shadowed areas. To ensure a higher probability of maintaining line of sight with transmitting objects, SBM systems often employ constellations of satellites in specific orbits. By strategically distributing the satellites, the system can increase the chances of having at least one satellite with a clear line of sight to an aircraft at any given time, even if others are obstructed due to terrain or other factors. The LOS requirement in SBM emphasizes the need for unobstructed paths between satellites and transmitting objects. It plays a vital role in ensuring the effectiveness and coverage of the surveillance system by enabling the reception of signals and accurate determination of the position, velocity, and other information of the tracked objects.

- **Radioelectric coverage:**

In the context of radioelectric coverage in SBM, it refers to the area or region in which the satellite-based system can receive and process ADS-B signals from aircraft or other transponders. Since space-based ADS-B relies on satellites, it has the advantage of providing coverage in remote areas, over oceans, and in regions where ground-based infrastructure is limited or non-existent. The radioelectric coverage in SBM is determined by the network of satellites in orbit and their orbital parameters. The satellites receive signals transmitted by ADS-B equipped aircraft and other objects, and these signals are then processed to determine the position, velocity, and other relevant information of the aircraft. The coverage area of a SBM system depends on various factors, including the number and distribution of satellites, their orbital altitude and inclination, the sensitivity and capabilities of the receivers onboard the satellites, and any limitations imposed by the system design.

To achieve global coverage, a constellation of satellites is typically deployed in specific orbital patterns to ensure that multiple satellites have line-of-sight visibility to a given area at any given time. The exact configuration and design of the constellation can vary depending on the specific system and its requirements. It is important to note that while SBM systems can provide wide-area coverage, they still rely on the presence of ADS-B signals from aircraft or other transponders. Therefore, the coverage is limited to areas where there is a sufficient density of ADS-B equipped aircraft or objects transmitting signals. Overall, SBM expands the radioelectric coverage for surveillance and tracking purposes, enabling enhanced monitoring and situational awareness of air traffic or other objects in areas where traditional ground-based systems face limitations.

- **Doppler frequency:**

In MLAT systems, the Doppler frequency is utilized to estimate the velocity or speed of a moving object. Multilateration is a technique used to determine the position of an object by measuring the time it takes for signals to travel from the object to multiple receivers or antennas at known locations. When an object is moving, the frequency of the signals it emits or reflects will be affected by the Doppler effect. By measuring the Doppler shift in the received signals at different receivers, the system can estimate the velocity vector of the object. The principle behind using Doppler frequency in MLAT systems is as follows: The object being tracked emits or reflects a signal, such as a radio wave or radar pulse. This signal is received by multiple antennas at known locations. The receivers measure the frequency of the received signal and compare it to the known frequency of the transmitted signal.

The difference in frequency, known as the Doppler shift, is directly related to the velocity of the object along the line of sight between the object and each receiver. By comparing the Doppler shifts measured at different receivers, the system can calculate the velocity vector of the object. This information, combined with the time measurements of signal arrival at each receiver, can be used to determine the position of the object. MLAT systems that utilize Doppler frequency for velocity estimation are commonly employed in various applications, including ATC surveillance radar systems, and tracking systems for vehicles or ships. They provide valuable information about the movement and speed of objects in real time, enabling efficient monitoring, navigation, and coordination of activities.

- **Dilution of Precision (DOP):**

DOP is a term used in navigation systems, including SBM, to quantify the accuracy and reliability of position measurements. It provides an indication of the quality of the positioning solution obtained from the multilateration system. In SBM, DOP is influenced by several factors, including the geometry of the satellites, the number and distribution of satellites in the constellation, and the position of the transmitting object (e.g., aircraft) relative to the satellites. The key DOP values commonly used in navigation systems are:

- **Position (3D) Dilution of Precision (PDOP):**

Also known as HDOP, is a measure of the horizontal position accuracy. It quantifies the effect of the satellite geometry on the precision of the position solution in the horizontal plane (latitude and longitude). A lower PDOP value indicates a better satellite geometry and, therefore, higher position accuracy.

- **VDOP:**
Measures the effect of satellite geometry on the precision of the position solution in the vertical dimension (altitude). It reflects the quality of the altitude measurement. Similar to PDOP, a lower VDOP value indicates better satellite geometry and higher altitude accuracy.
- **Time Dilution of Precision (TDOP):**
Represents the effect of satellite geometry on the precision of the time measurement used in the positioning solution. It is particularly relevant in systems that rely on precise time synchronization. A lower TDOP value indicates better satellite geometry and higher time accuracy.
- **Geometric Dilution of Precision (GDOP):**
It is a comprehensive measure that combines the effects of PDOP, VDOP, and TDOP. It provides an overall assessment of the geometric factors affecting the accuracy of the position, altitude, and time measurements.

By considering DOP values, users of SBM systems can evaluate the reliability and accuracy of the obtained position and other measurements. DOP values serve as indicators of the quality of the positioning solution. Lower DOP values generally indicate higher accuracy, while higher values suggest reduced accuracy due to factors such as sub-optimal satellite geometry or unfavorable positioning of the transmitting object in relation to the satellites. It is important to note that DOP values can vary based on the specific configuration of the satellite constellation, the number of satellites in view, and the geometry of the transmitting objects. Thus, optimizing the design of the satellite constellation and ensuring an adequate number of satellites could help mitigate the DOP and enhance the overall accuracy of the SBM system's positioning solution.

To facilitate the interpretation of DOP values, a qualitative scale is commonly used. This scale associates the quality of the system geometry with specific numerical DOP values. Table 2.1.1 provides a reference guide for interpreting DOP values and their corresponding quality levels. By referring to this table, users can assess the performance and reliability of the SBM system's positioning solution based on the DOP values obtained.

DOP value	Rating (quality)
< 1	Ideal
1-2	Excellent
2-5	Good
5-10	Moderate
10-20	Fair
> 20	Poor

Table 2.1.1: Qualitative scale for the DOP values

In this MLAT system, the analysis will focus on HDOP. The equivalence values provided in Table 2.1.1 serve as general indicators and can vary depending on the specific scenario being addressed. However, it is important to note that DOP values primarily depend on the geometric distribution of the stations, specifically their positions relative to each point within the surveillance volume. For a given level of measurement errors, the TPA or lower bounds of system accuracy depend on the DOP. Therefore, the DOP plays a significant role as the station deployment locations may not always align with the theoretically optimal geometric configurations. It is advisable to analyze the DOP in conjunction with the LOS considerations.

The DOP analysis is independent of the measurement or synchronization architecture but relies on the number of stations that meet the LOS requirements for a specific spatial point and the resulting geometry formed by those stations. To calculate HDOP, a minimum of three stations is required, while VDOP and PDOP necessitate the use of at least four stations. In the case of this SBM system, which operates in a wide area scenario such as the en-route phase, analyzing the HDOP would be the most appropriate, since the altitude used would be taken from the barometric altimeter placed onboard the aircraft that measures the pressure at a specific height and translates this pressure into height measured in feet. The elements of Q designated are stated in 1.1:

$$Q = \begin{bmatrix} \sigma_x^2 & \sigma_{xy} & \sigma_{xz} & \sigma_{xt} \\ \sigma_{xy} & \sigma_y^2 & \sigma_{yz} & \sigma_{yt} \\ \sigma_{xz} & \sigma_{yz} & \sigma_z^2 & \sigma_{zt} \\ \sigma_{xt} & \sigma_{yt} & \sigma_{zt} & \sigma_t^2 \end{bmatrix} \equiv \begin{bmatrix} a^2 & - & - & - \\ - & b^2 & - & - \\ - & - & c^2 & - \\ - & - & - & d^2 \end{bmatrix} \quad (1.1)$$

The notation used on the right part of the Q matrix equivalence corresponds to the local horizon plane and the local vertical in either a north, east, up coordinate system, where variables a , b , c , and d refer to the $EDOP$, $NDOP$, $VDOP$, and $TDOP$, respectively. The DOP parameters result in:

$$\begin{aligned} HDOP &= (a^2 + b^2)^{\frac{1}{2}} = (EDOP^2 + NDOP^2)^{\frac{1}{2}} \\ PDOP &= (a^2 + b^2 + c^2)^{\frac{1}{2}} = (EDOP^2 + NDOP^2 + VDOP^2)^{\frac{1}{2}} \\ GDOP &= (a^2 + b^2 + c^2 + d^2)^{\frac{1}{2}} = (EDOP^2 + NDOP^2 + VDOP^2 + TDOP^2)^{\frac{1}{2}} \end{aligned}$$

Notice GDOP is actually the square root of the trace of the Q matrix. Both the HDOP and VDOP are dependent on the coordinate system used. Since the clocks on the legacy International Cospas-Sarsat Programme LEO satellites are much less accurate than GPS clocks, discarding their time measurements would actually increase the geolocation solution accuracy. This procedure has been followed in the design of the MLAT system.

- **Theoretical Position Accuracy:**

Another parameter of the system is the TPA. It mainly shows the accuracy of calculating the target position for a particular spatial point, within the surveillance volume. This parameter, which includes both the effects of the measurement error and those of the DOP, is called theoretical because only reflects the best case (or lower bound) of the accuracy that can be obtained with a certain system geometry and an amount of measurements errors. For practical issues, this is the parameter used to obtain the system design. The method used to calculate the TPA is based on the CRLB analysis, a well-known technique in statistics which sets a lower bound on the variance of an unbiased estimator.

- **Error balance measurement:**

In SBM, error balance measurement refers to the process of estimating and compensating for errors in the position measurements obtained from the MLAT system. It involves analyzing various error sources and applying correction techniques to improve the accuracy and reliability of the position solution.

Some of the common error sources in SBM systems include:

1. **Satellite clock errors:**

The onboard clocks of satellites used in the multilateration system may have slight timing errors, which can introduce inaccuracies in the time measurements. By analyzing the timing information from multiple satellites, the system can estimate and correct for these clock errors.

2. **Signal propagation delays:**

The time it takes for the signals to travel from the transmitting object (e.g., aircraft) to the satellites can introduce errors in the distance measurements. These errors can arise due to atmospheric conditions, signal reflection, or refraction. Correction techniques, such as ionospheric modeling or differential corrections, can be applied to account for these propagation delays and improve the accuracy of distance measurements.

3. **Satellite orbit errors:**

Imperfections in the knowledge of the satellite orbits can lead to positioning errors. Precise orbit determination techniques, including GPS-based orbit determination or satellite laser ranging, can be employed to refine the satellite orbit information and minimize the associated errors.

4. **Multipath interference:**

In SBM, signals from the transmitting object may encounter reflections or obstructions that result in multipath interference. This interference can distort the received signals and lead to positioning errors. Advanced signal processing techniques, such as adaptive filtering or antenna diversity, can be utilized to mitigate multipath effects and improve accuracy.

5. **GDOP:**

As mentioned earlier, the geometric arrangement of satellites relative to the transmitting object can affect the accuracy of position measurements. By optimizing the satellite constellation design, adjusting satellite orbits, or employing additional satellites, the system can minimize the GDOP and improve the accuracy of the position solution.

To achieve error balance measurement, SBM systems typically employ sophisticated algorithms and techniques that analyze and compensate for the identified error sources. These techniques can include filtering, statistical estimation, least squares, or Kalman filtering methods to estimate and correct for the errors in the position measurements. By effectively managing and reducing errors through error balance measurement, SBM systems can provide more accurate and reliable positioning information for applications such as air traffic control, surveillance, or navigation.

- **System redundancy:**

System redundancy in SBM refers to the inclusion of backup or redundant components and capabilities in the multilateration system to ensure its continued operation and reliability in the event of failures or anomalies. Redundancy is essential in SBM systems due to their critical nature in providing surveillance and tracking services for air traffic control or other applications. It helps minimize the impact of failures or malfunctions on the overall system performance and ensures uninterrupted operation. Here are some common forms of redundancy employed in SBM systems:

1. **Satellite redundancy:**

A MLAT system may utilize multiple satellites in its constellation. Having redundant satellites ensures that even if one or more satellites experience failures or are taken out of service, there are still sufficient operational satellites to maintain coverage and provide reliable positioning information.

2. **Redundant ground control and processing infrastructure:**

The ground control segment and processing infrastructure of a SBM system can be designed with redundancy. This includes redundant control centers, processing servers, and backup systems to handle failures or outages. Redundancy in the ground segment helps maintain the system's ability to receive and process signals from the satellites and deliver accurate positioning data to users.

3. **Redundant communication links:**

Redundancy can also be implemented in the communication links between the satellites, ground control, and end-user systems. Multiple communication paths, such as redundant satellite downlinks or backup terrestrial communication links, ensure that data can be reliably transmitted and received even in the presence of failures or disruptions.

4. **Redundant power supply:**

SBM systems often incorporate redundant power supply systems to prevent service interruptions in the event of power failures or disruptions. This can involve redundant power sources, backup power generators, or Uninterruptible Power Supply (UPS) systems.

By implementing redundancy in various aspects of the system, SBM systems can enhance their reliability, availability, and fault tolerance. Redundancy helps minimize the impact of failures, increases system uptime, and ensures that critical surveillance and tracking services can be maintained even in challenging operational conditions. It is important to note that redundancy alone is not sufficient; proper monitoring, maintenance, and fault detection mechanisms are also necessary to identify and rectify failures promptly. This ensures that the redundant components or capabilities can seamlessly take over in case of a failure, maintaining the system's overall performance and integrity.

1.2 System Performance Parameters

This section provides an overview of the key parameters typically employed to assess the performance of a MLAT system. The primary parameters related to SPP include the PoD, PoFD, Probability of Identification (PoID), Probability of False Identification (PoFID), as well as system availability, capacity, and latency. These parameters play a crucial role in evaluating the effectiveness and reliability of an MLAT system.

- **Probability of Detection (PoD):**

The system PoD in SBM refers to the likelihood of successfully detecting and tracking a transmitting object, such as an aircraft or other targets, by the MLAT system. It quantifies the system's ability to reliably detect and maintain surveillance of objects within its coverage area. Several factors influence the probability of detection in SBM systems:

1. **SNR:**

The strength of the received signal compared to the background noise affects the ability to detect and extract useful information from the signals. Higher SNR values generally result in a higher probability of detection.

2. **Antenna gain and sensitivity:**

The gain and sensitivity of the antennas used in the system influence the ability to capture and process weak signals. Antennas with higher gain and sensitivity can improve the probability of detecting signals from distant or low-power transmitting objects.

3. **Transmitter power:**

The power of the transmitting object's signal plays a role in the probability of detection. Higher power signals are easier to detect, especially in situations where the received signal strength is relatively low.

4. **Interference and noise:**

Interference from other sources or environmental noise can affect the detection performance. Effective interference rejection techniques and noise filtering algorithms can improve the probability of detection in the presence of interfering signals or noise.

5. **System design and configuration:**

The design and configuration of the SBM system, including the number and distribution of satellites, the coverage area, and the selection of appropriate signal processing algorithms, can impact the probability of detection. Optimal system design and configuration can maximize the chances of detecting and tracking transmitting objects.

It is important to note that achieving a 100% probability of detection is often not feasible due to various factors, including system limitations, environmental conditions, and operational constraints. However, SBM systems strive to achieve high probabilities of detection to ensure reliable surveillance and tracking capabilities. By employing advanced signal processing techniques, optimizing system parameters, and considering the factors mentioned above, SBM systems aim to maximize the probability of detecting transmitting objects within their coverage area, enabling effective monitoring and tracking of air traffic or other targets.

- **Probability of False Detection (PoFD):**

On the other side, the probability of non-detection in SBM refers to the likelihood of a transmitting object, such as an aircraft or other targets, not being detected or tracked by the MLAT system. It represents the system's inability to identify and maintain surveillance of objects within its coverage area. Several factors can contribute to the probability of non-detection in SBM systems:

1. **Signal blockage or shadowing:**

Obstacles, such as buildings, terrain features, or natural obstructions, can block or attenuate the signals transmitted by the object. In such cases, the signals may not reach the satellites, resulting in non-detection.

2. **Insufficient signal strength:**

If the transmitting object's signal is weak or attenuated due to distance, interference, or other factors, it may not be detected by the MLAT system's receivers. Lower signal strength decreases the probability of detection.

3. **Low SNR:**

In environments with high levels of background noise or interference, the SNR of the received signals can be low. This can reduce the system's ability to detect and extract useful information from the signals, leading to a higher probability of non-detection.

4. **Inaccurate or incomplete position data:**

If the MLAT system fails to accurately estimate the position of the transmitting object based on the received signals, it may result in non-detection or incorrect tracking.

5. **System limitations and performance constraints:**

The overall design, configuration, and performance limitations of the MLAT system can impact the probability of non-detection. Factors such as the number and distribution of satellites, sensitivity of the receivers, system accuracy, and processing algorithms influence the system's ability to detect and track objects reliably.

MLAT systems continually strive to improve their detection capabilities by employing advanced signal processing techniques, enhancing receiver sensitivity, optimizing system parameters, and addressing challenges associated with Non-Line-of-Sight (NLOS) scenarios. These efforts aim to minimize the probability of non-detection and improve the overall reliability and effectiveness of SBM systems.

- **Probability of Identification (PoID):**

The PoID in SBM refers to the likelihood of successfully identifying the transmitting object, such as an aircraft or other targets, by the MLAT system. It quantifies the system's ability to accurately determine the identity of the object being tracked. Several factors influence the PoID in SBM systems:

1. **Unique identifiers:**

The transmitting objects, such as aircraft, are typically equipped with unique identification codes, such as the Mode-S address in ADS-B. The PoID is high when the system can accurately extract and associate the transmitted identification code with the corresponding object.

2. Data link integrity:

The integrity of the data link between the transmitting object and the MLAT system is crucial for accurate identification. The system relies on receiving and processing reliable and uncorrupted data to ensure correct identification.

3. Data link availability:

The availability of the data link between the transmitting object and the MLAT system affects the PoID. If the data link is intermittent or unavailable, it may result in incomplete or missing identification information, reducing the probability of accurate identification.

4. Data processing algorithms:

The algorithms employed by the MLAT system for data processing and identification play a significant role in the PoID. Advanced algorithms that account for signal quality, error correction, and data fusion techniques can improve the accuracy of identification.

5. Database integration:

Integrating external databases, such as aircraft registration databases or flight plans, with the MLAT system can enhance the PoID. By cross-referencing transmitted identification codes with known aircraft information, the system can verify and validate the identity of the tracked objects.

The PoID is closely related to the quality and integrity of the data received from the transmitting objects. Factors such as signal strength, data link availability, data processing algorithms, and database integration all contribute to the accuracy and reliability of identification in SBM systems.

Efforts to improve the PoID include continuous refinement of algorithms, robust data link protocols, integration with reliable databases, and effective error detection and correction techniques. By maximizing the PoID, SBM systems can provide accurate and reliable information on the identity of tracked objects, supporting applications such as ATC, surveillance, or situational awareness.

• Probability of False Identification (PoFID):

The PoFID in SBM refers to the likelihood of incorrectly identifying a transmitting object, such as an aircraft or other targets, by the MLAT system. It quantifies the system's potential for misidentifying objects or associating incorrect identification information with tracked signals. Several factors can contribute to the PoFID in SBM systems:

1. Signal ambiguity:

In situations where multiple transmitting objects are within the system's coverage area and their signals overlap or interfere with each other, the system may struggle to accurately identify each object. Signal ambiguity can lead to false identification or incorrect association of identification information.

2. Inaccurate identification codes:

Transmitting objects, such as aircraft, are typically equipped with unique identification codes, such as the Mode-S address in ADS-B. However, in some cases, these codes may be inaccurate, missing, or improperly transmitted, leading to incorrect identification by the MLAT system.

3. Data corruption or errors:

Errors in the received data, such as corrupted signals, communication issues, or data transmission errors, can result in incorrect identification. These errors can distort or alter the identification information, leading to false identifications.

4. System noise and interference:

Environmental noise, interference from other sources, or signal distortions can affect the accuracy of identification. In the presence of noise and interference, the system may misinterpret identification information or fail to associate it correctly with the transmitting object.

5. Data processing algorithms:

The algorithms used for data processing and identification within the MLAT system can impact the probability of false identification. Inaccurate or insufficiently robust algorithms may result in false identifications or incorrect association of identification codes.

To minimize the PoFID, SBM systems employ several measures:

1. Advanced signal processing:

Sophisticated signal processing techniques, such as noise filtering, interference rejection, and error correction algorithms, can improve the accuracy of identification and reduce the probability of false identifications.

2. Data validation and verification:

Implementing data validation and verification mechanisms within the system helps ensure the integrity and accuracy of the received identification information. These mechanisms can include checksums, cross-referencing with external databases, or comparison with redundant data sources.

3. Quality control and assurance:

Regular quality control checks, including system performance monitoring, error rate analysis, and data integrity assessments, help identify and address potential sources of false identification. By maintaining high quality control standards, system operators can minimize the probability of false identifications.

4. Algorithm refinement and testing:

Continual refinement and testing of the data processing algorithms used for identification are essential for improving accuracy and reducing false identification rates. Rigorous testing and validation against known scenarios and real-world data can help identify and rectify algorithmic deficiencies.

While it is challenging to achieve a 0% probability of false identification, SBM systems aim to keep false identification rates as low as possible through careful system design, algorithmic improvements, and robust data processing techniques. By minimizing false identifications, these systems can provide reliable and accurate identification information for applications such as air traffic control, surveillance, and tracking.

- **System availability against eventualities:**

System availability in SBM refers to the ability of the system to remain operational and provide its intended services under various eventualities or challenging circumstances. Ensuring high availability is crucial for critical applications such as air traffic control, surveillance, and navigation. To enhance system availability against eventualities, SBM systems incorporate several measures:

1. **Redundancy:**

Redundancy is a key approach to increase system availability. It involves duplicating critical components, such as satellites, ground infrastructure, communication links, and power supply systems. Redundancy ensures that backup components can seamlessly take over in case of failures, minimizing downtime and maintaining system operation.

2. **Fault tolerance and resilience:**

SBM systems are designed to be fault-tolerant and resilient to withstand failures or disruptions. This involves implementing fault detection mechanisms, error correction techniques, and automated recovery procedures. By quickly identifying and mitigating faults, the system can minimize service interruptions and maintain availability.

3. **Maintenance and monitoring:**

Regular maintenance activities, including system inspections, software updates, and equipment checks, are essential for ensuring system availability. Proactive monitoring and performance management help detect anomalies, address potential issues, and take preventive measures before they impact the system's availability.

4. **Contingency planning:**

SBM systems often have contingency plans in place to deal with unexpected events or emergencies. These plans outline procedures for handling disruptions, disasters, or other critical incidents. Contingency planning includes backup communication channels, backup control centers, and emergency response protocols to minimize downtime and restore system availability as quickly as possible.

5. **System health monitoring:**

Continuous monitoring of the system's health and performance allows for proactive identification of potential issues or degradation. Real-time monitoring of satellite health, communication links, signal quality, and other system parameters enables early detection of anomalies and timely corrective actions to maintain system availability.

6. **Disaster recovery:**

SBM systems incorporate disaster recovery strategies to address major disruptions such as natural disasters or system-wide failures. These strategies include backup data centers, data replication, data backups, and recovery procedures to restore the system's functionality and availability.

By implementing these measures, SBM systems aim to ensure high availability and robust operation even in the face of eventualities. Redundancy, fault tolerance, maintenance, monitoring, contingency planning, and disaster recovery strategies work together to minimize downtime, maintain system availability, and deliver reliable services for critical applications.

- **Maximum capacity of the MLAT system:**

The maximum capacity of a SBM system refers to the maximum number of transmitting objects, such as aircraft or other targets, that the system can effectively track and provide accurate positioning information for within its operational limits. The maximum capacity of a SBM system depends on several factors:

1. **System design and architecture:**

The design and architecture of the system, including the number and distribution of satellites, ground infrastructure, and processing capabilities, play a significant role in determining its capacity. A well-designed system with optimized resource allocation can accommodate a larger number of transmitting objects.

2. **Signal processing and data handling:**

The efficiency and speed of signal processing algorithms, data fusion techniques, and data handling capabilities impact the system's capacity. Advanced algorithms and efficient data processing techniques can enable the system to handle a larger number of simultaneous transmissions and provide accurate positioning information.

3. **Communication bandwidth:**

The available communication bandwidth between the satellites and the ground infrastructure affects the system's capacity. Sufficient bandwidth is necessary to handle the data traffic from multiple transmitting objects simultaneously.

4. **Update rate and refresh interval:**

The desired update rate and refresh interval of the positioning information also influence the system's capacity. Higher update rates require faster processing and data transmission, potentially affecting the maximum capacity of the system.

5. **System performance and accuracy requirements:**

The desired performance and accuracy requirements of the system can influence its capacity. Higher accuracy requirements may necessitate additional processing and computational resources, potentially affecting the maximum number of transmitting objects that can be tracked simultaneously.

It is important to note that the maximum capacity of a SBM system is not a fixed number and can vary based on the specific implementation, technological advancements, and operational constraints. Additionally, the capacity may differ for different types of transmitting objects, such as aircraft with different communication protocols or signal characteristics. System operators and designers continually work to enhance the capacity of SBM systems through advancements in technology, algorithm improvements, and system optimizations. These efforts aim to accommodate larger numbers of transmitting objects and meet the growing demands of applications such as ATC, surveillance, and tracking.

- **Latency in the communication network:**

Latency in the communication network of SBM refers to the delay or time taken for data to travel between the satellites and the ground infrastructure. It is an important consideration as it affects the timeliness of data transmission, processing, and the overall system performance. Several factors contribute to the latency in the communication network of SBM:

1. **Distance:**

The physical distance between the satellites and the ground infrastructure affects the latency. As the distance increases, the time taken for signals to travel between the two points also increases, resulting in higher latency.

2. **Signal propagation:**

The speed at which signals propagate through the medium (e.g., electromagnetic waves in space) impacts latency. While electromagnetic waves travel at the speed of light, there may still be a slight delay due to factors such as atmospheric conditions, signal processing, and transmission overhead.

3. **Data transmission protocol:**

The communication protocol used for transmitting data between the satellites and the ground infrastructure can influence latency. Some protocols have inherent delays or transmission overhead that can increase the overall latency.

4. **Network congestion:**

Network congestion, caused by high data traffic or limited bandwidth, can introduce additional delays in data transmission and processing, thereby increasing latency. The presence of other data-intensive applications or communication systems sharing the same network resources can impact latency.

5. **Signal processing and data handling:**

The time taken for processing and handling data within the system also contributes to latency. Data received from satellites needs to be processed, analyzed, and fused to determine the position of transmitting objects. The efficiency of signal processing algorithms and the overall system architecture can affect latency.

6. **Ground infrastructure and network capacity:**

The capacity and capabilities of the ground infrastructure, including network equipment, data centers, and processing systems, influence latency. Insufficient processing power or network capacity can result in longer processing times and increased latency.

Efforts are made to minimize latency in the communication network of SBM systems, as low latency is crucial for real-time applications like ATC. This can be achieved through optimizing network infrastructure, employing efficient communication protocols, utilizing high-speed data links, and implementing advanced signal processing techniques to expedite data processing. By reducing latency, SBM systems can provide timely and accurate positioning information, enabling efficient tracking and surveillance of transmitting objects in applications where real-time data is critical.

1.3 System Design vs Performance Parameters

As mentioned earlier, the design of the MLAT system requires the consideration of various design parameters that optimize its functions and, consequently, its performance. The system functions can be categorized into two subsets: equipment-dependent functions and those dependent on the entire system. The design of each function takes into account a set of system design parameters. Specifically, for the positioning function, these parameters include LOS, DOP, measurement error balance, theoretical system accuracy, and redundancy.

The proper configuration of these parameters is essential to ensure that the positioning function operates within predefined levels of accuracy under any circumstance. The PoD is closely related to the positioning function. If the calculated target position falls outside the operational accuracy levels, the system disregards the corresponding report, thereby reducing the PoD. Hence, it is crucial to maintain the theoretical system accuracy within the predefined levels. Additionally, the redundancy parameter plays a vital role in determining the PoD. Insufficient configuration of redundancy prevents the availability of an adequate number of stations required to achieve the required operational accuracy.

The dependency of latency on the positioning function is primarily operational rather than theoretical. The computational time is directly influenced by the localization algorithm used to calculate the position. If an unsuitable localization algorithm or strategy is employed, it can introduce a time delay that exceeds the maximum allowable latency. However, due to advancements in computer processing, this dependency can often be neglected. Furthermore, since it is an operational relationship, it is not explicitly considered during the design process, as no specific model can be applied to this dependency, even though its existence is acknowledged.

The operational system accuracy directly depends on the positioning function and is the most apparent dependency. It can be understood that the higher the theoretical accuracy, considering the effects of DOP and measurement errors, the higher the operational accuracy can be. The availability of the system is related to the positioning function through the system geometry, which is reflected by the DOP parameter. The system geometry must allow the system to maintain the same accuracy levels over time, even in the presence of station failures or other situations that reduce the number of available stations. Therefore, the redundancy parameter must be set to preserve the DOP levels. Lastly, there is another form of dependency between the design parameters of different functions. In the case of the positioning function, this dependency is unidirectional. For example, the measurement errors also depend on the design and manufacturing of the measurement devices in the receiving station or the CPS. However, due to the nature of this dependency, it is assumed that it does not exist and account for it by introducing a modeled uncertainty into the design process.

1.4 Coordinate Systems: LLA and ECEF

In MLAT applications, the coordinates commonly used are Latitude, Longitude, Altitude (LLA) and Earth-centered, Earth-fixed coordinate system (ECEF). LLA coordinates represent a geographic location on Earth using latitude (angular distance north or south of the equator), longitude (angular distance east or west of a reference meridian), and altitude (elevation above or below a reference ellipsoid). ECEF coordinates, on the other hand, represent a point's position relative to the Earth's center in a Cartesian coordinate system fixed to the Earth. It uses x, y, and z coordinates, where the x-axis points toward the intersection of the prime meridian and the equator, the y-axis points towards the east, and the z-axis points towards the North Pole.

In MLAT applications, the process involves converting the received signals' time differences into distance measurements, which are then used to determine the target's LLA or ECEF coordinates through MLAT techniques. These coordinate systems play a crucial role in accurately locating targets based on signal measurements from multiple reference points.

1.5 Solutions for MLAT Systems Design

The primary objective of MLAT systems is to achieve hyperbolic localization of targets equipped with transponders (or non-transponder devices for surface targets). Consequently, the design of these systems primarily focuses on optimizing this function, ensuring that a set of requirements and restrictions are met to the best possible extent. Specifically, designing an MLAT system involves determining the optimal spatial distribution of stations (system geometry) to satisfy specific performance levels described previously. This process heavily relies on the fundamental theory of MLAT system accuracy, particularly the understanding of how system geometry influences accuracy.

Several notable works in this field have contributed to its advancement. In [20], a novel procedure was proposed, which established a method for calculating the accuracy of a location estimator. This method linked the error covariance matrix to the moments and products of inertia of a mass configuration determined from the system geometry. Additionally, the author of [21] further expanded on the boundaries and limitations of the method described in [20]. In the realm of MLAT, [22] derived formulas to estimate the length and cosine directions of the semi-axes of error ellipsoids. These formulas relied on RMS errors and direction cosines of distance measurements obtained through MLAT.

Another noteworthy work is [23], which presented a method for estimating lower bounds on 2D localization errors in acoustic passive arrays. This method utilized the Cramér-Rao inequality and provided insights into the achievable accuracy of acoustic source localization. The publication [24] explored approximate formulas that establish a relationship between the accuracy of TDOA and differential DF measurements. These formulas were based on the "one-sigma width" of constant lines represented by the measured quantities on the Earth's surface, offering a straightforward means of estimating localization accuracy. In the context of sensor placement, [25] offered a step-by-step manual process for locating sensors that measure the bearing of acoustic signals emitted by targets. This process relied on inspecting the FIM to optimize sensor placement. Additionally, [26] presented a theoretical analysis of the CRLB for source localization using only TDOA measurements. The publication introduced ideal geometries known as platonic shapes, which minimize the variance bounds for localization. It was assumed that all stations had identical measurement errors.

Chapter 2

Satellite Constellation

2.1 Orbital Parameters

The orbital parameters of a satellite constellation refer to the characteristics that define the orbits of the satellites within the constellation. These parameters determine the geometry, coverage, and performance of the constellation. Here are some common orbital parameters and types of satellite constellations:

1. **Altitude:**

It refers to the height of the satellite above the Earth's surface. Satellites can be categorized into different altitude ranges, such as LEO, Medium Earth Orbit (MEO), and Geosynchronous Equatorial Orbit (GEO). LEO constellations typically operate between 200 and 2,000 kilometers, while MEO constellations operate around 8,000 to 20,000 kilometers. GEO satellites are positioned approximately 35,786 kilometers above the equator.

2. **Inclination:**

It is the angle between the orbital plane of a satellite and the Earth's equatorial plane. It determines the coverage area and the latitude range over which the satellites pass. Some constellations have polar orbits with high inclinations (nearly 90 degrees), covering the entire globe, while others have lower inclinations for more specific coverage areas.

3. **Eccentricity:**

It describes the shape of the orbit. It represents how elliptical or circular the orbit is. Satellites with low eccentricity have nearly circular orbits, while those with higher eccentricity have more elongated orbits.

4. **Number of satellites:**

This number varies depending on the application and desired coverage. Constellations can consist of a few satellites to hundreds or even thousands of satellites. More satellites generally provide better coverage and redundancy.

5. Constellation geometry:

The arrangement and distribution of satellites in a constellation can vary. Some constellations have evenly spaced satellites in circular orbits, while others employ more complex patterns, such as Walker constellations or phased constellations, to optimize coverage and minimize signal interference.

Common types of satellite constellations include:

1. GNSS:

GNSS constellations, like GPS, GLONASS, and Galileo, provide positioning, navigation, and timing services for worldwide use.

2. Earth observation:

These constellations consist of multiple satellites that capture imagery and data for various purposes such as weather monitoring, environmental analysis, and disaster management.

3. Communication:

Communication constellations, like Iridium and Starlink, use multiple satellites to provide global communication services, offering coverage in remote areas and supporting high-speed internet connectivity.

4. Remote sensing:

These constellations involve multiple satellites working together to collect data and images for scientific research, climate monitoring, and mapping applications.

The specific orbital parameters and constellation types can vary depending on the mission objectives, coverage requirements, and technological considerations of each satellite system.

In order to evaluate the MLAT system outlined, a LEO constellation will be used for the satellite deployment and subsequent analysis. A LEO constellation consists of a satellites orbit in a band between 160 km and 2,000 km above the surface of the planet. The Earth's gravitational force becomes stronger the closer you get. Because of this, LEO satellites, being relatively close to the Earth, have to move very fast, in order to counteract gravity.

For example, the International Space Station (ISS) is located at a relatively low altitude (400 km), moving at approximately 27,600 km per hour and orbiting the Earth about 16 times a day. Contrary to GEO satellites, many LEO and MEO satellites are often deployed in satellite constellations, because the coverage area provided by a single satellite only covers a small area that moves as the satellite travels at the high angular velocity needed to maintain its orbit. As a consequence, a big number of LEO satellites are needed to provide and maintain continuous coverage over a specific area.

2.2 Kepler's Laws of Planetary Motion

Kepler's laws of planetary motion are a set of three fundamental principles that describe the motion and behavior of planets (and other celestial bodies) in their orbits around the Sun. They were formulated by the German astronomer Johannes Kepler in the early 17-th century and are considered foundational in the field of celestial mechanics.

1. Kepler's First Law (Law of Ellipses):

Each planet's orbit around the Sun is an ellipse with the Sun at one of the two foci. This law dispelled the ancient notion of perfectly circular orbits and established the concept of elliptical orbits.

2. Kepler's Second Law (Law of Equal Areas):

A line connecting a planet to the Sun sweeps out equal areas in equal time intervals. This means that a planet moves faster when it is closer to the Sun (perihelion) and slower when it is farther away (aphelion). This law implies that the speed of a planet in its orbit is not constant but varies as it moves through different portions of its elliptical path.

3. Kepler's Third Law (Law of Harmonies):

The square of the orbital period (T) of a planet is proportional to the cube of its average distance from the Sun (a). Mathematically, it can be expressed as $T^2 = k * a^3$, where k is a constant of proportionality. This law establishes a relationship between a planet's orbital period and its distance from the Sun.

Kepler's laws of planetary motion were groundbreaking at the time, as they provided a more accurate and descriptive model of the solar system. They formed a crucial foundation for Isaac Newton's later development of the laws of gravitation and laid the groundwork for modern celestial mechanics. Today, Kepler's laws are still used to understand and predict the motion of planets, satellites, and other celestial bodies in space. They have applications in astronomy, astrophysics, spacecraft trajectory planning, and the study of exoplanetary systems, among other areas.

2.3 Newton's Laws of Motion

Newton's laws of motion are fundamental principles in classical physics that describe the relationship between the motion of an object and the forces acting upon it. They were formulated by Sir Isaac Newton in the late 17-th century and laid the foundation for classical mechanics.

1. Newton's First Law of Motion (Law of Inertia):

An object at rest tends to stay at rest, and an object in motion tends to stay in motion with the same velocity unless acted upon by an external force. In other words, an object will maintain its state of motion unless acted upon by an unbalanced force.

2. Newton's Second Law of Motion:

The acceleration of an object is directly proportional to the net force acting on it and inversely proportional to its mass. This can be mathematically expressed as $F = ma$, where F is the net force applied to the object, m is its mass, and a is the resulting acceleration.

3. Newton's Third Law of Motion (Law of Action-Reaction):

For every action, there is an equal and opposite reaction. When an object exerts a force on another object, the second object exerts an equal and opposite force on the first object. Forces always occur in pairs.

Newton's laws of motion are fundamental principles that apply to objects of varying sizes and velocities, enabling the understanding and prediction of motion in diverse scenarios. These laws form the basis of mechanics, covering celestial bodies, vehicles, and everyday objects. Widely utilized in engineering and physics, they facilitate calculations of forces, accelerations, velocities, and trajectories across systems, from simple to complex. However, it's essential to acknowledge their applicability in classical mechanics and at speeds significantly slower than that of light. For high velocities or extremely small objects, the principles of quantum mechanics and relativity come into play, necessitating different equations and theories to accurately describe their motion.

2.4 Satellite Dynamics

Satellite dynamics encompasses the study of satellite motion and behavior in space. It is essential for designing, operating, and controlling satellites to achieve desired orbits and mission objectives. The dynamics of a satellite are governed by classical mechanics and celestial mechanics. Gravity is the primary force, pulling the satellite towards the Earth and determining its orbit shape based on velocity, mass, and altitude. Mathematical models incorporating Newton's and Kepler's laws describe satellite motion. External forces such as atmospheric drag and solar radiation pressure also impact satellite orbits, especially in low Earth orbit. Control techniques, including propulsion systems and attitude control, are employed to maintain desired orbits. Satellite dynamics aids mission planning, utilizing software tools and simulations to optimize trajectories and evaluate requirements. This multidisciplinary field combines physics, mathematics, and engineering to understand and manipulate satellite motion, enabling successful missions and advancements in space exploration and satellite technology.

2.4.1 Keplerian Elements

Keplerian elements are a set of parameters used to describe the orbit of a satellite or any other object in space. They are based on Johannes Kepler's laws of planetary motion and provide a concise and standardized way to represent the characteristics of an orbit. The six Keplerian elements are as follows:

- **Semi-major axis (a):**

It represents half the length of the major axis of the elliptical orbit. The semi-major axis determines the average distance between the satellite and the central body (such as the Earth for Earth-orbiting satellites).

- **Eccentricity (e):**

It measures the shape of the orbit. Eccentricity determines how elongated or circular the orbit is. A value of 0 indicates a perfectly circular orbit, while a value between 0 and 1 represents an elliptical orbit.

- **Inclination (i):**

It defines the angle between the orbital plane and the reference plane (usually the Earth's equator). The inclination determines the tilt or inclination of the orbit with respect to the equator.

- **Right Ascension of the Ascending Node (RAAN) (Ω):**

It specifies the angle between the reference direction (usually vernal equinox) and the point where the satellite's orbit intersects the reference plane from south to north. It determines the orientation of the orbit in the reference frame.

- **Argument of perigee (ω):**

It represents the angle between the ascending node and the point of closest approach to the central body (perigee) within the orbital plane. It determines the orientation of the orbit within the orbital plane.

- **True anomaly (ν):**

It indicates the angle between the perigee and the satellite's current position in the orbit, measured from the focus of the elliptical orbit. It describes the satellite's position along its orbital path at a specific time.

By specifying these six Keplerian elements, one can fully describe the shape, size, orientation, and position of a satellite's orbit. They provide valuable information for orbital calculations, mission planning, satellite tracking, and analysis of orbital dynamics.

2.4.2 Satellite's Motion

Satellite motion in space is governed by classical mechanics and celestial mechanics. Once launched into orbit around a celestial body like Earth, a satellite follows a curved path. This motion consists of translational and rotational components. Translational motion refers to the satellite's movement along its orbital path, influenced primarily by the gravitational force exerted by the central body. Rotational motion involves the satellite spinning or rotating about its own axis, controlled by onboard systems.

The trajectory and characteristics of satellite motion depend on factors such as initial velocity, mass, altitude, and the gravitational field of the central body. Through orbital mechanics, scientists and engineers can calculate and predict the satellite's position, velocity, and acceleration at any given time. Accurate understanding and control of satellite motion are vital for maintaining the desired orbit, achieving mission objectives, and optimizing resource utilization. This requires precise mathematical models, computational tools, and robust control systems to manage the satellite's trajectory and orientation in space.

2.4.3 Orbit Perturbations

Orbit perturbations refer to deviations or disturbances in the motion of a satellite or other orbiting object from its ideal or predicted trajectory. These perturbations can be caused by various factors, both natural and man-made, and can have significant effects on the orbit and the satellite's performance. Here are some common sources of orbit perturbations:

- **Gravitational perturbations:**

Gravitational perturbations result from the gravitational influence of celestial bodies on orbiting objects. The Moon, the Sun, and other planets exert gravitational forces that cause slight variations in satellite orbits. These perturbations are more noticeable in highly elliptical or geostationary orbits, affecting position, velocity, and orbital period. Precise mathematical models and numerical techniques are used to account for these perturbations. By considering the masses, positions, and velocities of celestial bodies, gravitational forces on satellites can be calculated. Incorporating these forces into motion equations allows for prediction and analysis of orbital deviations. Understanding gravitational perturbations is crucial for maintaining orbit stability, enabling precise maneuvers, and ensuring desired satellite positions.

- **Atmospheric drag:**

Atmospheric drag, also known as atmospheric resistance or atmospheric braking, affects objects in Earth's orbit, especially in low Earth orbit (LEO). As satellites or spacecraft move through the atmosphere, collisions with gas molecules create a drag force opposing their motion. This results in energy loss, decreasing orbital speed and causing orbit decay. Factors influencing atmospheric drag include altitude, orbital velocity, atmospheric density, and surface area. Lower orbits experience denser layers and more significant drag. Satellite operators employ strategies like streamlined designs, altitude maintenance thrusters, and controlled reentry to mitigate drag effects. Accurate modeling and prediction of atmospheric drag are crucial for maintaining orbits, extending mission lifetimes, and managing space debris.

- **Solar radiation pressure:**

Solar radiation pressure is a phenomenon affecting satellites and spacecraft. Sunlight transfers momentum to objects, creating a force that opposes motion. It weakens orbital speed, alters altitude, and induces rotation. Designers consider solar radiation pressure when planning missions, optimizing spacecraft shape and attitude control. Accurate modeling is vital for precise orbital calculations and maintaining desired trajectories, especially for higher altitudes and large objects.

- **Atmospheric variations:**

Atmospheric variations in Earth's atmosphere can impact satellites and spacecraft. Factors like temperature, density, and humidity introduce uncertainties in trajectory and performance. Fluctuations in atmospheric density affect satellite drag and decay rates. Accurate modeling requires atmospheric data and helps optimize mission planning, spacecraft design, and collision avoidance.

Satellite operators employ advanced orbital analysis and control techniques to compensate for perturbations and preserve the desired orbit. Mathematical models, including numerical integration of motion equations, help predict and correct for these effects. Attitude adjustments, propulsion systems, and orbital maneuvers are utilized to counteract perturbations and ensure orbit stability.

2.5 Iridium constellation

The proposed SBM system requires a LEO satellite constellation for deployment. The chosen constellation for testing the simulator's performance is the Iridium satellite constellation. Developed by Motorola in the 1990s, it is currently owned and operated by Iridium Communications Inc. This network of communication satellites provides global coverage for various telecommunications services, enabling worldwide voice and data communication. It consists of 66 active satellites evenly distributed into six polar orbit planes, ensuring complete global coverage. Each satellite is in a LEO approximately 780 kilometers (485 miles) above the Earth's surface, enabling low-latency communication suitable for real-time applications. The Iridium satellites communicate with each other using ISLs to form a mesh network. This allows seamless communication and uninterrupted coverage across the constellation.

2.6 Proposed constellation

To evaluate the outlined MLAT system, a satellite constellation (made of 192 satellites) geometry is proposed, taking into account the requirement of it being a LEO constellation. It is important to note that no optimization process has been conducted to determine the best distribution of satellites. However, with the developed applications and tools, the composition and structure of satellites could be appropriately designed for specific areas of interest on Earth's surface. The proposed satellite structure, along with its potential implementation, is considered sufficient to meet all the objectives. Table 2.2.1 provides the key parameters of the constellation.

Planes	Inclination	Semi-major axis	Eccentricity	RAAN	Anomaly	Phase
12	90 °	7020000 m	0.00005	30 °	22.5 °	11.25 °

Table 2.2.1: Main parameters of the proposed constellation

The RAAN step refers to the longitude at which a spacecraft crosses the equatorial plane while moving from south to north. The descending node, however, occurs when the spacecraft passes through the equatorial plane, transitioning from the Northern Hemisphere to the Southern Hemisphere. The RAAN step can be found with the number of planes constituting the constellation, NP , and its expression is given by 2.1:

$$RAAN = \frac{360}{NP} \quad (2.1)$$

On the other hand, the true anomaly step represents an angular parameter that determines the position of a celestial body as it moves along a Keplerian orbit. It can be calculated using the number of satellites per plane, SPP , and its expression is given by 2.2:

$$Anomaly = \frac{360}{SPP} \quad (2.2)$$

Part III

Algorithms for Mode S MLAT

Chapter 1

Localization Problem

In SBM, localization algorithms are employed to determine the position of an object using measurements obtained from multiple satellites or measuring stations. These algorithms process the timing or ranging information from the signals transmitted by the satellites to calculate the object's location.

Localization in SBM poses unique challenges due to the nature of satellite-based surveillance. In this context, the localization problem involves determining the precise position of an object using measurements obtained from multiple satellites or measuring stations in space. Two key aspects contribute to the complexity of SBM localization.

Firstly, the sparse geometry of satellites in space presents a challenge in accurately estimating the object's position. Unlike ground-based MLAT systems that may have a denser network of measuring stations, SBM relies on a limited number of satellites in LEO or MEO constellations. This sparse geometry can result in longer signal paths and increased uncertainties in the ranging or timing measurements. Additionally, the varying geometry of satellites in motion adds complexity to the localization problem, as the relative positions of the satellites change over time.

Secondly, the presence of atmospheric and propagation effects introduces errors and uncertainties into the measurements, further complicating the localization process. Signals transmitted by the object may experience delays, distortions, or multipath effects as they propagate through the Earth's atmosphere. These atmospheric and propagation effects can introduce errors in the ranging or timing measurements received by the satellites. Compensating for these effects and accurately modeling them becomes crucial to achieve accurate localization results in SBM.

Addressing these challenges requires sophisticated algorithms that can handle sparse satellite geometries, account for atmospheric and propagation effects, and accurately estimate the object's position based on the available measurements. Advanced signal processing techniques, statistical estimation methods, and robust models for atmospheric and propagation effects are essential components of the solutions developed for SBM localization.

Chapter 2

The Inverse Problem

Inverse problems arise when it becomes necessary to determine the source responsible for generating certain physical phenomena. In a typical direct problem, one or a set of sources are known, along with a mathematical model that describes how the physical phenomena behave in relation to these sources. Consequently, the system's response can be obtained for any specific source. However, in the case where the source is unknown (for example, the position of a signal transmitter) while the response is known (such as a TOA/TDOA measurement corresponding to the signal emitted from the unknown source), it becomes crucial to reverse the situation by formulating an inverse model. This inverse model aims to determine the source of these responses. This formulation is referred to as the inverse problem, and a classical mathematical description would be as follows:

$$\int_{\Omega} source \times system d\Omega = answer \quad (2.1)$$

In this context, let Ω represent a domain that varies depending on the specific problem, and \times symbolize the particular interaction involved. The primary goal is to identify the source (referred to as "source"), based on a mathematical model that describes the system (known as "system"), and a set of data (typically noisy) that contains the corresponding response (referred to as "answer"). However, in practical terms, solving this problem often requires employing numerical methods. Consequently, it becomes necessary to convert the continuous model into a discrete representation, leading to the following formulation:

$$A\theta = \hat{m} \quad (2.2)$$

In this formulation, there is the coefficient matrix A , which characterizes the behavior of the system representing the physical phenomena. The unknown source is denoted as the column vector θ , while the column vector \hat{m} contains the response data, such as instrument measurements. The primary objective of any localization algorithm in MLAT systems is to establish and solve a system of equations similar to the following representation. This system of equations is obtained by manipulating the set of equations according to the data model in a way that explicitly yields the coefficient matrix A and the measurement vector \hat{m} . The resulting system of equations is then solved using a numerical algorithm. It is important to note that the specific form of each inverse localization problem depends on the pairing of the data model and the numerical algorithm, which govern the manipulation and solution of the equations.

Chapter 3

Singular Value Decomposition

The term Singular Value Decomposition (SVD) represents a powerful numerical tool utilized in the analysis of Ill-Conditioned Problem (ICP), specifically the Ordinary SVD (OSVD). It serves as the foundation for all the methods and procedures discussed in this SBM system design. Additionally, SVD aids in distinguishing between two distinct types of ICP: Rank-Deficient Problem (RDP) and Discrete Ill-Posed Problems (DIPP). Furthermore, this discussion will also encompass the concept of regularization methods employed to transform an ICP into a Well-Conditioned Problem (WCP). In the case of ICP, the matrix A that requires inversion typically contains two or more linearly dependent equations. One notable feature of SVD is its ability to identify these linear dependencies.

3.1 The Ordinary SVD (OSVD)

Assume a rectangular or square matrix $A \in \mathbb{R}^{m \times n}$, where without loss of generality $m \geq n$. The SVD of A is defined as the decomposition of the matrix into three independent matrices [27], [28]:

$$A = U \Sigma V^T = \sum_{i=1}^n u_i \sigma_i v_i^T \quad (3.1)$$

where $U = [u_1, \dots, u_N] \in \mathbb{R}^{m \times n}$ and $V = [v_1, \dots, v_N] \in \mathbb{R}^{n \times n}$ are matrices with orthonormal columns u_i and v_i , respectively, that satisfy the following identity:

$$U^T U = V^T V = I_n \quad (3.2)$$

being I_n the $n \times n$ identity matrix. In addition, Σ is a $n \times n$ diagonal with non-negative elements $(\sigma_1, \dots, \sigma_n)$ appearing in non-increasing order such that $\sigma_1 \geq \sigma_2 \geq \dots \geq \sigma_n \geq 0$. The singular values of A are the elements of matrix Σ . On the other hand, the column vectors u_i and v_i correspond to the left and right singular vectors of A , respectively. Numerical routines are employed to obtain the matrices U , Σ , and V . However, describing such procedures is out of the scope of this project. The SVD of matrix A gives two sets of orthonormal basis vectors (e.g., the columns of matrices U and V) that allow to transform matrix A into a diagonal matrix by projecting it on those two bases:

$$U^T AV = \Sigma = \begin{bmatrix} \sigma_1 & 0 & \cdots & 0 \\ 0 & \sigma_2 & \cdots & 0 \\ \vdots & \vdots & \ddots & \vdots \\ 0 & 0 & \cdots & \sigma_n \end{bmatrix}_{n \times n} \quad (3.3)$$

Matrix Σ allows to check some numerical properties of matrix A . For instance, a small singular (or a group of these) value indicates some linear dependencies in matrix A (i.e., a zero or very close to zero value of σ_n indicates that A is of the type ill-conditioned).

3.2 Null Space and Range of a Matrix

First, the concept of kernel, or null space [29] of a $m \times n$ matrix A is the set of all vectors θ_N satisfying that $A\theta_N = 0$. In general, the null space is denoted by the operator $N(\cdot)$, and its mathematical definition is expressed as follows:

$$N(A) = \{\theta_N \in K^n : A\theta_N = 0\} \quad (3.4)$$

where K is a field of real numbers, and 0 , the zero vector with m components. Then, the range, commonly known as the column space of a $m \times n$ matrix A , is the set of all possible linear combinations of its column vectors. Mathematically, if matrix A has columns vectors denoted as a_i , for $i = 1, \dots, n$, the range of A will be the set of vectors resulting from this linear combination:

$$\sum_{i=1}^n c_i a_i \quad (3.5)$$

where c_i is a scalar. Consequently, the range of a matrix can be understood as the collection of all linear combinations of its columns a_i . In the context of a linear system of equations, the range of matrix A represents the set of vectors \hat{m} for which the system $A\theta = \hat{m}$ possesses a solution.

3.3 The Generalized SVD (GSVD)

In parallel to the OSVD, there exists the Generalized SVD (GSVD), referring to a pair of matrices A and L . It is computed assuming that $A \in \mathbb{R}^{m \times n}$ and $L \in \mathbb{R}^{p \times n}$ (being L a full rank matrix), where $m \geq n \geq p$, and also $N(A) \cap N(L) = \{0\}$. The GSVD is nothing but a decomposition of the matrix pair (A, L) following:

$$A = U \begin{bmatrix} \Sigma & 0 \\ 0 & I_{n-p} \end{bmatrix} X^{-1} \quad (3.6)$$

$$L = V(M \ 0)X^{-1} \quad (3.7)$$

where $U \in \mathbb{R}^{m \times n}$ and $V \in \mathbb{R}^{p \times p}$ are orthonormal (i.e., $I_n = U^T U$, and $I_p = V^T V$). Moreover, $X \in \mathbb{R}^{n \times n}$ is a non-singular square matrix with $(A^T A)$ -orthogonal columns:

$$X^T A^T A X = \begin{bmatrix} \Sigma^2 & 0 \\ 0 & I_{n-p} \end{bmatrix} \quad (3.8)$$

Matrices Σ and M consist of two $p \times p$ diagonal matrices with non-negative elements $(\sigma_1, \dots, \sigma_p)$ and (μ_1, \dots, μ_p) , respectively. These elements are ordered as follows:

$$0 \leq \sigma_1 \leq \dots \leq \sigma_p \leq 1 \quad (3.9)$$

$$1 \geq \mu_1 \geq \dots \geq \mu_p \geq 0 \quad (3.10)$$

Both of them are normalized such that $\sigma_i^2 + \mu_i^2 = 1$, for $i = 1, \dots, p$. Additionally, for the generalized singular values γ_i of the matrix pair (A, L) appear in non-decreasing order and are defined as follows:

$$\gamma_i = \frac{\sigma_i}{\mu_i}, \quad i = 1, \dots, p \quad (3.11)$$

3.4 Ill-Conditioned Problems

The concept of a well-posed problem in mathematics originated from the definition put forth by French mathematician Jacques Hadamard in the 20-th century. According to Hadamard, mathematical models describing physical phenomena should possess the following properties:

1. Existence of a solution: A solution to the problem must exist.
2. Uniqueness of the solution: The solution must be unique.
3. Continuous dependence on initial conditions: The behavior of the solution should change continuously with respect to the initial conditions.

If all the necessary conditions are met, the problem is considered well-posed. However, if any of these conditions are not satisfied, the problem is classified as ill-posed according to Hadamard. Ill-posedness can arise from an incorrect mathematical model, requiring modification, or it may be inherent to the problem formulation itself. Inverse problems often fall into this category, such as the inverse heat equation, where determining the initial temperature distribution from final data is ill-conditioned, resulting in significant variations due to small changes in the data.

To obtain a numerical solution, continuum models are discretized. Although solutions may be continuous with respect to initial conditions, they can be prone to numerical instability when computed with finite precision or in the presence of data errors. Even for well-posed problems, they can still be ill-conditioned, meaning that small errors in initial data can lead to larger errors in computed solutions. Nonlinear complex systems, known as chaotic systems, are well-known examples of instability. However, if a problem is well-posed, there is a higher chance of finding a solution using a stable algorithm. Conversely, if a problem is not well-posed, it must be reformulated for numerical treatment, often involving the introduction of additional assumptions through regularization, such as assuming solution smoothness.

In the context of the MLAT localization problem, the data model depends on the type of measurements and the system geometry. Ill-conditioning is a common issue in MLAT localization, particularly when only TOA or TDOA measurements are utilized. In such cases, the ill-conditioning can be considered inherent to the problem formulation, and the target position must be calculated while accounting for these conditions. However, the TOA/TDOA data model can be enhanced by combining it with other types of measurements, such as AOA or FDOA, leading to a data model with improved numerical characteristics. There are various strategies to improve the TOA/TDOA data model, but each has its advantages and disadvantages, and their applicability may be limited. Solving a WCP problem is generally easier compared to solving an ICP problem, which can present several challenges. ICP problems arise in a wide range of engineering and scientific applications, including acoustics, astrometry, computerized tomography, geophysics, remote sensing, signal processing, and statistics, among others. Moreover, ICP problems are commonly encountered in the localization process for MLAT systems.

3.5 Regularization Methods for solving ICPs

In order to solve the ICP, it is crucial to employ strategies that fulfill the three Hadamard's conditions. These conditions aim to transform an ICP into a well-conditioned problem. These strategies are widely known as regularization methods. By incorporating additional information regarding the desired solution, regularization methods aim to enhance the stability of the coefficient matrix A [27], thereby obtaining a reliable and meaningful solution. The overall concept of this aspect is illustrated in Figure 3.3.1.

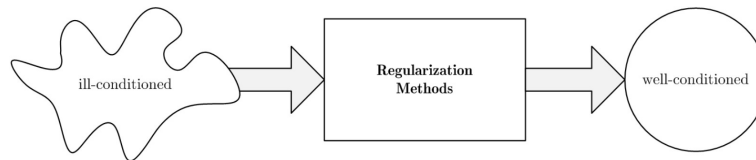


Fig. 3.3.1: Regularization strategy for turning ICP into WCP.

The fundamental concept behind regularization methods involves introducing a certain residual component associated with the regularized solution. The norm of this residual, known as the residual norm, can be mathematically defined as follows:

$$\rho(\theta) = \|A\theta - \hat{m}\|_2 \quad (3.12)$$

where $\|\cdot\|_2$ denotes the 2-norm operator [29], and then they can (in general terms) use one of the following schemes [27] to find a solution:

1. Minimize $\rho(\theta)$ subject to the constraint that θ belongs to a specified subset, i.e., $\theta \in S_\theta$.
2. Minimize $\rho(\theta)$ subject to the constraint that some measurement $\Omega(\theta)$ of the size of θ is less than some specified upper bound δ , i.e., $\Omega(\theta) \leq \delta$.

3. Minimize $\Omega(\theta)$ subject to the constraint $\rho(\theta) \leq \alpha$.
4. Minimize a linear combination of $\rho(\theta)^2$ and $\Omega(\theta)^2$: $\min\{\rho(\theta)^2 + \lambda^2\Omega(\theta)^2\}$, where λ is a specified weighting factor.

All the approaches mentioned above rely on the assumption that a regularized solution, which meets certain residual and constraint criteria, will provide a close approximation to the exact solution. However, regularization inherently introduces bias into the solution while statistically reducing the size of the covariance matrix. Before tackling an ICP problem, it is essential to evaluate various key aspects, as outlined in [27]. These important considerations include:

- What kind of ill-conditioning does the problem have?
- Is it possible to regularize?
- Which additional information is available?
- Is this additional information suitable for stabilization purposes?
- Which method is more adequate to efficiently and reliably solve the problem on a computer?
- How much stabilization should be added?

3.6 Classification of the ICPs

As introduced when describing the SVD of a given matrix, a differentiation of the two types of existing ICP and their characteristics can be done as follows:

- **Rank-Deficient Problem (RDP):**

Matrix A has a cluster of small singular values and there is also a well-determined gap between the large and small singular values, meaning that one or more rows and columns of A are linearly dependent.

- **Discrete Ill-Posed Problems (DIPP):**

There is no gap between the large and small singular values. Instead, all of these gradually decay to zero. This fact makes the notion of numerical rank to be not useful to analyze this class of ICP.

3.7 Analysis Parameters of ICPs

To determine the level of ill-conditioning of a matrix A , several key parameters can be used for a quick assessment. The choice of these parameters depends on the problem at hand, but generally, the condition number and rank of a matrix offer a rapid indication of its degree of ill-conditioning [27], [29]. Furthermore, when a problem involves a rank-deficient matrix, the numerical rank parameter becomes particularly valuable.

3.7.1 The Condition Number

The condition number of a given matrix A is defined as the ratio between its maximum and minimum singular values [27], [29]. In simpler terms, the condition number represents the relationship between the largest and smallest singular values, and it is computed numerically using the following expression:

$$\text{cond} = \frac{\sigma_1}{\sigma_n} \quad (3.13)$$

When the last singular value approaches to zero, a high condition number is found, therefore the matrix A can be considered as an ill-conditioned matrix.

3.7.2 The Rank of a Matrix

The rank of a matrix is a measure of the number of linearly independent columns it contains [29]. Based on the SVD of matrix A , the rank can be determined by counting the strictly positive singular values in the matrix [27]. However, in the presence of errors like measurement inaccuracies, approximation errors, discretization errors, or rounding errors, the conventional definition of rank loses its utility. In noisy conditions, certain columns that may appear mathematically independent can exhibit practical linear dependence. Consequently, the concept of numerical rank becomes more meaningful and applicable in such scenarios.

3.7.3 The Numerical Rank

The numerical rank of a matrix A corresponds to the number of columns in the matrix that can be considered practically linearly independent, taking into account a specific error threshold denoted by ϵ [27], [29]. Formally, the numerical rank is denoted by the real-valued integer r_ϵ , which satisfies the following expression:

$$r_\epsilon = r_\epsilon(A, \epsilon) = \min_{\|E\|_2 \leq \epsilon} \text{rank}(A + E) \quad (3.14)$$

In 3.14, for the numerical rank (r_ϵ), matrix E represents the perturbation matrix that contains the errors associated with matrix A [27], [29]. It is crucial to note the significant condition imposed on the norm of the perturbation matrix E in 3.14. The concept of numerical rank becomes meaningful and applicable only when the problem is classified as rank-deficient. In such cases, a distinct gap exists between certain singular values and the remaining ones, and the numerical rank, r_ϵ , satisfies the following inequality:

$$\sigma_{r_\epsilon} > \epsilon > \sigma_{r_\epsilon+1} \quad (3.15)$$

Moreover, the numerical ϵ -rank, as defined in 3.14, can be expressed in terms of the Frobenius norm $\|\cdot\|_F$. In this context, the numerical rank is the smallest integer k that satisfies the following condition [30]:

$$\sigma_{k+1}^2 + \dots + \sigma_n^2 \leq \epsilon^2 \quad (3.16)$$

3.8 Least Squares and the Pseudoinverse

The Least Squares (LS) method, commonly used in MLAT localization problems [29], is a classical numerical technique for solving over-determined systems of equations. In these situations, the number of equations exceeds the number of unknown parameters, making it impossible to obtain an exact solution. The LS method aims to find the optimal solution by minimizing the sum of squared differences between the measured values and the corresponding modeled values. This is achieved by minimizing the squared 2-norm of a residual function. For a linear system of equations, where A is an $m \times n$ ($m > n$) coefficient matrix, θ is an $n \times 1$ unknown vector, and \hat{m} is an $m \times 1$ known measurement vector, the LS method seeks a solution θ that minimizes the following function:

$$\|A\theta - \hat{m}\|_2^2 \quad (3.17)$$

If matrix A possesses linearly independent columns (indicating that it is full rank) and if the matrix $A^T A$ is invertible, then the least squares (LS) problem yields the following solution:

$$\hat{\theta} = (A^T A)^{-1} A^T \hat{m} \quad (3.18)$$

where the super script $\hat{\cdot}$ refers to a non-exact (estimated) solution. However, if matrix A contains linearly dependent columns, it is advisable to avoid utilizing the solution presented in 3.18, and instead, consider the following alternative:

$$\hat{\theta} = A^\dagger \hat{m} \quad (3.19)$$

where A^\dagger is defined as the pseudoinverse [29] matrix of A . In terms of the SVD of A , the pseudoinverse matrix A^\dagger is obtained as:

$$A^\dagger \equiv \sum_{i=1}^{\text{rank}(A)} v_i \sigma_i^{-1} u_i^T \quad (3.20)$$

being u_i and v_i the i -th left and right singular vectors of A , respectively, σ_i the i -th singular value of A , and the function $\text{rank}(\cdot)$, the rank of the matrix. When the solution $\hat{\theta}$ is obtained by using the pseudoinverse matrix, it is defined as the minimum 2-norm solution. The pseudoinverse of A can be also defined, in terms of U , Σ , and V , as:

$$A^\dagger = V_{n \times \text{rank}(A)} \Sigma_{\text{rank}(A) \times \text{rank}(A)} (U_{m \times \text{rank}(A)})^T \quad (3.21)$$

If matrix A is of full rank, then $\text{rank}(A) = n$ and, hence, the matrix $(A^T A)^{-1} A^T$ is equal to the pseudoinverse matrix † . For simplicity, it is common to employ this equivalence:

$$A^\dagger = (A^T A)^{-1} A^T \quad (3.22)$$

Hereby, 3.22 is indistinctly referred to as the pseudoinverse matrix, such that if A is not full rank, A^\dagger is obtained by 3.20 or 3.21.

Chapter 4

Localization Algorithms

This chapter proposes a general framework for analyzing and comparing localization algorithms. The traditional classification of localization algorithms into open form and closed form is acknowledged, but a broader classification compatible with the existing one is introduced. This new classification is based on a general framework that defines a localization algorithm as a combination of a data model and a numerical algorithm. Throughout the chapter, the framework and classification are elaborated, highlighting their relation to the traditional classification.

The chapter provides a concise overview of prominent localization algorithms found in the literature and aligns them with the proposed general framework. Additionally, a general procedure is outlined for analyzing the MLAT localization problem, aiming to identify sources of ill-conditioning and gain a comprehensive understanding of its extent. Simulation and comparison results for the localization algorithms are presented using real-world data in simulated scenarios. These results contribute to forming general conclusions regarding the performance of the examined localization algorithms.

Beyond describing the novel general framework and classification of localization algorithms, the main objective of this chapter is to demonstrate that there is no universally applicable algorithm that consistently provides the most statistically efficient (low dispersion and unbiased) and numerically efficient (stable with robust convergence) solutions for target localization under all conditions. This realization serves as the main motivation for the proposed localization strategy outlined in [17].

4.1 Basic concepts

The localization problem involves estimating the position of a target within a given geographical reference system based on a set of physical measurements obtained from signals emitted by aircraft or vehicles. Generally, the target position can be determined by solving a set of equations that relate it to each measurement, such as hyperbolic equations in the case of standard MLAT systems.

Localization algorithms aim to formulate this problem in a computationally implementable context. They consist of a data model and a numerical algorithm. The data model establishes an explicit relationship between the unknown parameter θ and a set of known parameters, including measurements and the positions of receiving stations. This relationship constructs a numerical inverse problem, which can be linear or nonlinear, although linear formulations are commonly employed for practical reasons.

The numerical algorithm is then employed to solve the resulting inverse problem, enabling the calculation of numerical data representing the target's position within a specific geographical reference system, such as the Cartesian coordinate system. In this section, a general framework is presented to encompass the overall structure of any localization algorithm. This framework serves multiple purposes: understanding the various localization algorithms described in this thesis, establishing a comprehensive classification scheme for these algorithms, facilitating comparative analysis between them, identifying their respective strengths and weaknesses, and discerning the novel contributions offered by the localization strategies presented. The development of this general framework involved an extensive review of relevant literature, followed by careful selection of the most significant and representative localization algorithms.

4.1.1 Data Model

Prior to delving into the various types of data models, it is essential to introduce the concept of a characteristic equation, as it plays a crucial role in explaining and comprehending the subsequent classification and description of localization algorithms. Essentially, a characteristic equation represents a mathematical scalar element that establishes a relationship between the unknown variables and the measurements obtained from a set of receiving stations and their corresponding positions. This scalar element, when expressed in a vector-matrix form for a given set of N_S stations, is referred to as a data model. In essence, the data model can be regarded as a generalized version of a characteristic equation.

Localization algorithms employ different data models, which can be classified into three main categories: statistical approach based models, numerical approach based models, and algebraic approach based models. Each of these categories possesses distinct characteristics, which are described below:

- **Statistical approach-based models:**

These data models rely on statistical principles and assumptions to establish the relationship between the unknown variables and the measurements. They often involve probabilistic formulations, such as Maximum Likelihood Estimator (MLE) or Bayesian inference, to estimate the target position. Statistical models are particularly suitable when dealing with uncertain measurements and incorporating prior knowledge about the system.

- **Numerical approach-based models:**

These data models utilize numerical methods to solve the localization problem. They typically involve the discretization of the problem domain, such as dividing the geographical area into a grid or mesh, and employing numerical techniques like finite element methods or finite difference methods. Numerical models are well-suited for handling complex geometries and continuous physical phenomena.

- **Algebraic approach-based models:**

These data models employ algebraic techniques to establish the relationship between the unknown variables and the measurements. They often involve linear or nonlinear equations, which can be solved using algebraic methods like least squares estimation or Newton's method. Algebraic models are commonly used in cases where the problem can be adequately approximated by a set of equations, and linear formulations are often preferred due to their computational efficiency.

By understanding the main characteristics of each type of data model, one can gain valuable insights into the underlying principles and methodologies employed by different localization algorithms.

4.1.2 Numerical Algorithm

The solution to the resulting linear inverse problem derived from any data model necessitates a numerical approach to obtain a numerical estimation for the target position. As discussed previously, the most widely employed numerical algorithm for solving such linear inverse problems is the method of LS, which utilizes the pseudoinverse matrix. Additionally, for statistical approach based models that involve iterative procedures due to the non-linearity of the resulting model, the Gauss-Newton method [31] is commonly utilized. Furthermore, regularization methods are also well-known in this context.

4.1.3 Classification of Localization Algorithms

A distinction between the two types of existing Localization Algorithm (LA)s and their respective characteristics can be outlined as follows:

- **Open Form Algorithms:**

Open form algorithms are a type of localization algorithms that operate in an iterative manner and do not require explicit mathematical formulations. They typically involve a search or optimization process to estimate the target position. Open form algorithms are flexible and can handle complex scenarios, but they may require more computational resources and have longer convergence times compared to closed form algorithms. These algorithms are often used when the underlying data model is non-linear or when the problem involves uncertainties and constraints that cannot be easily expressed in a closed form solution.

- **Closed Form Algorithms:**

Closed form algorithms, also known as direct or analytical algorithms, are a type of localization algorithms that provide a direct mathematical solution for estimating the target position. Unlike open form algorithms, closed form algorithms do not require iterative processes or search procedures. Instead, they involve solving a set of equations or applying specific mathematical formulas to obtain the desired solution. Closed form algorithms are typically more efficient in terms of computational resources and have faster convergence times compared to open form algorithms. They are commonly used when the data model is linear and the problem can be represented by a set of equations that can be solved analytically. However, closed form algorithms may have limitations in handling non-linearities or incorporating uncertainties and constraints that are inherent in some localization problems.

The following section will be describing the different closed form algorithms used for estimating the starting points for the Taylor-Series Expansion algorithm.

4.2 Closed Form Localization Algorithms

As introduced, these algorithms do not need an starting point unlike open form algorithms. However, they do introduce either a quadratic or a cubic noise term in the corresponding mathematical model that in some cases may lead to poorer accuracy levels. From [17], the most representative closed form algorithms which can be used to solve the localization problem in Mode S MLAT are those proposed by Smith and Abel [32], Friedlander [33], Schau and Robinson [34], Chan and Ho [35], and the application of Bancroft algorithm [36] (initially developed for GPS). All of them are described in the following subsections.

4.2.1 Smith and Abel

The algorithm proposed by Smith and Abel [32] is based on the principle of spherical interpolation. According to this principle, the difference in range between two stations, such as the i -th station and a reference station with known position, represents the distance from the i -th station to a sphere centered at the target position and passing through the reference station, assuming no noise. This algorithm is a one-step algorithm that provides a single solution for the target position.

The characteristic equation of this algorithm is derived by manipulating a single equation in the form of 2.6. This equation contains two unknown parameters: the target position and the range (or distance) from the target position to the reference point. Therefore, the algorithm utilizes two error functions in the least squares sense, known as the spherical LS criteria. The first criterion establishes an explicit relationship between the target position θ and its distance R_s from a known reference point (referred to as target range). The second criterion is used to directly solve for R_s , and this solution is then plugged into the first LS criterion to obtain the solution for the target position.

The algorithm assumes that both the target range and the target position are numerically independent, making it a numerical approach-based model. The algorithm is summarized below, considering that the coordinate system's origin is located at the position of the reference station (station 1), i.e., $\theta_i = \theta_i - \theta_1$, $R_1 = 0$, and $R_s = r_1$. The characteristic equation shown in 4.1 is formed by two stations (the i -th station and the reference one) and is expressed as follows:

$$2\theta_i^T \theta = R_i^2 - \hat{m}_{i,1}^2 - 2R_s \hat{m}_{i,1}, \quad i = 2, \dots, N_s \quad (4.1)$$

Since the measurements are not precisely performed, this algorithm proposes that 4.1 must actually be expressed in terms of an error, as stated in 4.2:

$$\epsilon_{i,1} = R_i^2 - \hat{m}_{i,1}^2 - 2R_s \hat{m}_{i,1} - 2\theta_i^T \theta, \quad i = 2, \dots, N_s \quad (4.2)$$

which expressed in vector-matrix form 4.3 leads to the following data model:

$$\epsilon = \delta - 2R_s \hat{m} - 2S\theta \quad (4.3)$$

where

$$\begin{aligned}
S &= \begin{bmatrix} x_2 & y_2 & z_2 \\ \vdots & \vdots & \vdots \\ x_{N_s} & y_{N_s} & z_{N_s} \end{bmatrix}_{(N_s-1) \times 3} \\
\delta &= \begin{bmatrix} R_2^2 - \hat{m}_{2,1}^2 \\ \vdots \\ R_{N_s}^2 - \hat{m}_{N_s,1}^2 \end{bmatrix}_{(N_s-1) \times 1}
\end{aligned} \tag{4.4}$$

The data model in 4.3 is linear in θ given R_s , and vice versa. In cases where the error vector exhibits linearity with respect to the unknowns, a solution for the target position θ , given R_s , can be obtained by minimizing the 2-norm of 4.3. This solution is commonly referred to as the LS solution and is expressed as follows:

$$\hat{\theta} = \frac{1}{2} S^\dagger (\delta - 2R_s \hat{m}) \tag{4.5}$$

where S^\dagger represents the pseudoinverse matrix of S . In addition, this solution can be viewed as the resolution of the following inverse problem:

$$S \hat{\theta} = \frac{1}{2} (\delta - 2R_s \hat{m}) \tag{4.6}$$

Since R_s is still unknown and no solution can be obtained using Equation 4.5, the authors in [32] suggest employing a secondary error function by substituting 4.5 into 4.3. Consequently, the authors derive the explicit solution for R_s as follows:

$$\epsilon' = \delta - 2R_s \hat{m} - S S^\dagger (\delta - 2R_s \hat{m}) = (I - S S^\dagger) (\delta - 2R_s \hat{m}) \tag{4.7}$$

or equivalently,

$$\epsilon' = P_s^\perp (\delta - 2R_s \hat{m}) \tag{4.8}$$

where

$$P_s^\perp = I - S S^\dagger \tag{4.9}$$

It becomes evident that the updated error equation is linear with respect to the single unknown variable R_s . Therefore, it can be resolved by minimizing the 2-norm of ϵ' in 4.8. This solution can be expressed as follows:

$$R_s = \frac{\hat{m}^T P_s^\perp P_s^\perp \delta}{2 \hat{m}^T P_s^\perp P_s^\perp \hat{m}} \tag{4.10}$$

A solution for the target position θ can be achieved by substituting the value from 4.10 into 4.5, leading to the following resulting expression:

$$\hat{\theta}_{Smith\&Abel} = \frac{1}{2} S^\dagger \left(I - \frac{\hat{m} \hat{m}^T P_s^\perp P_s^\perp}{\hat{m}^T P_s^\perp P_s^\perp \hat{m}} \right) \delta \tag{4.11}$$

This final solution can be interpreted as the resolution of the following inverse problem:

$$G_{Smith\&Abel} \hat{\theta}_{Smith\&Abel} = \hat{m}_{Smith\&Abel} \quad (4.12)$$

where

$$G_{Smith\&Abel} = S$$

$$\hat{m}_{Smith\&Abel} = \frac{1}{2} \left(I - \frac{\hat{m} \hat{m}^T P_s^\perp P_s^\perp}{\hat{m}^T P_s^\perp P_s^\perp \hat{m}} \right) \delta \quad (4.13)$$

The characteristic equation in this algorithm is formed using a pair of stations. In order to estimate a target location with n coordinates, at least $n + 1$ stations are required (e.g., three for 2D localization and four for 3D localization). However, it should be noted that the estimator's solution, as presented in 4.11, is statistically biased and sub-optimal. This is due to the assumption of mutual independence between the target position and range, and the absence of any constraints in the solution of the inverse problem to compensate for this assumption.

Furthermore, in this method, the coefficient matrix remains constant for a given system as it solely depends on the positions of the stations. Conversely, the measurement vector from 4.13 is a modified version of the pure range differences vector, introducing quadratic noise terms. The existence of this modified vector depends directly on the stability of calculating the pseudoinverse of S .

4.2.2 Friedlander

Friedlander proposed an algorithm [33] based on the spherical interpolation principle, similar to the Smith and Abel algorithm [32], as an alternative solution. Like the previous algorithm, Friedlander's method is a one-step algorithm that provides a single solution for the target position. The characteristic equation in this algorithm also contains two unknown and mutually dependent parameters: the target position and the target range.

The main difference between Friedlander's algorithm and Smith and Abel's algorithm lies in the way the problem is solved. Friedlander eliminates one of the unknown parameters, specifically the target range to the reference station r_1 (where station 1 is assumed as the reference station), by pre-multiplying the corresponding data model with a matrix that contains the measurement vector in its null space. By eliminating one of the mutually dependent parameters, Friedlander's algorithm provides a solution without any restrictions between the two parameters, resembling an assumption of mutual independence. Therefore, this algorithm is considered a numerical approach-based model.

While the author claims that Friedlander's algorithm is mathematically equivalent to Smith and Abel's algorithm [32], observations when executing the algorithms suggest that they exhibit different performance characteristics. Below, a summary of Friedlander's algorithm is presented. It is important to note that the formulation below does not specify the origin of the coordinate system at any receiving station's position but at an arbitrary point. The characteristic equation, formed by two stations (the i -th station and the reference station), is expressed as follows:

$$2(\theta_i - \theta_1)^T \theta = R_i^2 - R_1^2 - \hat{m}_{i,1}^2 - 2r_1 \hat{m}_{i,1}, \quad i = 2, \dots, N_s \quad (4.14)$$

It is worth noting that this equation is equivalent to the one presented by Smith and Abel in [32]. The primary distinction arises from the fact that 4.1 is derived by setting the coordinate system's origin at the reference station's position, whereas 4.14 sets the origin at an arbitrary point. Consequently, the data model, expressed in vector-matrix form, is as follows:

$$S_{Fried}\theta = \mu - r_1\hat{m} \quad (4.15)$$

where

$$S_{Fried} = \begin{bmatrix} x_2 - x_1 & y_2 - y_1 & z_2 - z_1 \\ \vdots & \vdots & \vdots \\ x_{N_s} - x_1 & y_{N_s} - y_1 & z_{N_s} - z_1 \end{bmatrix}_{(N_s-1) \times 3} \quad (4.16)$$

$$\mu = \frac{1}{2} \begin{bmatrix} R_2^2 - R_1^2 - \hat{m}_{2,1}^2 \\ \vdots \\ R_{N_s}^2 - R_1^2 - \hat{m}_{N_s,1}^2 \end{bmatrix}_{(N_s-1) \times 1}$$

Equivalently to Smith and Abel, the data model in 4.15 is linear in θ given r_1 and vice versa. At this juncture, the author suggests eliminating r_1 by pre-multiplying the data model in 4.15 with a matrix M that encompasses the measurement vector \hat{m} in its null space, satisfying $M\hat{m} = 0$. This transformation can be expressed as follows:

$$M = (I - Z)D \quad (4.17)$$

where

$$I = \begin{bmatrix} 1 & 0 & \cdots & 0 \\ 0 & 1 & \cdots & 0 \\ \vdots & \vdots & \ddots & \vdots \\ 0 & 0 & \cdots & 1 \end{bmatrix}_{(N_s-1) \times (N_s-1)}$$

$$D = \begin{bmatrix} \hat{m}_{2,1} & \cdots & 0 \\ \vdots & \ddots & \vdots \\ 0 & \cdots & \hat{m}_{N_s,1} \end{bmatrix}_{(N_s-1) \times (N_s-1)} \quad (4.18)$$

$$Z = \begin{bmatrix} 0 & 1 & \cdots & 0 \\ 0 & \ddots & \ddots & 0 \\ \vdots & \ddots & \ddots & 1 \\ 1 & 0 & \cdots & 0 \end{bmatrix}_{(N_s-1) \times (N_s-1)}$$

Matrix Z corresponds to a circular shift matrix, which can be obtained by circularly shifting the columns of the identity matrix one step to the right. Upon pre-multiplying 4.15, the inverse problem can be represented in the following form:

$$MS_{Fried}\theta = M\mu \quad (4.19)$$

where the corresponding solution is:

$$\hat{\theta}_{Fried} = (S_{Fried}^T M^T M S_{Fried})^{-1} S_{Fried}^T M^T M \mu \quad (4.20)$$

This solution can be considered as the solution of this inverse problem:

$$G_{Fried} \hat{\theta}_{Fried} = \hat{m}_{Fried} \quad (4.21)$$

with

$$\begin{aligned} G_{Fried} &= M S_{Fried}^T \\ \hat{m}_{Fried} &= M \mu \end{aligned} \quad (4.22)$$

The formation of a characteristic equation in this algorithm requires a set of two stations. To estimate the target location with a set of n coordinates, at least $n + 1$ stations are required (three for 2D localization and four for 3D localization). However, it has been demonstrated that the matrix M is always singular with a rank of $N_s - 2$, where N_s is the number of stations. Therefore, the author proposes using at least $n + 2$ equations instead of $n + 1$. Based on our simulations, it can be observed that not satisfying this condition is the main cause of poor algorithm performance under certain situations.

However, in practical terms, this assertion is not always true, and the algorithm provides similar overall performance levels as the Smith and Abel algorithm [32]. Similar to the Smith and Abel algorithm, this method is biased and not optimal, and the coefficient matrix of the inverse problem remains constant for a given system. Additionally, this algorithm utilizes a modified version of the pure range difference vector, introducing quadratic noise terms.

4.2.3 Schau and Robinson

The algorithm proposed by Schau and Robinson [34] is based on the spherical intersection principle, which states that the range distance from the target to any station of known position represents the radius of a sphere centered at the target position. This algorithm is a two-step process that provides two potential solutions for the target position, requiring a selection procedure to choose between them. The characteristic equation is derived by manipulating pairs of equations to obtain an expression similar to Smith and Abel [32], involving two unknown and mutually dependent parameters: the target position and the target range to a reference point.

Unlike other algorithms, Schau and Robinson utilize the unknown target ranges as functions of range differences between pairs of stations, as the former are not directly measured in standard MLAT systems. The solving procedure for this algorithm differs from Smith and Abel [32] and Friedlander [33]. It involves sequentially finding the two unknown parameters by solving two separate problems. First, the target range to a reference point is obtained by solving a quadratic equation, and then an inverse problem is solved to determine the target position. This inverse problem is solved twice, corresponding to each solution of the quadratic equation for the target range. This approach assumes numerical independence between the target position and range, thus constituting a numerical approach based model.

The algorithm can be summarized as follows. It is important to note that the formulation assumes the origin of the coordinate system to be at the position of the reference station (station 1), such that $\theta_i = \theta_i - \theta_1$, $R_1 = 0$, and $R_s = r_1$. The characteristic equation, formed by two stations (the i -th station and the reference station), is expressed as follows:

$$2\theta_i^T \theta = R_i^2 - \hat{m}_{i,1}^2 - 2R_s \hat{m}_{i,1}, \quad i = 2, \dots, N_s \quad (4.23)$$

Note that 4.23 is equal to that of Smith and Abel, shown in 4.1. This algorithm's data model is expressed in a vector-matrix form as follows:

$$\aleph \theta = \frac{1}{2}(\Delta - 2R_s \hat{m}) \quad (4.24)$$

where

$$\aleph = \begin{bmatrix} x_2 & y_2 & z_2 \\ \vdots & \vdots & \vdots \\ x_{N_s} & y_{N_s} & z_{N_s} \end{bmatrix}_{(N_s-1) \times 3} \quad (4.25)$$

$$\Delta = \begin{bmatrix} R_2^2 - \hat{m}_{2,1}^2 \\ \vdots \\ R_{N_s}^2 - \hat{m}_{N_s,1}^2 \end{bmatrix}_{(N_s-1) \times 1}$$

It should be noted that the matrices N and the vector θ in this algorithm are equivalent to the matrices \aleph and vector Δ in the Smith and Abel algorithm [32]. Although the same notation could have been used to maintain consistency with the original publications, a different notation was chosen instead. Similarly to Smith and Abel, the authors of this algorithm propose utilizing a spherical LS criterion to solve the inverse problem 4.24. This criterion leads to the following solution:

$$\hat{\theta} = \frac{1}{2} \aleph^\dagger (\Delta - 2R_s \hat{m}) \quad (4.26)$$

where \aleph^\dagger is the pseudoinverse matrix of \aleph . As expected, this solution is also equivalent to the one proposed by Smith and Abel in [32]. Indeed, at this point both algorithms are totally equivalent and their differences start with the way proposed for solving 4.26. When arriving to 4.4, Smith and Abel proposed to use a second spherical LS criterion, by substituting 4.4 into the first spherical LS criterion in 4.3, in order to explicitly obtain a unique solution for R_s and, with this value, solve the linear inverse problem. Schau, however, avoided using a second spherical LS criterion but instead introducing the LS solution 4.26 into the quadratic equation $R_s^2 = \theta^T \theta$ and thus, find its roots for R_s . After performing the necessary mathematical operations, the final quadratic equation in terms of R_s can be expressed as follows:

$$\begin{aligned} & R_s^2 [4 - 4\hat{m}^T (\aleph^\dagger)^T \aleph^\dagger \hat{m}] \\ & + R_s [2\hat{m}^T (\aleph^\dagger)^T \aleph^\dagger \Delta + 2\Delta^T (\aleph^\dagger)^T \aleph^\dagger \hat{m}] \\ & - [\Delta^T (\aleph^\dagger)^T \aleph^\dagger \Delta] = 0 \end{aligned} \quad (4.27)$$

The initial step of this algorithm involves determining the roots of 4.27. Subsequently, these two values are incorporated into the inverse problem expressed in 4.26 to obtain the respective solutions for the target position in the following manner:

$$\hat{\theta}_{Schau\&Robinson}^{1,2} = \frac{1}{2} \aleph^\dagger (\Delta - 2\hat{R}_s^{1,2} \hat{m}) \quad (4.28)$$

In practical applications, the ultimate solution must be selected from the two options presented in 4.28. To achieve this, an intuitive and empirical procedure should be implemented. Ultimately, the chosen solution from 4.28 can be regarded as the resolution to the following inverse problem:

$$G_{Schau\&Robinson}\hat{\theta}_{Schau\&Robinson}^{1,2} = \hat{m}_{Schau\&Robinson}^{1,2} \quad (4.29)$$

with

$$\begin{aligned} G_{Schau\&Robinson} &= \aleph \\ \hat{m}_{Schau\&Robinson}^{1,2} &= \frac{1}{2}(\Delta - 2R_s^{1,2}\hat{m}) \end{aligned} \quad (4.30)$$

To establish a characteristic equation in this algorithm, a pair of stations is required. For estimating a target location with a set of n coordinates, at least $n + 1$ stations are necessary (e.g., three for 2D localization and four for 3D localization). Similar to the Smith and Abel algorithm, the solution provided by 4.28 is biased and sub-optimal due to the assumption of mutual independence between the target position and range, without any compensating restriction in the inverse problem. Moreover, the quality of the solution depends on the selection procedure implemented to choose the final solution from the two possibilities. On the other hand, the coefficient matrix remains constant for a given system as it solely relies on the positions of the stations. However, the measurement vector from 4.30 is a modified version of the pure range difference vector, introducing quadratic noise terms, and its existence is directly influenced by the accuracy of finding the roots of the quadratic equation from 4.27, which might not exist in certain cases.

4.2.4 Chan and Ho

Chan and Ho [35] introduced this algorithm as an improvement over existing closed form algorithms, such as those proposed by Smith and Abel [32], Friedlander [33], and Schau and Robinson [34], which are sub-optimal in terms of statistical estimation. Similar to the Smith and Abel algorithm [32], Chan and Ho's approach is based on the spherical interpolation principle. However, it differs in that it presents a numerically corrected version and tackles the problem in two steps.

The first step, referred to as the initial estimation, involves calculating an initial solution for both the target position θ and the target range r_1 to the reference station. Unlike the aforementioned algorithms, which address direct problems, Chan and Ho's approach formulates both steps as inverse problems. The second step, known as the quadratic correction, imposes a known constraint between θ and r_1 to enhance the accuracy of θ . This two-step algorithm provides two possible solutions for the target location, necessitating the implementation of a procedure to select the appropriate one.

The primary objective of the second step is to address the inherent mutual dependence between the target position and range, which was assumed independently in previous algorithms. In a manner similar to Smith and Abel, the characteristic equation is derived during the first step, involving the two unknown parameters of target position and range. However, the key distinction from previous algorithms lies in the joint estimation of both parameters, rather than estimating the target range first and then the target position (as in Smith and Abel or Schau and Robinson) or eliminating the target range mathematically from the data model (as in Friedlander).

Despite this difference, the first step can be seen as equivalent to the Smith and Abel algorithm, as it also employs a spherical least squares criterion and assumes mutual independence between the target position and range. Hence, to address this limitation, Chan and Ho proposed the second step: a quadratic correction. This step involves determining a spatial increment that can be added to the initial estimation of the target position, effectively enforcing the constraint between the target position and range, thus improving the estimation accuracy.

Put simply, the purpose of the second step is to leverage the information redundancy inherent in spherical interpolation-based methods more effectively. This is achieved through a correction applied to the squared target coordinates, hence the term "quadratic correction." It is important to note that the second step, being a correction to an inverse problem rather than a localization problem itself, classifies the data model of this algorithm as belonging to the numerical approach based models. The algorithm is presented below. It is worth noting that the formulation does not establish the coordinate system's origin at any specific receiving station position, but rather at an arbitrary point. The characteristic equation, which involves two stations (the i -th station and the reference station), is expressed as follows:

$$2(\theta_i - \theta_1)^T \theta = R_i^2 - R_1^2 - \hat{m}_{i,1}^2 - 2r_1 \hat{m}_{i,1}, \quad i = 2, \dots, N_s \quad (4.31)$$

See that this equation is equivalent to the ones of Smith and Abel [32], Friedlander [33], and Schau and Robinson [34]. Considering the inherent imprecision in measurements, this algorithm also suggests formulating the aforementioned equation in terms of an error equation, as follows:

$$\epsilon_{i,1} = \frac{1}{2}(\hat{m}_{i,1}^2 - R_i^2 + R_1^2) + (\theta_i - \theta_1)^T \theta + r_1 \hat{m}_{i,1}, \quad i = 2, \dots, N_s \quad (4.32)$$

which expressed in vector-matrix form leads to the following data model:

$$\epsilon = h(\hat{m}) - G_a \begin{bmatrix} \hat{\theta}_a \\ \hat{r}_1 \end{bmatrix} \quad (4.33)$$

where $\hat{\theta}_a$ represents the initial estimate of θ , and \hat{r}_1 denotes the initial estimate of the target range to the reference station. Additionally, $h(\hat{m})$ is expressed as a function of the measurement vector of range differences to emphasize its probabilistic nature, as it is a random vector rather than a deterministic one.

$$G_a = - \begin{bmatrix} x_2 - x_1 & y_2 - y_1 & z_2 - z_1 & \hat{m}_{2,1} \\ \vdots & \vdots & \vdots & \vdots \\ x_{N_s} - x_1 & y_{N_s} - y_1 & z_{N_s} - z_1 & \hat{m}_{N_s,1} \end{bmatrix}_{(N_s-1) \times 4} \quad (4.34)$$

$$h(\hat{m}) = \frac{1}{2} \begin{bmatrix} \hat{m}_{2,1}^2 - (R_2^2 - R_1^2) \\ \vdots \\ \hat{m}_{N_s,1}^2 - (R_{N_s}^2 - R_1^2) \end{bmatrix}_{(N_s-1) \times 1}$$

The data model presented in 4.33 exhibits linearity with respect to both the target position and the target range, resembling similarities with previous algorithms. Under this assumption and considering the mutual independence of the target position and target range, a solution can be obtained by minimizing the 2-norm of 4.33. This solution, seen as the LS solution, is expressed as follows:

$$\begin{bmatrix} \hat{\theta}_a \\ \hat{r}_1 \end{bmatrix} \approx (G_a^T G_a)^{-1} G_a^T h(\hat{m}) = G_a^\dagger h(\hat{m}) \quad (4.35)$$

where G_a^\dagger represents the pseudoinverse matrix of G_a . This initial step clearly highlights the distinction between this algorithm and the previous ones. As mentioned in the introduction to this algorithm, Smith and Abel and Schau and Robinson arrive at the same data model (or its equivalent) and solve for the target range followed by the target position. In contrast, Friedlander eliminates r_a from the data model by pre-multiplying it with a matrix that contains the measurement vector in its null space. On the other hand, this algorithm directly estimates both parameters simultaneously in a single inverse problem. Furthermore, 4.35 can be viewed as the solution to the following inverse problem:

$$G_a \begin{bmatrix} \hat{\theta}_a \\ \hat{r}_1 \end{bmatrix} = h(\hat{m}) \quad (4.36)$$

The second step of the algorithm involves correcting the previous solutions $\hat{\theta}_a$ and r_1 by calculating a spatial increment that enforces satisfaction of the following equality constraint:

$$(\hat{\theta}_{a,1} - x_1)^2 + (\hat{\theta}_{a,2} - y_1)^2 + (\hat{\theta}_{a,3} - z_1)^2 = \hat{r}_1^2 \quad (4.37)$$

It is important to note that this equality constraint is applied to the squared coordinates. Therefore, it can be resolved by solving a straightforward inverse problem, given by:

$$\hat{\theta}'_a = (G'^T G'_a)^{-1} G'^T h'(\hat{\theta}_a) \quad (4.38)$$

where

$$G'_a = \begin{bmatrix} 1 & 0 & 0 \\ 0 & 1 & 0 \\ 0 & 0 & 1 \\ 1 & 1 & 1 \end{bmatrix}_{4 \times 3} \quad (4.39)$$

$$h'(\hat{\theta}_a) = \begin{bmatrix} (\hat{\theta}_{a,1} - x_1)^2 \\ (\hat{\theta}_{a,2} - y_1)^2 \\ (\hat{\theta}_{a,3} - z_1)^2 \\ \hat{r}_1^2 \end{bmatrix}_{4 \times 1}$$

Finally, the two solutions provided by this algorithm are:

$$\hat{\theta}_{Chan\&Ho}^{1,2} = \pm \sqrt{\hat{\theta}'_a} + \begin{bmatrix} x_1 \\ y_1 \\ z_1 \end{bmatrix} \quad (4.40)$$

The first inverse problem for localization, expressed in 4.36, can be interpreted as the resolution of the following general inverse problem:

$$G_{Chan\&Ho,1} \hat{\theta}_{Chan\&Ho,1} = \hat{m}_{Chan\&Ho,1} \quad (4.41)$$

with

$$\begin{aligned} G_{Chan\&Ho,1} &= G_a \\ \hat{\theta}_{Chan\&Ho,1} &= \begin{bmatrix} \hat{\theta}_a \\ \hat{r}_1 \end{bmatrix} \\ \hat{m}_{Chan\&Ho,1} &= h(\hat{m}) \end{aligned} \quad (4.42)$$

whilst the second one, shown in 4.38, can be seen as another inverse problem:

$$G_{Chan\&Ho} \hat{\theta}_{Chan\&Ho}^{1,2} = \hat{m}_{Chan\&Ho} \quad (4.43)$$

with

$$\begin{aligned} G_{Chan\&Ho} &= G'_a \\ \hat{m}_{Chan\&Ho} &= h'(\hat{\theta}_a) \end{aligned} \quad (4.44)$$

In order to form a characteristic equation within this algorithm, a set of two stations is required. However, since the first inverse problem estimates a total of $n + 1$ unknowns (including n coordinates and r_1) in the most general case, estimating a target location with n coordinates necessitates at least $n + 2$ stations (e.g., four stations for 2D localization or five stations for 3D localization). It is crucial to emphasize that our simulations have shown that the solutions provided for the target range r_1 are not useful (e.g., $r_1 < 0$) when the number of stations is insufficient (i.e., only $n + 1$ stations for estimating n coordinates). In such cases, the second step of the algorithm significantly degrades the positional accuracy achieved by the first step. Similarly, we have observed that solely using the solution for the target position obtained from the first step (i.e., the parameter $\hat{\theta}_a$) yields performance similar to the Smith and Abel algorithm [32].

Furthermore, the authors of this algorithm claim in [35] that it provides an unbiased solution with a small standard deviation close to its CRLB when the noise level is moderate. However, our simulations, both in simulated and real scenarios, have not confirmed these claims. We have also found that using the covariance matrix of measurement errors, i.e., weighted LS, to solve the inverse problem in 4.36, as suggested by the algorithm's authors, only holds true when the covariance matrix can be accurately estimated. This is not the case in MLAT systems where the stations within the same system may exhibit highly diverse conditions. In such cases, utilizing the covariance matrix of measurement errors can actually lead to performance degradation.

The accuracy of the initial estimations, $\hat{\theta}_a$ and r_1 , is crucial for the performance of this method, as the quality of the second step's quadratic correction directly depends on them. In the first step, the coefficient matrix is non-constant and introduces noise terms due to the inclusion of range difference measurements. Similarly, the measurement vector in 4.42 is a modified version of the pure range difference measurements and introduces quadratic noise terms as it includes the squares of the range difference measurements. While the authors of the algorithm claim that it is statistically optimal and can be seen as an approximation of the MLE in the small error region, our extensive simulations indicate that this assertion is not true in practice, particularly for applications in MLAT systems.

4.2.5 Bancroft

The Bancroft algorithm, initially developed by Bancroft [36] for GPS applications, was later adapted for MLAT systems by Geyer and Daskalakis [37]. However, we refer to it as the Bancroft algorithm because the latter work is a direct application of Bancroft's original method. Unlike other algorithms, the Bancroft algorithm utilizes TOA measurements instead of TDOA or range difference measurements.

This algorithm is a one-step approach that provides two possible solutions for the target position. Therefore, an intuitive procedure must be implemented to select the appropriate solution. The characteristic equation of the Bancroft algorithm is derived through algebraic manipulation of the TOA equations, resulting in a data model that is further simplified using the Lorentz inner product for time-space vectors [38].

Notably, the Bancroft algorithm does not rely on statistical or numerical assumptions, making it an algebraic approach-based model. The summarized formulation below does not specify the origin of the coordinate system at any particular receiving station position, but rather at an arbitrary point. After algebraic manipulation of the TOA, the characteristic equation of this algorithm is expressed as follows:

$$2(x_i x + y_i y + z_i z - c^2 \hat{t}_i t_e) = x^2 + y^2 + z^2 - c^2 t_e^2 + x_i^2 + y_i^2 + z_i^2 - c^2 \hat{t}_i^2 \quad (4.45)$$

where $\hat{t}_i = \widehat{TOA}_i$, i.e., the i -th TOA measurement, and t_e , the signal emission time. By expressing 4.45 in the vector-matrix form as shown in 4.46, this data model is obtained:

$$2A_l s_a = \Lambda \mathbf{1} + v \quad (4.46)$$

where

$$\begin{aligned} A_l &= \begin{bmatrix} x_1 & y_1 & z_1 & -c\hat{t}_1 \\ \vdots & \vdots & \vdots & \vdots \\ x_{N_s} & y_{N_s} & z_{N_s} & -c\hat{t}_{N_s} \end{bmatrix}_{N_s \times 4} \\ s_a &= \begin{bmatrix} \theta \\ ct_e \end{bmatrix}_{4 \times 1} \\ \Lambda &= \langle s_a, s_a \rangle = x^2 + y^2 + z^2 - c^2 t_e^2 \\ \mathbf{1} &= \begin{bmatrix} 1 \\ \vdots \\ 1 \end{bmatrix}_{N_s \times 1} \\ v &= \begin{bmatrix} \langle s_1, s_1 \rangle \\ \vdots \\ \langle s_{N_s}, s_{N_s} \rangle \end{bmatrix}_{N_s \times 1} = \begin{bmatrix} x_i^2 + y_i^2 + z_i^2 - c^2 \hat{t}_i^2 \\ \vdots \\ x_{N_s}^2 + y_{N_s}^2 + z_{N_s}^2 - c^2 \hat{t}_{N_s}^2 \end{bmatrix}_{N_s \times 1} \end{aligned} \quad (4.47)$$

In the given data model of 4.46, the operator $\langle \rangle$ represents the Lorentz inner product between two vectors. When both vectors are the same, the parameter Λ corresponds to the Lorentzian norm. Assuming that matrix A_l is non-singular, the explicit solution to the data model is:

$$s_a = \frac{1}{2}\Lambda A_l^\dagger \mathbf{1} + \frac{1}{2}A_l^\dagger v = \Lambda d + e \quad (4.48)$$

where

$$\begin{aligned} d &= \frac{1}{2}A_l^\dagger \mathbf{1} \\ e &= \frac{1}{2}A_l^\dagger v \end{aligned} \quad (4.49)$$

Since the unknowns d and e are involved, this algorithm suggests taking the Lorentzian norm of both sides of 4.48. This operation yields a quadratic equation given by:

$$\alpha\Lambda^2 + \beta\Lambda + \gamma = 0 \quad (4.50)$$

with the coefficients

$$\begin{aligned} \alpha &= \langle d, d \rangle \\ \beta &= 2\langle d, e \rangle \\ \gamma &= \langle e, e \rangle \end{aligned} \quad (4.51)$$

and whose solution is easily obtained by:

$$\Lambda^{1,2} = \frac{-\beta \pm \sqrt{\beta^2 - 4\alpha\gamma}}{2\alpha} \quad (4.52)$$

Finally, the two potential solutions offered by this algorithm can be obtained by substituting the values of Λ obtained using 4.52 into 4.48, resulting in the following expressions:

$$\hat{s}_a^{1,2} = \Lambda^{1,2}d + e \quad (4.53)$$

The characteristic equation in this algorithm can be formed with only one station since it is based on TOA measurements. However, it requires an additional parameter to be estimated: the signal emission time t_e . Therefore, to estimate a target location with n coordinates, a minimum of $n + 1$ stations is necessary (e.g., three stations for 2D localization or four stations for 3D localization).

In this method, the matrix that needs to be inverted is not exact, as it includes the TOA measurements, which naturally introduce noise terms. Moreover, the calculation of the inverse for matrix A_l may not be stable, as the fourth column typically contains quantities that are several orders of magnitude greater than the rest. Additionally, this algorithm introduces quadratic noise terms as the vector v includes the squares of the TOA measurements. Furthermore, it is worth noting that the roots provided by 4.52 can sometimes be complex numbers. In such cases, the real part of the complex number must be extracted.

4.3 Open Form Localization Algorithms

These algorithms use an iterative procedure and need for a suitable starting point (most of the times information about θ) which is normally provided by the closed form algorithms (already commented). The most established open form algorithm to solve the hyperbolic system of equations in Mode S MLAT is based on the Taylor-Series Expansion algorithm [39], [40].

4.3.1 Taylor-Series Expansion

The initial presentation of this method can be found in [40], where the author employed an algebraic procedure to describe the application of Taylor-Series Expansion. This approach aimed to linearize 2.6 and derive an explicit mathematical model for calculating the unknown position θ .

Subsequently, in [39], an accuracy analysis was presented for passive localization systems. In this reference, the author introduced an equivalent formulation to the one presented in [40], but with a statistical approach. This statistical procedure provides deeper insights into the real problem.

Therefore, the Taylor-Series Expansion method is summarized following the procedure outlined in [39]. For real standard Mode S MLAT systems that utilize only range difference measurements, it is more general to express 2.6 as follows:

$$\hat{m}_{i,1} \equiv cTDOA_i = [f_i(x, y, z) - f_1(x, y, z)] + n_{i,1} \quad (4.54)$$

Here, $n_{i,1}$ represents the noise associated with the range difference measurement between the i -th station and the reference station. The level of noise primarily relies on each station's capability to receive, time-tag, and transmit the corresponding TOA measurement to the CPS. However, in a general context, the noise is assumed to follow a zero-mean Gaussian distribution. The $N_s - 1$ range difference equations in the form of 4.54 can be expressed in vector notation as follows:

$$\hat{m} = m(\theta) + n \quad (4.55)$$

where \hat{m} is a $N_s - 1$ column vector which contains all the range difference measurements, $m(\theta)$ is also a $N_s - 1$ column vector of the form:

$$\begin{bmatrix} f_i(x, y, z) - f_1(x, y, z) \\ \vdots \\ f_{N_s}(x, y, z) - f_1(x, y, z) \end{bmatrix}_{(N_s-1) \times 1} \quad (4.56)$$

In this case, n is the equivalent range difference noise measurement vector of $N_s - 1$ size assumed to be of zero mean and Gaussian distributed with covariance matrix given by:

$$N = E[(n - E[n])(n - E[n])^T] \quad (4.57)$$

where $E[\]$ denotes the expectation operator. The structure of the covariance matrix depends on the techniques used to estimate the TOA/TDOA values. Consequently, the likelihood function for the unknown target position is given by [39]:

$$\Lambda = \frac{1}{(2\pi)^{\frac{N_s-1}{2}} \det(N(\theta))^{\frac{1}{2}}} e^{-\frac{1}{2}\{(\hat{m}-m(\theta))^T N(\theta)^{-1}(\hat{m}-m(\theta))\}} \quad (4.58)$$

Here, $\det(N(\theta))$ represents the determinant of the $N_s - 1 \times N_s - 1$ measurement covariance matrix $N(\theta)$. Therefore, the target position, given a specific system and a set of measurements, is determined by maximizing the likelihood function in 4.58 and minimizing the following function:

$$Q(\theta) = (\hat{m} - m(\theta))^T N(\theta)^{-1} (\hat{m} - m(\theta)) \quad (4.59)$$

To find the θ that minimizes 4.59, the function $m(\theta)$ is linearized by a Taylor-Series Expansion centered in a starting point $\theta_0 = [x_0, y_0, z_0]^T$. Only the terms of zero and first order are retained, resulting in the following expression:

$$m(\theta) = m(\theta_0) + G(\theta - \theta_0) \quad (4.60)$$

Here, G refers to the TDOA Jacobian matrix of the form:

$$G_i = \frac{1}{c} \begin{bmatrix} \frac{x_i - x_2}{r_2} - \frac{x_i - x_1}{r_1} & \frac{y_i - y_2}{r_2} - \frac{y_i - y_1}{r_1} & \frac{z_i - z_2}{r_2} - \frac{z_i - z_1}{r_1} \\ \vdots & \vdots & \vdots \\ \frac{x_i - x_{N_s}}{r_{N_s}} - \frac{x_i - x_1}{r_1} & \frac{y_i - y_{N_s}}{r_{N_s}} - \frac{y_i - y_1}{r_1} & \frac{z_i - z_{N_s}}{r_{N_s}} - \frac{z_i - z_1}{r_1} \end{bmatrix}_{(N_s-1) \times 3} \quad (4.61)$$

By defining $\hat{m}_\Delta = \hat{m} - m(\theta_0)$ and $\Delta\theta = \theta - \theta_0$, Q in 4.59 can be rewritten as:

$$Q(\Delta\theta) = (\hat{m}_\Delta - G\Delta\theta)^T N(\theta)^{-1} (\hat{m}_\Delta - G\Delta\theta) \quad (4.62)$$

The derivatives of 4.62 with respect to each component of $\Delta\theta$ need to be computed, and then set to zero in order to obtain a direct expression for $\Delta\theta$. Through several algebraic manipulations, it can be shown that:

$$\hat{\theta} = (G^T N(\theta)^{-1} G)^{-1} G^T N(\theta)^{-1} \hat{m}_\Delta + \theta_0 \quad (4.63)$$

By changing θ to $\hat{\theta}$ in order to emphasize that it is the variable estimated by the MLE in 4.58, it is customary to remove the term $N(\theta)$ from 4.63. This assumption treats the covariance matrix as an identity matrix, although in reality it is generally not equal to it. This assumption simplifies the mathematical treatment, although it does not accurately reflect the actual noise distribution among stations. Additionally, 4.63 should be refined through several iterations until a satisfactory level of accuracy is achieved. This iterative procedure can be expressed as follows:

$$\hat{\theta}^k = (G(\hat{\theta}^{k-1})^T G(\hat{\theta}^{k-1}))^{-1} G(\hat{\theta}^{k-1})^T \hat{m}_\Delta(\hat{\theta}^{k-1}) + \hat{\theta}^{k-1}, \quad k = 1, \dots, K \quad (4.64)$$

Here, $\hat{\theta}_0 = \theta_0$, $\hat{m}_\Delta(\hat{\theta}^{k-1}) = \hat{m} - m(\theta^{k-1})$, and K is the maximum number of refinement iterations. It is important to note that θ_0 does not necessarily need to be an initial estimation of the true target position θ . In certain applications, the starting point can be assumed as a fixed value across the entire coverage area. The choice of the starting point θ_0 often has a significant impact on the convergence of the method, which will be further analyzed in this section.

Finally, the iterative process outlined in 4.64 requires a stopping criterion, typically determined by the Euclidean difference between the solution at the k -th iteration and the k -th - 1 iteration. If the difference between these two solutions is smaller than a predefined spatial threshold, the algorithm terminates the iterative procedure. Otherwise, it continues with the refinement process. This stopping criterion can be expressed as follows:

$$\|\hat{\theta}^k - \hat{\theta}^{k-1}\|_2 = \begin{cases} \leq \Delta_s, & s \\ > \Delta_s, & c \end{cases} \quad (4.65)$$

where Δ_s is the predefined spatial threshold. s and c refer to *stop* and *continue*, depending on the case. Moreover, 4.64 can also be seen as a LS solution of the MLAT localization problem, which actually is the 2-norm solution, it is, the solution that satisfies:

$$\hat{\theta} = \underset{\theta}{\operatorname{argmin}} \|G\theta - \hat{m}\|_2^2 \quad (4.66)$$

As seen in [29], the denoted matrix G^\dagger refers to the pseudoinverse matrix of $(G^T G)^{-1} G^T$; the iterative estimator in 4.64 can be alternatively expressed as follows:

$$\hat{\theta}^k = G^\dagger(\hat{\theta}^{k-1}) \hat{m}_\Delta(\hat{\theta}^{k-1}) + \hat{\theta}^{k-1}, \quad k = 1, \dots, K \quad (4.67)$$

This approach may not always yield satisfactory accuracies due to the presence of linearly dependent equations in the matrix G under certain operational conditions. In such cases, the solutions from 4.64 or 4.67 tend to have large errors. Consequently, it can be concluded that solving the localization problem using the LS approach has certain disadvantages. One significant numerical disadvantage is associated with the violation of Hadamard's conditions. The LS solution obtained from the pseudoinverse matrix does not always satisfy all three Hadamard's conditions. As a result, in some cases, the solution provided by 4.64 may significantly deviate from the exact solution, resulting in an ill-conditioned localization problem. However, on the positive side, this algorithm offers the important advantage of linear noise dependency, whereas closed-form algorithms exhibit quadratic noise dependency.

Providing an initial estimation of the position, commonly referred to as a starting point, is crucial. Depending on the specific application scenario, this starting point can be predetermined as a fixed value or estimated through a prior execution of a closed-form algorithm. However, relying solely on the LS solution does not always guarantee convergence of the method. Therefore, when performing surveillance beyond the system perimeter, typically in WAM, it becomes necessary to employ a closed-form algorithm to obtain a suitable starting point for the localization process. Utilizing a closed-form algorithm to estimate the starting point is justified due to its robustness to noise, and subsequently applying a Taylor expansion method improves upon the previous solution. It is important to note that the vertical component of the position is often the most ill-conditioned, impacting all numerical methods. Determining the most appropriate approach to determine the starting point depends on factors such as system geometry, radioelectric coverage, and the number of available receiving stations. Nonetheless, practical strategies can be employed to estimate the starting point accurately.

4.4 Review of the Localization Algorithms

The summarized key characteristics of the seven localization algorithms analyzed are presented in Table 3.4.1. It should be noted that the number of target position coordinates to be estimated is denoted by n , where n can be either 2 or 3 depending on the type of localization (2D or 3D). The columns labeled *Steps* and *Solutions* indicate the number of steps required to solve each algorithm and the number of solutions obtained, respectively. The column *SATS* represents the number of stations or satellites necessary to form a single equation, while *Min. Rx* denotes the minimum number of receiving stations required for the system to function correctly. Each algorithm introduces different noise contributions, indicated as *Noise terms*. The *Data model* that characterizes each algorithm is also provided.

It is important to note that the only iterative algorithm among them is the open form Taylor-Series Expansion algorithm (it is not a regularization method), whereas the remaining closed form algorithms provide direct solutions. Additionally, it is observed that all the algorithms are solved within a specific number of steps, and the number of solutions matches the number of steps required, except for the Bancroft algorithm, which yields two solutions from a single solving step.

Algorithm	Steps	Solutions	SATS	Min. Rx	Noise terms	Data Model
Smith & Abel	1	1	2	$n + 1$	Quadratic	Numerical
Friedlander	1	1	2	$n + 1$	Quadratic	Numerical
Schau & Robinson	2	2	2	$n + 1$	Quadratic	Numerical
Chan & Ho	2	2	2	$n + 2$	Quadratic	Numerical
Bancroft	1	2	2	$n + 1$	Linear & Quadratic	Algebraic
Taylor-Series	1	1	2	$n + 1$	Linear	Statistical

Table 3.4.1: Characteristics of the localization algorithms

Chapter 5

Regularization Algorithms

In SBM, regularization algorithms are employed to improve the accuracy and stability of the positioning solutions by mitigating the effects of noise, measurement errors, and other uncertainties. These algorithms incorporate regularization techniques that introduce additional constraints or penalties to the mathematical model used for position estimation. Here are a few common regularization algorithms used in SBM:

- **Tikhonov Regularization:**

Tikhonov regularization, also known as ridge regression, is a widely used technique to stabilize and improve the accuracy of ill-conditioned or noisy multilateration problems. It introduces a regularization term into the objective function that penalizes large or complex solutions. This additional term helps control the trade-off between accuracy and stability, effectively reducing the impact of measurement errors and improving the overall robustness of the estimated position.

- **Total Variation (TV) Regularization:**

This regularization is a technique used to preserve the sharpness or sparsity of the estimated positions. It is particularly useful when dealing with problems involving edges or discontinuities in the object's location. By adding a penalty term based on the total variation of the estimated position, the algorithm encourages sparse or piecewise smooth solutions, which can lead to more accurate localization results.

- **Sparsity-Inducing Regularization:**

Sparsity-inducing regularization methods, such as L1 regularization (Lasso), promote solutions that have a small number of non-zero components or parameters. These methods are particularly useful in scenarios where only a few satellites or measuring stations provide reliable measurements. By encouraging sparsity, these algorithms can enhance the system's resilience to measurement errors and reduce the impact of outliers, leading to more accurate position estimates.

- **Bayesian Regularization:**

Bayesian regularization techniques incorporate prior knowledge or assumptions about the object's position into the estimation process. Bayesian approaches utilize probability distributions to represent uncertainty and update the distributions based on the available measurements. By incorporating prior information or assumptions about the position, these algorithms can improve the accuracy and stability of the estimated solutions.

- **Constraint-Based Regularization:**

Constraint-based regularization methods impose additional constraints on the estimated position to improve the overall solution quality. These constraints can be geometric, physical, or statistical in nature, depending on the specific problem and requirements. By incorporating constraints such as bounding the position within a certain region or enforcing smoothness properties, these algorithms can enhance the accuracy and validity of the estimated positions.

These regularization algorithms are often used in combination with the localization algorithms mentioned earlier, such as TOA, TDOA, AOA, or FDOA, to enhance the positioning results. The choice of regularization algorithm depends on the characteristics of the problem, the available measurements, and the specific requirements of the multilateration system. The objective is to strike a balance between accuracy, stability, robustness, and computational efficiency.

5.1 Basic Concepts

There are various options available for constructing and solving the localization problem in MLAT systems. However, it has been observed that in certain scenarios, due to factors such as system geometry, measurement noise, and the quality of the starting point (in the case of open form algorithms), the corresponding inverse problem can become ill-conditioned. As a result, the estimated target position may not be accurate or may exhibit large errors, making it unreliable.

To address the issue of ill-conditioning, both hardware and software-based solutions have been developed. In terms of hardware, one approach is to increase the number of stations. Typically, ill-conditioning tends to arise when the number of stations is less than seven or eight. By adding more stations, the problem of ill-conditioning can be mitigated. Another hardware-based solution involves incorporating additional measurement capabilities, such as AOA, to improve the data model. This, in turn, helps transform the ill-conditioned coefficient matrix into a well-conditioned one, improving the overall reliability of the localization process.

However, while these solutions are effective, they often require significant financial investments. Alternatively, software-based solutions can be explored, offering two possible options. The first option involves using a horizontal (2D) projection of the localization algorithms, solving the resulting system of equations using the pseudoinverse matrix. Although this approach initially yields a well-conditioned coefficient matrix, it introduces a spatial bias due to the projection from 3D to 2D, affecting the solution but not the measurements.

The second software-based option is to implement closed form localization algorithms from a family of algorithms. These algorithms have the advantage of not requiring a starting point, which can be a source of ill-conditioning. However, they introduce quadratic and cubic relationships between the solution (target position) and the measurement noise. In some cases, it is necessary to choose between the two possible solutions provided by these algorithms. While horizontal projection is also possible for this type of algorithm, the issue of spatial bias remains.

Having discussed the fundamentals of inverse problems and the localization problem in MLAT systems, as well as the different solutions available, this section explores several regularization methods applied to solve the MLAT localization problem. These methods can be categorized into two families: Direct Regularization Method (DRM) and Indirect Regularization Method (IRM). The solutions presented in this chapter can be considered a software-based strategy aimed at overcoming the disadvantages mentioned earlier for both software and hardware-based solutions.

5.1.1 Classification of Regularization Algorithms

The two types of existing Regularization Algorithm (RA)s can be differentiated based on the following characteristics:

- **Direct Regularization Method (DRM):**

These algorithms are a type of regularization technique used in various fields, including signal processing and inverse problems. DRM involves incorporating prior knowledge or constraints on the solution directly into the regularization framework. The main idea behind DRM is to impose certain properties or structures on the solution space to improve the quality and reliability of the estimated solution. This can be achieved by adding penalty terms or regularization functions to the objective function being optimized. These penalty terms control the trade-off between data fidelity and the desired properties of the solution, such as smoothness, sparsity, or non-negativity. DRM provides a flexible approach that allows for the incorporation of different types of constraints, depending on the specific problem at hand. By effectively utilizing available information, DRM can enhance the accuracy and stability of the solution, particularly in situations where the inverse problem is ill-posed or ill-conditioned.

- **Indirect Regularization Method (IRM):**

These algorithms are a class of techniques used to solve inverse problems by modifying the data instead of directly incorporating constraints into the regularization framework. IRM aims to improve the ill-posedness of the problem by pre-processing the data through various methods such as denoising, filtering, or transforming the data to a different domain. These pre-processing steps aim to enhance the quality of the data and improve its conditioning, making it more amenable to standard inversion techniques. By reducing noise, artifacts, or uncertainties in the data, IRM indirectly regularizes the inverse problem and improves the stability and accuracy of the solution. IRM methods are often tailored to specific problem domains and require a deep understanding of the underlying physics or characteristics of the data. Overall, IRM provides an alternative approach to regularization, focusing on data modification to mitigate the ill-posedness and enhance the performance of subsequent inversion algorithms.

5.2 Direct Regularization Methods

This section focuses on explaining the practical implementation of various DRM discussed in the classification of regularization approaches. DRM encompass a range of techniques utilized to address ill-posed linear inverse problems. Some common types of DRM include:

- Tikhonov Regularization
- Singular Value Decomposition (SVD)-based Methods
 - Truncated SVD (T-SVD)
 - T-SVD with Sub-set Selection (T-SVD-SS)
- Total Least Squares (TLS)-based Methods
 - Truncated TLS (T-TLS)

The implementation of the regularization methods discussed in this section is specifically designed to complement the Taylor-series expansion method. The primary challenge hereby in achieving convergence for solving the MLAT localization problem lies in the ill-conditioning of the coefficient matrix involved. By incorporating and solving the localization problem using regularization methods, our aim is to transform the weaknesses of this localization algorithm (such as the reliance on a high-quality starting point and limited or no convergence) into strengths, while still retaining its inherent advantages, such as statistical optimality. The findings and contributions presented in this chapter have been previously described and analyzed in publications such as [41].

5.2.1 Tikhonov Regularization

The Tikhonov regularization method, independently developed by Tikhonov and Phillips [42], [43] has been widely employed in various engineering and scientific applications to address ill-conditioned problems. It is commonly referred to as Tikhonov regularization due to its association with Tikhonov. The fundamental concept of this method involves incorporating a priori information regarding the size and smoothness of the desired solution, expressed through a semi-norm. In general, Tikhonov regularization aims to minimize not only the residual 2-norm but also a trade-off between the residual 2-norm and the 2-norm of the final solution. This principle is mathematically represented by the following function [27], [42]:

$$\operatorname{argmin}\{\|G\theta - \hat{m}\|_2^2 + \lambda^2\|L\theta\|_2^2\} \quad (5.1)$$

Here, the regularization parameter λ governs the relative importance assigned to minimizing the regularization term $\|L\theta\|_2$. This term, also known as the discrete smoothing norm or $\Omega(\theta)$, contributes to the overall objective. The matrix $L \in \mathbb{R}^{n \times n}$ (where $n = 3$ for (x,y,z) localization) is referred to as the regularization matrix. To apply the Taylor-Series Expansion method using Tikhonov regularization, it is necessary to reformulate the likelihood function (see 4.58) to incorporate the minimization of 5.1. Consequently, the likelihood function for the Tikhonov method can be expressed as follows:

$$\Lambda(\theta) = \frac{1}{(2\pi)^{\frac{N_s-1}{2}} \det(N(\theta))^{\frac{1}{2}}} e^{-\frac{1}{2}\{(\hat{m}-m(\theta))^T N(\theta)^{-1}(\hat{m}-m(\theta)) + \lambda^2(L\theta)^T L\theta\}} \quad (5.2)$$

where $\theta = [x, y, z]^T$ is the target position, and \hat{m} is the range difference measurements vector. In this application, it is defined the MLE as the regularized MLE, and the solution of this is the value of θ that maximizes 5.2. In this way, the regularized MLE minimizes the following function:

$$Q(\theta) = (\hat{m} - m(\theta))^T N(\theta)^{-1} (\hat{m} - m(\theta)) + \lambda^2 (L\theta)^T L\theta \quad (5.3)$$

Similar to the Taylor-Series method solved using the LS approach, it is necessary to expand the non-linear function $m(\theta)$ using a Taylor series centered around a starting point $\theta_0 = [x_0, y_0, z_0]^T$. This process results in the following minimization function:

$$Q(\Delta\theta) = (\hat{m}_\Delta - G\Delta\theta)^T N(\theta)^{-1} (\hat{m}_\Delta - G\Delta\theta) + \lambda^2 (L\Delta\theta)^T L\Delta\theta \quad (5.4)$$

To determine the value of $\Delta\theta$ that minimizes the function $Q(\Delta\theta)$, the derivatives of 5.4 with respect to each component of $\Delta\theta$ are calculated. Then, these derivatives are set to zero to obtain an explicit expression for $\Delta\theta$. The procedure can be summarized as follows:

$$\nabla_{\Delta\theta} Q(\Delta\theta)|_{\Delta\theta=\Delta\hat{\theta}} = -G^T N(\theta)^{-1} \hat{m}_\Delta + G^T N(\theta)^{-1} G\Delta\hat{\theta} + \lambda^2 L^T L\Delta\hat{\theta} = 0 \quad (5.5)$$

where 5.5 has been evaluated at $\Delta\hat{\theta} = \hat{\theta} - \theta_0$. Then,

$$(G^T N(\theta)^{-1} G + \lambda^2 L^T L)\Delta\hat{\theta} = G^T N(\theta)^{-1} \hat{m}_\Delta \quad (5.6)$$

and the unknown variable $\Delta\hat{\theta}$ can be obtained by:

$$\Delta\hat{\theta} = (G^T N(\theta)^{-1} G + \lambda^2 L^T L)^{-1} G^T N(\theta)^{-1} \hat{m}_\Delta \quad (5.7)$$

Here, 5.7 is therefore the regularized MLE solution to the Taylor-Series expansion method. From 5.7, the following expression can be extracted:

$$A_\lambda^{-1} = (G^T N(\theta)^{-1} G + \lambda^2 L^T L)^{-1} G^T N(\theta)^{-1} \quad (5.8)$$

where A_λ^{-1} is known in the literature [27], [42] as the Tikhonov's regularized inverse matrix. The estimated target parameter is finally calculated:

$$\hat{\theta}_\lambda = A_\lambda^{-1} \hat{m}_\Delta + \theta_0 \quad (5.9)$$

The estimated parameter vector $\hat{\theta}$ is denoted as $\hat{\theta}_\lambda$ to emphasize that it represents the Tikhonov solution. In this regularized estimator, the covariance matrix $N(\theta)$ is assumed to be an identity matrix, removing its dependence on the true target position θ . Additionally, to improve the accuracy of the regularized estimator in 5.9, it should be refined through several iterations. The resulting regularized iterative procedure can be expressed as follows:

$$\hat{\theta}_\lambda^k = A_\lambda^{-1} (\hat{\theta}_\lambda^{k-1}) \hat{m}_\Delta (\hat{\theta}_\lambda^{k-1}) + \hat{\theta}_\lambda^{k-1}, \quad k = 1, \dots, K \quad (5.10)$$

Here, $\hat{\theta}_\lambda^0$ is initialized as θ_0 , $\hat{m}_\Delta(\hat{\theta}_\lambda^{k-1})$ represents the difference between the estimated and actual measurements, and K denotes the maximum number of refinement iterations. It should be noted that θ_0 is not necessarily a previous estimation of the true target position θ . In certain applications, the starting point can be assumed as a fixed value for the entire coverage area. The choice of θ_0 significantly affects the convergence of the method, although in this particular application, it has been found that the performance of this solution is less sensitive compared to the LS solution.

To ensure the proper application of regularized MLE, it is crucial to select the appropriate regularization parameter λ and regularization matrix L to obtain a valid solution. The choice of the regularization matrix L is closely related to the statistical properties of the target position vector θ , specifically the correlation between the coordinates (x,y,z). Assuming that the components of θ are non-random and uncorrelated, which is a reasonable assumption [19], a common approach is to set the regularization matrix L as the identity matrix of size $n \times n$. Furthermore, in [44], the author demonstrated that the existence of a minimum expected value for the residual error in the Tikhonov method can only be guaranteed when L is the identity matrix. Otherwise, the Tikhonov solution may deviate significantly from the exact solution. Therefore, unless otherwise specified, the regularization matrix used in the remainder of this thesis is assumed to be $L = I_{3 \times 3}$.

Determining the appropriate regularization parameter λ is not as straightforward as selecting the regularization matrix. The literature offers various numerical methods and procedures to calculate or estimate an approximate value for the regularization parameter. It is worth noting that the choice of λ is closely related to the SVD spectrum of matrix G . Therefore, it becomes evident that the SVD spectrum should be examined in order to calculate the regularization parameter within the solution of 5.10. In the upcoming subsection, the solution of 5.10 will be presented using an SVD routine instead of relying on a numerical method to directly obtain the inverse matrix 5.8. Additionally, a procedure will be described to estimate the suitable regularization parameter λ .

5.2.1.1 Solving Regularized MLE by SVD

The expression from 5.10 can be solved using a numerical routine to directly compute the inverse matrix A_λ^{-1} . However, it is crucial to examine the SVD spectrum to estimate the regularization parameter. The SVD spectrum provides valuable information about the ill-conditioning of the problem. The expression for calculating the Tikhonov regularized MLE solution using the SVD is presented in [27], [29] as follows:

$$\hat{\theta}_\lambda^k = \left(\sum_{i=1}^n f_i^{k-1} \frac{(u_i^{k-1})^T \hat{m}_\Delta(\hat{\theta}_\lambda^{k-1})}{\sigma_i^{k-1}} v_i^{k-1} \right) + \hat{\theta}_\lambda^{k-1}, \quad k = 1, \dots, K \quad (5.11)$$

where u_i and v_i correspond to the left and right singular vectors of G , respectively. On the other hand, σ_i refers to the i -th singular value of G , and these values are obtained following a SVD routine. Here, if $G \in \mathbb{R}^{m \times n}$ (in this application, m is the number of receiving stations and $n = 3$ (three dimensions)), then the SVD of G is a decomposition of the form [27], [29]:

$$G = U \Sigma V^T = \sum_{i=1}^n u_i \sigma_i v_i^T \quad (5.12)$$

where $U = (u_1, \dots, u_i) \in \mathbb{R}^{(N_s-1) \times n}$ and $V = (v_1, \dots, v_i) \in \mathbb{R}^{n \times n}$ are matrices with orthonormal columns, and Σ is a diagonal matrix such that $\Sigma = \text{diag}(\sigma_1, \dots, \sigma_i)$. Finally, f_i are known in the literature [27], [42] as the Tikhonov's filter factors. For this specific application, $L = I_{n \times n}$, these filter factors are obtained in the following way:

$$f_i = \frac{\sigma_i^2}{\sigma_i^2 + \lambda^2} \quad (5.13)$$

5.2.1.2 Effect of the Tikhonov Regularization

In order to gain a better understanding of how the Tikhonov method operates in the context of the localization problem, let us explicitly derive the matrix A_λ . For the sake of simplicity, we will omit the superscript k in the remaining descriptions of the regularized MLE. The matrix A_λ can be expressed as follows:

$$A_\lambda = (A_\lambda^{-1})^{-1} = ((G^T N(\theta)^{-1} G + \lambda^2 L^T L)^{-1} G^T N(\theta)^{-1})^{-1} \quad (5.14)$$

After a few operations, 5.14 takes the following form:

$$A_\lambda = G + \lambda^2 (G^T N(\theta)^{-1})^{-1} L^T L \quad (5.15)$$

By expressing 5.15 in terms of the SVD of matrix G (i.e., $G = U \Sigma V^T$), and neglecting the covariance matrix $N(\theta)$, matrix A_λ can be expressed this way:

$$\begin{aligned} A_\lambda &= U \Sigma V^T + \lambda^2 U \Sigma^{-1} V^T \\ A_\lambda &= U (\Sigma + \lambda^2 \Sigma^{-1}) V^T \\ A_\lambda &= U \Sigma \Gamma_\lambda V^T \\ A_\lambda &= U \Sigma_\lambda V^T \end{aligned} \quad (5.16)$$

Here, $\Gamma_\lambda = \text{diag}(\frac{1}{f_1}, \dots, \frac{1}{f_n})$ represents a diagonal matrix with elements corresponding to the Tikhonov filter factors f_j . The matrix $\Sigma_\lambda = \Sigma \Gamma_\lambda$ denotes the matrix of singular values of A_λ . This expression of 5.16 can be understood as the singular value decomposition (SVD) of matrix A_λ , where the left and right singular vectors are identical to those of matrix G , and the singular values are an amplified version of the singular values of matrix G . Geometrically, the matrices U and V provide sets of orthonormal basis vectors, represented by their column vectors.

In this context, the singular values serve as spectrum components of a matrix, and they are the sole distinguishing factor between two matrices that share the same orthonormal basis, as exemplified by A_λ and G . Therefore, considering that matrix G encompasses information about the system geometry, it can be inferred that A_λ represents a modified version of the system's geometry, wherein its singular value spectrum is an altered version of that of matrix G . In other words, the utilization of the regularized estimator can be viewed as a correction to the system geometry, transforming the ill-conditioned scenario into an equivalent well-conditioned one.

However, it is important to note that since the minimum residual norm solution can only be obtained using the pseudoinverse matrix, and given that matrix A_λ is different from matrix G , the regularized MLE solution always introduces a bias compared to the exact solution [27]. Nevertheless, as we will demonstrate later, in many cases this bias can be negligible if the appropriate regularization matrix and regularization parameter are chosen.

5.2.1.3 Regularization Error of the Tikhonov Regularization

When employing any regularization method, a certain degree of error is introduced due to the approximations made to enable the solution of the ill-conditioned problem [27]. Substituting 4.55, 4.60 and 5.8 into 5.9, and remembering $\hat{m}_\Delta = \hat{m} - m(\theta_0)$ and $\Delta\hat{\theta} = \hat{\theta} - \theta_0$, the expression of $\hat{\theta}_\lambda$ can be rewritten this way:

$$\hat{\theta}_\lambda = \theta + (G^T N(\theta)^{-1} G + \lambda^2 L^T L)^{-1} G^T N(\theta)^{-1} \{m(\theta) - m(\theta_0) - A_\lambda(\theta - \theta_0) + n\} \quad (5.17)$$

In 5.17, it is shown that the estimated target position is affected by an error that depends on two components, one is the regularized linearization error and the other one is the error due to the measurements noise. For the Tikhonov method, the error [27] can be expressed in the following manner:

$$\begin{aligned} \theta - \hat{\theta}_\lambda &= G^\dagger m_\Delta(\theta) - A_\lambda^{-1} \hat{m}_\Delta \\ \theta - \hat{\theta}_\lambda &= (G^\dagger - A_\lambda^{-1}) m_\Delta(\theta) - A_\lambda^{-1} n \end{aligned} \quad (5.18)$$

where G^\dagger is the pseudoinverse matrix of G , $\hat{m}_\Delta = m_\Delta(\theta) + n$, and $m_\Delta(\theta) = m(\theta) - m(\theta_0)$. The first term in 5.18 represents the regularization error, which provides information about the error in the system geometry correction. The second term corresponds to the perturbation error, which accounts for measurement noise such as instrumental errors and propagation effects.

When only a minimal amount of regularization is applied ($0 \ll \lambda \ll 1$), the Tikhonov filter factors approach 1, and the overall error is primarily influenced by the perturbation error $A_\lambda^{-1} n$. This situation is known as under-smoothing, and the resulting solution $\hat{\theta}_\lambda$ tends to converge towards the conventional non-regularized solution, namely the least squares (LS) solution.

Conversely, when a substantial amount of regularization is utilized ($\lambda \gg 0$), the filter factors become considerably small ($f_i \ll 1$), and the overall error is predominantly governed by the regularization error. This scenario is referred to as over-smoothing, and in the context of the localization problem, the solution $\hat{\theta}_\lambda$ tends to converge towards θ_0 . In terms of the singular value decomposition (SVD) of matrix G , the computation of the overall error can be expressed as follows:

$$\theta - \hat{\theta}_\lambda = \sum_{i=1}^n (1 - f_i) \frac{u_i^T m_\Delta(\theta)}{\sigma_i} v_i - \sum_{i=1}^n f_i \frac{u_i^T n}{\sigma_i} v_i \quad (5.19)$$

Finally, upon analyzing 5.18 or 5.19, it becomes apparent that the proper implementation of the Tikhonov method aims to achieve a balance between the two components of error, namely the regularization error and the perturbation error.

5.2.1.4 Estimation of the Regularization Parameter

The selection or estimation of the regularization parameter is a crucial aspect in the application of regularization methods. Various methods and procedures exist to calculate an approximate value for the regularization parameter. In [27], the author classifies these methods into two categories based on the assumption about the 2-norm of the measurement error $\|n\|_2$. The first category consists of methods that rely on a priori knowledge or a good estimation of $\|n\|_2$. The second category includes methods that do not require any a priori knowledge or estimation of $\|n\|_2$ but instead extract this information from the given measurement vector \hat{m} .

Within the first category, one notable method is the discrepancy principle [45], which takes into account the 2-norm of the measurement error or its generalized version (generalized discrepancy principle), which also considers possible errors E in the coefficient matrix G (in the context of this application, the differential Jacobian matrix). The fundamental idea behind these methods is that if the equation $G\theta = m$ (where θ and m are the exact quantity vectors) holds exactly, then the correct regularization parameter is the one for which the residual error $\|G\hat{\theta}_\lambda - \hat{m}\|_2$ is equal to a specific value determined by a relation between the a priori upper bounds δ_e and δ_E for $\|n\|_2$ and $\|E\|_2$, respectively. In other words, the value of λ should satisfy the following condition:

$$\|G\hat{\theta}_\lambda - \hat{m}\|_2 = \delta_e \quad (5.20)$$

where $\|n\|_2 \leq \delta_e$, and the generalized version:

$$\|G\hat{\theta}_\lambda - \hat{m}\|_2 = \delta_0^{exact} + \delta_e + \delta_E \|\theta\|_2 \quad (5.21)$$

where δ_0^{exact} is an incompatibility measure of the inverse problem. In the second category of methods, the objective is to minimize a function that approximates the total error, thereby obtaining a regularization parameter that achieves an optimal balance between the regularization and perturbation errors in θ_λ . Some of these methods include the approach described in [46] and the quasi-optimality criterion [47]. Additionally, there are other methods that do not require information about $\|n\|_2$. These include the Generalized Cross Validation (GCV) [27], [48] and the L-curve criterion. These methods are based on the assumption that a good approximation for the regularization parameter is one that minimizes specific functions. In the case of the GCV method, it utilizes a function called the GCV function [48], while the L-curve criterion employs a function known as the L-curve, which depicts the relationship between the 2-norm of the regularized solution and the corresponding residual 2-norm.

It is important to note that all of the aforementioned methods yield regularization parameter values that enable accurate numerical solutions for various applications, such as image processing, remote sensing, EM scattering, etc. However, they typically involve a significant computational burden as they require solving an optimization problem to find a parameter that satisfies certain equalities (in the case of the first category of methods) or minimizing specific functions (in the case of the second category of methods, GCV method, and L-curve criterion). Consequently, the computation time required for implementing these methods may not be suitable for real-time localization in MLAT systems.

In the context of ATC operations, where data update time and system capacity are crucial factors, the aforementioned methods for calculating the regularization parameter are not suitable for real-time localization in MLAT systems. These methods involve significant computational requirements and are not feasible within the constraints of ATC operations.

Two strategies are proposed to estimate the regularization parameter that are more suitable for real-time localization in MLAT systems. The first strategy involves evaluating the problem using several regularization parameter values, typically no more than three, and selecting the one that yields the best results. The second strategy is based on analyzing the spectrum of singular values of the problem and deriving the regularization parameter from that analysis. These strategies provide efficient and practical approaches to estimate the regularization parameter in real-time scenarios.

- **Residual error evaluation:**

The first option for this application is to solve the problem for one, two or three regularization parameters and then choose that solution that corresponds with the minimum residual error. This option is valid for this application because the typical size of the coefficient matrices is normally smaller than 10×3 . Obviously to implement this strategy a relative rigorous analysis of the problem scenario must be carried out. In general, the residual error for an inverse problem is given by:

$$error_j = \frac{\|G(\hat{\theta}_{\lambda_j})\hat{\theta}_{\lambda_j} - \hat{m}\|_2}{\|\hat{m}\|_2}, \quad j = 1, \dots, k \quad (5.22)$$

where k refers to the total evaluated values. For the Taylor-Series Expansion method, the matrix G is an approximation of an exact coefficient matrix, then 5.22 could not be a correct value for the residual error with respect to the true target position. Therefore, it is proposed to calculate the residual error by replacing the regularized solution $\hat{\theta}_{\lambda_j}$ in the non-linear TDOA function in G as follows:

$$error_j = \frac{\|h_{\lambda_j} - \hat{m}\|_2}{\|\hat{m}\|_2}, \quad j = 1, \dots, k \quad (5.23)$$

where vector h_{λ_j} is given by:

$$h_{\lambda_j} = \begin{bmatrix} TDOA_{2,1}(\hat{\theta}_{\lambda_j}) \\ \vdots \\ TDOA_{N_S,1}(\hat{\theta}_{\lambda_j}) \end{bmatrix}_{(N_S-1) \times 1} \quad (5.24)$$

In this strategy, the quality of the regularized solution is evaluated by directly utilizing the non-linear problem instead of relying solely on the classical expression of the matrix-vector product. This approach allows for a more accurate assessment of the regularized solution's quality by considering the specific characteristics and complexities of the non-linear problem at hand.

- **Singular value spectrum inspection:**

The second option involves a real-time inspection of the singular values spectrum of the coefficient matrix G . Before delving into the description of the proposed procedure, it is important to introduce the concepts of the resolution matrix and averaging kernels. In any regularization method, the resolution matrix [27] is defined as follows:

$$\Xi \equiv A_{\lambda}^{-1}G \quad (5.25)$$

The resolution matrix quantifies the amount of smoothing introduced by any particular regularization method. In this sense, the regularized solution $\hat{\theta}_\lambda$ can be written in the following way:

$$\begin{aligned}\hat{\theta}_\lambda &= A_\lambda^{-1} \hat{m}_\Delta + \theta_0 \\ \hat{\theta}_\lambda &= A_\lambda^{-1} (m_\Delta(\theta) + n) + \theta_0 \\ \hat{\theta}_\lambda &= \Xi \Delta \theta + A_\lambda^{-1} n + \theta_0\end{aligned}\tag{5.26}$$

In the case of the LS solution, obtained using the pseudoinverse matrix (which yields the solution with minimum residual 2-norm), the resolution matrix is given by $\Xi = I_3$. Therefore, for a well-conditioned problem, the expected value of θ_{LS} is such that $E[\hat{\theta}_{LS}] = 0$. However, in any regularization method, the resolution matrix differs from I_3 , and the regularized solution $\hat{\theta}_\lambda$ represents a smoothed version of θ . Specifically, each component of the first term in 5.26 corresponds to a weighted average of all elements in θ . The second term in 5.26 represents the contribution of measurement noise, and the third term is the starting point for the Taylor series expansion method.

In Tikhonov regularization, the level of smoothing is determined by the regularization parameter λ , and it follows that if $\lambda = 0$, then $\Xi = I_3$, whereas if $\lambda = \infty$, then $\Xi = 0_3$. In the former case, the regularized solution $\hat{\theta}_\lambda$ approaches the LS solution $\hat{\theta}_{LS}$ (under-smoothing case), while in the latter case, $\hat{\theta}_\lambda$ approaches θ_0 (over-smoothing case). Thus, the resolution matrix provides insight into the precision with which the regularized solution can approximate the exact solution. On the other hand, in order to quantitatively analyze the level of smoothing for each component of the regularized solution, it is necessary to examine each row of the resolution matrix Ξ . The i -th smoothed component [27] can be expressed as follows:

$$(\Xi \theta)_i = \zeta_i^T \theta, \quad i = 1, \dots, 3\tag{5.27}$$

In the literature [27], the set of rows ζ_i^T are known as averaging kernels of the problem, which are used to quantify the influence of observations on the estimated parameters in the regularization process. In order to address ill-conditioned problems, it is crucial to determine the appropriate level of smoothing. The relationship between the i -th averaging kernel ζ_i^T and the i -th Tikhonov filter factor f_i is directly related. If f_i decreases, the amplitudes of ζ_i^T decrease, resulting in increased smoothing for the i -th component of the regularized solution $\hat{\theta}_\lambda$. Conversely, if f_i increases, the amplitudes of ζ_i^T increase, leading to decreased smoothing for the i -th component. Based on the hypothesis that the vertical component of the target position is more ill-conditioned in Mode S Multilateration systems, a formulation is proposed to introduce more smoothing specifically for the vertical component, whose formulation takes the following form:

$$\lambda_k = \sigma_3^k + w(\sigma_2^k - \sigma_3^k)\tag{5.28}$$

where λ_k , σ_2^k , σ_3^k are the regularization parameter value, and the second and third singular values of matrix G , respectively, for the k -th refinement iteration of the Taylor-Series expansion method. Note that factor w controls the weight of the term $(\sigma_2^k - \sigma_3^k)$, and after many observations, it has been observed that it depends mainly on the available number of stations and the operational scenario.

Several studies have extensively investigated the accuracy performance of Local Area Multilateration (LAM)/WAM systems. It has been observed that the 2D problem is typically better conditioned than the vertical problem within the coverage area of the system. However, for areas outside the system perimeter, the conditioning of the 2D and vertical problems becomes similar. Furthermore, a strategy is proposed to update the weight factor, denoted as w , for LAM/WAM localization problems. This strategy suggests adjusting the value of w during refinement iterations. The hypothesis behind this approach is that as the refinement iterations progress, the 2D convergence becomes more stable and the level of ill-conditioning decreases. Consequently, the value of w should be reduced accordingly, as lower ill-conditioning implies a lower regularization parameter (λ). For this type of applications, 5.28 is modified as follows 5.29:

$$\lambda_k = \sigma_3^k + w^k(\sigma_2^k - \sigma_3^k) \quad (5.29)$$

where

$$w^k = \begin{cases} 0.8w^{k-1}, & \sigma_2^k \geq \sigma_2^{k-1} \\ w^{k-1}, & \text{otherwise} \end{cases}, \quad k = 3, \dots, K \quad (5.30)$$

where K is the total number of Taylor iterations. For WAM scenarios like the one proposed for the SBM system (far targets and a number of receiving stations greater than five), $w = 0.03$ is used. However, if LAM MLAT applications should be evaluated, the value of the parameter would be $w = 0.3$, as detailed in [17].

5.2.2 SVD-based Methods

Other regularization methods used to improve the smoothness of the final target position solution rely on the decomposition of singular values, known as SVD-based methods. The classical solution by SVD is in connection with the LS problem. The classical SVD says that, if G is invertible, then its inverse is given by [27], [29]:

$$G^{-1} = \sum_{i=1}^n \frac{v_i u_i^T}{\sigma_i} \quad (5.31)$$

and then, the solution $\hat{\theta}$ is given by:

$$\hat{\theta} = \sum_{i=1}^n \frac{u_i^T \hat{m}_\Delta}{\sigma_i} v_i + \theta_0 \quad (5.32)$$

On the other hand, the pseudoinverse matrix [27] G^\dagger of G is defined as:

$$G^\dagger \equiv \sum_{i=1}^{\text{rank}(G)} \frac{v_i u_i^T}{\sigma_i} \quad (5.33)$$

and, the LS solution to the problem $\|G\theta - \hat{m}\|_2$ is given by:

$$\hat{\theta}_{LS} = G^\dagger \hat{m} = \sum_{i=1}^{\text{rank}(G)} \frac{u_i^T \hat{m}_\Delta}{\sigma_i} v_i + \theta_0 \quad (5.34)$$

The solution obtained through the pseudoinverse meets the first two conditions of Hadamard, but fails to satisfy the third condition. The subsequent results section will demonstrate that when dealing with highly ill-conditioned problems, the solution derived from 5.34 does not produce precise results. In localization problems involving Mode S MLAT, it is typical to have an abundance of measurements from the stations, surpassing the minimum requirement for solving the system of equations. This scenario is known as an over-determined system of hyperbolic equations, and its explicit solution can be expressed as follows:

$$\hat{\theta}_{LS}^{over} = (G^T G)^{-1} G^T \hat{m}_\Delta + \theta_0 = G^\dagger \hat{m}_\Delta + \theta_0 \quad (5.35)$$

In this case, where $G^\dagger = (G^T G)^{-1} G^T$, it is evident that the solution in 5.35 is completely equivalent to the one in 4.63. The only distinction is that the LS solution has been presented in the SVD domain. Furthermore, the solution obtained from 5.35 must also undergo iteration using the same procedure as described in 4.64.

5.2.2.1 Solution by Truncated SVD (T-SVD)

This section explains the solution provided by the T-SVD method, a modified version of SVD. When the matrix G is not precisely rank deficient but instead becomes numerically rank deficient due to an error ϵ , it is advisable to avoid using the classical SVD solution. Instead, it is recommended to employ the rank- k_ϵ matrix G_{k_ϵ} , as defined in references [27] and [29]:

$$G_{k_\epsilon} = \sum_{i=1}^{k_\epsilon} u_i \sigma_i v_i^T \quad (5.36)$$

Here, k_ϵ represents a discrete value commonly referred to as the discrete regularization parameter or truncation parameter for T-SVD. In practice, it is often chosen as $k_\epsilon = r_\epsilon$, which corresponds to the numerical rank of the matrix G in the presence of an error level ϵ . In simpler terms, the main idea behind the T-SVD method is to select a specific number, denoted by k_ϵ , of the largest singular values of the matrix G to form a new coefficient matrix G_{k_ϵ} . This approach aims to enhance the numerical properties of G by disregarding singular values that are close to zero. To further elaborate, let's consider the iterative location estimator in the context of T-SVD as indicated in 4.64. The T-SVD method enables us to express it in the following manner:

$$\hat{\theta}_{k_\epsilon}^k = (G_{k_\epsilon} (\hat{\theta}_{k_\epsilon}^{k-1})^T G_{k_\epsilon} (\hat{\theta}_{k_\epsilon}^{k-1}))^{-1} G_{k_\epsilon} (\hat{\theta}_{k_\epsilon}^{k-1})^T \hat{m}_\Delta (\hat{\theta}_{k_\epsilon}^{k-1}) + (\hat{\theta}_{k_\epsilon}^{k-1}) \quad (5.37)$$

for $k = 1, \dots, K$, being $\hat{\theta}_{k_\epsilon}^k$ the solution provided by the T-SVD, and $\hat{\theta}_{k_\epsilon}^0$ the starting point as required for Taylor-Series-based methods. The covariance matrix of the measurement errors here is assumed to be an identity matrix. In addition, k refers to the iteration index, whilst k_ϵ corresponds to the regularization parameter for T-SVD. In this sense, the numerical solution of 5.37 can be expressed in terms of the SVD matrix of G by using 5.36 as indicated in [27], whose expression is:

$$\hat{\theta}_{k_\epsilon}^k = G_{k_\epsilon}^\dagger(\hat{\theta}_{k_\epsilon}^{k-1})\hat{m}_\Delta(\hat{\theta}_{k_\epsilon}^{k-1}) + \hat{\theta}_{k_\epsilon}^{k-1} = \sum_{i=1}^{k_\epsilon} \frac{(u_i^{k-1})^T \hat{m}_\Delta(\hat{\theta}_{k_\epsilon}^{k-1})}{\sigma_i^{k-1}} v_i^{k-1} + \hat{\theta}_{k_\epsilon}^{k-1} \quad (5.38)$$

also evaluated for $k = 1, \dots, K$. Generally, the type of scenarios where T-SVD can be applied is the same than those used for the Tikhonov regularization. For this reason, the stop criteria described in 4.65 can also be applied here.

The solution derived from 5.38 is a unique solution that possesses the minimum 2-norm and ensures stability. Consequently, this solution satisfies all three Hadamard's conditions. However, a crucial aspect when using 5.38 is the proper selection of the error level ϵ or the regularization parameter k_ϵ . The error level ϵ is derived from the assumption that the matrix G can be expressed as $G = G^{exact} + E$, where G^{exact} is precisely rank deficient, and E represents a perturbation of G^{exact} . The perturbation can arise from various sources. In [27], the author proposes that the error level ϵ should satisfy $\|E\|_2$. However, since the perturbation matrix and its 2-norm are unknown, the previously mentioned strategy for estimating the matrix rank becomes less effective in this scenario.

The selection or estimation of the regularization parameter plays a crucial role in applying T-SVD regularization. Unlike Tikhonov regularization, which has a continuous parameter, T-SVD regularization relies on a discrete parameter with specific differences in estimation or selection. As indicated in 5.36, the discrete regularization parameter can range from zero to n , where n represents the number of target position coordinates to be estimated, typically three in the case of general MLAT localization. However, if the regularization parameter is set to $k_\epsilon = 3$, no regularization is applied, resulting in the LS solution 4.64. On the other hand, when the regularization parameter is $k_\epsilon = 0$, all singular values of the Jacobian differential matrix G are ignored, rendering 5.38 incapable of providing a valid solution. Therefore, for MLAT localization problems, it seems that the regularization parameter k_ϵ can only assume two values (1 or 2) when regularization is needed, and one value (3) when no regularization is required.

Similarly, there are various methods available to estimate the regularization parameter for T-SVD regularization. However, it's important to note that the limitations mentioned earlier also apply to this method. Based on observations and findings, a viable approach for selecting the regularization parameter is to solve the problem outlined in 5.38 for $k_\epsilon = 2$ and $k_\epsilon = 3$. Extensive testing has shown that setting $k_\epsilon = 1$ does not provide useful solutions due to significant information loss, so it is not further considered. Following the procedure proposed for Tikhonov regularization, a similar strategy can be employed for T-SVD regularization. Additionally, an equivalent approach described in [42] can be used to improve the performance of this type of applications using T-SVD regularization. The strategy is as follows:

$$k_\epsilon^k = \begin{cases} 3, & \sigma_2^k \geq \sigma_2^{k-1} \\ 2, & \text{otherwise} \end{cases}, \quad k = 3, \dots, K \quad (5.39)$$

where K is the total number of Taylor iterations, and $k_\epsilon^1 = k_\epsilon^2 = 2$ for WAM/LAM applications.

5.2.2.2 T-SVD with Sub-set Selection

In addition to the T-SVD solution, there is another SVD-based method known as T-SVD-SS. This method is quite similar to the previously described approach, with the difference being that instead of selecting the entire set of k_ϵ columns, the k_ϵ most linearly independent columns from matrix G are extracted. To achieve this, a permutation matrix Π is utilized to minimize the condition number of the resulting sub-matrix \hat{G}_{k_ϵ} . The new matrix is formed by taking the first k_ϵ columns of the matrix $G\Pi$. The solution for T-SVD-SS is given by references [27] and [29]:

$$\hat{\theta}_{k_\epsilon}^{basic} = \Pi \begin{pmatrix} \hat{G}_{k_\epsilon}^\dagger \hat{m}_\Delta \\ 0 \end{pmatrix} + \begin{pmatrix} \theta_0 \\ 0 \end{pmatrix} \quad (5.40)$$

The solution $\hat{\theta}_k^{basic}$ in 5.40 has zero values in the positions corresponding to the neglected columns of matrix G . The permutation matrix Π can be easily obtained using a QR factorization routine described in [29]. The T-SVD-SS approach is characterized by its dependence on estimating an error level in the QR factorization. However, estimating the error level ϵ poses significant challenges in finding an approximate and suitable value. This can result in a QR factorization that produces a matrix \hat{G}_{k_ϵ} equal to the original matrix G , thereby losing the benefits of proper regularization for improving estimations. Consequently, the T-SVD-SS method will not be further described. Moreover, extensive trials and simulations have demonstrated that this method does not yield accurate or reliable results for the intended application. Therefore, T-SVD-SS is considered inappropriate for SBM systems.

5.2.3 TLS-based methods

The methods discussed earlier focus solely on potential errors in the measurement vector \hat{m} . They assume that error sources in solving the general inverse problem $G\theta = \hat{m}$ are confined to the measurement vector \hat{m} . However, there are situations where the matrix G may not be precisely known or contains errors due to measurements or approximations of the exact operator. Additionally, linearization or discretization errors may arise. To address these cases, the TLS method was developed [49] to solve the inverse problem while considering both the potential errors in the coefficient matrix G and their magnitude relative to those in the measurement vector \hat{m} . The main idea of TLS method is to allow a residual vector and a residual matrix. In this context, the solution to the inverse problem involves finding a vector θ that minimizes the following optimization problem:

$$\min \|(G, \hat{m}) - (\tilde{G}, \hat{m}')\|_F \quad \text{subject to } \hat{m}' = \tilde{G}\theta \quad (5.41)$$

where \tilde{G} is the perturbed coefficient matrix, \hat{m}' is the equivalent perturbed version of the measurement vector, and $\|\cdot\|_F$ denotes the Frobenius norm which, for a general $m \times n$ matrix A is defined as in [29]:

$$\|A\|_F = \sqrt{\sum_{i=1}^{\min(m,n)} \sigma_i^2} \quad (5.42)$$

where σ_i represents the i -th singular value of matrix A . Therefore, the solution to the localization problem using 5.41 can be expressed in terms of the SVD of the augmented matrix $[G, \hat{m}_\Delta]$ as follows:

$$[G, \hat{m}_\Delta] = \bar{U} \bar{\Sigma} \bar{V}^T \quad (5.43)$$

being $\bar{\Sigma}$ the matrix of singular values of $[G, \hat{m}_\Delta]$, and it takes the following form:

$$\hat{\theta}_{TLS}^k = -\bar{v}_{1:n,n+1}^{k-1} \frac{1}{\bar{v}_{n+1,n+1}^{k-1}} + \theta_0^{k-1}, \quad k = 1, \dots, K \quad (5.44)$$

Here, $\bar{v}_{1:n,n+1}^{k-1}$ represents the $(n+1)$ -th right singular vector of 5.43, with dimensions $n \times 1$, corresponding to the $(k-1)$ -th iteration of the Taylor series. In other words, 5.43 is computed using $[G(\hat{\theta}_{TLS}^{k-1}), \hat{m}_\Delta(\hat{\theta}_{TLS}^{k-1})]$. In cases where the problem is ill-conditioned, especially with a rank-deficient coefficient matrix, it is advisable to avoid using the solution 5.44 obtained from TLS. Instead, similar to the T-SVD approach, it is recommended to use the truncated version of TLS for more reliable results.

5.2.3.1 Solution by Truncated TLS (T-TLS)

In a similar manner to the SVD and T-SVD solutions, when matrix G is either rank deficient or numerically rank deficient, it is common practice to discard all singular values that are zero or close to zero from the augmented matrix $[G, \hat{m}]$. The resulting problem, using the truncated matrix, is known as T-TLS [49]. It represents a modified version of the original ill-conditioned problem, where the modification is based on both the matrix G and the measurement vector \hat{m} . By introducing the truncation parameter k_{T-TLS} , which denotes the number of retained singular values from $[G(\hat{\theta}_{TLS}^{k-1}), \hat{m}_\Delta(\hat{\theta}_{TLS}^{k-1})]$, the matrix \bar{V} can be partitioned into a $(n+1) \times (n+1)$ matrix as follows:

$$\bar{V} = \begin{pmatrix} \bar{V}_{11} & \bar{V}_{12} \\ \bar{V}_{21} & \bar{V}_{22} \end{pmatrix} \quad (5.45)$$

where $\bar{V}_{11} \in \mathbb{R}^{n \times k_{T-TLS}}$, then, the iterative localization estimator in the sense of T-TLS can be obtained the following way:

$$\hat{\theta}_{k_{T-TLS}}^k = -\bar{V}_{12}^{k-1} (\bar{V}_{22}^\dagger)^{k-1} + \hat{\theta}_{k_{T-TLS}}^{k-1} = -\bar{V}_{12} (\bar{V}_{22}^T)^{k-1} \|\bar{V}_{22}^{k-1}\|_2^{-2} + \hat{\theta}_{k_{T-TLS}}^{k-1} \quad (5.46)$$

It is necessary to ensure that $\bar{V}_{22} \neq 0$ when partitioning the matrix \bar{V} as described. It should be noted that if $k_{T-TLS} = n$, then $\hat{\theta}_{k_{T-TLS}} = \hat{\theta}_{T-TLS}$. The selection of the truncation parameter k_{T-TLS} is crucial for the correct implementation of this method. Similar to the principle used for T-SVD, different values are used for T-TLS. In this case, the values are $k_{T-TLS} = 1$ and $k_{T-TLS} = 2$, instead of the values 2 and 3 used for T-SVD.

However, due to the size of the coefficient matrix, there are limited options for appropriate truncation parameter values. For ill-conditioned situations, it is advisable to set $k_{T-TLS} = 2$. It is important to highlight a significant difference between these two methods in terms of truncation parameter selection.

In the T-SVD algorithm, a larger regularization parameter results in less regularization introduced. On the other hand, in T-TLS, a larger regularization parameter leads to greater regularization. This distinction highlights how the algorithms are modified: for T-SVD, the modification depends solely on the coefficient matrix G , while for T-TLS, both the coefficient matrix G and the measurement vector \hat{n} are modified.

5.3 Indirect Regularization Methods

As mentioned earlier, regularization methods like Indirect Regularization Method (IRM) rely on iterative schemes that involve matrix-vector products to access the coefficient matrix. One notable characteristic of IRM is that it does not require explicit calculations to obtain the coefficient matrix, unlike Direct Regularization Method (DRM). There are various types of IRM that can be employed to solve ill-posed linear inverse problems. Some examples include:

- The Landweber iteration: applicable to both linear and nonlinear cases.
- The Iteratively Regularized Landweber method: an extension of the Landweber iteration.
- The Gauss-Newton method: primarily used in nonlinear cases.
- The Iteratively Regularized Gauss-Newton method: an extension of the Gauss-Newton method.

Providing a detailed description and analysis of these four regularization methods exceeds the scope of this project. However, comprehensive information on these methods can be found in publications such as [31] and [50].

5.4 Localization strategy for SBM systems

Extensive analysis and simulations have yielded insights for developing a comprehensive localization strategy for MLAT systems. No single algorithm consistently achieves optimal performance, so a recommended approach is combining closed form and open form algorithms for a near-optimal strategy. Implementing simple yet effective strategies further enhances performance.

The strategy involves two steps: area detection and localization. In area detection, estimating the target's potential location area is crucial. Using two methods simultaneously is advisable, extracting relevant navigation data from messages and applying a closed form algorithm for an initial position. The localization process follows area detection and operates at a specific update rate defined by EUROCAE. It combines closed form and Taylor-based algorithms with regularized estimators, such as Tikhonov or T-SVD based. Analyzing scenarios helps determine suitable estimators.

Based on area detection information, projected or non-projected closed form algorithms are used to calculate the initial position. A selected regularized estimator refines the position estimation. For applications like SBM, using barometric altitude or the closed form algorithm's altitude is recommended. Overall, this comprehensive strategy achieves accurate and reliable position estimation for MLAT systems.

Part IV

Examples

Chapter 1

Graphical User Interface (GUI)

To effectively showcase the project results, a user-friendly graphical interface, referred to as GUI, has been meticulously developed within Matlab using the internal app designer. This interface empowers the user to execute simulations by configuring various inputs, selecting operating modes, and specifying desired output results. The two operating modes will be elucidated, highlighting their key aspects.

The meticulously designed interface encompasses over 50 distinct inputs that cater to various aspects of running a simulation. Figure 4.1.1 provides a visual representation of the interface design, aiding in understanding its layout and components.

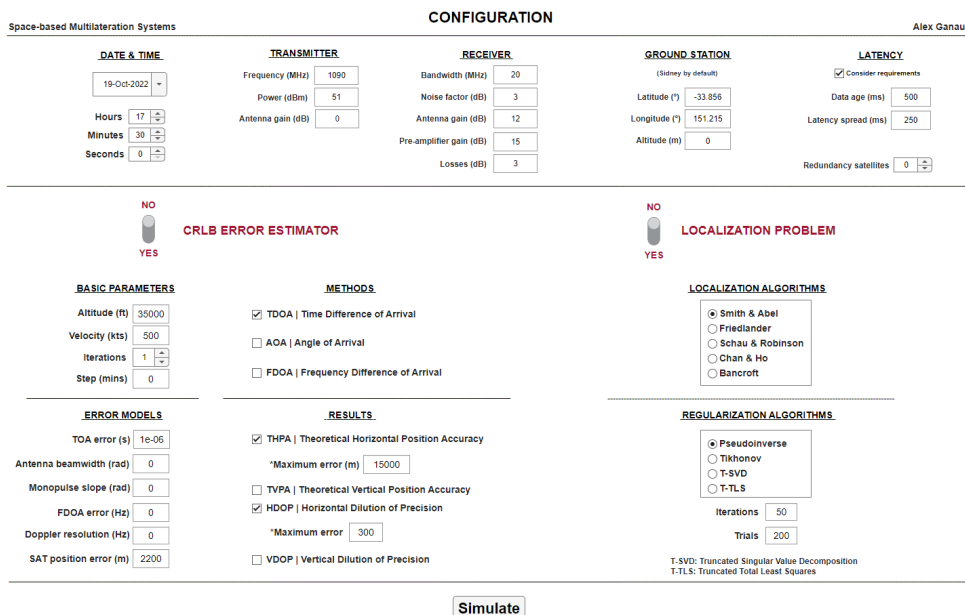


Fig. 4.1.1: Matlab GUI.

The descriptions of the two different operating modes are:

- **CRLB error estimator:**

This operational mode computes the CRLB of a system defined by a given constellation and several measurement error terms that can be configured separately. The CRLB represents the lowest error that could be achieved for a particular configuration. The analysis also considers the number of satellites that could be used to estimate the aircraft position at a given point considering the effect of the ISL network.

To accomplish this, it is crucial to find specific paths for satellite communication, meeting the necessary latency requirements to prevent losses of information. Two requirements have been defined: the data age, which denotes the maximum allowable lifetime of information over a single link before reaching the GS, and the latency spread, representing the maximum available time window to receive all the packets without any loss of information. The GS has been considered to be in Sydney (without loss of generality), with latitude/longitude coordinates of -33.856° and 151.215° .

- **Localization problem:**

The second operating mode is aimed at estimating the position of an airplane, denoted as θ , using an inverse problem approach. The localization algorithms employed in this project provide an initial estimate, which is then refined and made more accurate through the use of regularization algorithms in an iterative manner. The inverse problem involves determining the unknown position of the airplane based on the available data and measurements. It is a challenging task due to various factors such as measurement errors, noise, and limited information. The localization algorithms play a crucial role in providing an initial estimation of the airplane's position, which serves as a starting point for further refinement.

Once the initial estimate is obtained, regularization algorithms are employed to improve the accuracy and reliability of the position estimation. These algorithms utilize mathematical techniques to impose constraints and smoothness on the estimated position, effectively reducing the impact of noise and measurement errors. Through an iterative process, the regularization algorithms refine the position estimate until a more precise solution is achieved. By combining localization algorithms with regularization algorithms, this operating mode aims to achieve accurate and robust estimation of the airplane's position, enabling improved tracking and monitoring capabilities.

Furthermore, the estimation errors generated by these algorithms are displayed alongside the CRLB obtained from the error estimator. This visual representation enables easy comparison of results along a trajectory, simulating different flight routes of airplanes. By juxtaposing the estimation errors with the CRLB, it becomes convenient to assess the performance and accuracy of the estimation algorithms throughout the simulated flights.

Chapter 2

Iridium constellation

First, studies will be carried out using the Iridium Constellation. Figure 4.2.1 shows the satellite scenario with the distributed satellites, for a fixed simulation date and time (Oct 19, 2022 | 17:30:00), and Figure 4.2.2 displays the sensor network of the constellation, it is, the coverage area that characterizes the orbiting satellites. Since the orbital period of the Iridium constellation is 100.4 minutes, it has been decided to analyze five different cases separated 20 minutes each, so the total period is covered. The simulation parameters used for the initial case are those shown in Figure 4.1.1.

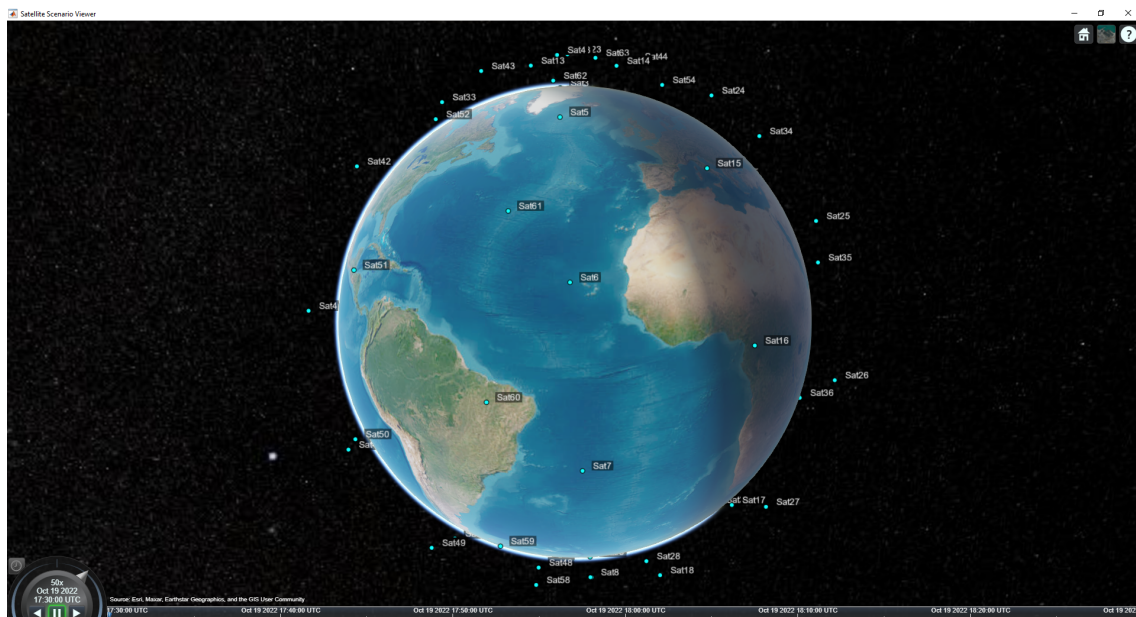


Fig. 4.2.1: Iridium constellation: Satellite distribution.

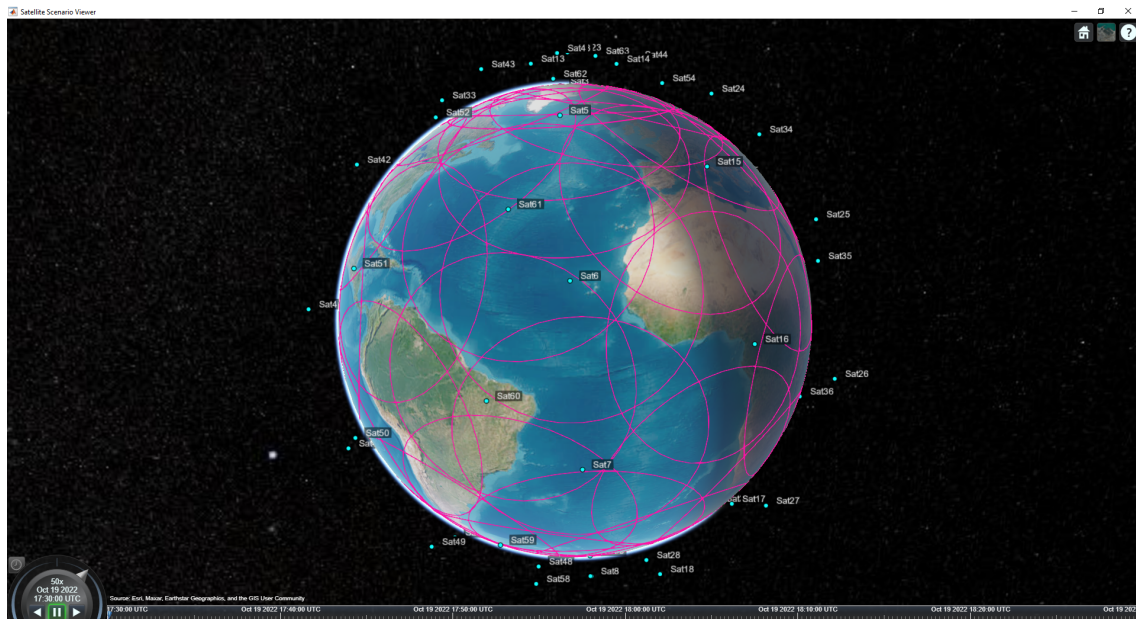


Fig. 4.2.2: Iridium constellation: Satellite sensors.

About simulations and results displaying values of -1, -2, or -3, the following should be clarified:

- **-1**, when the number of available satellites is smaller than the minimum of satellites required for establishing connections.
- **-2**, when the THPA obtained is greater than the maximum admitted horizontal error.
- **-3**, when the HDOP obtained is greater than the maximum admitted horizontal DOP.

2.1 North Atlantic

The area selected corresponding to the North Atlantic region is shown in Figure 4.2.3, and is made of 40 points, with 5 variations in latitude and 8 in longitude.

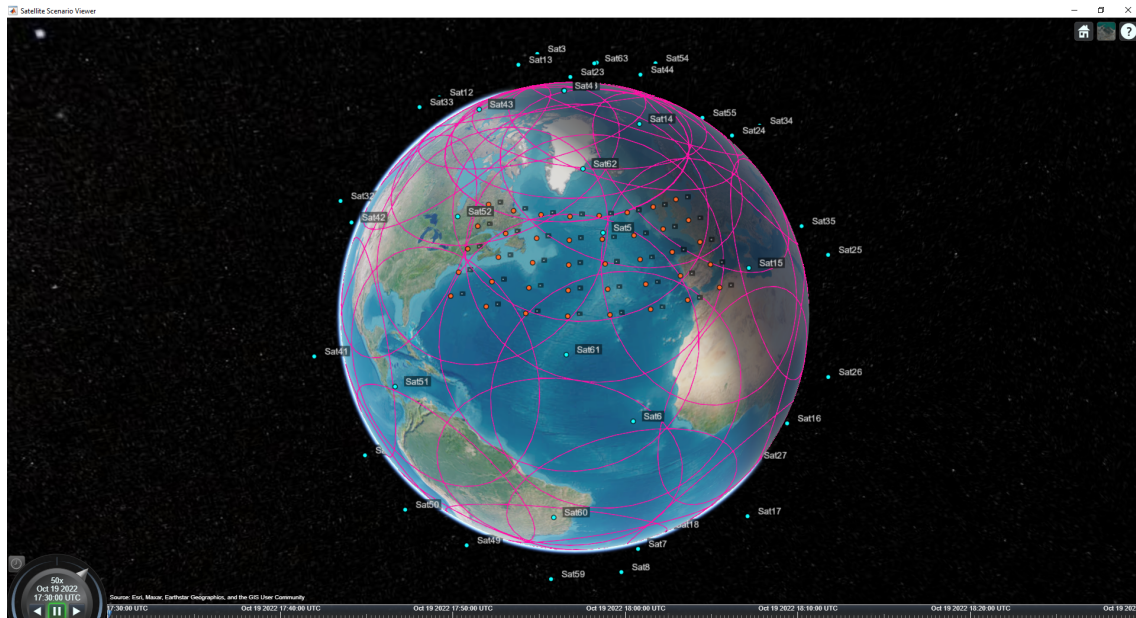


Fig. 4.2.3: Region I: North Atlantic airspace.

Figure 4.2.4 shows the connections between the points and the satellites.

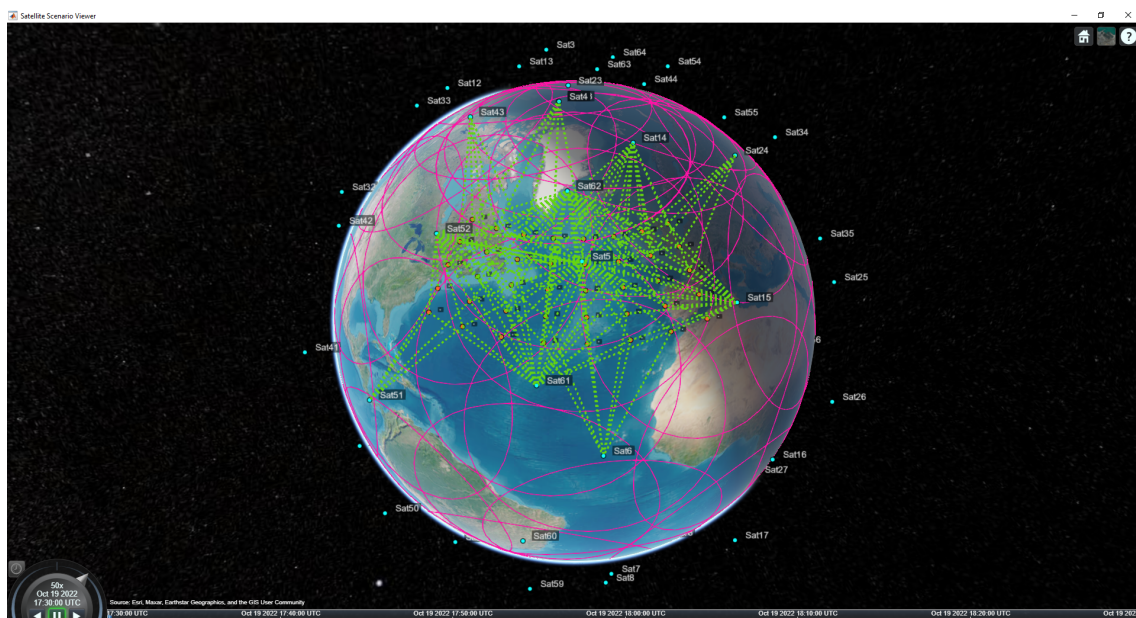


Fig. 4.2.4: North Atlantic: Simultaneous connections.

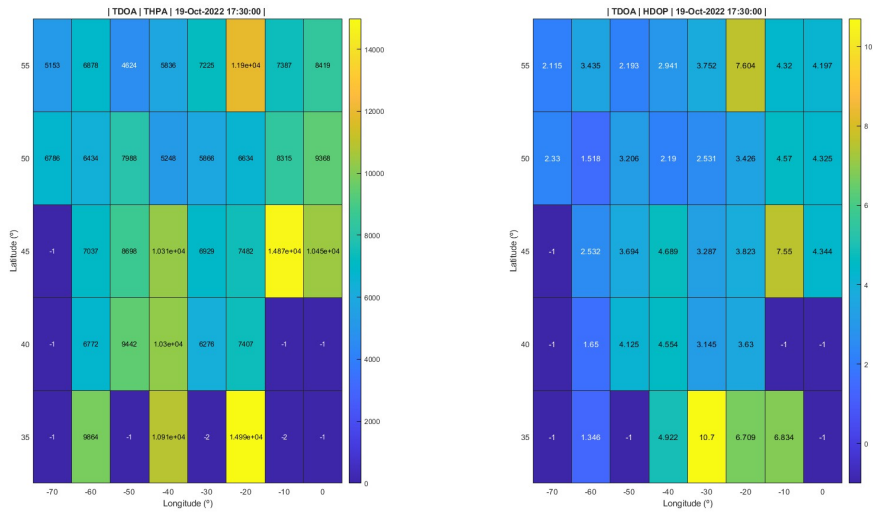


Fig. 4.2.5: Iridium | North Atlantic | TOA: 17:30h.

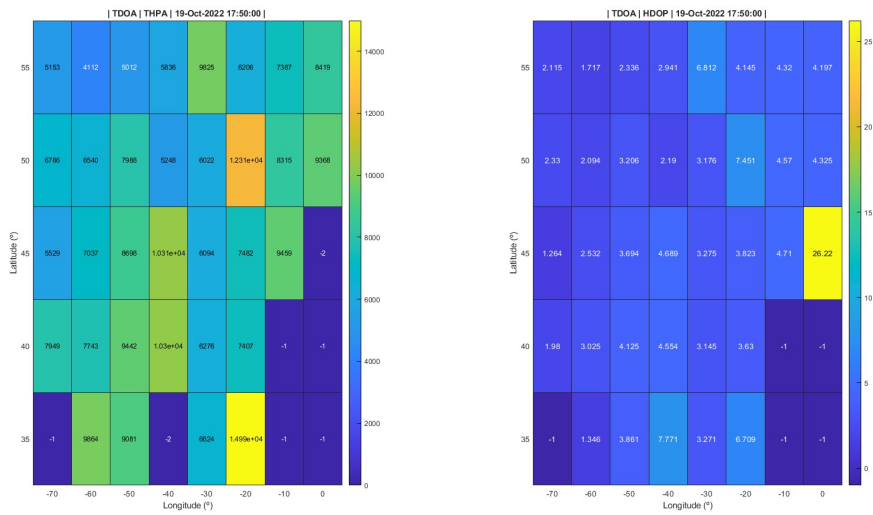


Fig. 4.2.6: Iridium | North Atlantic | TOA: 17:50h.

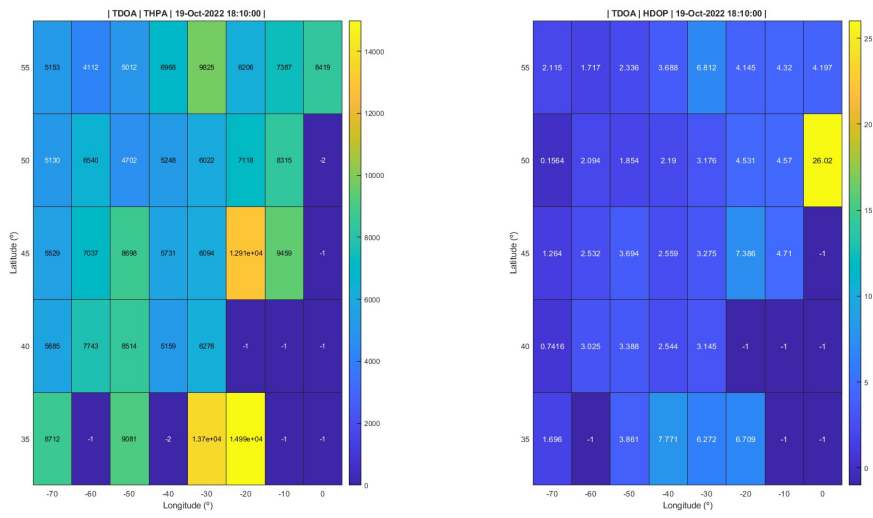


Fig. 4.2.7: Iridium | North Atlantic | TOA: 18:10h.

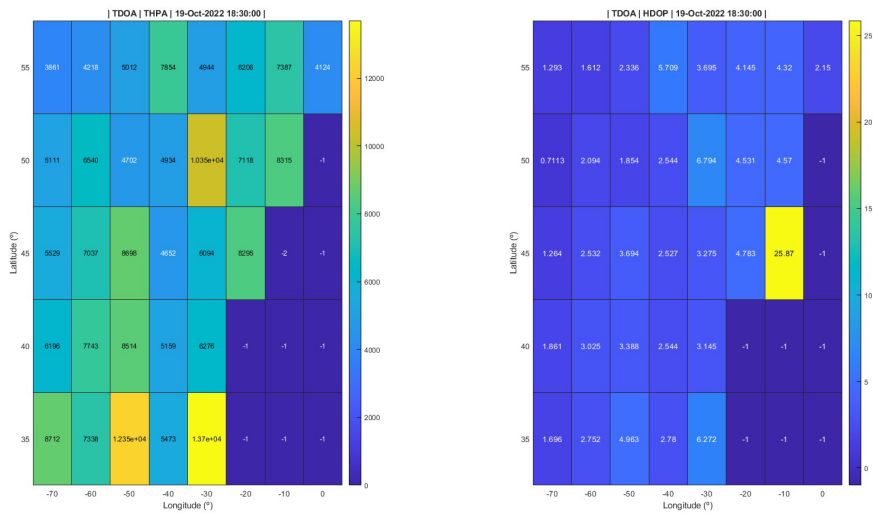


Fig. 4.2.8: Iridium | North Atlantic | TOA: 18:30h.

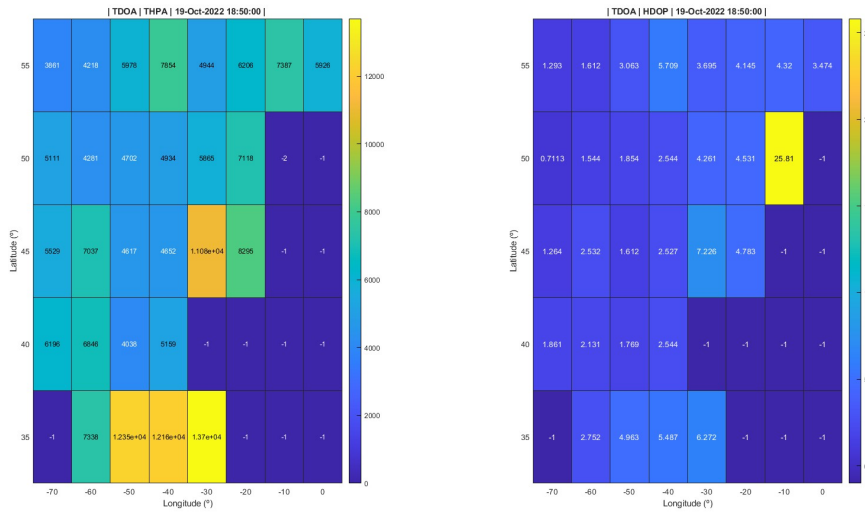


Fig. 4.2.9: Iridium | North Atlantic | TOA: 18:50h.

2.2 South Atlantic

The region corresponding to the South Atlantic airspace can be appreciated in Figure 4.2.10, and is made of 49 points, with 7 variations in latitude and 7 in longitude.

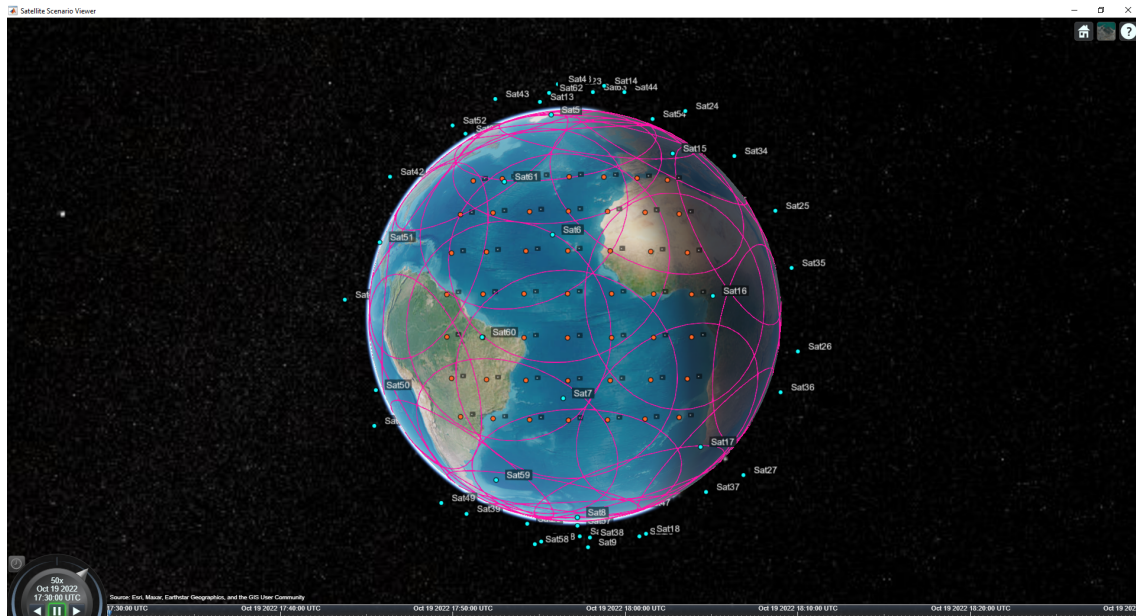


Fig. 4.2.10: Region II: South Atlantic airspace.

Connections between the points and the satellites can be appreciated in Figure 4.2.11.

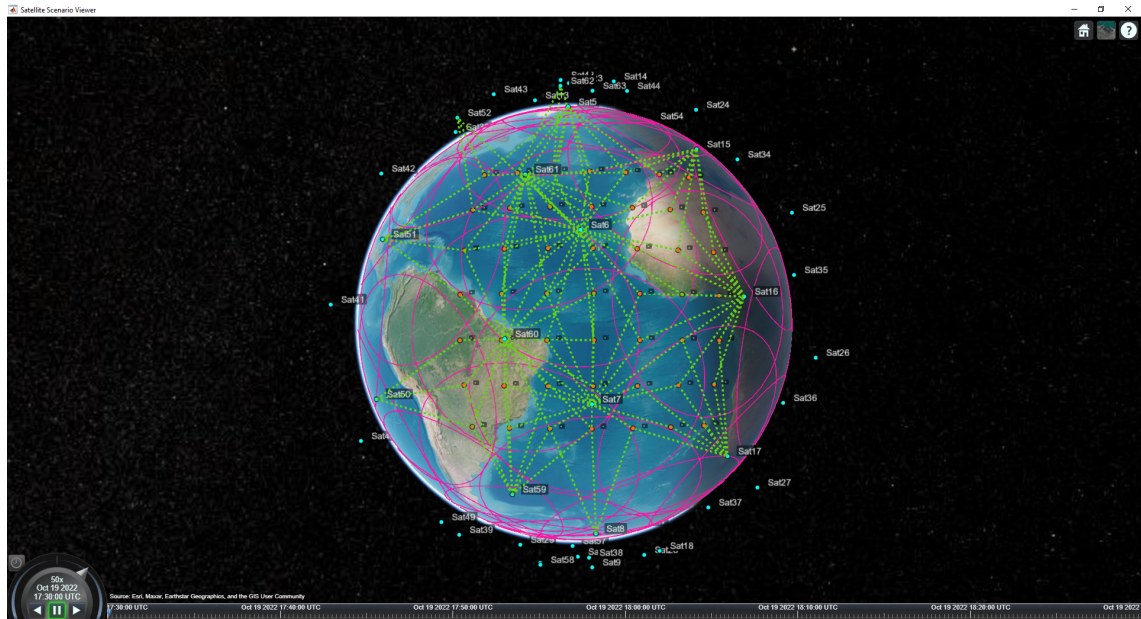


Fig. 4.2.11: South Atlantic: Simultaneous connections.

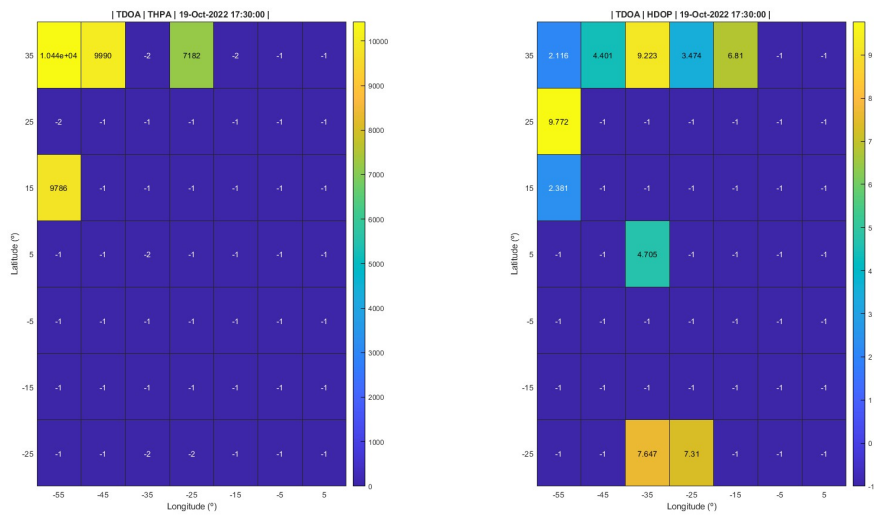


Fig. 4.2.12: Iridium | South Atlantic | TOA: 17:30h.

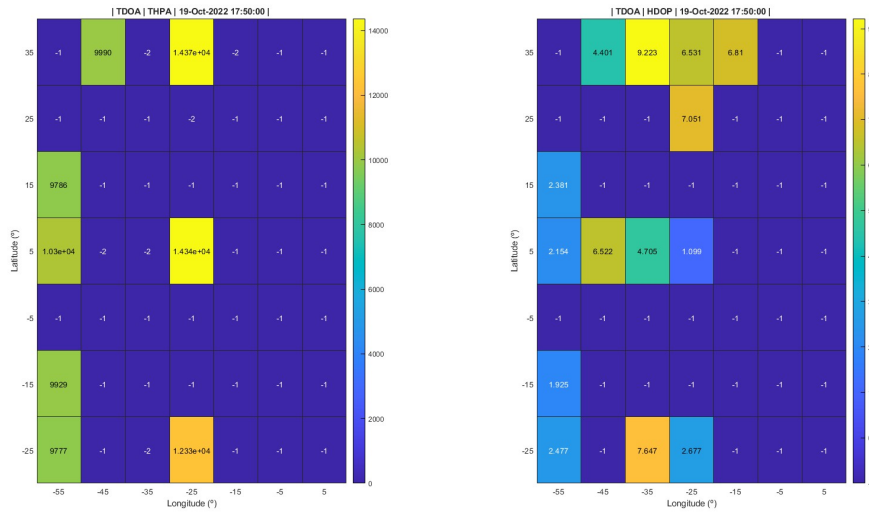


Fig. 4.2.13: Iridium | South Atlantic | TOA: 17:50h.

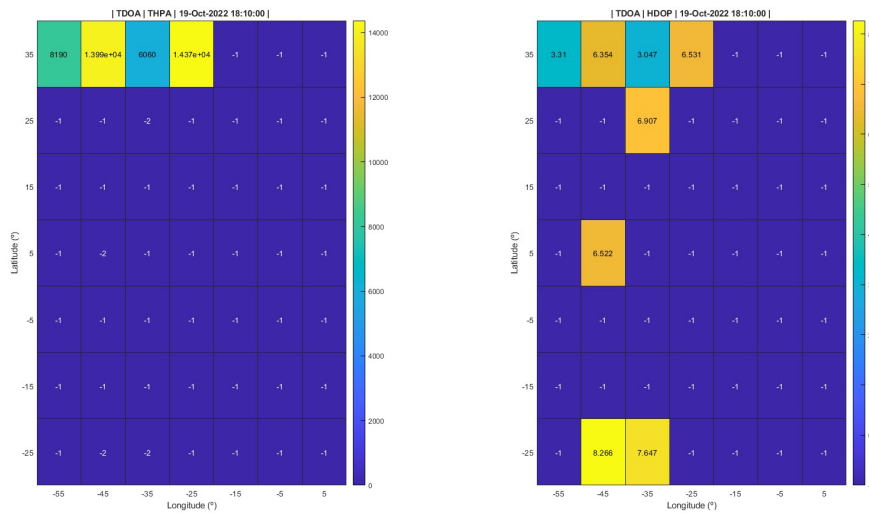


Fig. 4.2.14: Iridium | South Atlantic | TOA: 18:10h.

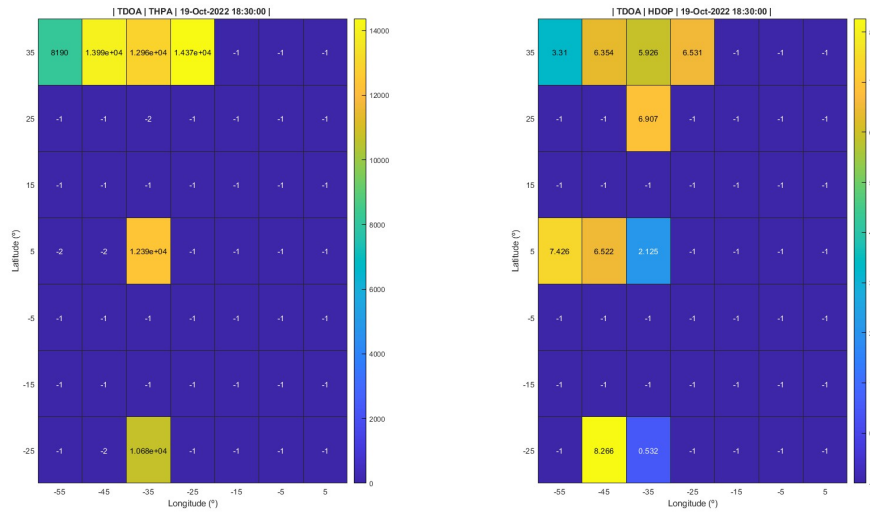


Fig. 4.2.15: Iridium | South Atlantic | TOA: 18:30h.

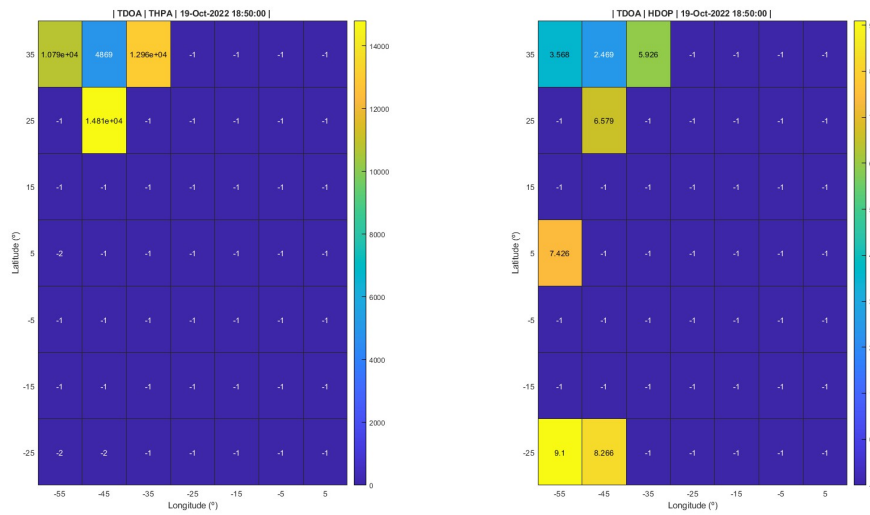


Fig. 4.2.16: Iridium | South Atlantic | TOA: 18:50h.

2.3 Key points

On the verge of results obtained with the Iridium constellation, the following points can be concluded:

- **North Atlantic airspace:**

- **HDOP:**

While Iridium satellites offer global coverage, there are certain locations where the number of satellites capable of receiving the emitted squitter signal from an airplane is insufficient to compute the position by MLAT, which requires a minimum of four satellites for the TDOA case studied. With alternative measurements, the required number of satellites would be smaller, therefore, more connections should take place.

A significant portion of these points lack adequate satellite coverage, it is, the minimum number of satellites tends not to be accomplished. In the graphs, these cases are represented as "-1". To address this challenge, a new satellite constellation is proposed as a solution to alleviate the connectivity issue encountered.

- **THPA:**

In situations where no connections occur, it is not possible to obtain a valid horizontal error. Moreover, for certain points that actually have an associated HDOP value, elevated horizontal errors are obtained, surpassing the user-defined threshold (set at 15 km) on the interface. In such cases, the simulation results display a "-2".

- **South Atlantic airspace:**

- **HDOP:**

Due to the unsuitable geometry of the Iridium constellation, in the South Atlantic region, connections cannot be established effectively along the equator. Consequently, a significant number of interest points in this area remain unconnected.

- **THPA:**

The horizontal accuracy errors rely on the ability to establish valid connections, and the analysis reveals that only a small percentage of the total interest points exhibit both an HDOP and a THPA error, although some may exceed the predefined threshold. In order to tackle this challenge, a proposed solution emerges in the form of a new satellite constellation, aimed at improving the connectivity issue at hand.

Chapter 3

Proposed constellation

Next, the proposed constellation, which was introduced in *Part II - Chapter 2 - Section 2.6: Proposed constellation*, will be analyzed. The spatial arrangement and coverage area of the satellites are illustrated in Figures 4.3.1 and 4.3.2, respectively.

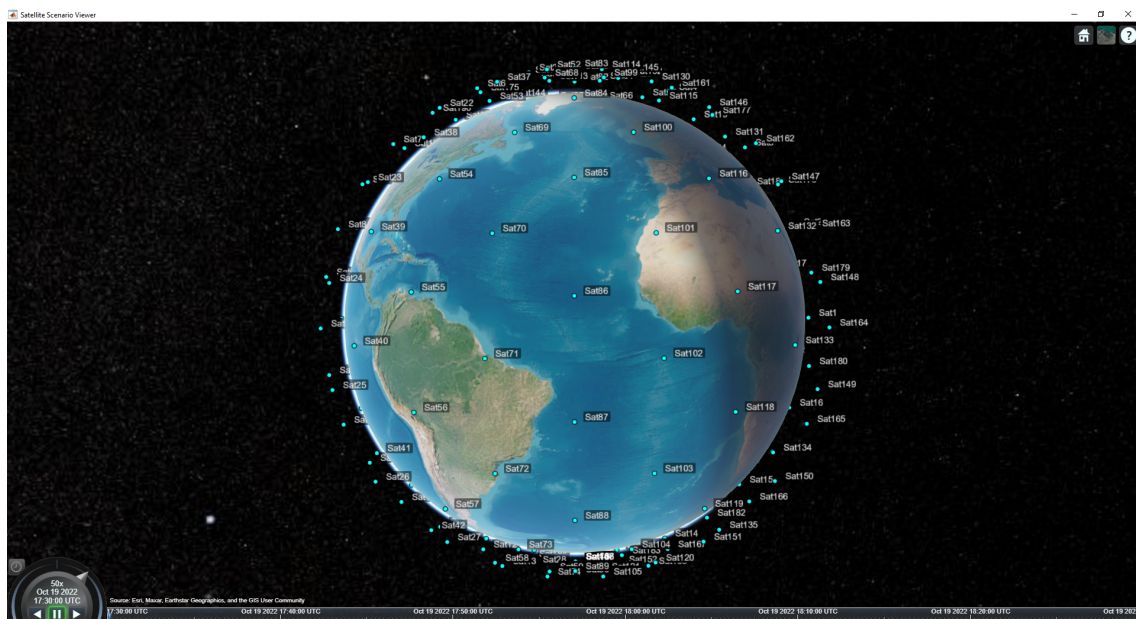


Fig. 4.3.1: Proposed constellation: Satellites distribution.

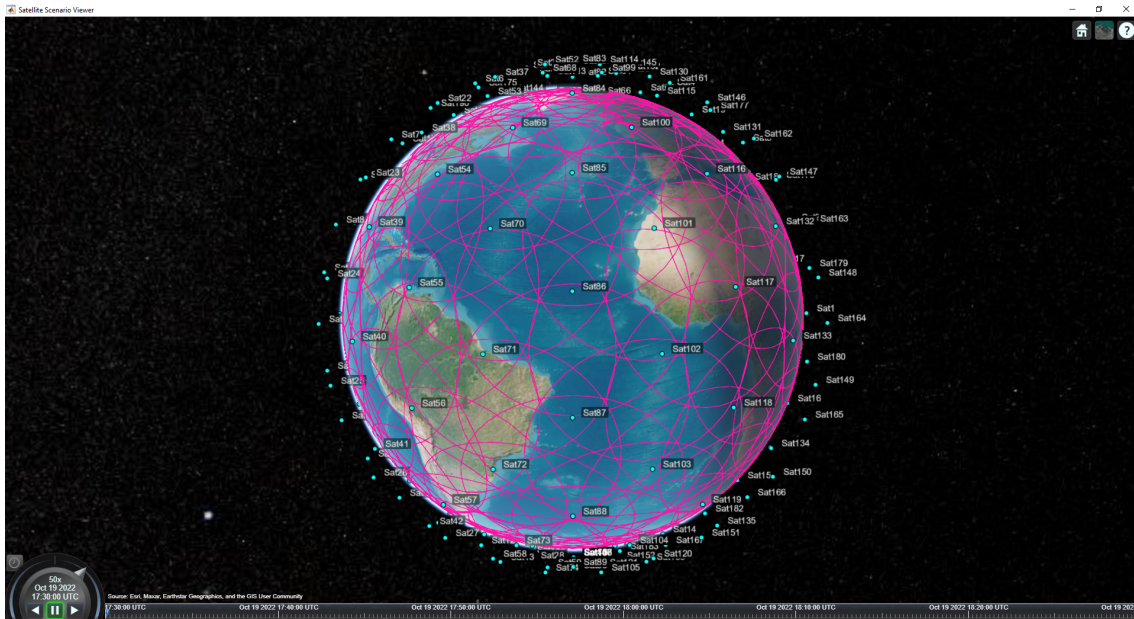


Fig. 4.3.2: Proposed constellation: Satellites sensors.

To demonstrate how the error estimator behaves with the proposed constellation, it is advisable to conduct several use cases. These cases rely on the different source error measurements, which have been elaborated in *Part I - Chapter 2 - Section 2.3.4: Hybrid MLAT Systems: Error Models*, and appear outlined in Table 4.3.1:

Error	1	2	3	4	5	6	7	8
TOA (μs)	1	1	1	1	1	0.1	0.01	0.001
SAT position (m)	2200	550	100	50	25	50	50	50

Table 4.3.1: Error models for the different use cases.

The first case uses the errors in time and satellite positioning that align with the values utilized for Iridium. For a fixed TOA error ($1 \mu\text{s}$), variations in the satellite position error have been tested to find a consistent and appropriate value to reach, approximately, the threshold value in which the influence of the satellite position error does not change (or improve) anymore the results. Simulations are carried out for positioning errors from 2200 to 25 m. The ideal case would be to have a null satellite position error, but since this will never be realistic nor feasible to achieve, given that the results show no significant improvements when changing from 50 to 25 m, the subsequent investigation will proceed considering 50 m as a feasible (and more realistic) solution, in terms of estimating the true satellites positions. Further tests are conducted by varying the time error to explore its impact on the analyses (from $1 \mu\text{s}$ to 1 ns), and thus, propose a final error model for the MLAT system designed. The TOA error selected is 10 ns, since applying 1 ns does not improve the results. By adjusting the time and positioning errors, the remaining and dominant contributor to the estimated errors is the SNR, which is not open to changes given that some of the solutions would encompass approaching the satellites to the Earth, or the airplanes to emit with higher power, which is actually limited.

3.1 Case 1: TOA error = 1 μ s | SAT position error = 2200 m

3.1.1 North Atlantic

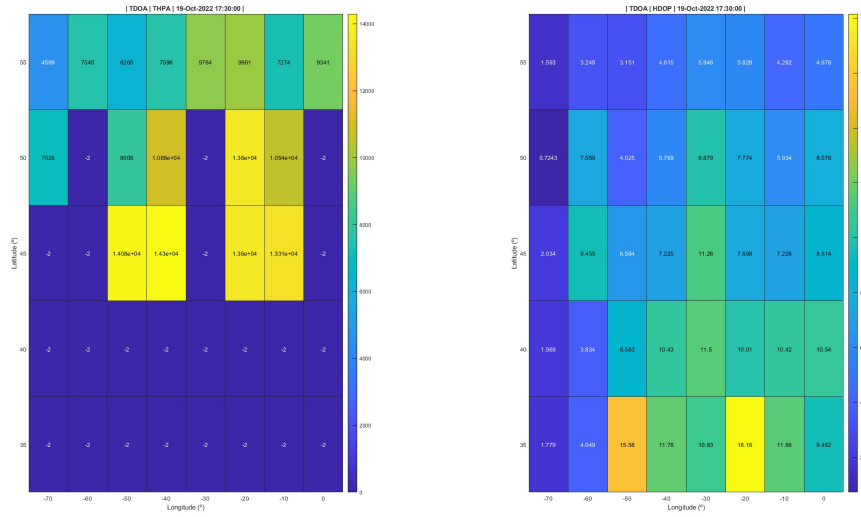


Fig. 4.3.3: Case 1 | North Atlantic | TDOA | THPA + HDOP | 17:30h.

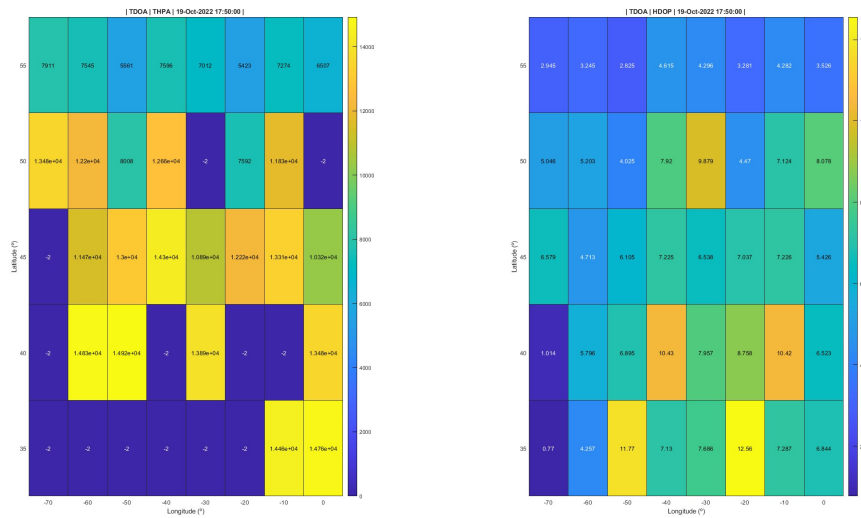


Fig. 4.3.4: Case 1 | North Atlantic | TDOA | THPA + HDOP | 17:50h.

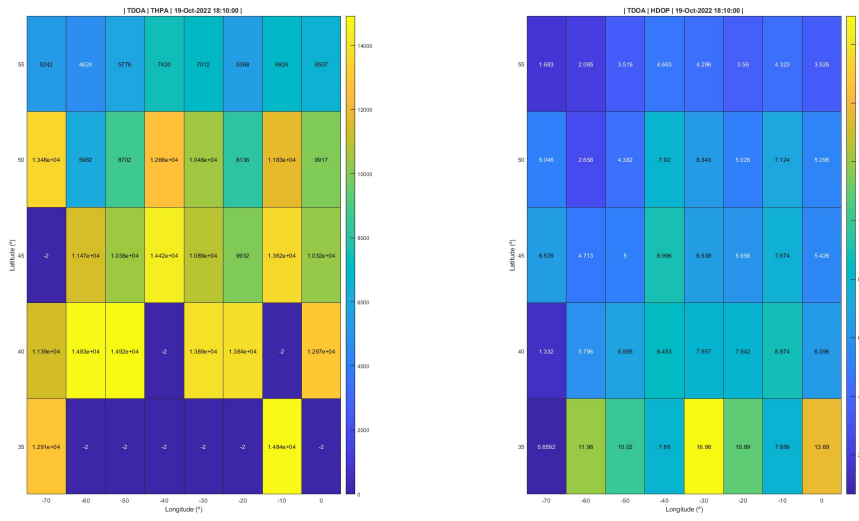


Fig. 4.3.5: Case 1 | North Atlantic | TDOA | THPA + HDOP | 18:10h.

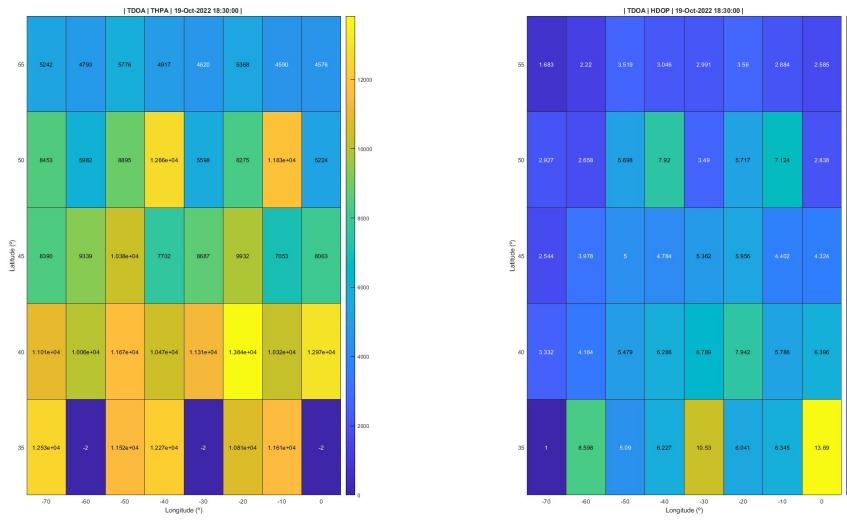


Fig. 4.3.6: Case 1 | North Atlantic | TDOA | THPA + HDOP | 18:30h.

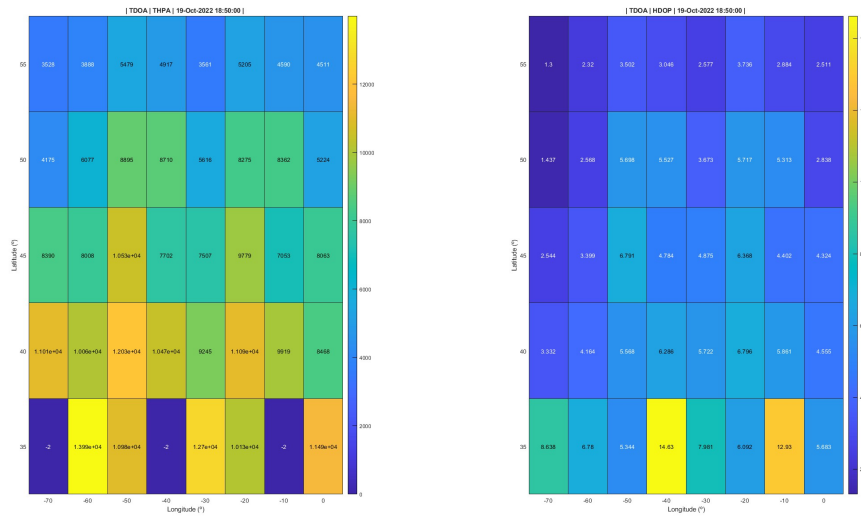


Fig. 4.3.7: Case 1 | North Atlantic | TDOA | THPA + HDOP | 18:50h.

3.1.2 South Atlantic

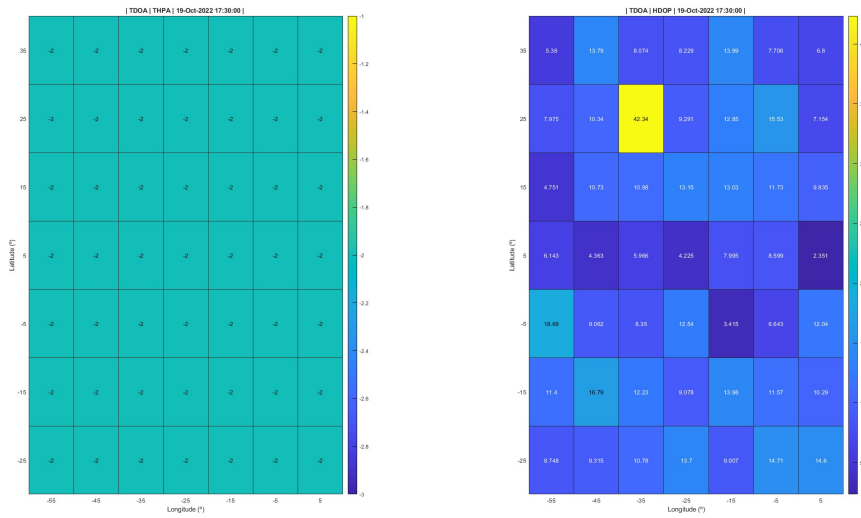


Fig. 4.3.8: Case 1 | South Atlantic | TDOA | THPA + HDOP | 17:30h.

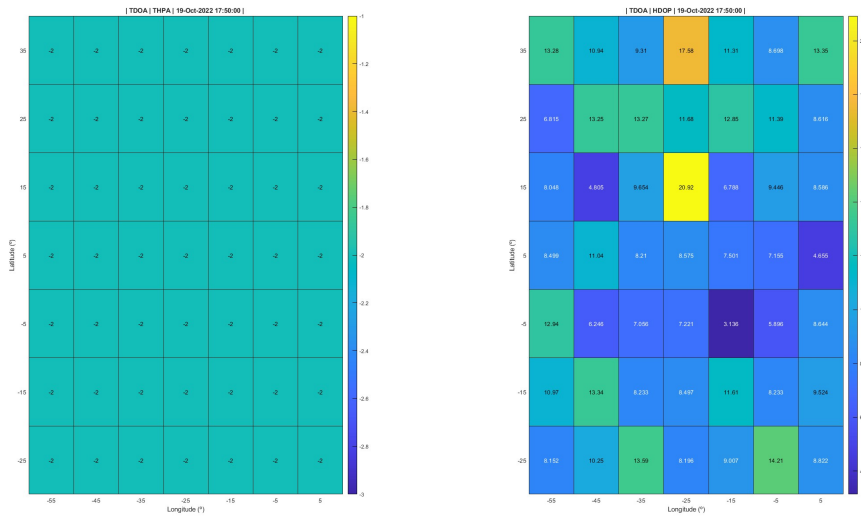


Fig. 4.3.9: Case 1 | South Atlantic | TDOA | THPA + HDOP | 17:50h.

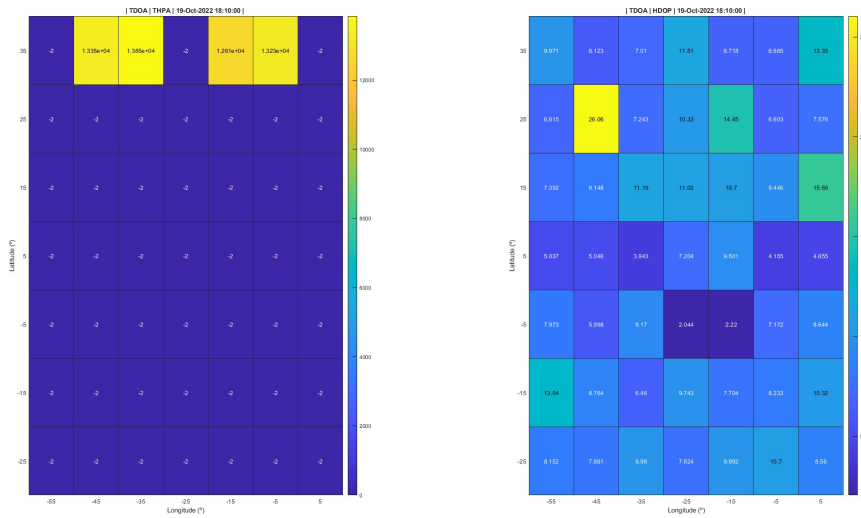


Fig. 4.3.10: Case 1 | South Atlantic | TDOA | THPA + HDOP | 18:10h.

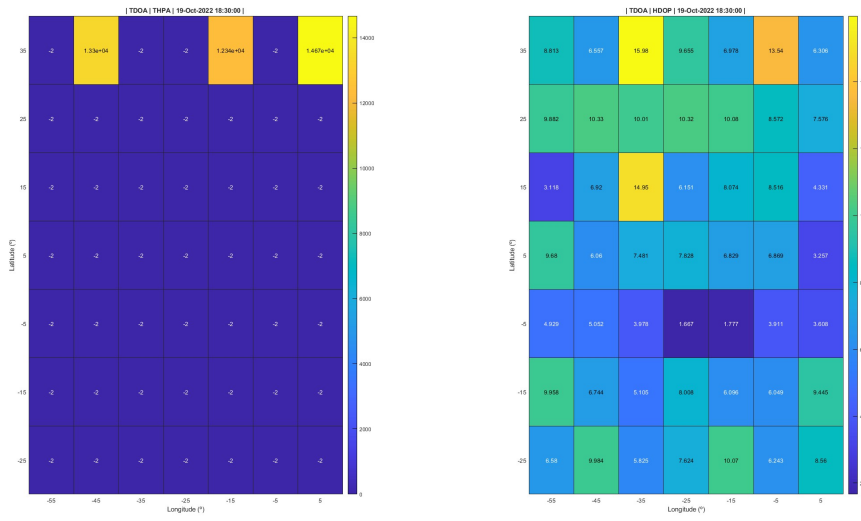


Fig. 4.3.11: Case 1 | South Atlantic | TODOA | THPA + HDOP | 18:30h.

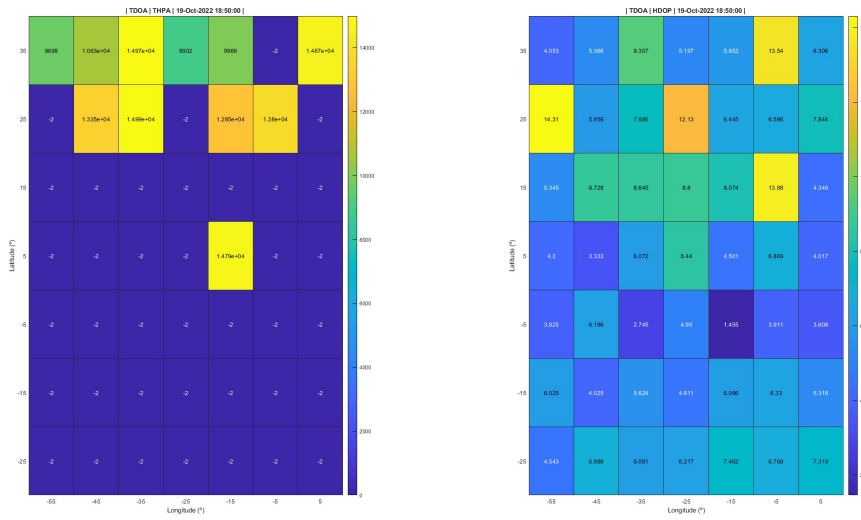


Fig. 4.3.12: Case 1 | South Atlantic | TODOA | THPA + HDOP | 18:50h.

3.1.3 Key points

On the verge of results obtained with the proposed constellation, the following points can be concluded:

- **North Atlantic airspace:**

- **HDOP:**

- The proposed system geometry not only enhances the quality of results, but also guarantees that all points have an associated HDOP value, even if some may be a bit elevated, compared to the average values. The suggested satellite constellation enables a more complete coverage area of analysis. This already tackles the huge disadvantage presented by the Iridium constellation.

- **THPA:**

- The majority of points exhibit a certain level of horizontal error. In certain instances, the calculated error exceeds the horizontal error threshold set at 15 km. Consequently, and as done previously, a value of "-2" is assigned to these non-valid results. All the simulations demonstrate that a solution (a certain accuracy error) exists for every point in the area, as a connection is well-established. However, in certain scenarios, the theoretical error falls short of the required validity for the specific application designed, hence exceeding the predefined threshold.

- **South Atlantic airspace:**

- **HDOP:**

- The system's geometry in this particular area demonstrates favorable characteristics in terms of the DOP achieved through the utilization of the proposed constellation with respect to using the Iridium constellation. Consequently, all points within the area possess an associated HDOP. This indicates a high level of confidence in the accuracy of the positioning information obtained for each point.

- **THPA:**

- In this specific area, a distinct pattern emerges. Connections are established for all points, but the majority of them exhibit high horizontal errors, exceeding the threshold set at 15 km, particularly in the first two simulations. Although the remaining points yield smaller errors, they are still considered elevated and unsuitable for the intended application.

In the remaining use cases, the simulations will focus solely on the North Atlantic airspace region. This approach allows for a comparative analysis of different solutions, aiming to identify a consistent model based on TOA error and satellite position error. Furthermore, only the THPA error will be displayed, as the HDOP remains constant throughout all the use cases, given that the satellite constellation remains unchanged.

3.2 Case 2: TOA error = 1 μ s | SAT position error = 550 m

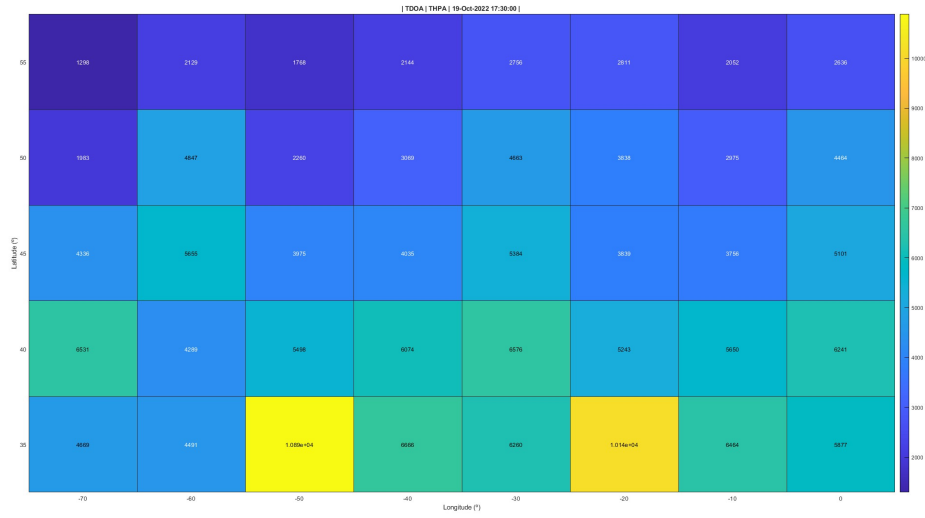


Fig. 4.3.13: Case 2 | TOA | THPA | 17:30h.

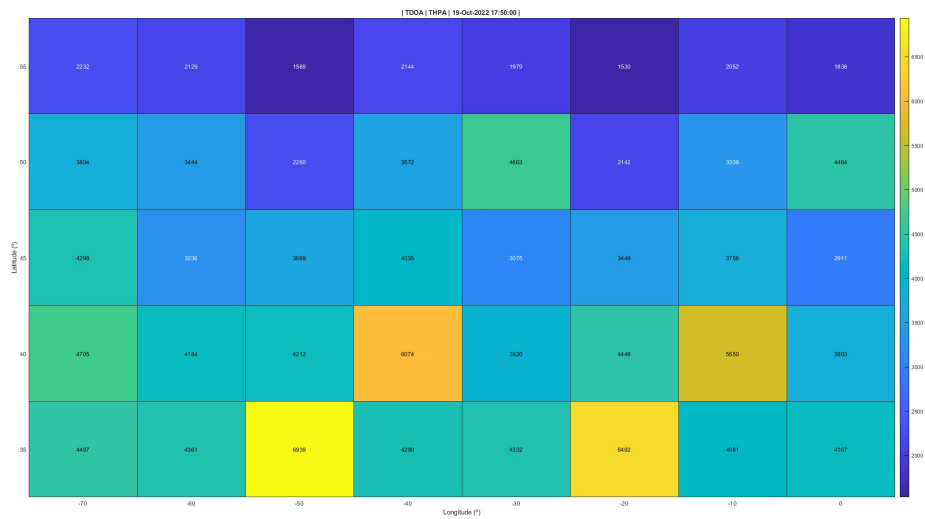


Fig. 4.3.14: Case 2 | TOA | THPA | 17:50h.

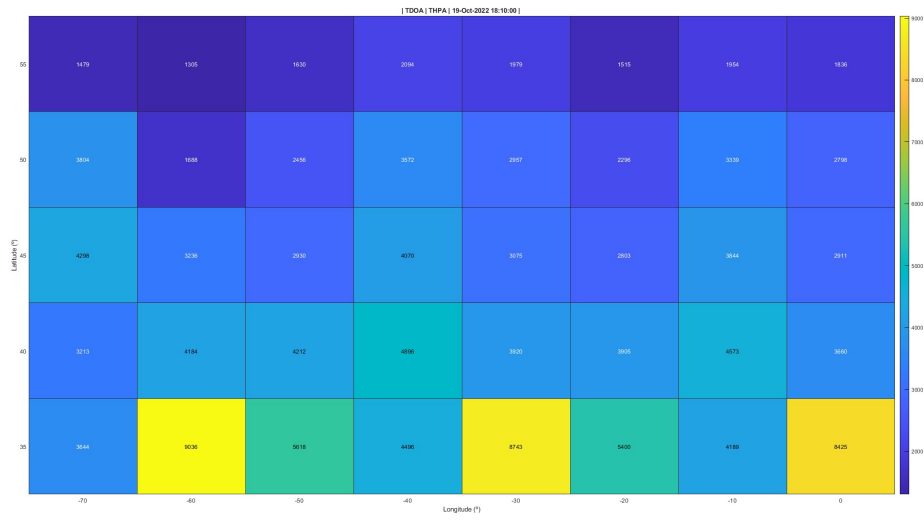


Fig. 4.3.15: Case 2 | TDOA | THPA | 18:10h.

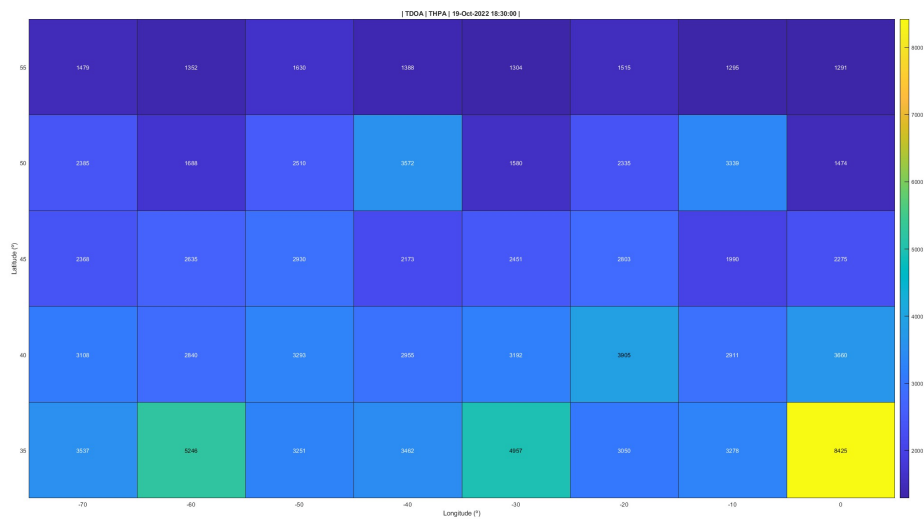


Fig. 4.3.16: Case 2 | TDOA | THPA | 18:30h.

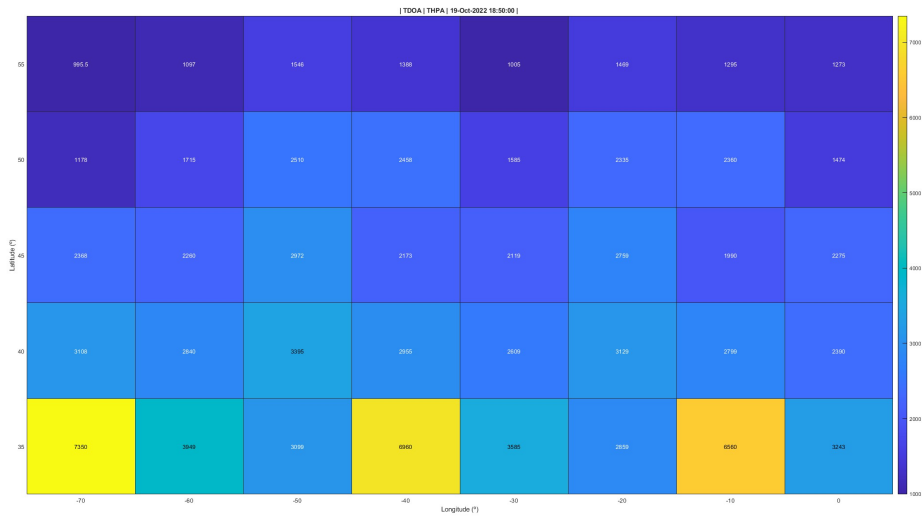


Fig. 4.3.17: Case 2 | TDOA | THPA | 18:50h.

3.3 Case 3: TOA error = 1 μ s | SAT position error = 100 m

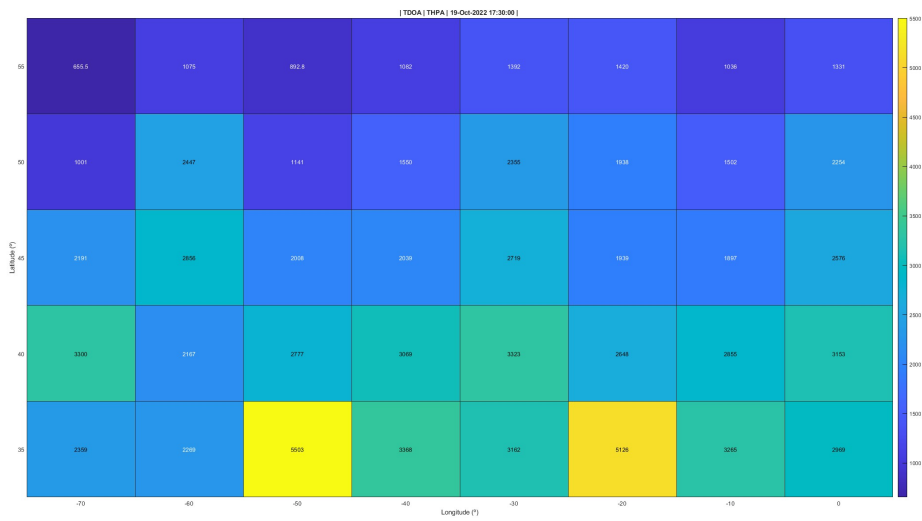


Fig. 4.3.18: Case 3 | TDOA | THPA | 17:30h.

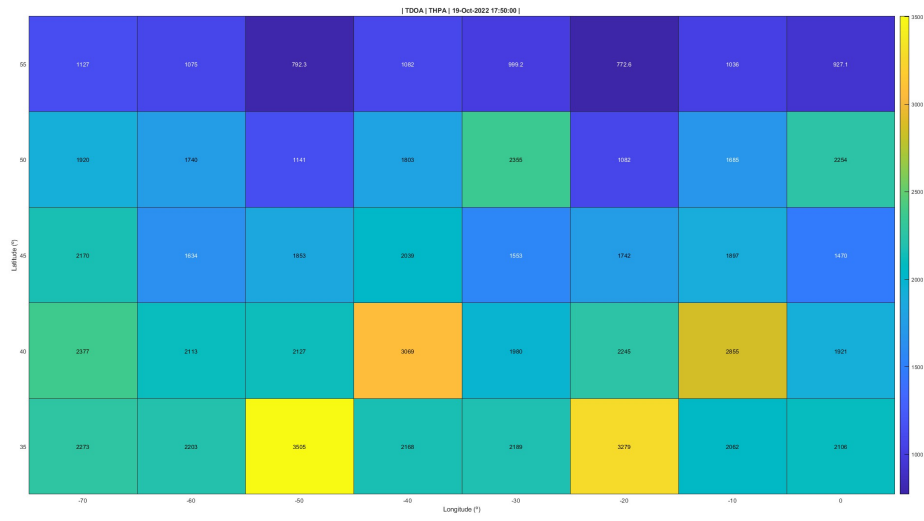


Fig. 4.3.19: Case 3 | TDOA | THPA | 17:50h.

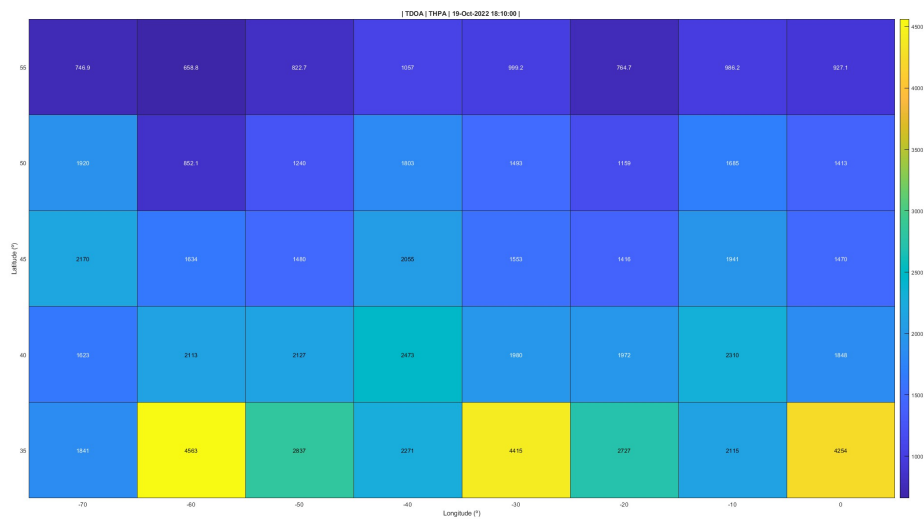


Fig. 4.3.20: Case 3 | TDOA | THPA | 18:10h.

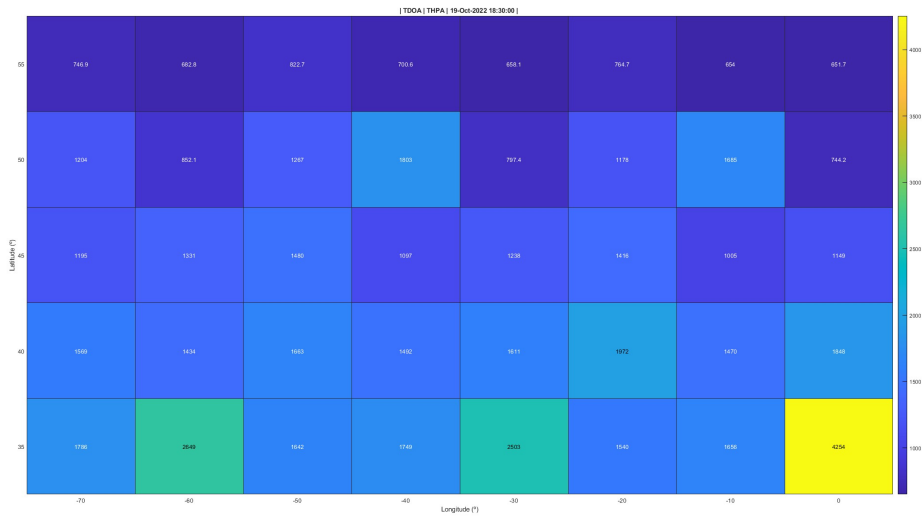


Fig. 4.3.21: Case 3 | TDOA | THPA | 18:30h.

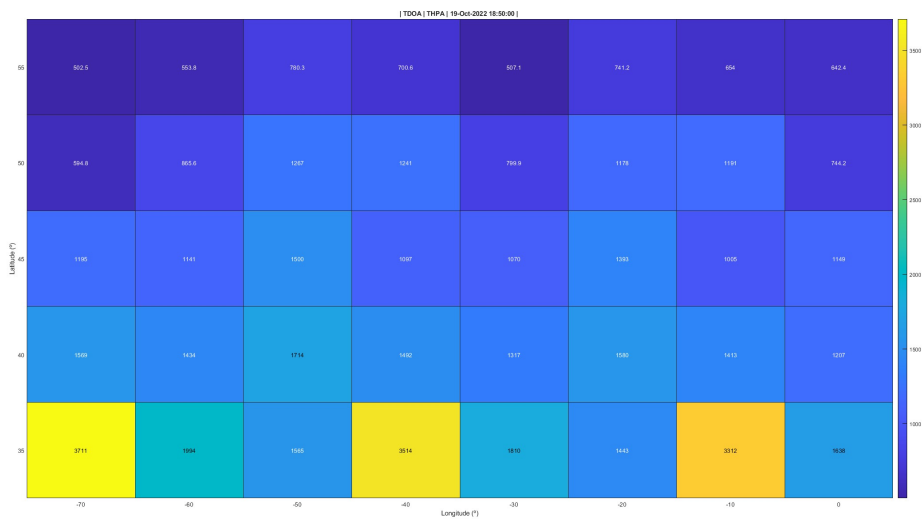


Fig. 4.3.22: Case 3 | TDOA | THPA | 18:50h.

3.4 Case 4: TOA error = 1 μ s | SAT position error = 50 m

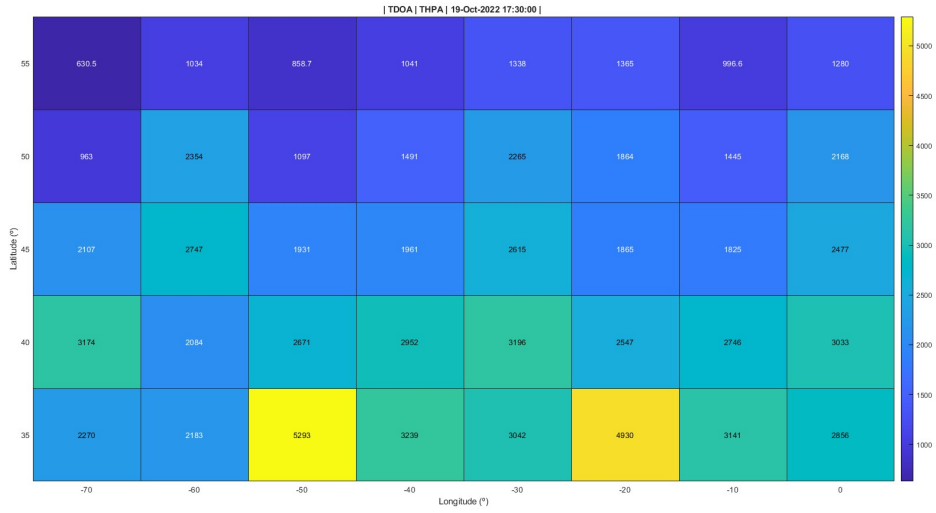


Fig. 4.3.23: Case 4 | TDOA | THPA | 17:30h.

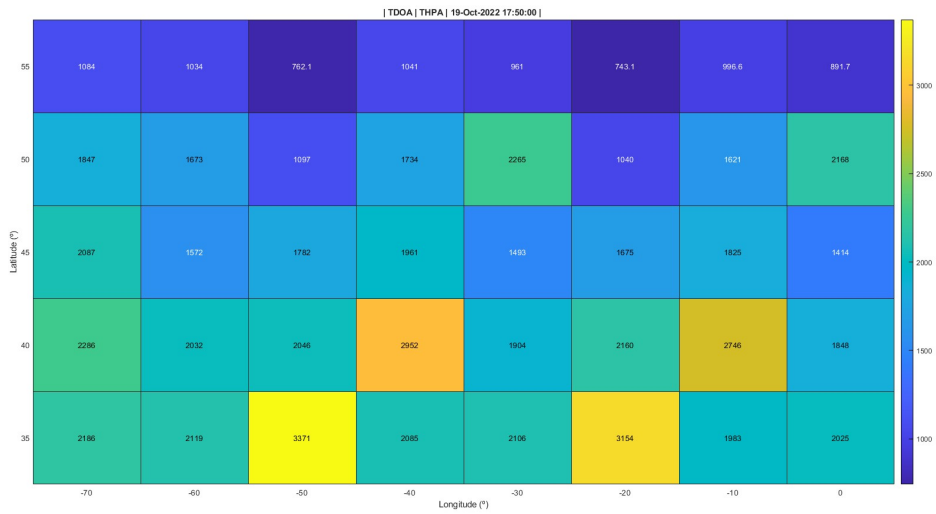


Fig. 4.3.24: Case 4 | TDOA | THPA | 17:50h.

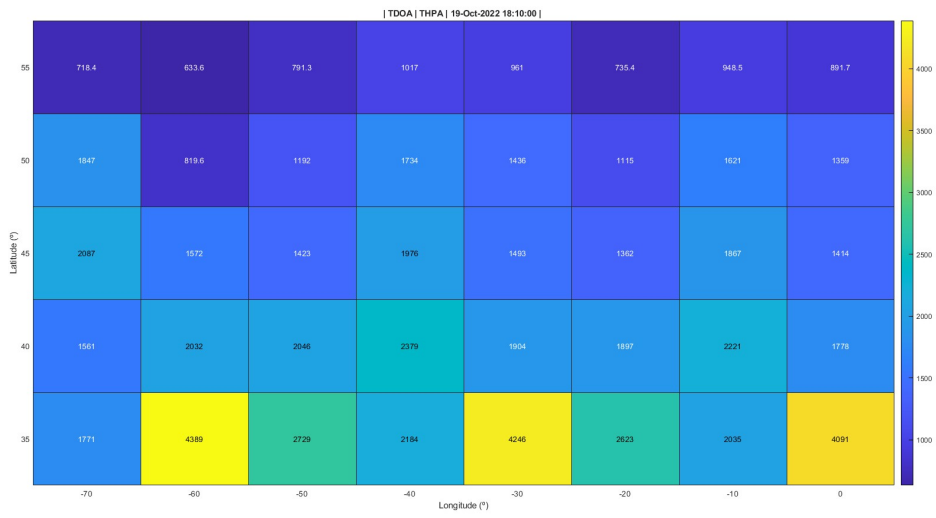


Fig. 4.3.25: Case 4 | TDOA | THPA | 18:10h.

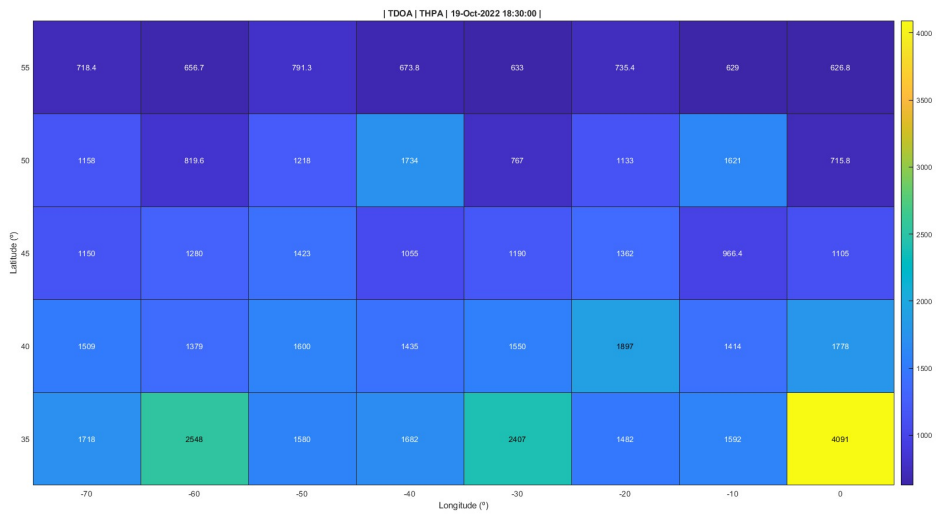


Fig. 4.3.26: Case 4 | TDOA | THPA | 18:30h.

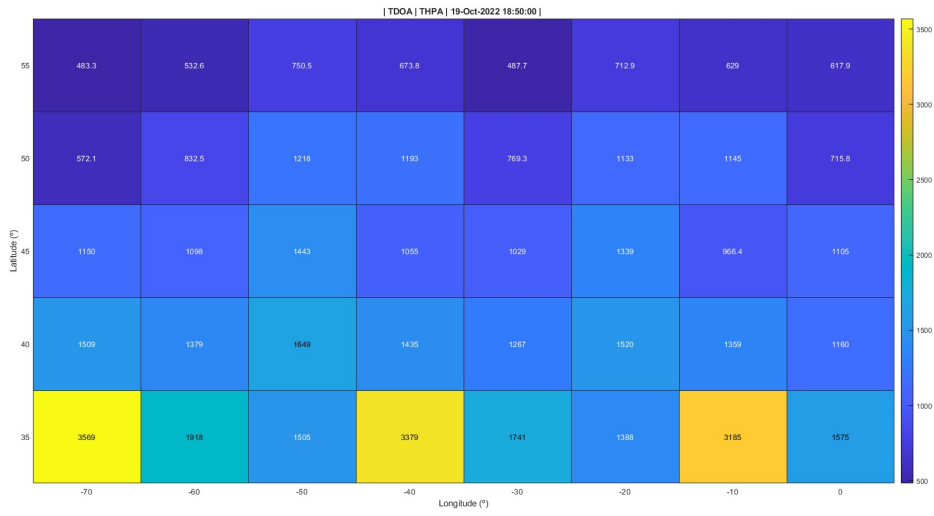


Fig. 4.3.27: Case 4 | TDOA | THPA | 18:50h.

3.5 Case 5: TOA error = 1 μ s | SAT position error = 25 m

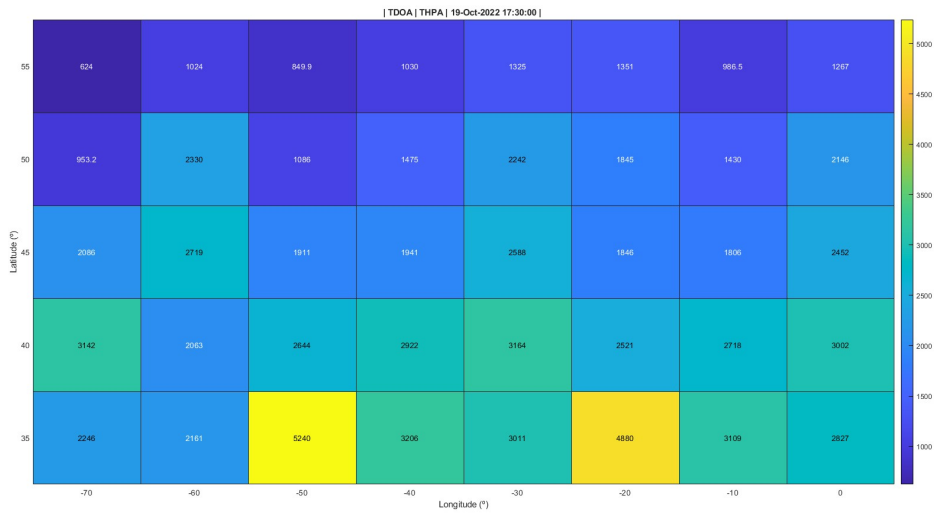


Fig. 4.3.28: Case 5 | TDOA | THPA | 17:30h.

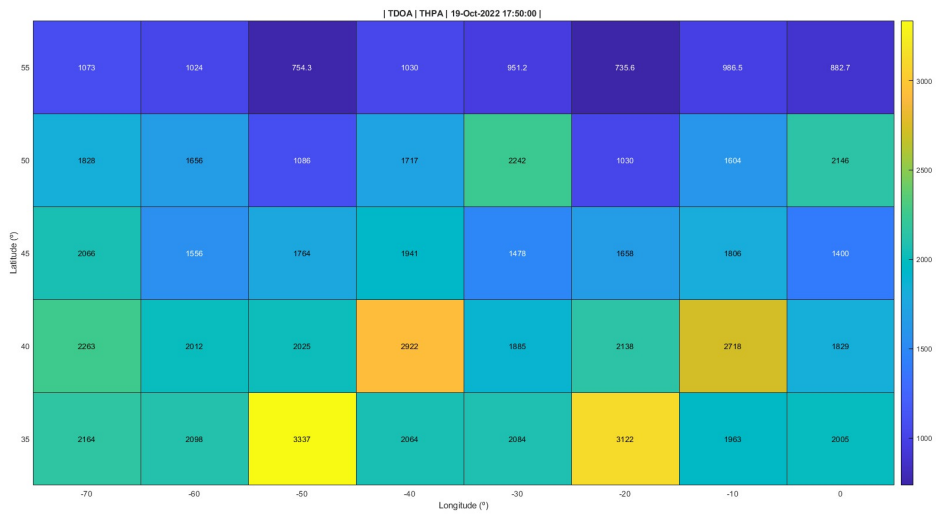


Fig. 4.3.29: Case 5 | TDOA | THPA | 17:50h.

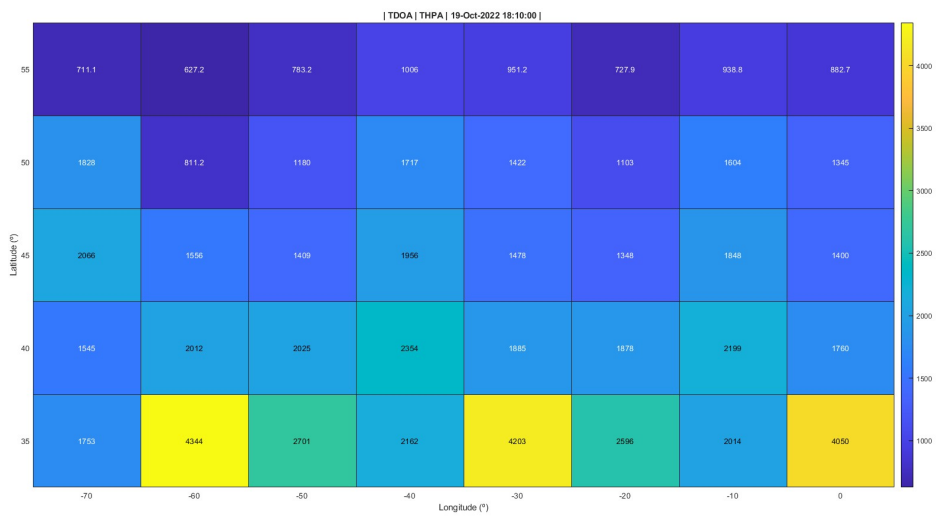


Fig. 4.3.30: Case 5 | TDOA | THPA | 18:10h.

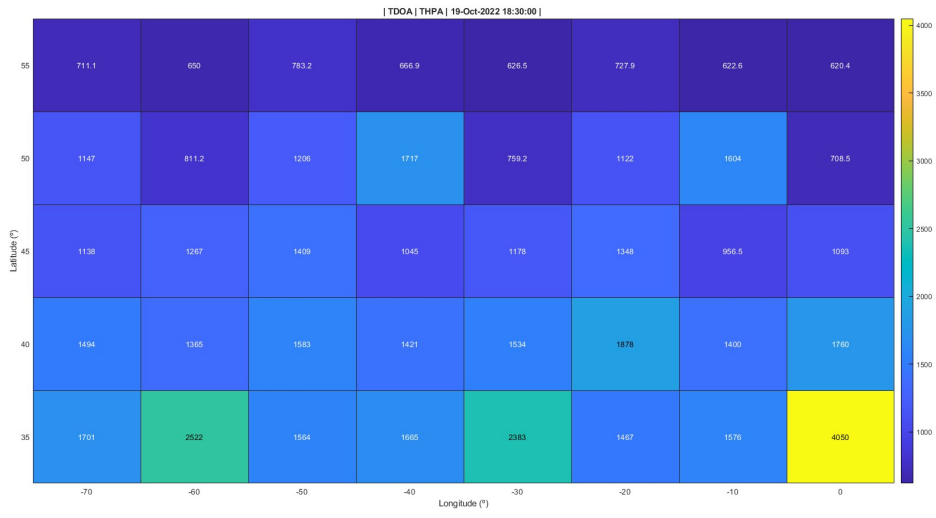


Fig. 4.3.31: Case 5 | TDOA | THPA | 18:30h.

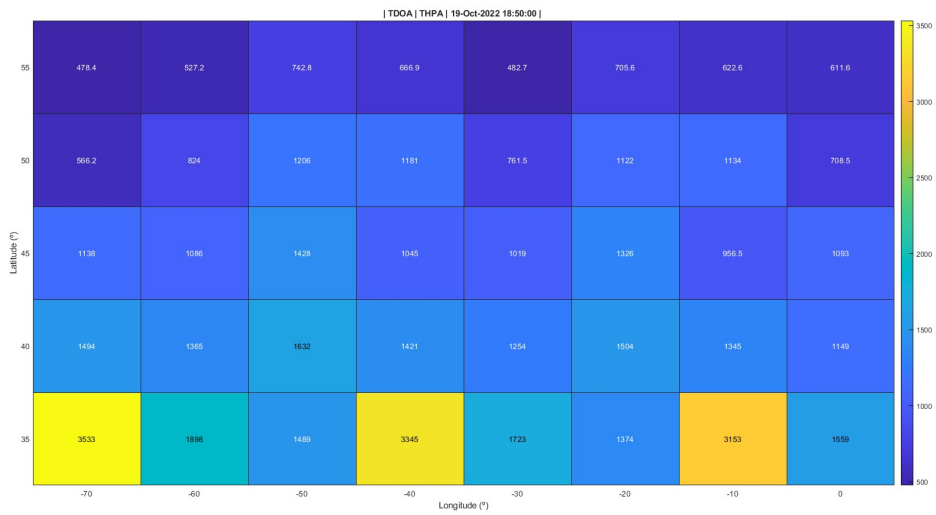


Fig. 4.3.32: Case 5 | TDOA | THPA | 18:50h.

3.6 Case 6: SAT position error = 50 m | TOA error = 100 ns

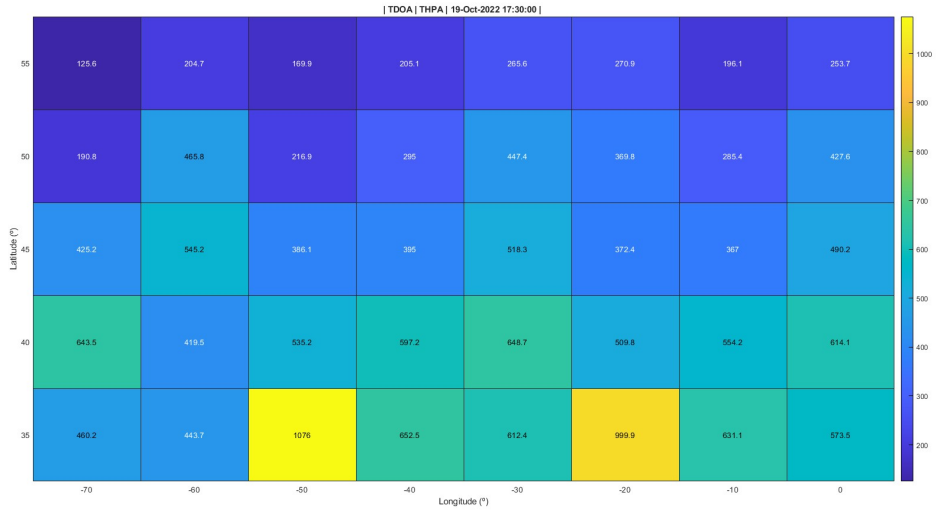


Fig. 4.3.33: Case 6 | TDOA | THPA | 17:30h.

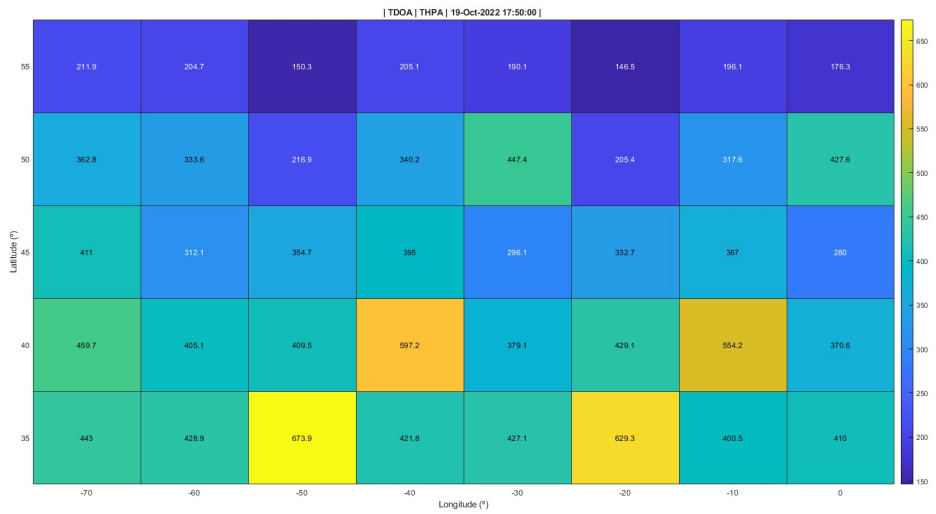


Fig. 4.3.34: Case 6 | TDOA | THPA | 17:50h.



Fig. 4.3.35: Case 6 | TDOA | THPA | 18:10h.

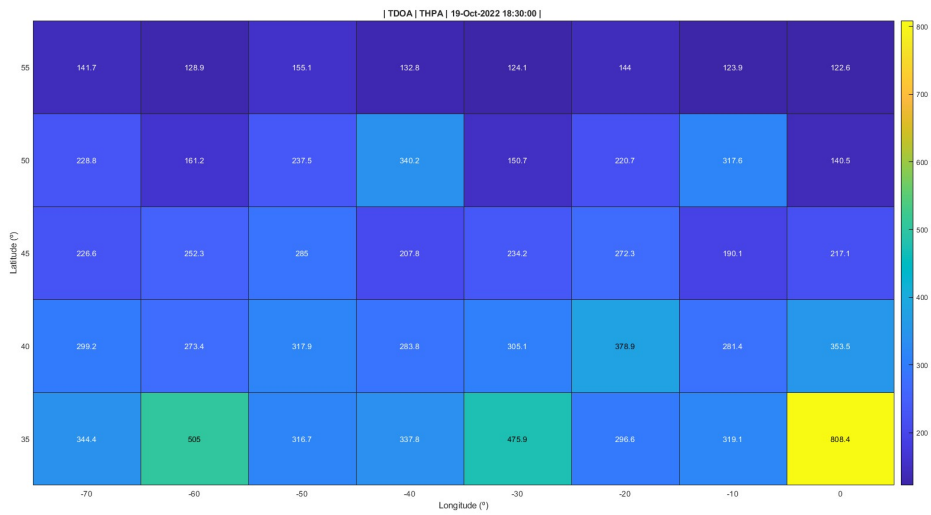


Fig. 4.3.36: Case 6 | TDOA | THPA | 18:30h.

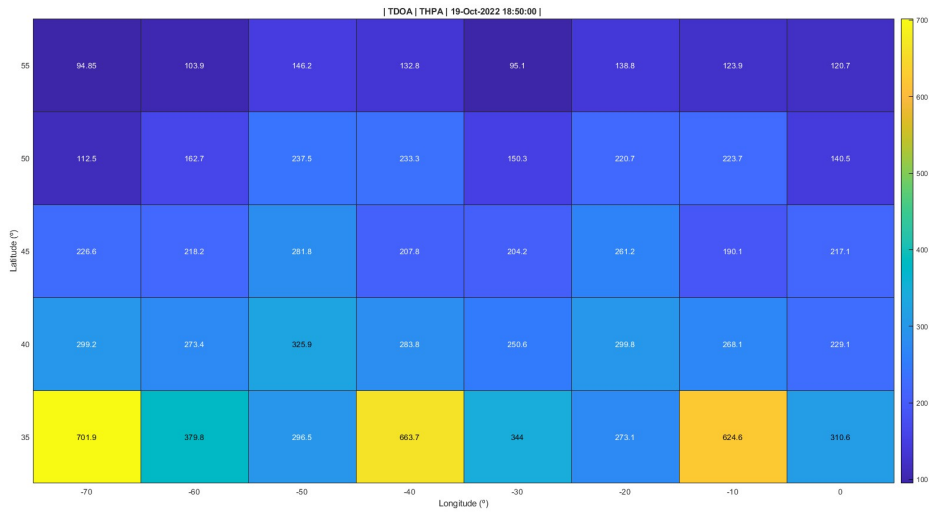


Fig. 4.3.37: Case 6 | TDOA | THPA | 18:50h.

3.7 Case 7: SAT position error = 50 m | TOA error = 10 ns

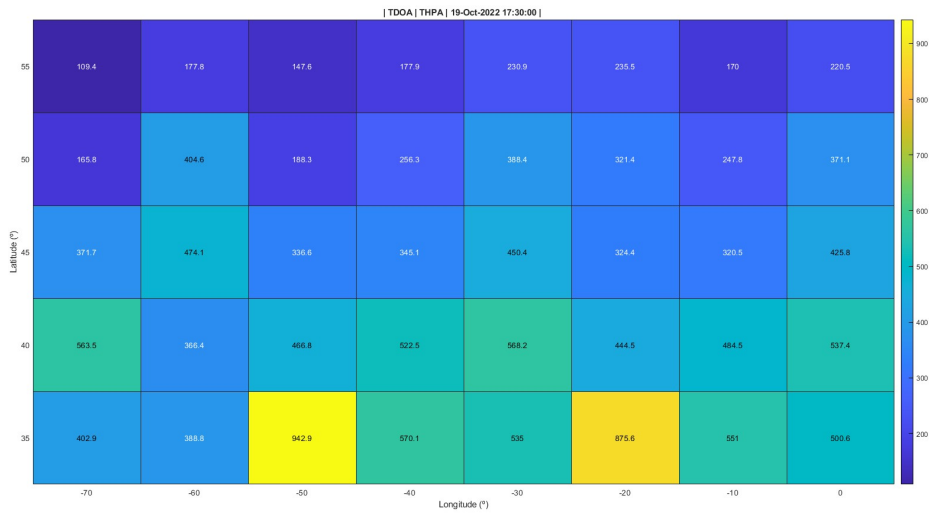


Fig. 4.3.38: Case 7 | TDOA | THPA | 17:30h.

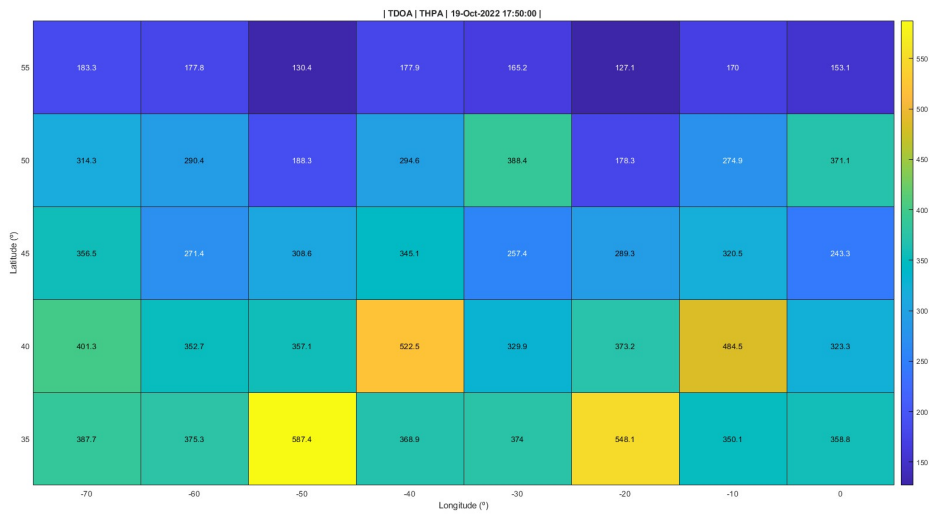


Fig. 4.3.39: Case 7 | TOA | THPA | 17:50h.



Fig. 4.3.40: Case 7 | TOA | THPA | 18:10h.

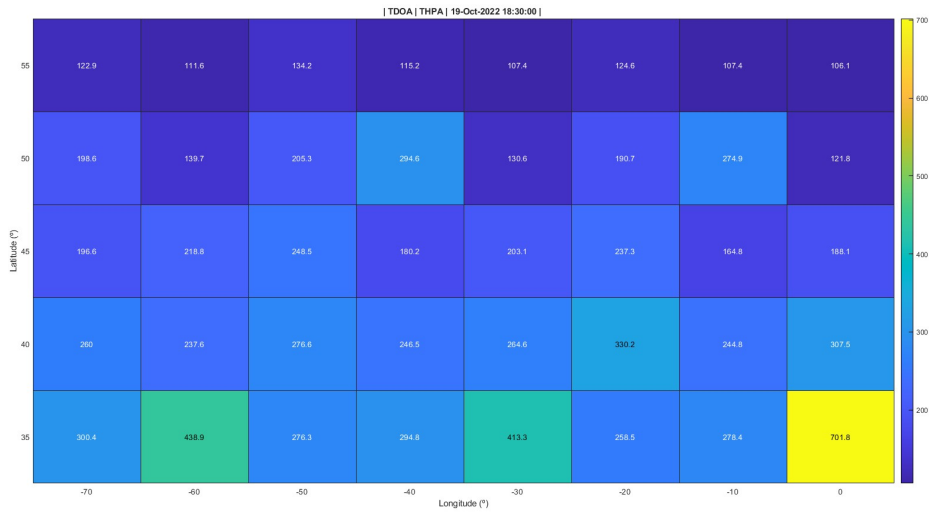


Fig. 4.3.41: Case 7 | TDOA | THPA | 18:30h.

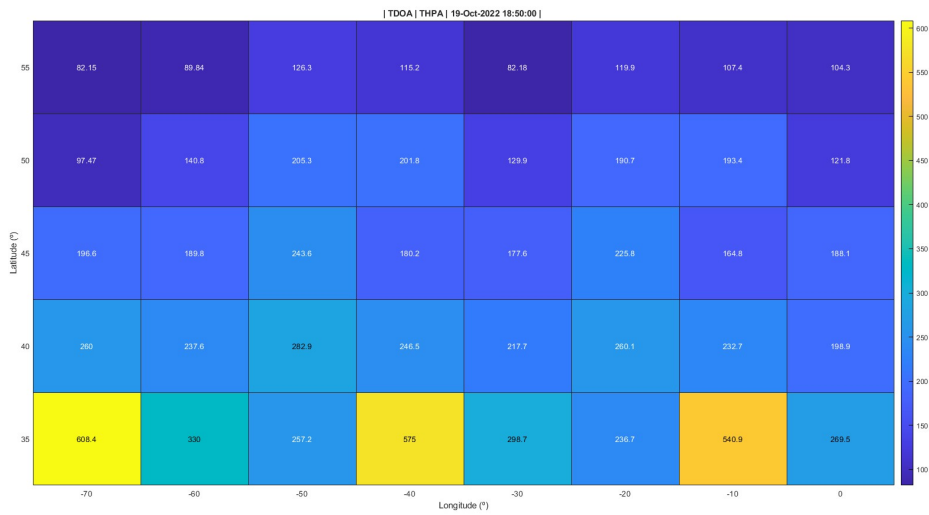


Fig. 4.3.42: Case 7 | TDOA | THPA | 18:50h.

3.8 Case 8: SAT position error = 50 m | TOA error = 1 ns

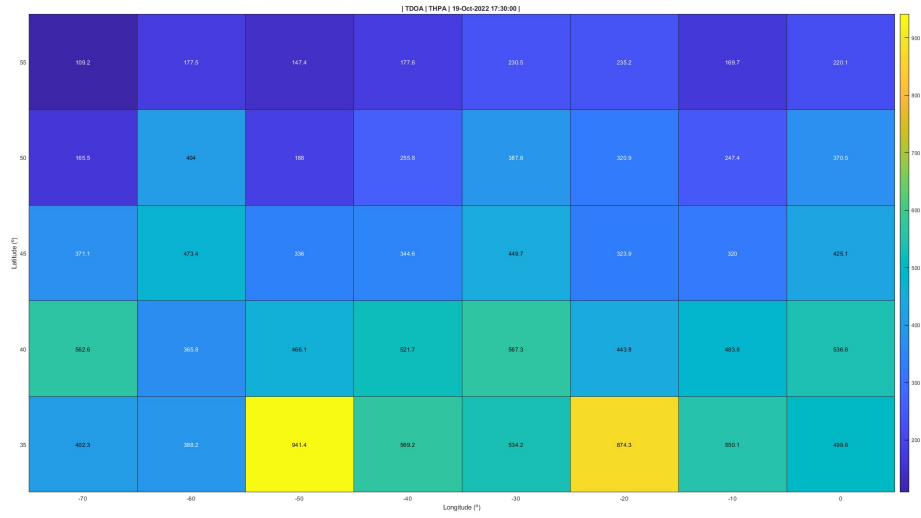


Fig. 4.3.43: Case 8 | TOA | THPA | 17:30h.

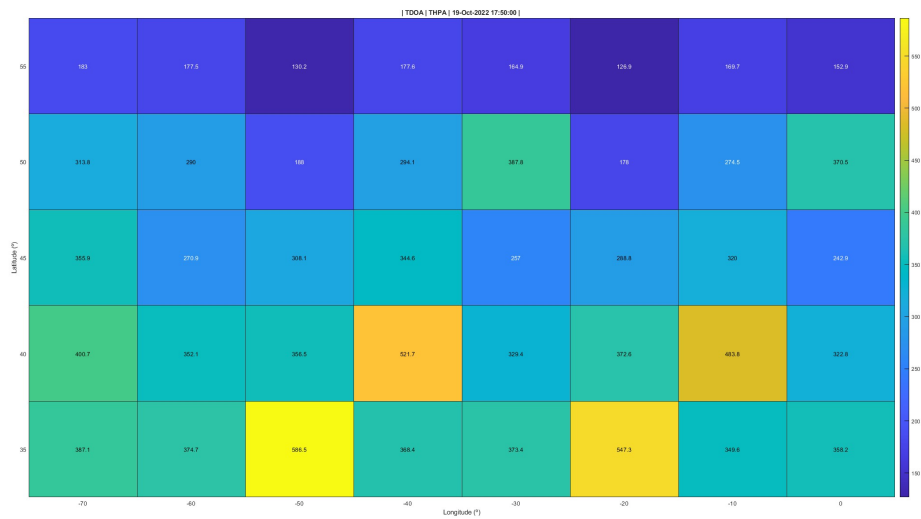


Fig. 4.3.44: Case 8 | TOA | THPA | 17:50h.

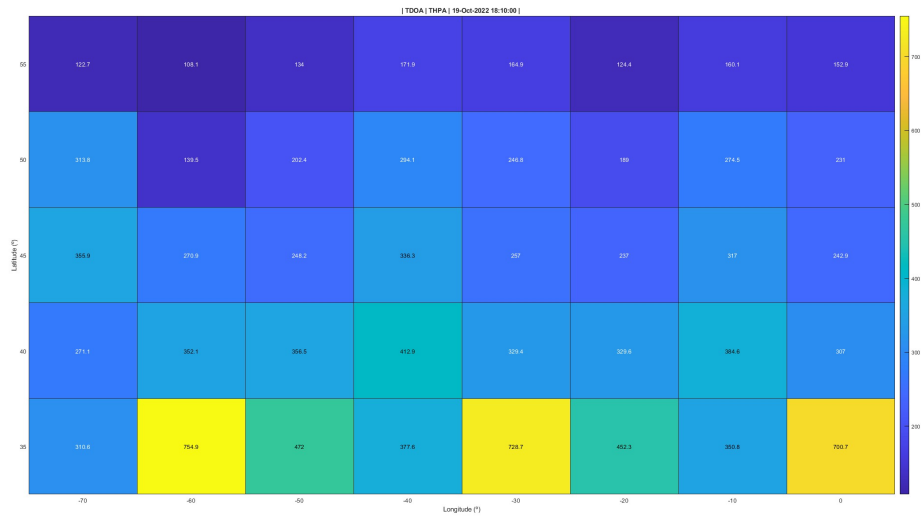


Fig. 4.3.45: Case 8 | THPA | 18:10h.

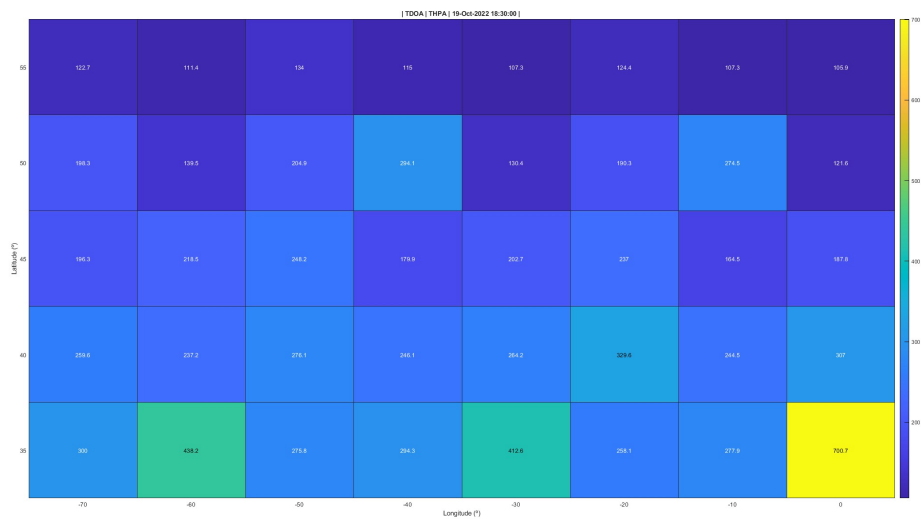


Fig. 4.3.46: Case 8 | THPA | 18:30h.

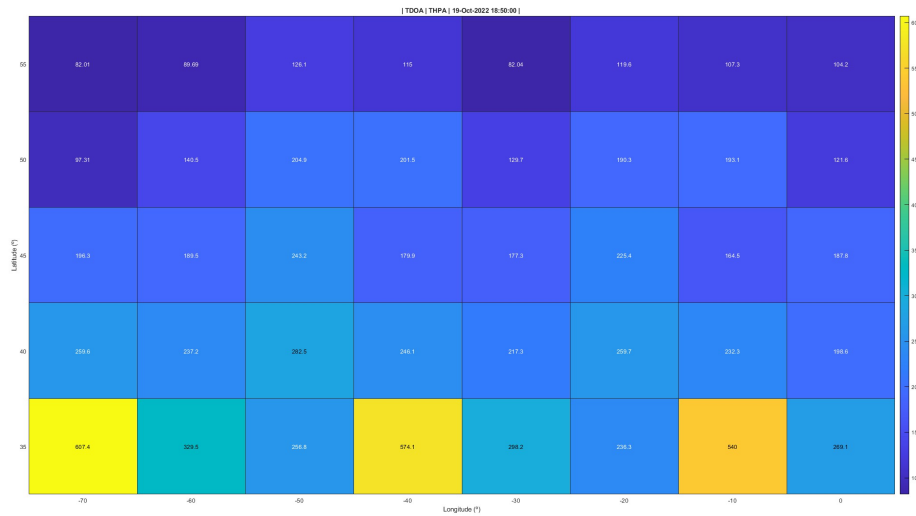


Fig. 4.3.47: Case 8 | TDOA | THPA | 18:50h.

3.9 Key points

On the verge of results obtained with the proposed constellation, for the North Atlantic airspace region, the following points can be concluded:

- **HDOP | THPA:**

Beginning with the same error values employed for the Iridium constellation, extensive testing has demonstrated a significant improvement in both the HDOP and the THPA values. This improvement guarantees the establishment of feasible connections across all areas of analysis. The revised system shows enhanced accuracy and trustworthiness, providing more reliable positioning information.

- **Satellite position error:**

Through adjustments made to the first error measurement source of the system, the true satellites position error, significant improvements have been observed in the THPA values. Initially, a considerable number of "2" cells were present for an error of 2200 m. However, following the corresponding adjustments, the THPA estimations improved to accuracy errors smaller than 10 km. These improvements continued until reaching the best accuracies of the system, in the range of hundreds of meters. This notable enhancement in accuracy was achieved with a satellite position error as low as 50 m, maintaining constant the time error.

- **TOA error:**

The second error measurement source refers to the TOA error introduced. The first analyses were carried out with an invariant time error in order to check the overall behavior while adjusting the positioning error of the satellites. After obtaining an adequate position error (50 m), variations in the TOA error were performed. As results show, changing from 10^{-6} to 10^{-8} has proved to significantly improve the estimations.

However, using a TOA error of 1 ns does not change nor improve the solutions. For this reason, it has been decided to use 10 ns as threshold. On the other hand, there is the remaining error, which is mainly introduced by the SNR.

- **Proposed error model:**

After performing all these simulations, a final model is proposed based on the two error measurement sources that characterize the system:

- **TOA error:** 10^{-8} s = 10 ns
- **SAT position error:** 50 m

These values have been demonstrated (corresponding to *Case 7*) to be suitable for the intended MLAT application. Therefore, it is recommended that the embedded receivers within the satellites adopt (or try to approach as much as possible) these error models to get accuracy errors similar to those shown in the simulations.

As a result, the localization problem will be further characterized and analyzed based on the proposed errors obtained from the performed CRLB analysis. These analyses will provide valuable insights into the performance and accuracy of the localization system as a whole.

3.10 Trajectory-based

The first operating mode focuses on analyzing the Cramér-Rao Lower Bound (CRLB) errors in specific areas of interest on the map. These areas have been defined as the North and South Atlantic regions. In this mode, the localization problem is applied to trajectories that simulate the routes of various airplanes. These trajectories have been intentionally designed to cover parts of the North and South Atlantic regions, which are crucial for analysis purposes. Both trajectories are listed and visualized in Tables 4.3.2 and 4.3.3, as well as Figures 4.3.48 and 4.3.49 respectively. These representations provide a clear overview of the flight routes and enable a detailed examination of the localization performance in the North and South Atlantic regions.

Latitude (°)	Longitude (°)	Altitude (ft)
51.21	-0.11	20000
53.13	-8.61	25000
54.41	-16.98	30000
55.09	-24.77	35000
55.71	-32.73	35000
55.79	-43.18	35000
54.84	-49.78	35000
52.86	-55.17	30000
49.19	-62.11	25000
45.45	-67.41	20000

Table 4.3.2: Trajectory I - North Atlantic Region

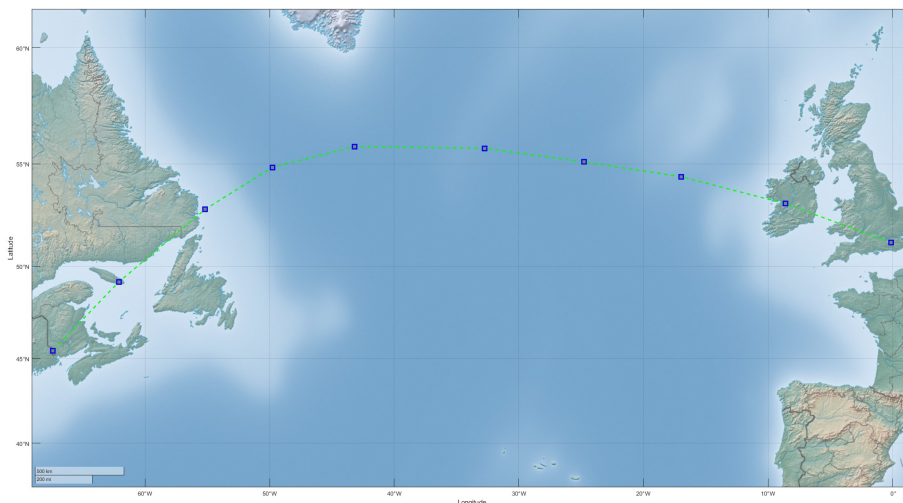


Fig. 4.3.48: Trajectory I - North Atlantic Region.

Latitude (°)	Longitude (°)	Altitude (ft)
41.51	-1.84	20000
35.12	-9.43	25000
28.32	-14.28	30000
22.16	-19.87	35000
16.53	-22.08	35000
8.34	-24.94	35000
-0.35	-29.62	35000
-6.44	-34.25	30000
-14.37	-36.92	25000
-21.83	-43.02	20000

Table 4.3.3: Trajectory II - South Atlantic Region



Fig. 4.3.49: Trajectory II - South Atlantic Region.

The tracks of the NAT region, which represents a structured set of transatlantic flight routes within the North Atlantic airspace region, governed by North Atlantic Organized Track System (NAT-OTS) are shown in Figure 4.3.50 (original work by Coisabh, Feb. 2017) [51].

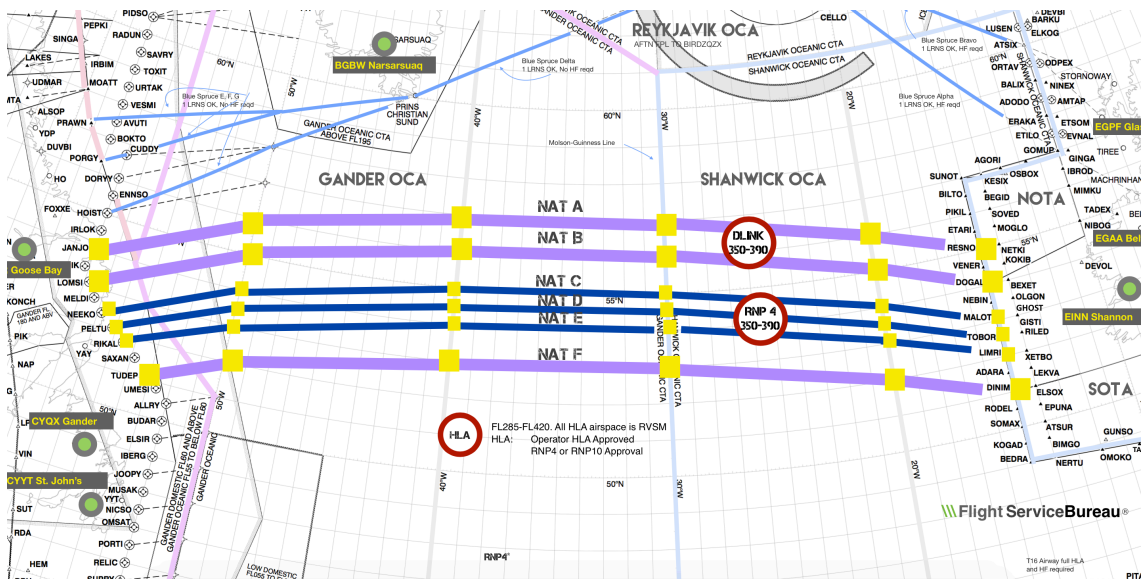


Fig. 4.3.50: North Atlantic Tracks westbound crossing.

For each localization algorithm, an additional process will be conducted using three out of the four algorithms available in the GUI: Taylor + pseudoinverse, and the regularization methods of Tikhonov and T-SVD. After numerous trials, it has been observed that the T-TLS algorithm yields very bad regularized estimations compared to the starting points provided by the localization algorithms. As a result, this procedure will not be further analyzed for this MLAT application.

Demonstrating the functionality of the localization and regularization algorithms is of utmost importance. The following images illustrate the estimated positions and regularized results obtained from several algorithms developed for this particular application. Initially, the localization method proposed by Chan and Ho [35] is examined. Figure 4.3.51 showcases the estimated positions generated by the algorithm, representing the two "target" estimations along with the reference point, which corresponds to the airplane. Subsequently, in Figure 4.3.52, the regularized positions obtained through the utilization of the Tikhonov method [42] are presented.

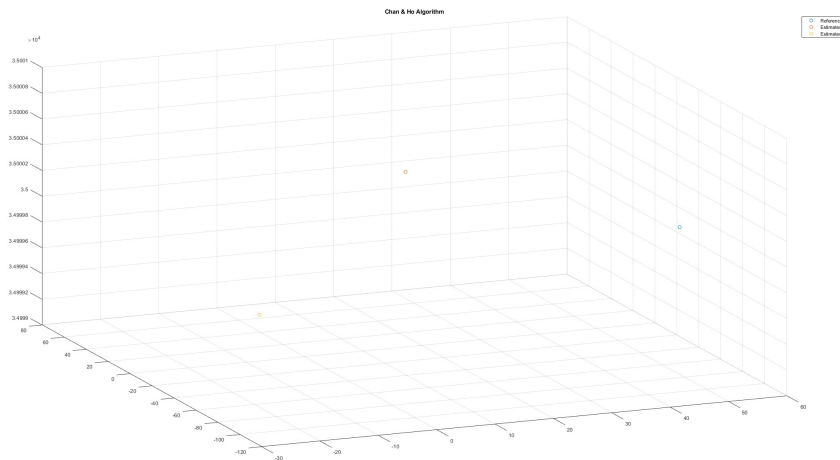


Fig. 4.3.51: Chan & Ho: Estimated positions

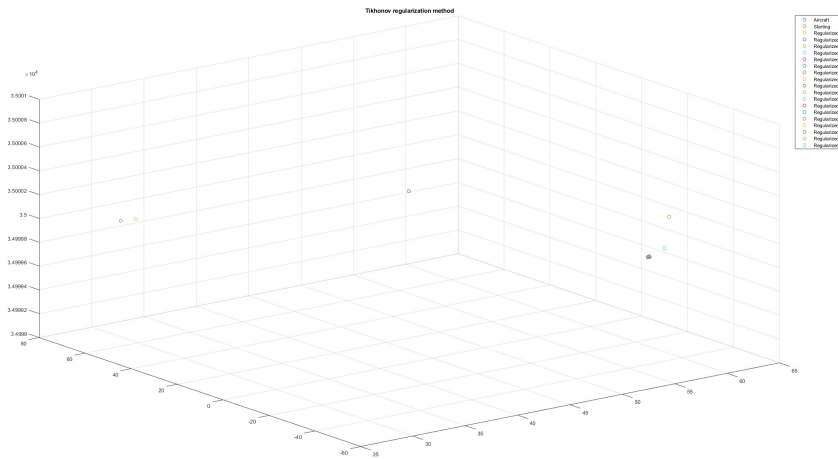


Fig. 4.3.52: Tikhonov: Regularized positions

The starting point for the regularization method is determined by selecting the closest estimation to the reference point among the two solutions presented in Figure 4.3.51. Figure 4.3.52 illustrates the iterative nature of the regularization process, where the initial point from Chan and Ho’s algorithm gradually approaches the aircraft point with each iteration, eventually converging to a solution. The regularization algorithm halts when the error between two consecutive points falls below a predefined threshold (set to 10 meters), indicating the attainment of a sufficiently accurate solution. A similar procedure is followed for another example, employing Bancroft’s [36] and the T-SVD regularization method, as depicted in Figures 4.3.53 and 4.3.54, respectively.

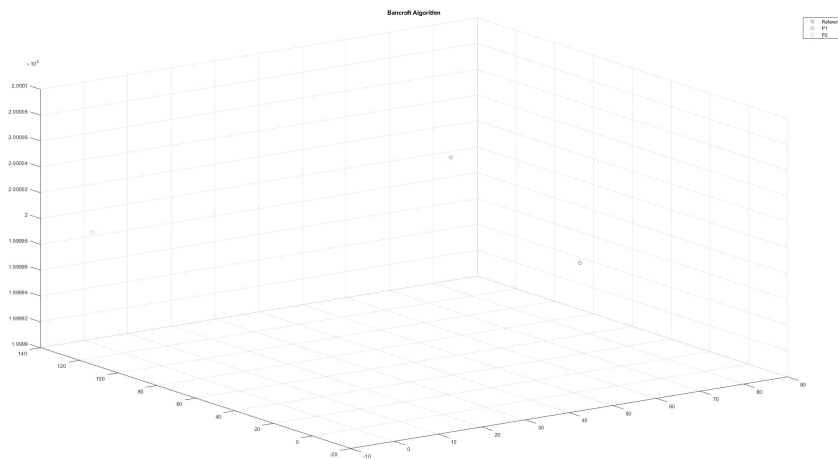


Fig. 4.3.53: Bancroft: Estimated positions

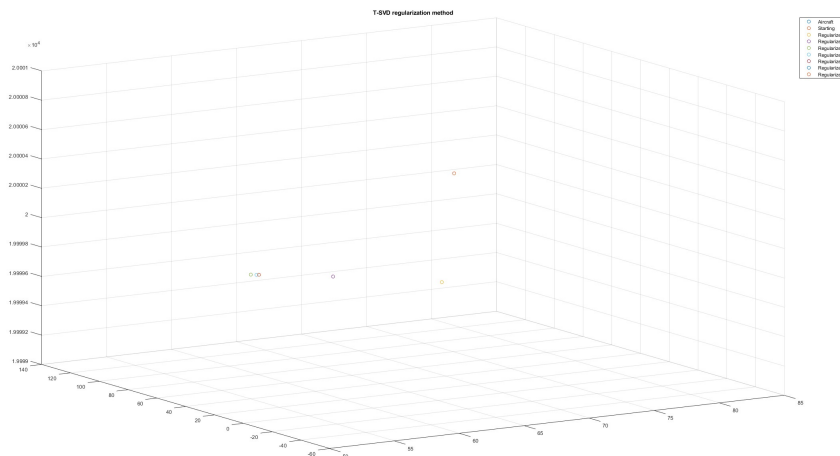


Fig. 4.3.54: T-SVD: Regularized positions

The process described above follows a consistent pattern. It begins by selecting the closest estimation to the reference point as the starting point. This initial estimation serves as a baseline. From there, iterative refinements are made to improve the accuracy of the estimation. The goal is to achieve the desired level of accuracy through successive iterations. Each iteration refines the estimation further, bringing it closer to the true value. This process continues until the desired level of accuracy is achieved.

Having previously covered the process of obtaining estimated positions and the subsequent regularization process, it is of utmost importance to delve into a comprehensive analysis of each algorithm developed within this context. Such an analysis enables us to gain a deeper understanding of the unique strengths, weaknesses, and performance characteristics associated with each algorithm. By examining the behavior of each algorithm individually, we can discern their respective advantages and limitations. This understanding will assist in making informed decisions regarding their suitability for specific applications or scenarios. By scrutinizing their performance characteristics, we can determine their efficiency, accuracy, and robustness.

Identifying the strengths of each algorithm provides insights into the aspects in which it excels. These could include rapid convergence, high precision, or suitability for handling specific types of data. On the other hand, recognizing the weaknesses of each algorithm helps us comprehend the areas in which it may struggle or require improvements, such as sensitivity to noise, computational complexity, or limited applicability to certain data distributions. Moreover, analyzing the performance characteristics of each algorithm enables us to compare and contrast their effectiveness. This evaluation may involve assessing factors such as computational efficiency, memory requirements, scalability, and the ability to handle large data sets or real-time applications. By understanding these aspects, we can make informed choices about selecting the most appropriate algorithm for a given task.

Overall, a comprehensive analysis of the behavior of each developed algorithm provides valuable insights into their respective strengths, weaknesses, and performance characteristics. This knowledge empowers researchers, engineers, and practitioners to make informed decisions and optimizations, ultimately enhancing the efficacy and applicability of the algorithms in question.

3.10.1 Trajectory I: North Atlantic

1. Smith & Abel + Pseudoinverse:

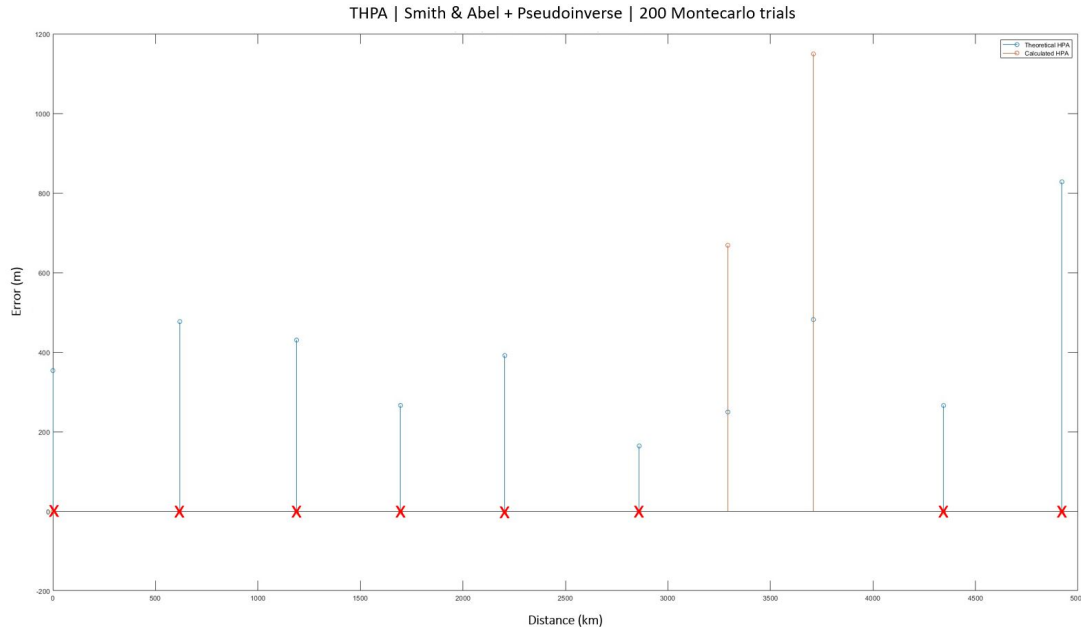


Fig. 4.3.55: North Atlantic | Smith & Abel + Pseudoinverse: Graph.

Error statistics and Horizontal Position Accuracy (HPA) using Smith & Abel + Pseudoinverse for 200 Montecarlo trials:

Lat. (°)	Lon. (°)	Alt. (ft)	Mean xEast (m)	Mean yNorth (m)	Mean Cond. number	St. dev. xEast (m)	St. dev. yNorth (m)	Calculated HPA (m)	THPA (m)
51.21	-0.11	20000.00	3024832.75	-1830290.61	22.11	3107351.47	1898522.69	-2.00	353.59
53.13	-8.61	25000.00	2799132.49	-4877625.99	24.21	3878186.85	6760656.36	-2.00	476.59
54.41	-16.98	30000.00	-5993536.62	-11109446.49	43.32	4031030.55	7473108.13	-2.00	430.17
55.09	-24.77	35000.00	-771908.79	-655881.91	33.32	968152.33	773940.86	-2.00	265.86
55.71	-32.73	35000.00	-3456065.20	-4760974.39	28.54	4003705.24	5524353.69	-2.00	391.33
55.79	-43.18	35000.00	1217988.53	-1096405.40	12.71	3386181.09	3046671.85	-2.00	163.98
54.84	-49.78	35000.00	-23.21	-23.74	12.83	460.60	484.49	668.49	249.25
52.86	-55.17	30000.00	-60.33	-43.56	13.72	759.30	862.96	1149.45	481.73
49.19	-62.11	25000.00	14371.64	5083.41	7.06	62970.97	22136.46	-2.00	265.67
45.45	-67.41	20000.00	-216244.80	-640576.85	21.12	1139807.03	3375302.64	-2.00	827.93

Fig. 4.3.56: North Atlantic | Smith & Abel + Pseudoinverse: Statistics.

A brief summary of the results is included:

- Points with horizontal errors larger than 15 km: 8 out of 10 (80 %)
- Highest valid calculated horizontal error: 1149.45 m
- Point with highest horizontal error: (52.86°, -55.17°, 30000 ft)

2. Smith & Abel + Tikhonov:

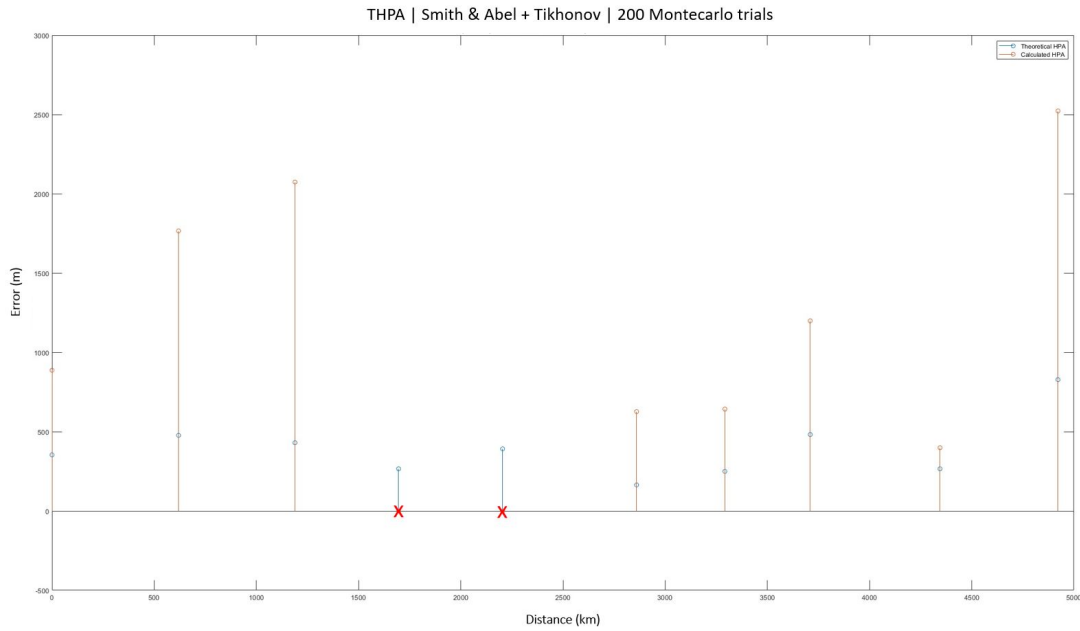


Fig. 4.3.57: North Atlantic | Smith & Abel + Tikhonov: Graph.

Error statistics and Horizontal Position Accuracy (HPA) using Smith & Abel + Tikhonov for 200 Montecarlo trials:

Lat. (°)	Lon. (°)	Alt. (ft)	Mean xEast (m)	Mean yNorth (m)	Mean Cond. number	St. dev. xEast (m)	St. dev. yNorth (m)	Calculated HPA (m)	THPA (m)
51.21	-0.11	20000.00	-10.47	9.38	12.78	748.79	475.75	887.15	353.59
53.13	-8.61	25000.00	104.34	-173.30	20.95	874.05	1534.27	1765.77	476.59
54.41	-16.98	30000.00	20.62	89.78	19.89	1024.28	1803.38	2073.97	430.17
55.09	-24.77	35000.00	-24319.22	-18198.79	10.87	343135.46	256855.67	-2.00	265.86
55.71	-32.73	35000.00	-74517.83	-103514.27	14.57	476257.69	645065.05	-2.00	391.33
55.79	-43.18	35000.00	0.58	0.56	8.56	457.10	427.53	626.15	163.98
54.84	-49.78	35000.00	-3.01	1.19	12.83	442.54	465.38	642.20	249.25
52.86	-55.17	30000.00	7.49	7.16	13.72	777.40	912.36	1198.65	481.73
49.19	-62.11	25000.00	11.67	-15.02	6.85	348.76	193.14	398.67	265.67
45.45	-67.41	20000.00	68.40	123.64	20.67	710.30	2419.80	2521.90	827.93

Fig. 4.3.58: North Atlantic | Smith & Abel + Tikhonov: Statistics.

A brief summary of the results is included:

- Points with horizontal errors larger than 15 km: 2 out of 10 (20 %)
- Highest valid calculated horizontal error: 2521.90 m
- Point with highest horizontal error: (45.45°, -67.41°, 20000 ft)

3. Smith & Abel + T-SVD:

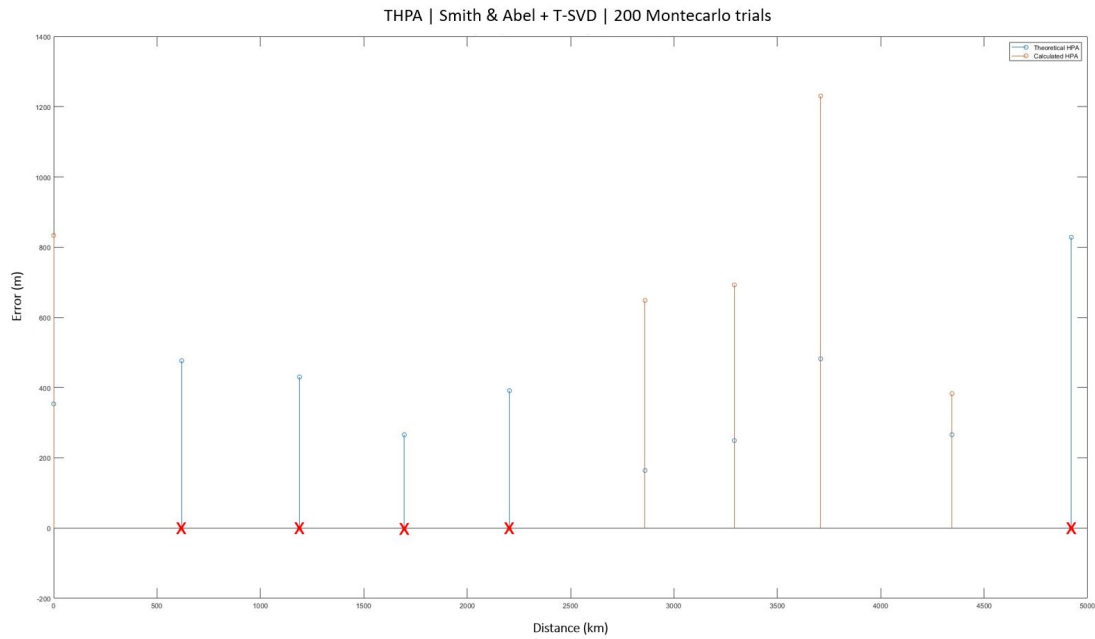


Fig. 4.3.59: North Atlantic | Smith & Abel + T-SVD: Graph.

Error statistics and Horizontal Position Accuracy (HPA) using Smith & Abel + T-SVD for 200 Montecarlo trials:

Lat. (°)	Lon. (°)	Alt. (ft)	Mean xEast (m)	Mean yNorth (m)	Mean Cond. number	St. dev. xEast (m)	St. dev. yNorth (m)	Calculated HPA (m)	THPA (m)
51.21	-0.11	20000.00	-55.81	19.43	12.78	705.01	444.23	833.30	353.59
53.13	-8.61	25000.00	132648.50	-230813.51	21.04	934010.76	1625199.02	-2.00	476.59
54.41	-16.98	30000.00	-1777927.68	-3290053.19	26.01	3083621.51	5707264.39	-2.00	430.17
55.09	-24.77	35000.00	-1035176.39	-817228.03	24.61	1339468.63	1037497.30	-2.00	265.86
55.71	-32.73	35000.00	-169103.19	-229416.55	14.86	741522.34	1007158.09	-2.00	391.33
55.79	-43.18	35000.00	-33.60	17.35	8.56	468.59	447.93	648.24	163.98
54.84	-49.78	35000.00	-31.36	-36.80	12.53	478.17	500.69	692.34	249.25
52.86	-55.17	30000.00	85.75	89.76	13.72	810.52	925.60	1230.32	481.73
49.19	-62.11	25000.00	11.77	-2.02	6.85	334.07	186.95	382.82	265.67
45.45	-67.41	20000.00	-29088.75	-86686.26	20.73	412126.63	1228219.39	-2.00	827.93

Fig. 4.3.60: North Atlantic | Smith & Abel + T-SVD: Statistics.

A brief summary of the results is included:

- Points with horizontal errors larger than 15 km: 5 out of 10 (50 %)
- Highest valid calculated horizontal error: 1230.32 m
- Point with highest horizontal error: (52.86°, -55.17°, 30000 ft)

1. Friedlander + Pseudoinverse:

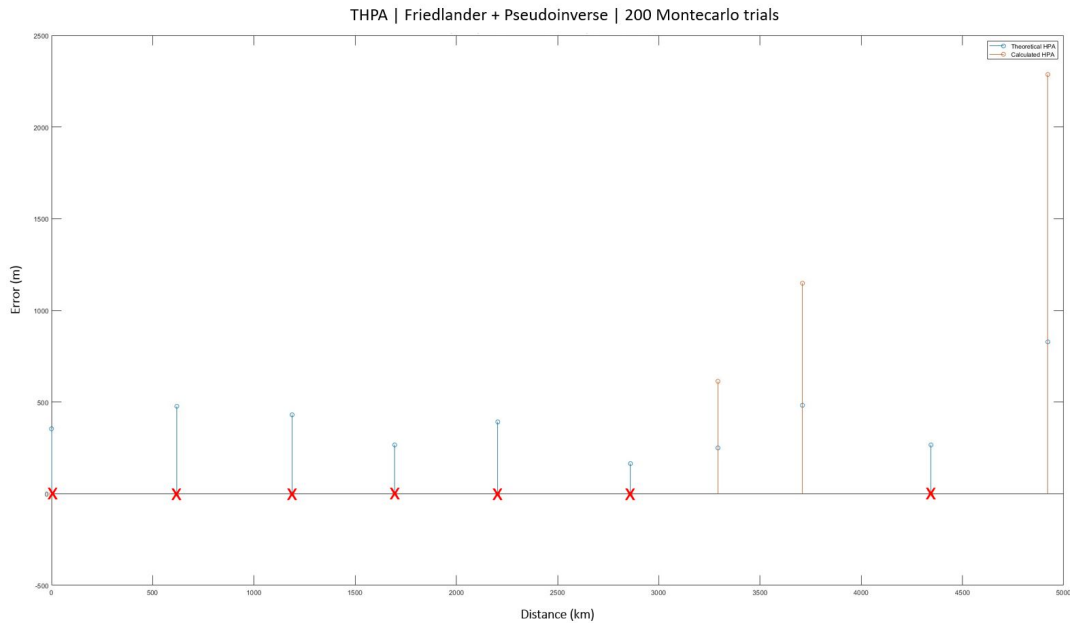


Fig. 4.3.61: North Atlantic | Friedlander + Pseudoinverse: Graph.

Error statistics and Horizontal Position Accuracy (HPA) using Friedlander + Pseudoinverse for 200 Montecarlo trials:

Lat. (°)	Lon. (°)	Alt. (ft)	Mean xEast (m)	Mean yNorth (m)	Mean Cond. number	St. dev. xEast (m)	St. dev. yNorth (m)	Calculated HPA (m)	THPA (m)
51.21	-0.11	20000.00	1562464.00	-923056.78	18.94	2818349.23	1671934.79	-2.00	353.59
53.13	-8.61	25000.00	5253387.84	-9166552.94	29.03	4803249.36	8383136.76	-2.00	476.59
54.41	-16.98	30000.00	-5354351.24	-9928920.36	42.26	5058372.10	9384041.13	-2.00	430.17
55.09	-24.77	35000.00	-734704.71	-636441.45	36.56	1104736.11	857956.64	-2.00	265.86
55.71	-32.73	35000.00	-5784644.72	-7989447.19	40.64	5551743.48	7682316.25	-2.00	391.33
55.79	-43.18	35000.00	2668218.70	-2393622.64	18.17	4677534.92	4196630.85	-2.00	163.98
54.84	-49.78	35000.00	-22.31	-32.88	12.83	429.11	437.33	612.69	249.25
52.86	-55.17	30000.00	53.89	49.80	13.72	766.07	854.55	1147.66	481.73
49.19	-62.11	25000.00	1437.12	499.20	6.87	20185.66	7169.27	-2.00	265.67
45.45	-67.41	20000.00	27.49	116.87	20.67	653.02	2191.29	2286.52	827.93

Fig. 4.3.62: North Atlantic | Friedlander + Pseudoinverse: Statistics.

A brief summary of the results is included:

- Points with horizontal errors larger than 15 km: 7 out of 10 (70 %)
- Highest valid calculated horizontal error: 2286.52 m
- Point with highest horizontal error: (45.45°, -67.41°, 20000 ft)

2. Friedlander + Tikhonov:

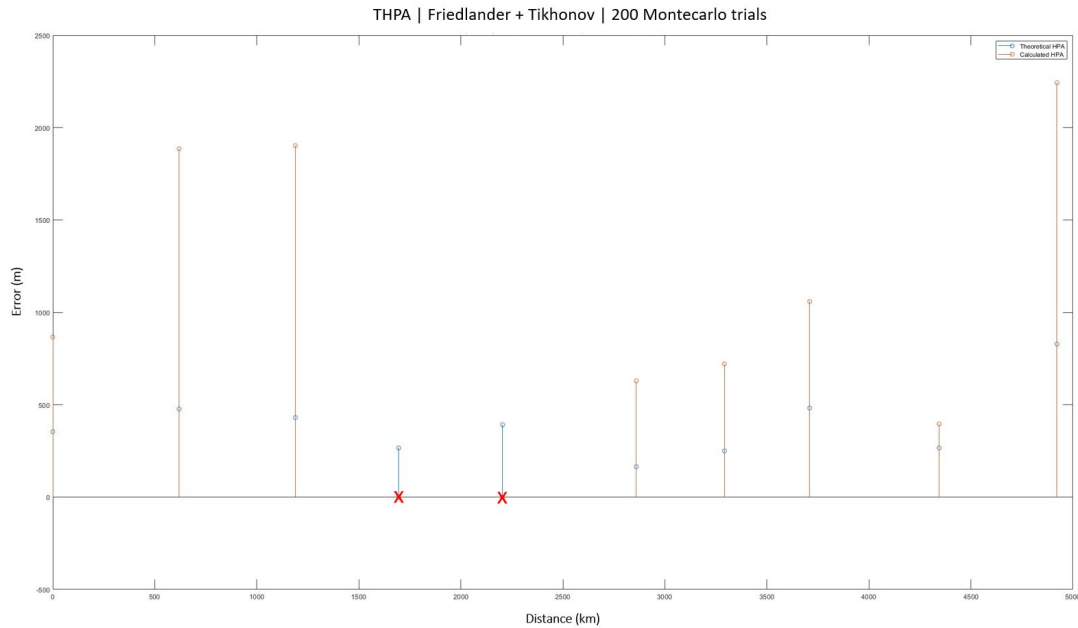


Fig. 4.3.63: North Atlantic | Friedlander + Tikhonov: Graph.

Error statistics and Horizontal Position Accuracy (HPA) using Friedlander + Tikhonov for 200 Montecarlo trials:

Lat. (°)	Lon. (°)	Alt. (ft)	Mean xEast (m)	Mean yNorth (m)	Mean Cond. number	St. dev. xEast (m)	St. dev. yNorth (m)	Calculated HPA (m)	THPA (m)
51.21	-0.11	20000.00	27.21	-19.64	12.78	729.43	466.93	866.08	353.59
53.13	-8.61	25000.00	-25.34	36.09	20.95	950.34	1628.14	1885.21	476.59
54.41	-16.98	30000.00	14.70	31.07	19.89	958.93	1642.66	1902.07	430.17
55.09	-24.77	35000.00	-1365331.72	-1039017.91	19.12	1928226.08	1454622.92	-2.00	265.96
55.71	-32.73	35000.00	-17737.07	-23830.56	14.41	181401.56	29232.76	-2.00	351.33
55.79	-43.18	35000.00	-0.93	12.53	8.56	461.61	426.39	628.40	163.98
54.84	-49.78	35000.00	56.90	54.56	12.83	494.28	524.53	720.73	249.25
52.86	-55.17	30000.00	74.69	66.40	13.72	697.76	795.50	1058.45	481.73
49.19	-62.11	25000.00	27.69	-4.28	6.85	344.22	194.89	395.56	265.67
45.45	-67.41	20000.00	-139.32	-463.28	20.67	634.11	2151.02	2242.54	827.93

Fig. 4.3.64: North Atlantic | Friedlander + Tikhonov: Statistics.

A brief summary of the results is included:

- Points with horizontal errors larger than 15 km: 2 out of 10 (20 %)
- Highest valid calculated horizontal error: 2242.54 m
- Point with highest horizontal error: (45.45°, -67.41°, 20000 ft)

3. Friedlander + T-SVD:

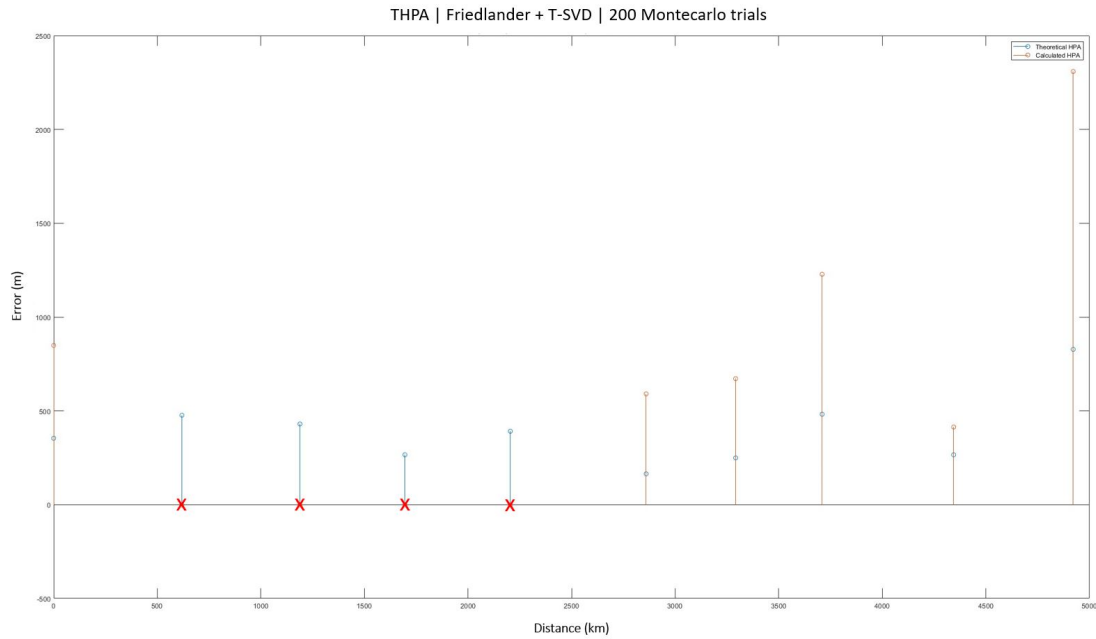


Fig. 4.3.65: North Atlantic | Friedlander + T-SVD: Graph.

Error statistics and Horizontal Position Accuracy (HPA) using Friedlander + T-SVD for 200 Montecarlo trials:

Lat. (°)	Lon. (°)	Alt. (ft)	Mean xEast (m)	Mean yNorth (m)	Mean Cond. number	St. dev. xEast (m)	St. dev. yNorth (m)	Calculated HPA (m)	THPA (m)
51.21	-0.11	20000.00	78.17	-50.90	12.78	717.68	453.29	848.84	353.59
53.13	-8.61	25000.00	507008.52	-881255.52	21.18	1673539.80	2909046.16	-2.00	476.59
54.41	-16.98	30000.00	-428168.86	-793021.70	21.48	1789585.55	3314677.46	-2.00	430.17
55.09	-24.77	35000.00	-599044.34	-506716.96	28.09	1025055.44	808860.83	-2.00	265.86
55.71	-32.73	35000.00	-241130.37	-330892.60	15.23	1150570.67	1580557.41	-2.00	391.33
55.79	-43.18	35000.00	-11.83	6.72	8.56	432.53	402.16	590.61	163.98
54.84	-49.78	35000.00	-14.53	-19.83	12.53	459.62	489.72	671.62	249.25
52.86	-55.17	30000.00	1.58	-0.19	13.72	819.55	914.24	1228.01	481.73
49.19	-62.11	25000.00	41.92	-24.55	6.65	363.74	197.65	413.97	265.67
45.45	-67.41	20000.00	14.41	49.47	20.67	652.45	2215.00	2309.10	827.53

Fig. 4.3.66: North Atlantic | Friedlander + T-SVD: Statistics.

A brief summary of the results is included:

- Points with horizontal errors larger than 15 km: 4 out of 10 (40 %)
- Highest valid calculated horizontal error: 2309.10 m
- Point with highest horizontal error: (45.45°, -67.41°, 20000 ft)

1. Schau & Robinson + Pseudoinverse:

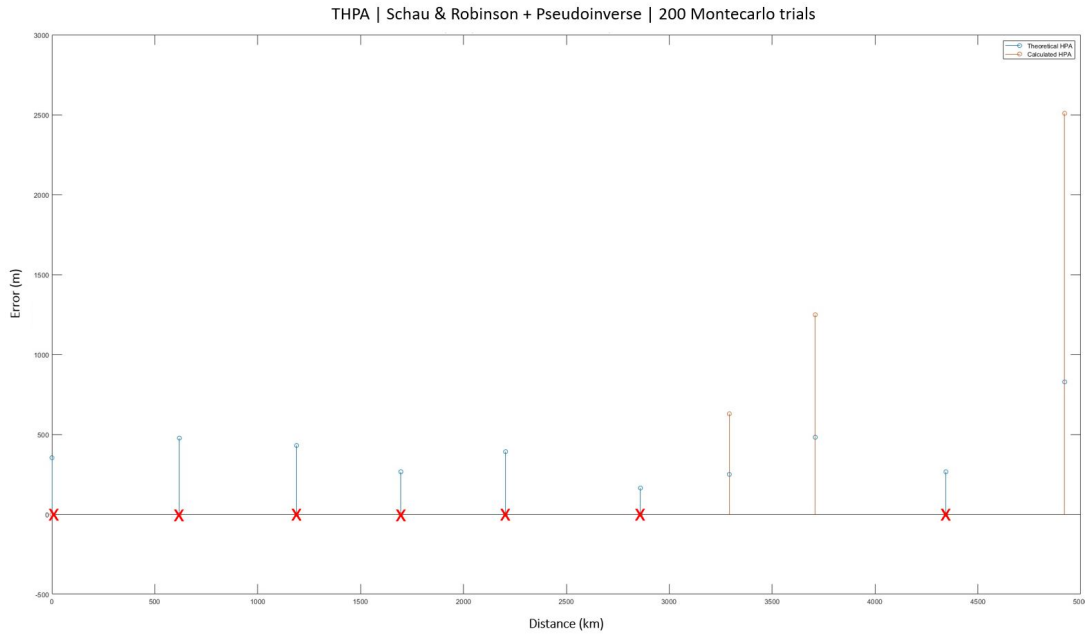


Fig. 4.3.67: North Atlantic | Schau & Robinson + Pseudoinverse: Graph.

Error statistics and Horizontal Position Accuracy (HPA) using Schau & Robinson + Pseudoinverse for 200 Montecarlo trials:

Lat. (°)	Lon. (°)	Alt. (ft)	Mean xEast (m)	Mean yNorth (m)	Mean Cond. number	St. dev. xEast (m)	St. dev. yNorth (m)	Calculated HPA (m)	THPA (m)
51.21	-0.11	20000.00	2484122.06	-1329124.32	40.22	2951307.70	1748583.68	-2.00	353.59
53.13	-8.61	25000.00	5580657.57	-9732604.56	29.72	4364081.98	7613918.91	-2.00	476.59
54.41	-16.98	30000.00	-4861205.94	-9006079.76	38.64	4325629.83	8019039.42	-2.00	430.17
55.09	-24.77	35000.00	-642415.44	-525029.20	24.85	1228727.25	946739.55	-2.00	265.96
55.71	-32.73	35000.00	-4802171.09	-6630682.18	35.98	5258630.01	7272176.87	-2.00	351.33
55.79	-43.18	35000.00	5177040.51	-4628915.51	28.56	5416588.13	4846090.37	-2.00	163.98
54.84	-49.78	35000.00	-0.30	-0.99	12.83	433.68	455.06	628.62	249.25
52.86	-55.17	30000.00	2.27	-4.48	13.72	824.39	936.81	1247.89	481.73
49.19	-62.11	25000.00	1462.41	502.40	6.87	20932.82	7063.27	-2.00	265.67
45.45	-67.41	20000.00	-30.94	-154.84	20.67	698.53	2409.03	2508.27	827.93

Fig. 4.3.68: North Atlantic | Schau & Robinson + Pseudoinverse: Statistics.

A brief summary of the results is included:

- Points with horizontal errors larger than 15 km: 7 out of 10 (70 %)
- Highest valid calculated horizontal error: 2508.27 m
- Point with highest horizontal error: (45.45°, -67.41°, 20000 ft)

2. Schau & Robinson + Tikhonov:

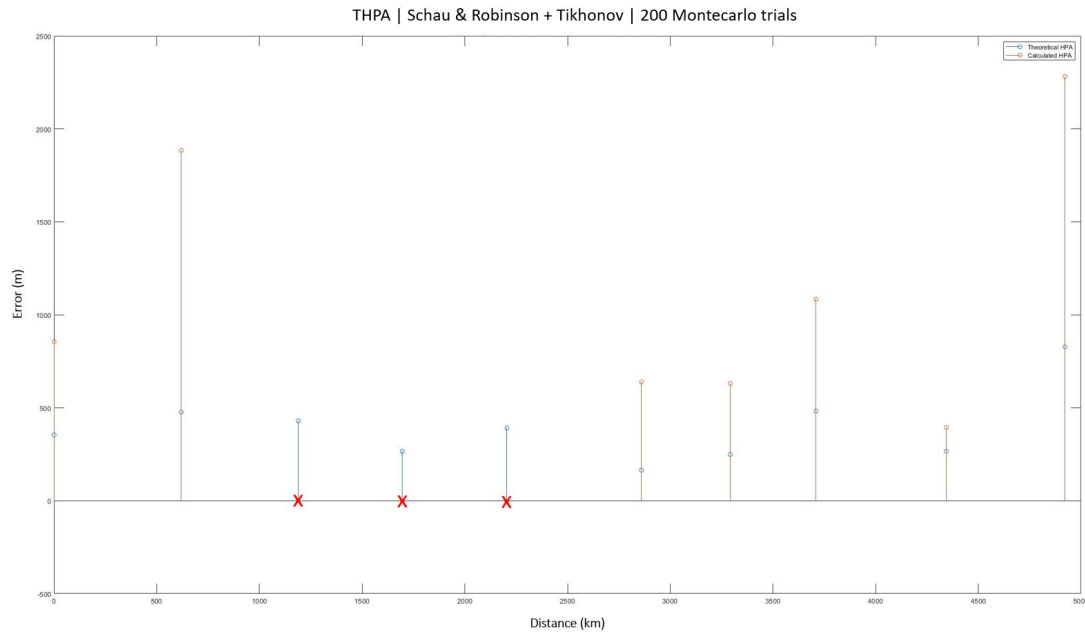


Fig. 4.3.69: North Atlantic | Schau & Robinson + Tikhonov: Graph.

Error statistics and Horizontal Position Accuracy (HPA) using Schau & Robinson + Tikhonov for 200 Montecarlo trials:

Lat. (°)	Lon. (°)	Alt. (ft)	Mean xEast (m)	Mean yNorth (m)	Mean Cond. number	St. dev. xEast (m)	St. dev. yNorth (m)	Calculated HPA (m)	THPA (m)
51.21	-0.11	20000.00	-44.14	24.69	12.78	714.17	472.15	856.13	353.59
53.13	-8.61	25000.00	30.38	-33.57	20.95	936.56	1635.20	1884.42	476.59
54.41	-16.98	30000.00	-40217.55	-73611.33	19.97	399882.15	732077.29	-2.00	430.17
55.09	-24.77	35000.00	-233312.25	-176524.12	12.16	948556.01	716096.50	-2.00	265.86
55.71	-32.73	35000.00	-48775.67	-65999.87	14.50	379619.56	514277.73	-2.00	391.33
55.79	-43.18	35000.00	-11.99	10.19	8.56	464.58	439.22	639.33	163.98
54.84	-49.78	35000.00	-5.33	-8.93	12.83	436.18	455.45	630.63	249.25
52.86	-55.17	30000.00	-43.29	-36.80	13.72	707.07	821.41	1083.81	481.73
49.19	-62.11	25000.00	-6.83	-0.26	6.85	343.04	194.79	394.48	265.67
45.45	-67.41	20000.00	-30.55	-108.24	20.67	647.12	2187.73	2281.43	827.93

Fig. 4.3.70: North Atlantic | Schau & Robinson + Tikhonov: Statistics.

A brief summary of the results is included:

- Points with horizontal errors larger than 15 km: 3 out of 10 (30 %)
- Highest valid calculated horizontal error: 2281.43 m
- Point with highest horizontal error: (45.45°, -67.41°, 20000 ft)

3. Schau & Robinson + T-SVD:

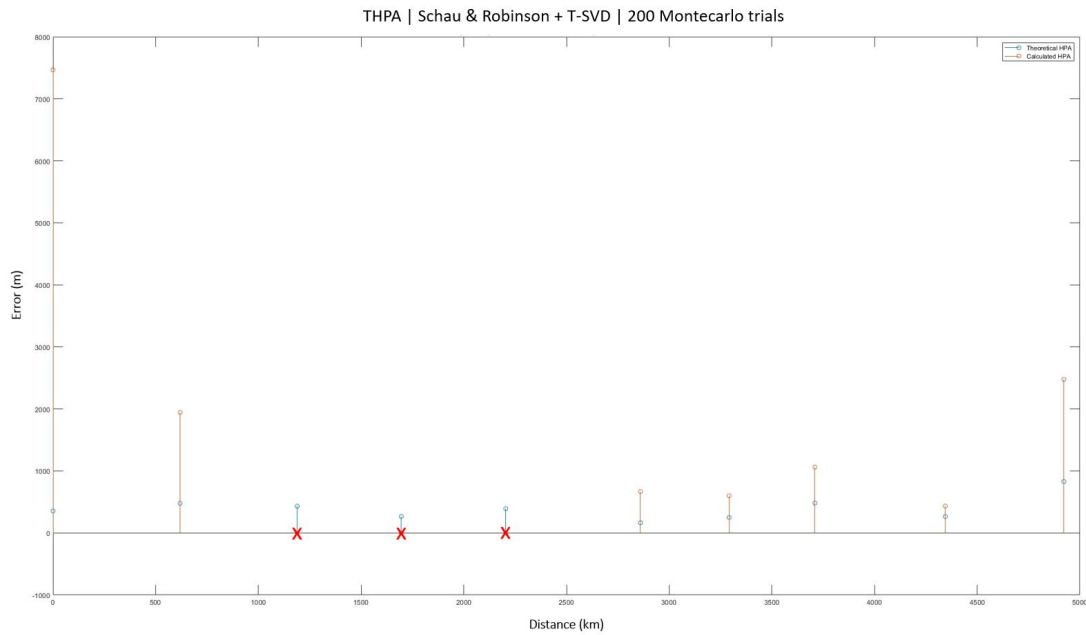


Fig. 4.3.71: North Atlantic | Schau & Robinson + T-SVD: Graph.

Error statistics and Horizontal Position Accuracy (HPA) using Schau & Robinson + T-SVD for 200 Montecarlo trials:

Lat. (°)	Lon. (°)	Alt. (ft)	Mean xEast (m)	Mean yNorth (m)	Mean Cond. number	St. dev. xEast (m)	St. dev. yNorth (m)	Calculated HPA (m)	THPA (m)
51.21	-0.11	20000.00	410.68	-272.98	12.78	6274.30	4048.41	7467.02	353.59
53.13	-8.61	25000.00	31.77	-39.77	20.95	959.55	1689.62	1943.08	476.59
54.41	-16.98	30000.00	-110621.27	-204854.10	20.29	910847.32	1686606.28	-2.00	430.17
55.09	-24.77	35000.00	-475523.28	-378778.32	18.40	1116234.11	861988.52	-2.00	265.86
55.71	-32.73	35000.00	-103476.91	-141276.45	14.71	699297.92	957901.39	-2.00	391.33
55.79	-43.18	35000.00	15.44	-10.38	8.56	486.90	456.05	667.12	163.98
54.84	-49.78	35000.00	19.33	19.38	12.93	407.06	438.96	598.65	249.25
52.86	-55.17	30000.00	18.68	14.94	13.72	696.82	798.95	1060.13	451.73
49.19	-62.11	25000.00	47.78	-28.44	6.85	378.75	208.34	432.26	265.67
45.45	-67.41	20000.00	-23.65	-61.75	20.67	690.70	2377.57	2475.87	827.93

Fig. 4.3.72: North Atlantic | Schau & Robinson + T-SVD: Statistics.

A brief summary of the results is included:

- Points with horizontal errors larger than 15 km: 3 out of 10 (30 %)
- Highest valid calculated horizontal error: 7467.02 m
- Point with highest horizontal error: (51.21°, -0.11°, 20000 ft)

1. Chan & Ho + Pseudoinverse:

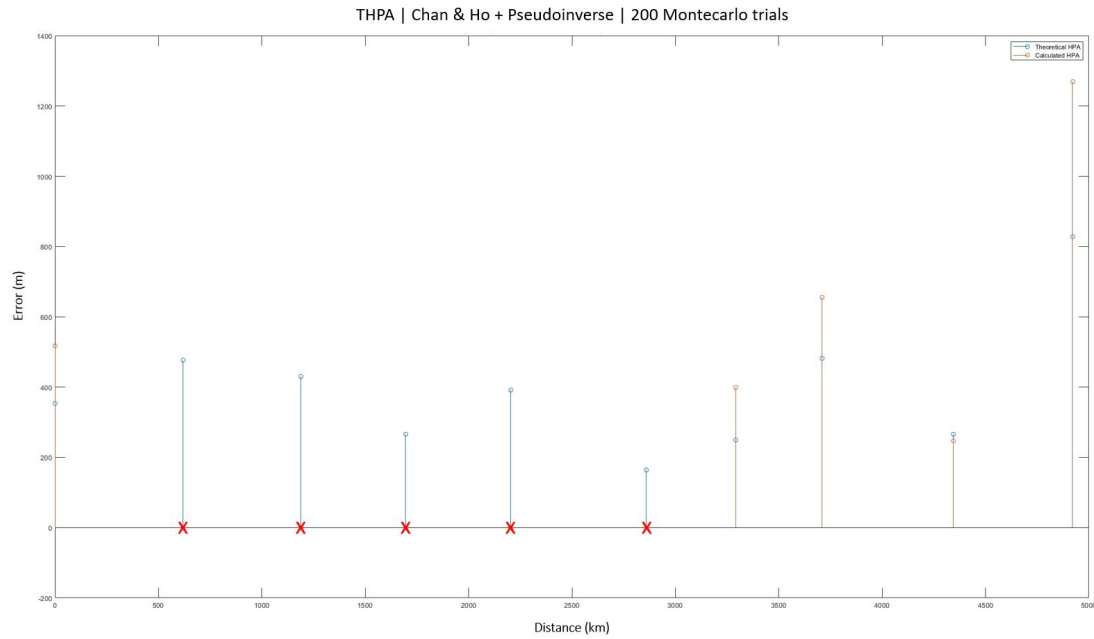


Fig. 4.3.73: North Atlantic | Chan & Ho + Pseudoinverse: Graph.

Error statistics and Horizontal Position Accuracy (HPA) using Chan & Ho + Pseudoinverse for 200 Montecarlo trials:

Lat. (°)	Lon. (°)	Alt. (ft)	Mean xEast (m)	Mean yNorth (m)	Mean Cond. number	St. dev. xEast (m)	St. dev. yNorth (m)	Calculated HPA (m)	THPA (m)
51.21	-0.11	20000.00	23.26	-16.73	12.78	436.63	277.22	517.20	353.59
53.13	-8.61	25000.00	1647442.21	-2869511.76	22.66	3156418.50	5499166.65	-2.00	476.59
54.41	-16.98	30000.00	-1030290.41	-1907728.03	23.66	2644743.17	4897985.57	-2.00	430.17
55.09	-24.77	35000.00	-1925931.85	-1568039.36	49.89	1116387.33	800908.89	-2.00	265.86
55.71	-32.73	35000.00	-4638347.92	-6394089.44	33.68	3926240.46	5418253.05	-2.00	391.33
55.79	-43.18	35000.00	595156.17	-529204.73	11.17	2361978.18	2100269.68	-2.00	163.98
54.84	-49.78	35000.00	-23.55	-21.15	12.83	274.29	289.54	398.83	249.25
52.86	-55.17	30000.00	-24.26	-21.68	13.72	434.28	490.93	655.45	481.73
49.19	-62.11	25000.00	-9.22	3.69	6.85	212.90	125.09	246.93	265.67
45.45	-67.41	20000.00	-33.71	-109.81	20.67	359.60	1217.20	1269.21	827.93

Fig. 4.3.74: North Atlantic | Chan & Ho + Pseudoinverse: Statistics.

A brief summary of the results is included:

- Points with horizontal errors larger than 15 km: 5 out of 10 (50 %)
- Highest valid calculated horizontal error: 1269.21 m
- Point with highest horizontal error: (45.45°, -67.41°, 20000 ft)

2. Chan & Ho + Tikhonov:

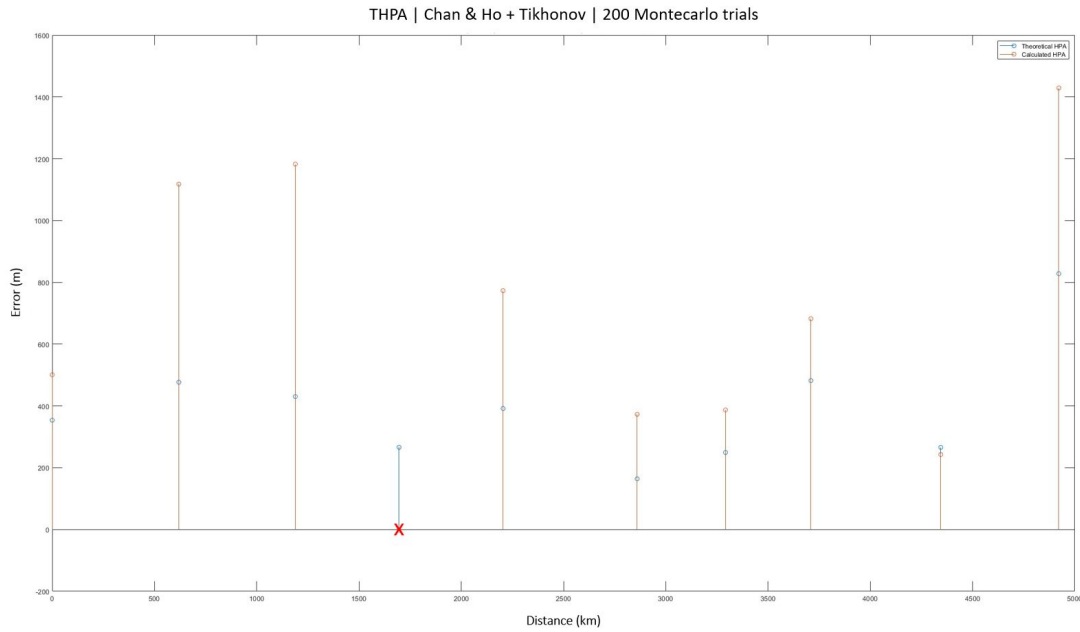


Fig. 4.3.75: North Atlantic | Chan & Ho + Tikhonov: Graph.

Error statistics and Horizontal Position Accuracy (HPA) using Chan & Ho + Tikhonov for 200 Montecarlo trials:

Lat. (°)	Lon. (°)	Alt. (ft)	Mean xEast (m)	Mean yNorth (m)	Mean Cond. number	St. dev. xEast (m)	St. dev. yNorth (m)	Calculated HPA (m)	THPA (m)
51.21	-0.11	20000.00	3.08	-3.24	12.78	426.31	262.70	500.75	353.59
53.13	-8.61	25000.00	-12.97	22.92	20.95	561.92	965.90	1117.47	476.59
54.41	-16.98	30000.00	-22.95	-42.53	19.89	594.29	1022.18	1182.38	430.17
55.09	-24.77	35000.00	-3692672.24	-2771377.97	32.27	1999641.05	1498622.80	-2.00	265.86
55.71	-32.73	35000.00	32.41	43.27	14.35	457.06	623.06	772.73	391.33
55.79	-43.18	35000.00	25.78	-20.24	9.56	274.56	252.11	372.76	163.98
54.04	-49.78	35000.00	19.19	20.90	12.83	283.61	283.19	386.90	249.25
52.86	-55.17	30000.00	-11.26	-12.79	13.72	442.06	519.45	682.09	481.73
49.19	-62.11	25000.00	-20.16	10.30	6.85	210.53	120.71	242.68	265.67
45.45	-67.41	20000.00	-13.17	-38.09	20.67	394.75	1373.06	1428.68	827.93

Fig. 4.3.76: North Atlantic | Chan & Ho + Tikhonov: Statistics.

A brief summary of the results is included:

- Points with horizontal errors larger than 15 km: 1 out of 10 (10 %)
- Highest valid calculated horizontal error: 1428.68 m
- Point with highest horizontal error: (45.45°, -67.41°, 20000 ft)

3. Chan & Ho + T-SVD:

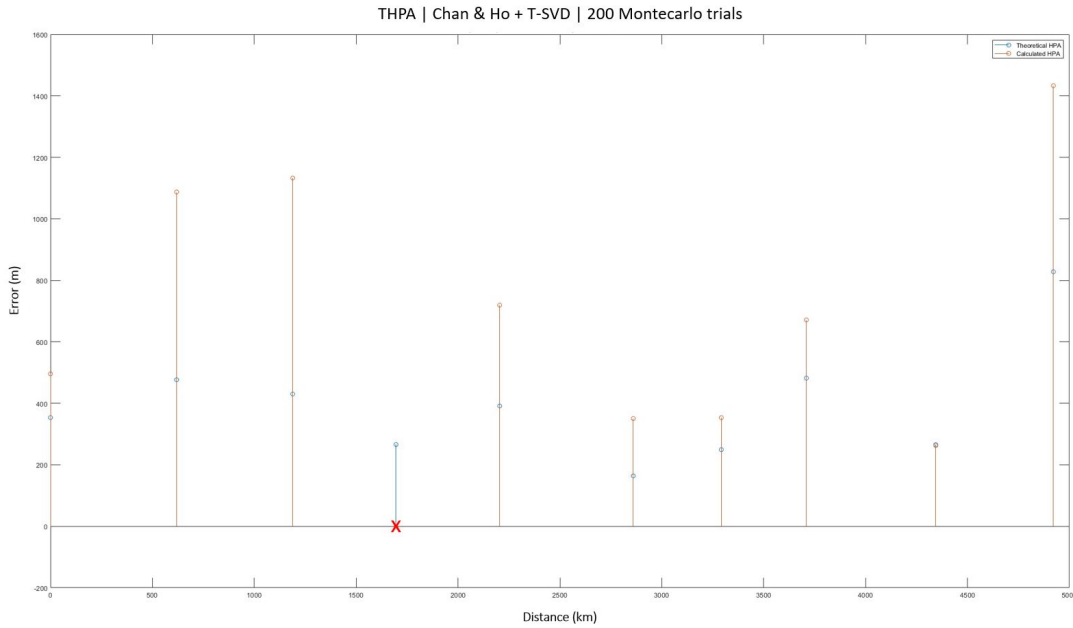


Fig. 4.3.77: North Atlantic | Chan & Ho + T-SVD: Graph.

Error statistics and Horizontal Position Accuracy (HPA) using Chan & Ho + T-SVD for 200 Montecarlo trials:

Lat. (°)	Lon. (°)	Alt. (ft)	Mean xEast (m)	Mean yNorth (m)	Mean Cond. number	St. dev. xEast (m)	St. dev. yNorth (m)	Calculated HPA (m)	THPA (m)
51.21	-0.11	20000.00	61.50	-40.95	12.78	418.97	265.42	495.96	353.59
53.13	-8.61	25000.00	-41.72	75.60	20.95	541.15	942.84	1087.10	476.59
54.41	-16.98	30000.00	61.88	128.77	19.89	567.62	980.12	1132.62	430.17
55.09	-24.77	35000.00	-29929.84	-22243.30	10.91	423152.11	314580.48	-2.00	265.86
55.71	-32.73	35000.00	-39.07	-38.45	14.35	424.33	580.64	719.16	391.33
55.79	-43.18	35000.00	-12.78	12.25	8.56	251.30	244.21	350.41	163.98
54.84	-49.78	35000.00	-38.15	-42.81	12.83	240.97	258.30	353.25	249.25
52.86	-55.17	30000.00	-65.29	-68.83	13.72	446.15	501.59	671.29	481.73
49.19	-62.11	25000.00	22.81	-11.09	6.85	230.86	124.80	262.44	265.67
45.45	-67.41	20000.00	14.72	34.91	20.67	415.30	1371.50	1433.00	827.93

Fig. 4.3.78: North Atlantic | Chan & Ho + T-SVD: Statistics.

A brief summary of the results is included:

- Points with horizontal errors larger than 15 km: 1 out of 10 (10 %)
- Highest valid calculated horizontal error: 1433.00 m
- Point with highest horizontal error: (45.45°, -67.41°, 20000 ft)

1. Bancroft + Pseudoinverse:

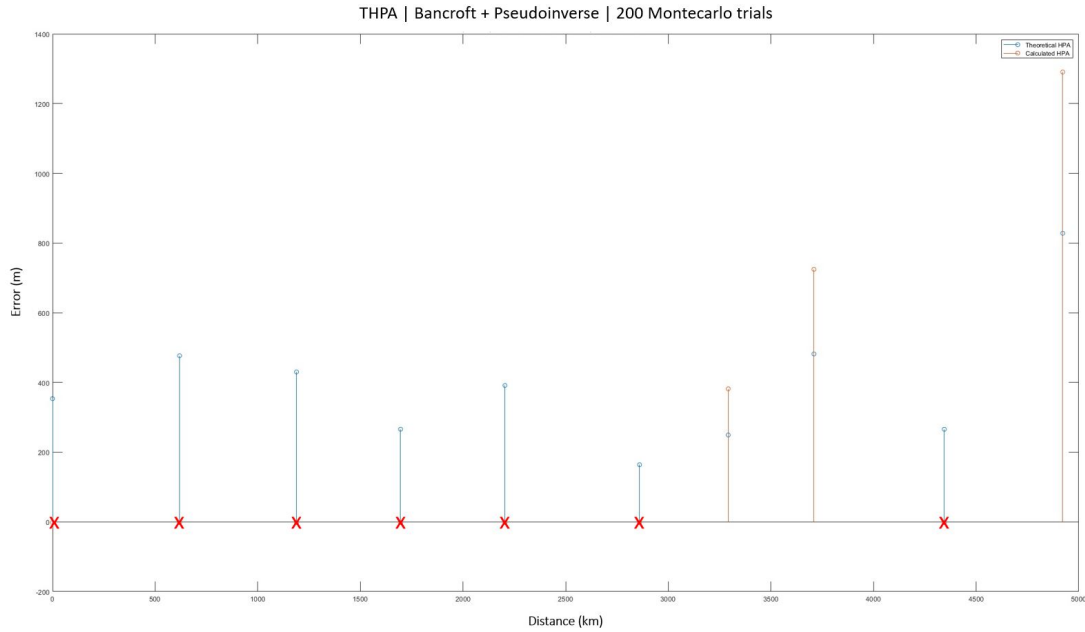


Fig. 4.3.79: North Atlantic | Bancroft + Pseudoinverse: Graph.

Error statistics and Horizontal Position Accuracy (HPA) using Bancroft + Pseudoinverse for 200 Montecarlo trials:

Lat. (°)	Lon. (°)	Alt. (ft)	Mean xEast (m)	Mean yNorth (m)	Mean Cond. number	St. dev. xEast (m)	St. dev. yNorth (m)	Calculated HPA (m)	THPA (m)
51.21	-0.11	20000.00	5942609.13	-3421447.93	40.21	3901302.61	2329621.90	-2.00	353.59
53.13	-8.61	25000.00	1714731.65	-2986028.66	22.66	3159758.03	5504139.26	-2.00	476.59
54.41	-16.98	30000.00	-1807755.02	-3348145.58	26.64	3410694.42	6319381.77	-2.00	430.17
55.09	-24.77	35000.00	-998333.40	-798889.63	27.65	1381590.71	1063912.32	-2.00	265.86
55.71	-32.73	35000.00	-2520993.88	-3477515.59	25.22	4042136.38	5581465.66	-2.00	391.33
55.79	-43.18	35000.00	5844165.28	-5264654.32	27.71	5622174.50	5058402.71	-2.00	163.98
54.84	-49.78	35000.00	32.09	26.46	12.83	264.32	275.49	381.79	249.25
52.86	-55.17	30000.00	-26.68	-30.71	13.72	478.59	543.92	724.50	481.73
49.19	-62.11	25000.00	10023.99	3546.61	6.99	52720.50	18693.15	-2.00	265.67
45.45	-67.41	20000.00	26.92	97.66	20.67	375.81	1234.59	1290.52	827.93

Fig. 4.3.80: North Atlantic | Bancroft + Pseudoinverse: Statistics.

A brief summary of the results is included:

- Points with horizontal errors larger than 15 km: 7 out of 10 (70 %)
- Highest valid calculated horizontal error: 1290.52 m
- Point with highest horizontal error: (45.45°, -67.41°, 20000 ft)

2. Bancroft + Tikhonov:

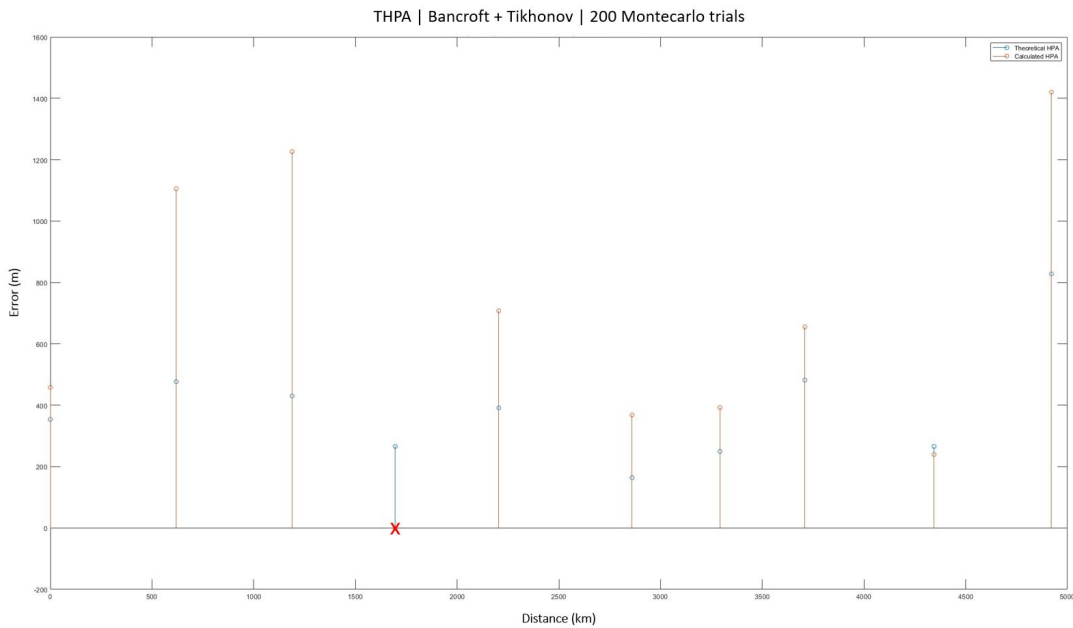


Fig. 4.3.81: North Atlantic | Bancroft + Tikhonov: Graph.

Error statistics and Horizontal Position Accuracy (HPA) using Bancroft + Tikhonov for 200 Montecarlo trials:

Lat. (°)	Lon. (°)	Alt. (ft)	Mean xEast (m)	Mean yNorth (m)	Mean Cond. number	St. dev. xEast (m)	St. dev. yNorth (m)	Calculated HPA (m)	THPA (m)
51.21	-0.11	20000.00	-74.94	55.51	12.70	391.08	238.98	458.31	353.59
53.13	-8.61	25000.00	-0.89	3.15	20.95	550.13	958.95	1105.54	476.59
54.41	-16.98	30000.00	61.35	102.00	19.89	610.77	1063.58	1226.47	430.17
55.09	-24.77	35000.00	-956041.45	-717918.15	16.32	1898846.93	1425156.67	-2.00	265.86
55.71	-32.73	35000.00	-12.28	-23.98	14.35	410.44	570.61	707.60	391.33
55.79	-40.18	35000.00	-17.29	21.25	8.56	267.35	253.33	368.31	163.98
54.84	-49.78	35000.00	-21.20	-23.97	12.83	267.92	296.47	382.23	249.25
52.86	-55.17	30000.00	16.62	23.30	13.72	427.95	496.32	655.34	401.73
49.19	-62.11	25000.00	-3.78	2.31	6.85	211.22	113.60	239.83	265.67
45.45	-67.41	20000.00	-30.33	-114.77	20.67	401.50	1361.88	1419.83	827.93

Fig. 4.3.82: North Atlantic | Bancroft + Tikhonov: Statistics.

A brief summary of the results is included:

- Points with horizontal errors larger than 15 km: 1 out of 10 (10 %)
- Highest valid calculated horizontal error: 1419.83 m
- Point with highest horizontal error: (45.45°, -67.41°, 20000 ft)

3. Bancroft + T-SVD:

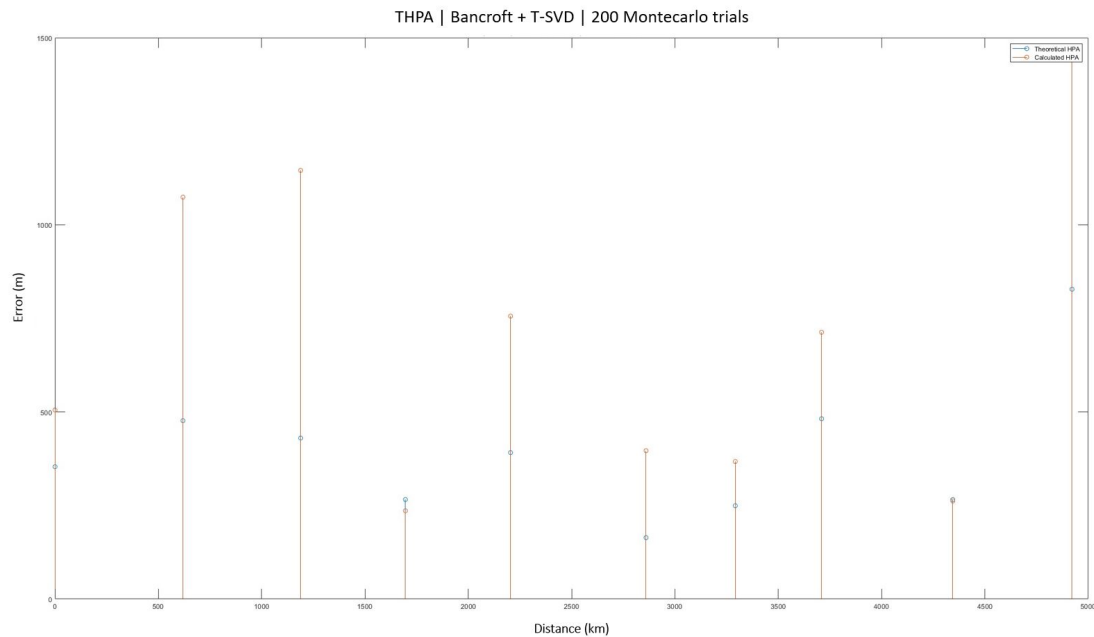


Fig. 4.3.83: North Atlantic | Bancroft + T-SVD: Graph.

Error statistics and Horizontal Position Accuracy (HPA) using Bancroft + T-SVD for 200 Montecarlo trials:

Lat. (°)	Lon. (°)	Alt. (ft)	Mean xEast (m)	Mean yNorth (m)	Mean Cond. number	St. dev. xEast (m)	St. dev. yNorth (m)	Calculated HPA (m)	THPA (m)
51.21	-0.11	20000.00	-8.87	8.97	12.78	429.35	266.14	505.14	353.59
53.13	-8.61	25000.00	-22.55	50.63	20.95	535.31	931.08	1073.99	476.59
54.41	-16.98	30000.00	-28.82	-33.28	19.89	572.17	992.32	1145.46	430.17
55.09	-24.77	35000.00	14.51	12.20	10.79	184.68	146.71	235.87	265.96
55.71	-32.73	35000.00	5.32	9.85	14.35	446.68	610.04	756.05	391.33
55.79	-43.18	35000.00	3.20	-0.21	8.56	293.23	266.78	396.43	163.98
54.84	-49.78	35000.00	-32.79	-32.65	12.83	255.95	263.70	367.49	249.25
52.86	-55.17	30000.00	15.82	22.43	13.72	470.66	535.43	712.89	481.73
49.19	-62.11	25000.00	-6.57	1.25	6.85	231.20	123.19	261.97	265.67
45.45	-67.41	20000.00	36.14	149.58	20.67	409.78	1384.27	1443.64	827.93

Fig. 4.3.84: North Atlantic | Bancroft + T-SVD: Statistics.

A brief summary of the results is included:

- Points with horizontal errors larger than 15 km: 0 out of 10 (0 %)
- Highest valid calculated horizontal error: 1443.64 m
- Point with highest horizontal error: (45.45°, -67.41°, 20000 ft)

The conducted tests have demonstrated the feasibility of estimating aircraft positions using the inverse localization problem with a LEO satellite constellation. The results are obtained through a two-step error calculation process. Firstly, a theoretical horizontal error (referred to as THPA) is determined for each point along the flight trajectory using the CRLB approach. The inverse localization problem then provides calculated accuracy errors, which are compared to the theoretical errors given by the CRLB. The comparison graphs effectively depict the behavior of this limit in the MLAT system. The discrete blue points represent the theoretical horizontal errors, while the orange points indicate the error estimations obtained through the inverse problem. In most cases, the theoretical limit is lower than the calculated error.

However, there are certain points where the inverse problem yields inaccurate solutions, resulting in large horizontal errors that exceed the threshold set at 15 km. This discrepancy can be attributed to the poor performance of the localization algorithms, which occasionally provide starting points that deviate significantly from the actual point of interest. As a result, the algorithms fail to converge to the expected solution, leading to the assignment of "-2" for these cases in the tables. In the graphs, these cases appear as a red x -symbol at 0, indicating no solutions (more specifically, large horizontal errors) have been calculated. By examining the summaries provided at the conclusion of each simulation case, a recurring pattern can be discerned. Points of interest located at lower altitudes (resulting in larger distances between airplanes and satellites) exhibit less accurate error estimations compared to those situated at higher altitudes, also known as Flight Level (FL)s. Notably, the point with coordinates (45.45°, -67.41°, 20000 ft) appears to be the one with worse calculated errors (of those which do not surpass 15 km).

The set of simulations performed reveals three key points that can be extracted:

- **THPA:**

Considering the proposed constellation and the error values obtained from the CRLB analyses, the THPA is computed for every single point of the trajectory. These selected error models have proved to be adequate to finding the theoretical error for every point, without leaving a single point solution-less. Typically, this THPA represents the minimum achievable horizontal error. The inverse localization problem is used to obtain the actual error. In certain cases, however, and with specific regularization methods, the calculated error can be slightly smaller due to the biased nature of the regularization algorithms.

- **Localization & regularization algorithms:**

Upon examining the performance of the implemented algorithms in this SBM application, it appears that all five algorithms are initially viable for estimating the position of targets using the inverse problem. However, the simulations provide a clearer understanding of their relative performance, indicating that two algorithms outshine the rest in terms of accuracy and reliability for estimating the target position. These two algorithms are Chan & Ho and Bancroft. Based on the results, the Taylor + Pseudoinverse algorithm proves to be the least effective in terms of improving the initial target position. Hence, it is highly recommended to go for a regularization algorithm, like the ones implemented here, the Tikhonov and T-SVD methods.

- **Influence of the starting point:**

In general, bad performances of the localization algorithms result in poor estimations of the starting points which directly affect to the subsequent process of improving the initial positions, trying to get as close as possible to the reference point (i.e., the position of the airplane). Despite having a good condition number at a specific point, starting with a bad estimation of it will end up with large calculated errors because the final estimation actually differs considerably from the reference point.

The South Atlantic region will be tested using only the two best-performing localization algorithms (Chan & Ho and Bancroft). However, the process of improving the initial estimations will continue to be analyzed with the Taylor + pseudoinverse algorithm, and the two regularization algorithms implemented for this application, the Tikhonov and T-SVD methods.

3.10.2 Trajectory II: South Atlantic

1. Chan & Ho + Pseudoinverse:

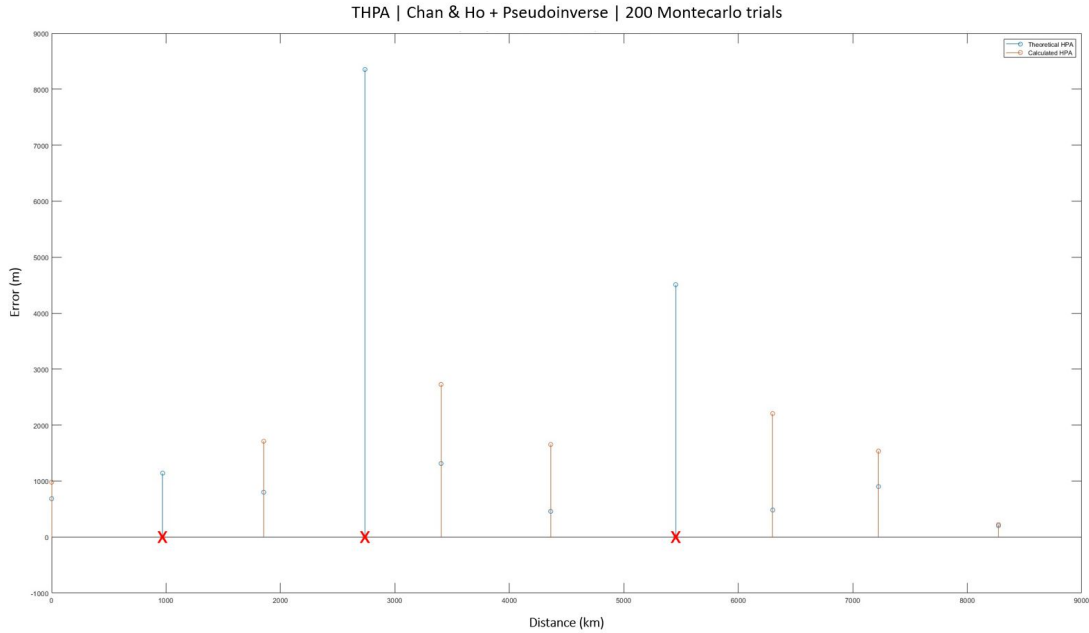


Fig. 4.3.85: South Atlantic | Chan & Ho + Pseudoinverse: Graph.

Error statistics and Horizontal Position Accuracy (HPA) using Chan & Ho + Pseudoinverse for 200 Montecarlo trials:

Lat. (°)	Lon. (°)	Alt. (ft)	Mean xEast (m)	Mean yNorth (m)	Mean Cond. number	St. dev. xEast (m)	St. dev. yNorth (m)	Calculated HPA (m)	THPA (m)
41.51	-1.84	20000.00	-8.33	6.47	19.28	811.67	549.46	980.16	685.03
35.12	-9.43	25000.00	-225025.61	-315658.04	33.74	1832797.78	2571271.80	-2.00	1142.22
28.32	-14.28	30000.00	-251.21	97.43	13.50	1612.35	575.21	1711.88	800.41
22.16	-19.87	35000.00	22931975.34	6074252.81	365.05	562524950.60	149075347.47	-2.00	8353.31
16.53	-22.08	35000.00	-123.92	-84.19	30.74	2410.99	1272.63	2726.25	1313.92
8.34	-24.94	35000.00	111.05	-94.87	26.51	1307.85	1012.45	1653.95	458.85
-0.35	-29.62	35000.00	-2052379.60	15848.22	64.45	12644178.06	104717.33	-2.00	4509.13
-6.44	-34.25	30000.00	196.52	88.92	14.60	2106.69	654.23	2205.94	481.73
-14.37	-36.92	25000.00	-24.21	119.88	26.17	546.73	1434.41	1535.07	902.29
-21.83	-43.02	20000.00	18.39	-3.14	9.72	221.18	33.94	223.77	203.23

Fig. 4.3.86: South Atlantic | Chan & Ho + Pseudoinverse: Statistics.

A brief summary of the results is included:

- Points with horizontal errors larger than 15 km: 3 out of 10 (30 %)
- Highest valid calculated horizontal error: 2726.25 m
- Point with highest horizontal error: (16.53°, -22.08°, 35000 ft)

2. Chan & Ho + Tikhonov:

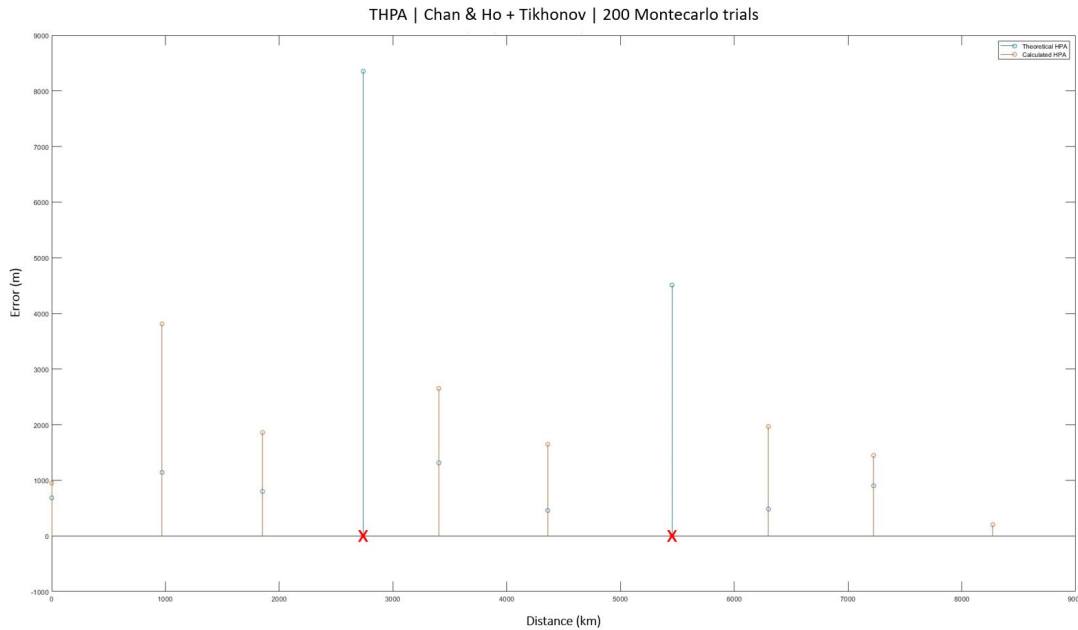


Fig. 4.3.87: South Atlantic | Chan & Ho + Tikhonov: Graph.

Error statistics and Horizontal Position Accuracy (HPA) using Chan & Ho + Tikhonov for 200 Montecarlo trials:

Lat. (°)	Lon. (°)	Alt. (ft)	Mean xEast (m)	Mean yNorth (m)	Mean Cond. number	St. dev. xEast (m)	St. dev. yNorth (m)	Calculated HPA (m)	THPA (m)
41.51	-1.84	20000.00	-18.04	14.38	19.28	786.85	533.62	950.73	885.03
35.12	-9.43	25000.00	-10.15	-4.06	33.35	2281.86	3052.07	3810.78	1142.22
28.32	-14.28	30000.00	-175.89	61.39	13.50	1752.27	623.33	1859.83	800.41
22.16	-19.87	35000.00	2193431.29	584377.80	56.79	3987195.53	1091632.09	-2.00	8353.31
16.53	-22.08	35000.00	16.75	6.16	30.74	2331.15	1261.57	2650.63	1313.92
8.94	-24.94	35000.00	56.50	21.66	26.51	1292.93	1022.67	1648.49	458.85
-0.35	-29.62	35000.00	-70149.18	538.62	64.76	991452.28	7715.43	-2.00	4509.13
-6.44	-34.25	30000.00	-59.61	13.09	14.60	1876.25	582.54	1964.61	481.73
-14.37	-36.92	25000.00	48.31	-88.34	26.17	513.47	1354.37	1448.44	902.29
-21.83	-43.02	20000.00	15.83	-2.89	9.72	200.93	33.24	203.66	203.23

Fig. 4.3.88: South Atlantic | Chan & Ho + Tikhonov: Statistics.

A brief summary of the results is included:

- Points with horizontal errors larger than 15 km: 2 out of 10 (20 %)
- Highest valid calculated horizontal error: 3810.78 m
- Point with highest horizontal error: (35.12°, -9.43°, 25000 ft)

3. Chan & Ho + T-SVD:

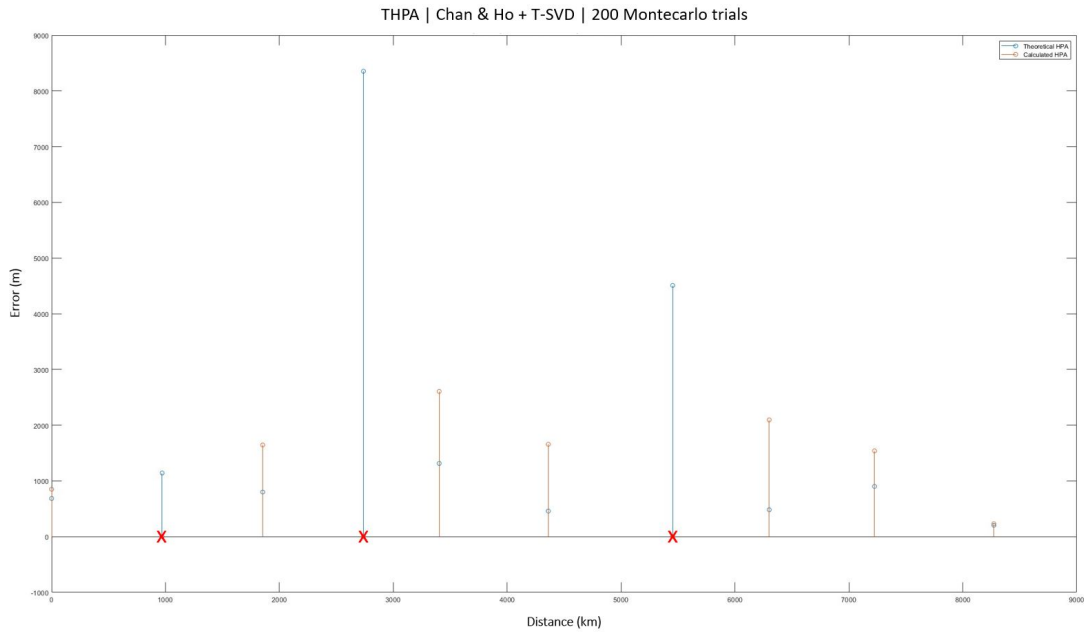


Fig. 4.3.89: South Atlantic | Chan & Ho + T-SVD: Graph.

Error statistics and Horizontal Position Accuracy (HPA) using Chan & Ho + T-SVD for 200 Montecarlo trials:

Lat. (°)	Lon. (°)	Alt. (ft)	Mean xEast (m)	Mean yNorth (m)	Mean Cond. number	St. dev. xEast (m)	St. dev. yNorth (m)	Calculated HPA (m)	THPA (m)
41.51	-1.94	20000.00	-41.23	29.59	19.28	702.96	479.37	850.86	685.03
38.12	-9.43	25000.00	-87502.98	-122734.25	33.53	1231919.62	1728251.85	-2.00	1142.22
28.32	-14.28	30000.00	-5.09	10.88	13.50	1549.47	552.24	1644.94	800.41
22.16	-19.87	35000.00	-12112556.33	-3213767.76	120.15	116135819.33	30804668.12	-2.00	8353.31
16.53	-22.08	35000.00	150.54	70.33	30.74	2306.21	1213.15	2605.83	1313.92
8.34	-24.94	35000.00	-101.09	52.74	26.50	1284.59	1046.70	1657.03	458.85
-0.35	-29.62	35000.00	-80772.31	744.41	64.80	1143274.14	9568.73	-2.00	4509.13
-6.44	-34.25	30000.00	101.64	3.43	14.60	2003.32	611.47	2094.56	481.73
-14.37	-36.92	25000.00	-18.55	6.10	26.17	539.10	1441.47	1538.98	902.29
-21.83	-43.02	20000.00	-14.02	0.57	9.72	228.93	35.28	231.63	203.23

Fig. 4.3.90: South Atlantic | Chan & Ho + T-SVD: Statistics.

A brief summary of the results is included:

- Points with horizontal errors larger than 15 km: 3 out of 10 (30 %)
- Highest valid calculated horizontal error: 2605.83 m
- Point with highest horizontal error: (16.53°, -22.08°, 35000 ft)

1. Bancroft + Pseudoinverse:

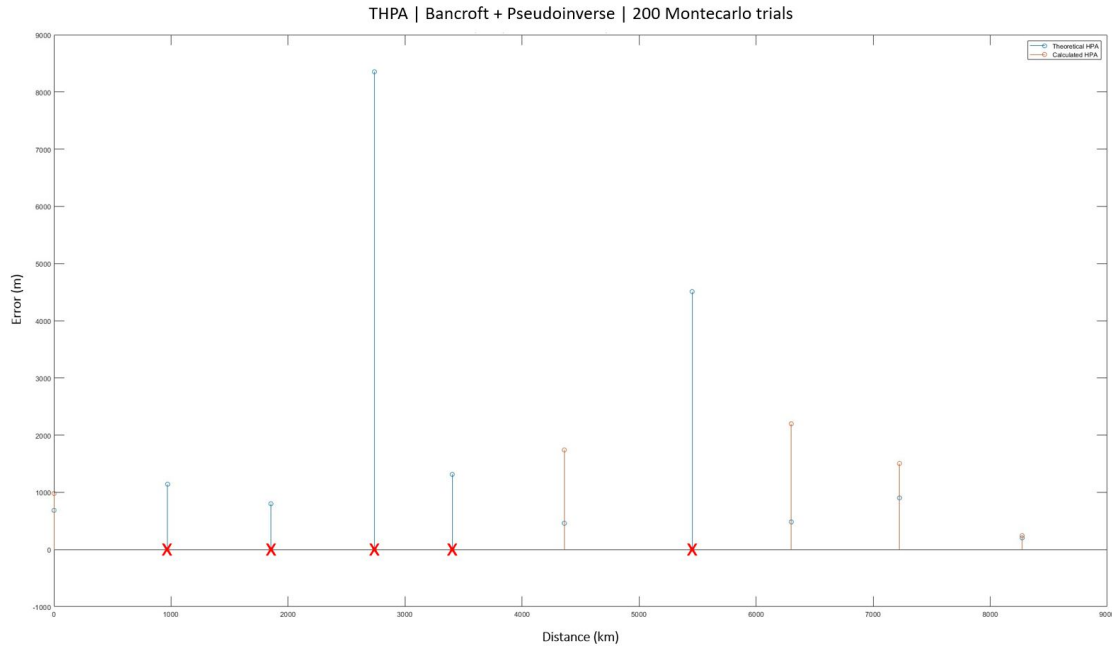


Fig. 4.3.91: South Atlantic | Bancroft + Pseudoinverse: Graph.

Error statistics and Horizontal Position Accuracy (HPA) using Bancroft + Pseudoinverse for 200 Montecarlo trials:

Lat. (°)	Lon. (°)	Alt. (ft)	Mean xEast (m)	Mean yNorth (m)	Mean Cond. number	St. dev. xEast (m)	St. dev. yNorth (m)	Calculated HPA (m)	THPA (m)
41.51	-1.84	20000.00	-9.87	8.90	19.28	812.78	548.11	990.33	685.03
35.12	-9.43	25000.00	-66717.97	-93652.95	33.45	943018.28	1323363.55	-2.00	1142.22
28.32	-14.28	30000.00	1327866.47	-538843.92	16.00	4869232.75	1976157.28	-2.00	800.41
22.16	-19.87	35000.00	23279068.28	6169850.67	262.69	226780189.73	59966452.98	-2.00	8353.31
16.53	-22.08	35000.00	20184.38	17372.01	30.71	284371.32	244799.99	-2.00	1313.92
8.34	-24.94	35000.00	-79.85	80.62	26.50	1387.05	1052.01	1740.88	458.85
-0.35	-29.62	35000.00	-2537356.11	21217.95	64.29	8493909.25	71605.64	-2.00	4509.13
-6.44	-34.25	30000.00	210.86	36.72	14.60	2123.57	571.95	2199.25	481.73
-14.37	-36.92	25000.00	-5.82	59.59	26.17	804.92	1417.21	1504.47	902.29
-21.83	-43.02	20000.00	-10.17	-2.76	9.72	238.46	38.59	241.57	203.23

Fig. 4.3.92: South Atlantic | Bancroft + Pseudoinverse: Statistics.

A brief summary of the results is included:

- Points with horizontal errors larger than 15 km: 5 out of 10 (50 %)
- Highest valid calculated horizontal error: 2199.25 m
- Point with highest horizontal error: (-6.44°, -34.25°, 30000 ft)

2. Bancroft + Tikhonov:

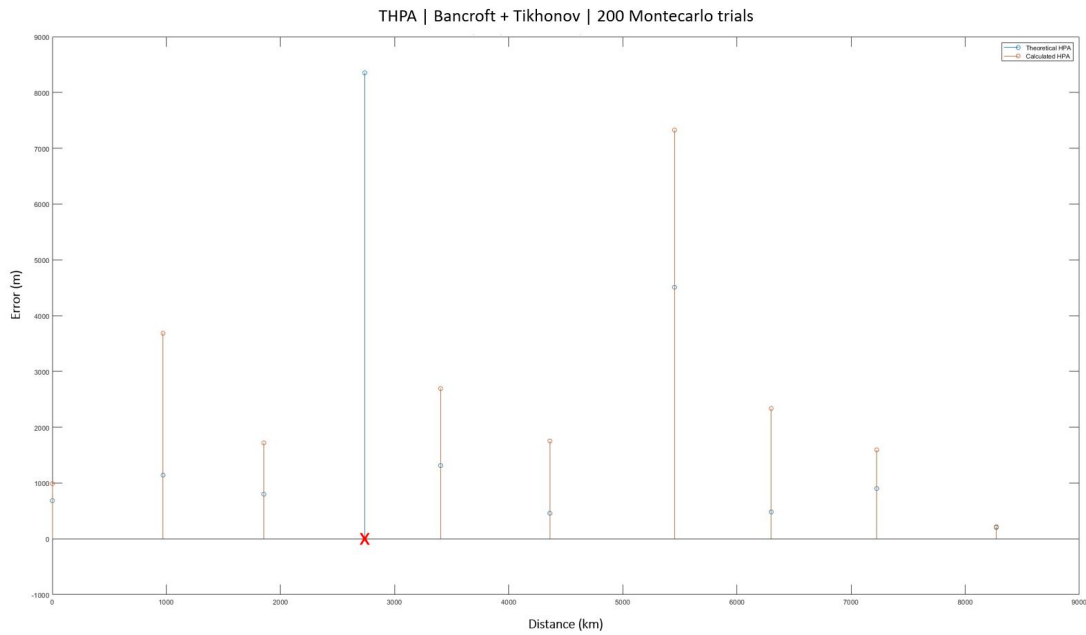


Fig. 4.3.93: South Atlantic | Bancroft + Tikhonov: Graph.

Error statistics and Horizontal Position Accuracy (HPA) using Bancroft + Tikhonov for 200 Montecarlo trials:

Lat. (°)	Lon. (°)	Alt. (ft)	Mean xEast (m)	Mean yNorth (m)	Mean Cond. number	St. dev. xEast (m)	St. dev. yNorth (m)	Calculated HPA (m)	THPA (m)
41.51	-1.84	20000.00	-53.91	24.37	19.28	817.07	559.17	990.09	685.03
35.12	-9.43	25000.00	139.02	223.80	33.35	2197.49	2958.16	3685.06	1142.22
28.32	-14.28	30000.00	162.93	-62.73	13.50	1618.92	500.37	1719.30	800.41
22.16	-19.87	35000.00	2956910.26	790805.86	61.45	7947908.43	2142289.17	-2.00	8353.31
16.53	-22.08	35000.00	185.36	67.59	30.74	2375.21	1272.07	2694.40	1313.92
8.34	-24.94	35000.00	-91.29	33.01	26.50	1365.51	1100.33	1753.67	458.85
-0.35	-29.62	35000.00	551.60	31.93	64.87	7287.25	750.30	7325.78	4509.13
-6.44	-34.25	30000.00	115.61	32.26	14.60	2236.14	681.25	2337.61	481.73
-14.37	-36.92	25000.00	5.79	-26.25	26.17	567.28	1490.50	1594.81	902.29
-21.83	-43.02	20000.00	-5.16	0.62	9.72	215.31	35.10	218.16	203.23

Fig. 4.3.94: South Atlantic | Bancroft + Tikhonov: Statistics.

A brief summary of the results is included:

- Points with horizontal errors larger than 15 km: 1 out of 10 (10 %)
- Highest valid calculated horizontal error: 7325.78 m
- Point with highest horizontal error: (-0.35°, -29.62°, 35000 ft)

3. Bancroft + T-SVD:

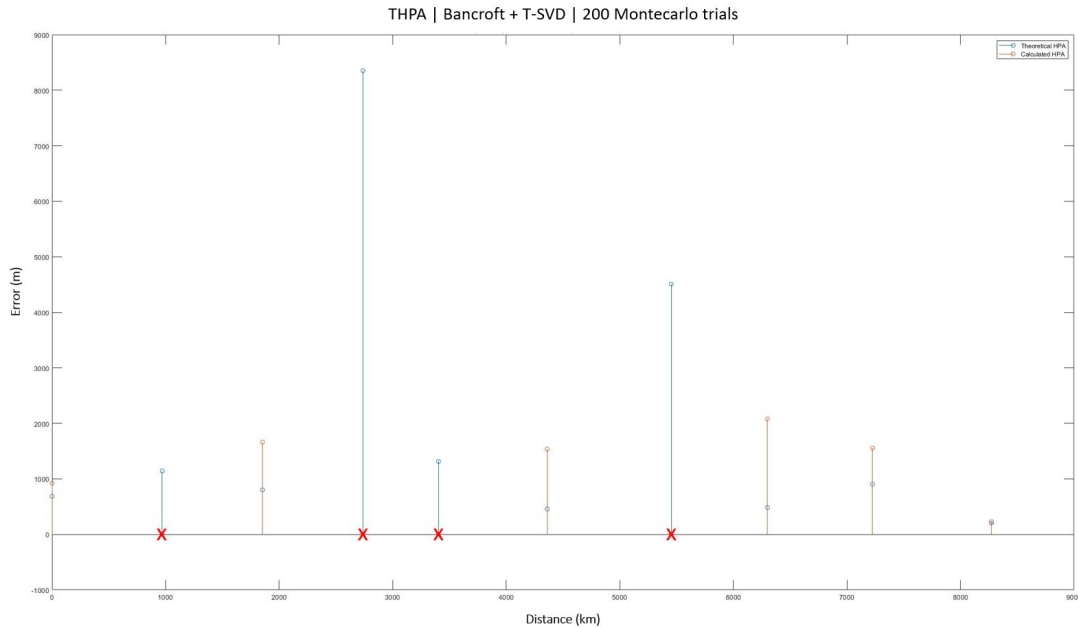


Fig. 4.3.95: South Atlantic | Bancroft + T-SVD: Graph.

Error statistics and Horizontal Position Accuracy (HPA) using Bancroft + T-SVD for 200 Montecarlo trials:

Lat. (°)	Lon. (°)	Alt. (ft)	Mean xEast (m)	Mean yNorth (m)	Mean Cond. number	St. dev. xEast (m)	St. dev. yNorth (m)	Calculated HPA (m)	THPA (m)
41.51	-1.84	20000.00	137.02	-91.57	19.28	764.96	519.64	924.76	685.03
35.12	-9.43	25000.00	-1122685.29	-1575556.01	35.60	4322031.38	6065898.89	-2.00	1142.22
28.32	-14.28	30000.00	38.72	-14.38	13.50	1562.06	565.64	1661.31	800.41
22.16	-19.87	35000.00	-12942457.48	-3420752.30	193.97	96874943.02	25706688.99	-2.00	8353.31
16.53	-22.08	35000.00	79039.89	68079.61	30.62	552941.40	476642.54	-2.00	1313.92
8.34	-24.94	35000.00	7.02	-4.81	26.51	1189.22	970.48	1534.86	458.85
-0.35	-29.62	35000.00	545720.94	-7603.10	65.40	8864027.67	116543.17	-2.00	4509.13
-6.44	-34.25	30000.00	-196.67	-68.43	14.60	1893.83	593.95	2080.41	481.73
-14.37	-36.92	25000.00	43.22	-74.08	26.17	542.75	1458.68	1556.38	902.29
-21.83	-43.02	20000.00	-13.51	-2.83	9.72	226.92	35.37	229.66	203.23

Fig. 4.3.96: South Atlantic | Bancroft + T-SVD: Statistics.

A brief summary of the results is included:

- Points with horizontal errors larger than 15 km: 4 out of 10 (40 %)
- Highest valid calculated horizontal error: 2080.41 m
- Point with highest horizontal error: (-6.44°, -34.25°, 30000 ft)

The tests conducted on the South Atlantic trajectory have exhibited a behavior similar to that of the North Atlantic route. Both localization algorithms yield valid starting points, facilitating the subsequent estimation process without difficulties. However, the issue with the pseudoinverse algorithm persists in this case as well. It remains the least effective algorithm used to improve the initial solutions, resulting in less accurate estimations (as evident from the abundance of "∞" values in the tables). This problem is generally resolved when employing either the Tikhonov or the T-SVD regularization methods. The latter provide better horizontal accuracies than the Taylor + pseudoinverse algorithm. As a consequence, it is advised not to use the pseudoinverse to try to improve the initial target position estimations, rather make use of a regularized method that will perform better and provide more accurate solutions.

Part V

Conclusions

Chapter 1

Overall Findings

With the realization of this project, several conclusions can be drawn based on the findings and outcomes of both operating modes. These conclusions include:

- **CRLB error estimator:**

Experiments have been conducted considering the impact of two important factors in terms of their effect on the system's performance. These two factors are as follows:

1. **System's geometry**
2. **Error measurement sources**

1. **System's geometry:**

Conclusions regarding this factor are outlined considering both types of constellation:

- **Iridium constellation:**

The utilization of the Iridium constellation, characterized by errors in time and satellite positioning, as opposed to a constellation specifically designed for the intended application, reveals a significant disparity in the outcomes.

When employing the Iridium approach, the system's performance deviates considerably from the desired objectives. The coverage provided by this constellation proves to be virtually impractical, as numerous areas suffer from minimal or nonexistent overlap. Establishing an MLAT system solely based on time measurements needs a minimum number of receiving stations—specifically, at least four satellites.

These satellites must have a direct LOS or radio visibility with the aircraft, while also satisfying other requirements such as latency. Consequently, as observed in the analysis of various points in the northern and southern Atlantic regions, connections either fail to establish due to the insufficient number of satellites or, if a connection is established, the resulting errors are excessively large, surpassing the predefined threshold of 15 km.

- **Proposed constellation:**

In contrast, employing the proposed constellation with the same error models yields a significantly enhanced estimation of horizontal errors. Moreover, the issue encountered with Iridium, where even calculating HDOP was impossible due to insufficient satellites, is completely resolved with the proposed constellation. The improved geometry and satellite distribution enable a greater number of connections, regardless of the specific area or point of interest under analysis.

2. Error measurement sources:

This second factor entails three different components that affect the system's performance. Those components are the TOA error, the error associated to the deviation in the true satellites positions, and the SNR.

Results have demonstrated the importance of finding an appropriate value for the satellite position error. After conducting different tests considering errors from 2200 to 25 m, and the latter showing similar performances as an error of 50 m, it has been decided to use 50 m as threshold. Then, adjustments in the TOA error have also been performed, comparing different possibilities and selecting 10 ns as a feasible error model. The third error contributor is the SNR, which depends on both the signal strength emitted from the aircraft (maximum emission power is limited by the aeronautical standards), and the distances between the satellites and the aircrafts. As a consequence, the SNR remains unchangeable.

To sum up, by refining the different error for both time and satellite positioning, a compact and adequate model is obtained, whose results reveal a significant enhancement in the calculation of the theoretical horizontal error compared to the initial case studied (also used with Iridium). The errors, which initially exceeded the threshold set at 15 km, are now reduced to hundreds of meters for all points within the study area. *Case 7* is representative of the error models selected, and used for the trajectory-based study.

- **Localization problem:**

- **Behavior of the THPA:**

In general, and as expected, the CRLB provides a certain THPA that is considered to be the minimum achievable error (for this application, the most relevant error is the horizontal). However, and as some of the graphs show (belonging to solutions obtained using a regularization algorithm), due to the biased nature of this type of inverse problems, some of the calculated errors are slightly smaller than the theoretical value (THPA).

- **Performance of the algorithms:**

Even with improved geometry, the inverse problem that must be solved to compute the estimated positions is typically ill-conditioned for several reasons, leading to difficulties in obtaining accurate solutions:

- * Measurement errors, particularly those related to the actual satellites positions.
- * The distance between the initial starting point and the actual location of the aircraft.

Therefore, non-regularized algorithms such as Taylor + pseudoinverse are not guaranteed to converge to a valid solution. That means that regularized algorithms must be used. The results of the numerical experiments demonstrate that the two best localization algorithms are Chan and Ho, and Bancroft, whereas the best candidates for computing the final estimated positions are Tikhonov and T-SVD. Even in this case, if the starting point is far from the actual aircraft position, the algorithms may diverge. With regards to the Tikhonov algorithm, and considering both the expressions of the Tikhonov regularization parameter (shown in 5.29) and the weighting factor that directly affects the refinement iterations (shown in 5.30), the best suited value of the weighting factor has been deeply assessed, showing that a good option is $w = 0.03$.

- **SBM system:**

After describing the conclusions associated to each operating mode, it is convenient to portray some overall conclusions regarding the MLAT system as a whole, which are:

- The two modes devised to assess the performance of a SBM system, which aims to offer real-time aircraft position information and enhance ATC/ATM systems, have demonstrated successful operation. In an initial assessment, these modes have provided both valid theoretical errors and consistent and reliable calculated errors derived from the estimation process conducted by the algorithms, following the inverse problem.
- It is yet to be determined whether the system, which already exhibits good performance, would enhance further through the implementation of a range of additional measures (AOA and/or FDOA) aimed at improving the performance of a given satellite constellation. Alternatively, another approach could involve proposing a design that prioritizes specific areas of interest, either by emphasizing global coverage (as in the initial mode studied) or by considering trajectories along the globe.
- For the considered constellation and error models, the uncertainty of the aircraft position estimated by means of a SBM system would be acceptable not only to cross-check the ADS-B-derived data for integrity assessment purposes but also to provide a second, GPS-independent surveillance layer.

For the given constellation and error models, the uncertainty associated with the aircraft position estimation using an SBM would be deemed acceptable. This level of uncertainty serves two important purposes:

- * **Integrity Assessment:**

It allows for cross-checking the data obtained from ADS-B to verify its integrity. By comparing the aircraft's estimated position from the SBM system with the ADS-B-derived data, any inconsistencies or anomalies can be identified, enabling integrity assessment of the ADS-B information.

- * **Independent Surveillance Layer:**

The aircraft's position estimation provided by the SBM system serves as a valuable second layer of surveillance that is not reliant solely on GPS. This additional layer of surveillance enhances the overall reliability and redundancy of the aircraft tracking system, offering an alternative source of position information that can be used in conjunction with GPS data.

Chapter 2

Future Work

After the realization of this project, several future work points can be identified for further exploration and development. These future work points include:

- **Extend the localization & regularization algorithms to hybrid cases:**

The project can be extended to handle hybrid localization scenarios, such as incorporating AOA or FDOA measurements along with the existing localization algorithms. This would allow for more accurate and robust positioning in diverse environments.

- **Validate the proposed error models using experimental data:**

To enhance the reliability and accuracy of the project, it is essential to validate the error models used in the localization algorithms. This can be achieved by collecting experimental data and comparing the results obtained from the algorithms with the ground truth.

- **Study the effect of the communication network on the MLAT system performance:**

Investigate the impact of the underlying communication network, specifically the physical and network layers, on the performance of the MLAT system. Analyze factors such as signal quality, interference, and propagation characteristics, as well as network congestion and latencies, to optimize the system's performance in real-world scenarios.

- **Apply non-linear tracking algorithms to derive aircraft positions:**

Explore non-linear tracking algorithms that can directly derive the position of aircraft without requiring the solution of an inverse problem. This approach could potentially improve the efficiency and accuracy of aircraft tracking in the MLAT system.

By focusing on these future work points, the project can be further enhanced (E-MLAT), leading to advancements in hybrid localization techniques, improved error modeling, better understanding of network effects, and the implementation of more efficient tracking algorithms.

Chapter 3

Acknowledgments

I am deeply grateful to Dr. Juan V. Balbastre, the esteemed leader of the *Air Navigation Systems* group at *Valencia Polytechnic University*. Words cannot fully convey my appreciation for the opportunity he bestowed upon me to join the research team in early 2021 and contribute to my Bachelor's Thesis. Over the course of two and a half years, I have had the privilege of working on innovative solutions for ATC/ATM, and this transformative journey culminates with the completion of my Master's Thesis on Space-based Multilateration (SBM) Systems.

I am acutely thankful to Dr. Balbastre for his profound knowledge and expertise in the captivating realms of aviation and aerospace, which have enthralled my passion since childhood. His insights and proficiency have not only shaped me as an individual but also as a diligent researcher. Moreover, I want to thank him for his significant role in paving the path for my professional journey, acting as a vital catalyst that propelled me from being a student to embarking on my professional career as an engineer at *RTX | Collins Aerospace Applied Research & Technology*.

I would like to thank my colleagues at the Telecom Engineering School and the research group for their support throughout these years. Specifically, I hold the friendship of Andrés and Alejandro in deep regard, as I consider myself fortunate to have met them on the very first day of university. Their companionship has been priceless in shaping my life throughout these six years.

Lastly, I want to express my utmost gratitude to my parents, particularly my mother. All their confidence in my abilities has been a guiding beacon, fueling my determination to overcome challenges, embrace opportunities, and strive for greatness. Their unwavering support has been the foundation upon which my achievements stand, and I will forever cherish their love, guidance, and belief in me.

Remember, shoot for the moon.

Bibliography

- [1] *Annex 10 to the Convention on International Civil Aviation – Volume IV Surveillance and Collision Avoidance System. ICAO 2014.*
- [2] *European Mode S Station Functional Specification - SUR/MODES/EMS/SPE-01. Eurocontrol 2005.*
- [3] *ADS-B Horizontal Position Accuracy - EUROCONTROL NMD/NS/SCC 2016. J. Steinleitner, 2016.*
- [4] *Global Air Navigation Plan – Doc 9750-AN/963 Fifth Edition 2016. ICAO 2016.*
- [5] “Concept of Operations Mode S in Europe (Mode S CONOPS) - SUR.ET2.ST02.1000-CNP-01-00. Eurocontrol 1996.” In: ().
- [6] “The CASCADE Programme (ADS-B and Multilateration). Eurocontrol 2004.” In: ().
- [7] “ARTAS (ATM Surveillance Tracker and Server). Eurocontrol 2004.” In: (). URL: <https://www.eurocontrol.int/product/artas>.
- [8] “SASS-C (Surveillance Analysis Support System for ATC Centres). Eurocontrol 2002.” In: (). URL: <https://www.eurocontrol.int/online-tool/surveillance-analysis-support-system-atc-centres>.
- [9] URL: <https://www.eurocontrol.int/service/automatic-dependent-surveillance-broadcast>.
- [10] “NAT Doc 008 Application of separation minima North Atlantic Region – 1st edition Amendment 10. ICAO 2020.” In: ().
- [11] *North Atlantic tracks at Flight Level 330 and below to be abolished. NATS 2022.* URL: <https://nats.aero/blog/2022/02/north-atlantic-tracks-at-flight-level-330-and-below-to-be-abolished/>.
- [12] “Summary of discussions and conclusions of the fifty-fourth meeting of the North Atlantic systems planning group. ICAO – Paris, France 2018.” In: ().
- [13] *ENAIRE – STARTICAL, 2021.* URL: https://www.enaire.es/es_ES/2021_05_18/ndp_proyecto_startical.
- [14] *Aireon.* URL: <https://aireon.com/>.
- [15] *ICAO Cir 326 AN/188 Assessment of ADS-B and Multilateration Surveillance to Support Air Traffic Services and Guidelines for Implementation 2012 ISBN 978-92-9231-980-9.*
- [16] B. Forssell. “Radionavigation Systems: Artech House, 2008.” In: ().
- [17] *New Strategies to Improve Multilateration Systems in the Air Traffic Control.* 2013.
- [18] G. Richard Curry. “Radar System Performance Modeling, Second Edition”. In: *Artech House* (2004).

- [19] Gaspare Galati et al. "Lower bounds of accuracy for enhanced mode-S distributed sensor networks". In: *IET Radar, Sonar and Navigation* 6 (Mar. 2012), pp. 190–201. DOI: 10.1049/iet-rsn.2011.0197.
- [20] Harry B. Lee. "A Novel Procedure for Assessing the Accuracy of Hyperbolic Multilateration Systems". In: *IEEE Transactions on Aerospace and Electronic Systems* AES-11.1 (1975), pp. 2–15. DOI: 10.1109/TAES.1975.308023.
- [21] Harry B. Lee. "Accuracy Limitations of Hyperbolic Multilateration Systems". In: *IEEE Transactions on Aerospace and Electronic Systems* AES-11.1 (1975), pp. 16–29. DOI: 10.1109/TAES.1975.308024.
- [22] J. F. Cline. "Multilateration Error Ellipsoids". In: *IEEE Transactions on Aerospace and Electronic Systems* AES-14.4 (1978), pp. 665–667. DOI: 10.1109/TAES.1978.308693.
- [23] P. Schultheiss and E. Weinstein. "Lower bounds on the localization errors of a moving source observed by a passive array". In: *IEEE Transactions on Acoustics, Speech, and Signal Processing* 29.3 (1981), pp. 600–607. DOI: 10.1109/TASSP.1981.1163622.
- [24] Paul C. Chestnut. "Emitter Location Accuracy Using TDOA and Differential Doppler". In: *IEEE Transactions on Aerospace and Electronic Systems* AES-18.2 (1982), pp. 214–218. DOI: 10.1109/TAES.1982.309230.
- [25] J.S. Abel. "Optimal sensor placement for passive source localization". In: (1990), 2927–2930 vol.5. DOI: 10.1109/ICASSP.1990.116239.
- [26] B. Yang and J. Scheuing. "Cramer-Rao bound and optimum sensor array for source localization from time differences of arrival". In: 4 (2005), iv/961–iv/964 Vol. 4. DOI: 10.1109/ICASSP.2005.1416170.
- [27] Per Christian Hansen. *Rank-Deficient and Discrete Ill-Posed Problems*. Society for Industrial and Applied Mathematics, 1998. DOI: 10.1137/1.9780898719697. eprint: <https://epubs.siam.org/doi/pdf/10.1137/1.9780898719697>. URL: <https://epubs.siam.org/doi/abs/10.1137/1.9780898719697>.
- [28] Richard J. Hanson. "A Numerical Method for Solving Fredholm Integral Equations of the First Kind Using Singular Values". In: *SIAM Journal on Numerical Analysis* 8.3 (1971), pp. 616–622. ISSN: 00361429. URL: <http://www.jstor.org/stable/2949679> (visited on 05/16/2023).
- [29] G. H. Golub and C. F. V. Loan. "Matrix Computations". In: *Third ed. Baltimore: the Johns Hopkins University Press* (1996).
- [30] Per Christian Hansen. "Analysis of Discrete Ill-Posed Problems by Means of the L-Curve". In: *SIAM Review* 34.4 (1992), pp. 561–580. DOI: 10.1137/1034115. eprint: <https://doi.org/10.1137/1034115>. URL: <https://doi.org/10.1137/1034115>.
- [31] *Convergence rates for iteratively regularized Gauss–Newton method subject to stability constraints*. Vol. 400. 2022, p. 113744. DOI: <https://doi.org/10.1016/j.cam.2021.113744>. URL: <https://www.sciencedirect.com/science/article/pii/S0377042721003666>.
- [32] J. Smith and J. Abel. "The spherical interpolation method of source localization". In: *IEEE Journal of Oceanic Engineering* 12.1 (1987), pp. 246–252. DOI: 10.1109/JOE.1987.1145217.
- [33] B. Friedlander. "A passive localization algorithm and its accuracy analysis". In: *IEEE Journal of Oceanic Engineering* 12.1 (1987), pp. 234–245. DOI: 10.1109/JOE.1987.1145216.

- [34] H. Schau and A. Robinson. "Passive source localization employing intersecting spherical surfaces from time-of-arrival differences". In: *IEEE Transactions on Acoustics, Speech, and Signal Processing* 35.8 (1987), pp. 1223–1225. DOI: 10.1109/TASSP.1987.1165266.
- [35] Y.T. Chan and K.C. Ho. "An efficient closed-form localization solution from time difference of arrival measurements". In: ii (1994), II/393–II/396 vol.2. DOI: 10.1109/ICASSP.1994.389638.
- [36] Stephen Bancroft. "An Algebraic Solution of the GPS Equations". In: *IEEE Transactions on Aerospace and Electronic Systems* AES-21 (1985), pp. 56–59.
- [37] M. Geyer and A. Daskalakis. "Solving passive multilateration equations using Bancroft's algorithm". In: 2 (1998), F41/1–F41/8 vol.2. DOI: 10.1109/DASC.1998.739825.
- [38] Stephen Bancroft. "An Algebraic Solution of the GPS Equations". In: *IEEE Transactions on Aerospace and Electronic Systems* AES-21.1 (1985), pp. 56–59. DOI: 10.1109/TAES.1985.310538.
- [39] *Statistical Theory of Passive Location Systems*. Vol. AES-20. 2. 1984, pp. 183–198. DOI: 10.1109/TAES.1984.310439.
- [40] *Position-Location Solutions by Taylor-Series Estimation*. Vol. AES-12. 2. 1976, pp. 187–194. DOI: 10.1109/TAES.1976.308294.
- [41] *On the application of singular value decomposition and Tikhonov regularization to ill-posed problems in hyperbolic passive location*. Vol. 57. 7. 2013, pp. 1999–2008. DOI: <https://doi.org/10.1016/j.mcm.2012.03.004>. URL: <https://www.sciencedirect.com/science/article/pii/S0895717712000611>.
- [42] *Tikhonov, A.N. (1963) Solution of Incorrectly Formulated Problems and the Regularization Method. Soviet Mathematics Doklady, 4, 1035-1038.*
- [43] David L. Phillips. "A Technique for the Numerical Solution of Certain Integral Equations of the First Kind". In: *J. ACM* 9.1 (Jan. 1962), pp. 84–97. ISSN: 0004-5411. DOI: 10.1145/321105.321114. URL: <https://doi.org/10.1145/321105.321114>.
- [44] Allan J. MacLeod. "Finite-dimensional regularization with nonidentity smoothing matrices". In: *Linear Algebra and its Applications* 111 (1988), pp. 191–207. ISSN: 0024-3795. DOI: [https://doi.org/10.1016/0024-3795\(88\)90059-6](https://doi.org/10.1016/0024-3795(88)90059-6). URL: <https://www.sciencedirect.com/science/article/pii/0024379588900596>.
- [45] Vladimir Alekseevich Morozov. "On the solution of functional equations by the method of regularization". In: *Doklady Mathematics* 7 (1966), pp. 414–417.
- [46] Helmut Gfrerer. "An A Posteriori Parameter Choice for Ordinary and Iterated Tikhonov Regularization of Ill-Posed Problems Leading to Optimal Convergence Rates". In: *Mathematics of Computation* 49.180 (1987), pp. 507–522. ISSN: 00255718, 10886842. URL: <http://www.jstor.org/stable/2008325> (visited on 05/17/2023).
- [47] Martin Hanke and Toomas Raus. "A General Heuristic for Choosing the Regularization Parameter in Ill-Posed Problems". In: *SIAM Journal on Scientific Computing* 17.4 (1996), pp. 956–972. DOI: 10.1137/0917062. eprint: <https://doi.org/10.1137/0917062>. URL: <https://doi.org/10.1137/0917062>.
- [48] Gene H. Golub, Michael Heath, and Grace Wahba. "Generalized Cross-Validation as a Method for Choosing a Good Ridge Parameter". In: *Technometrics* 21.2 (1979), pp. 215–223. ISSN: 00401706. URL: <http://www.jstor.org/stable/1268518> (visited on 05/17/2023).

- [49] Sabine Van Huffel and Joos Vandewalle. *The Total Least Squares Problem*. Society for Industrial and Applied Mathematics, 1991. DOI: 10.1137/1.9781611971002. eprint: <https://epubs.siam.org/doi/pdf/10.1137/1.9781611971002>. URL: <https://epubs.siam.org/doi/abs/10.1137/1.9781611971002>.
- [50] *A compressive Landweber iteration for solving ill-posed inverse problems*. Vol. 24. Nov. 2008, p. 065013. DOI: 10.1088/0266-5611/24/6/065013.
- [51] Wikipedia. *North Atlantic Tracks*. 2017. URL: https://en.wikipedia.org/wiki/North_Atlantic_Tracks.

Part VI

Sustainable Development Goals (SDGs)

Associating a project with the SDGs is essential because it provides a framework for addressing the world's most pressing challenges and promoting sustainable development on a global scale. Table 6.0.1 gathers the impact of the thesis' topic into each of the SDGs. In addition, an overview list with a brief explanation of how this master's thesis relates to each of the SDGs is also included.

SDG	Description	High	Medium	Low	Not applicable
1	Zero Hunger				✓
2	Zero Poverty				✓
3	Good Health				✓
4	Quality Education				✓
5	Gender Equality				✓
6	Clean Water and Sanitation				✓
7	Renewable Energy			✓	
8	Good Jobs and Economic Growth		✓		
9	Innovation and Infrastructure	✓			
10	Reduced Inequalities				✓
11	Sustainable Cities and Communities			✓	
12	Responsible Consumption		✓		
13	Climate Action	✓			
14	Life Below Water				✓
15	Life on Land				✓
16	Peace and Justice				✓
17	Partnerships for the Goals			✓	

Table 6.0.1: Sustainable Development Goals (SDGs)

SBM has various connections to several SDGs, which are SDG 7, 8, 9, 11, 12, 13, and 17. Here's a brief overview of these connections:

- **SDG 7 (Renewable Energy):**

SBM can support the development and management of renewable energy infrastructure by providing accurate tracking and monitoring of transportation and logistics activities related to the renewable energy sector. This can help optimize energy production, reduce downtime, and improve overall energy management.

- **SDG 8 (Good Jobs and Economic Growth):**

SBM can contribute to economic growth by enhancing transportation and logistics efficiency, resulting in improved trade and commerce. It can optimize supply chains, enhance infrastructure planning, and support the development of innovative transportation solutions, leading to job creation and economic development.

- **SDG 9 (Innovation and Infrastructure):**

SBM plays a crucial role in advancing infrastructure and innovation by providing real-time data on transportation and logistics activities. This information can be used to optimize infrastructure planning, improve transportation systems, and support the development of smart cities and sustainable infrastructure.

- **SDG 11 (Sustainable Cities and Communities):**

SBM can contribute to sustainable urban development by improving transportation systems and supporting efficient mobility within cities. It can help manage traffic flow, enhance emergency response coordination, and enable sustainable transportation planning, leading to more livable and resilient cities.

- **SDG 12 (Responsible Consumption):**

SBM can support responsible consumption and production by providing real-time data on transportation activities, enabling better monitoring of supply chains and reducing waste in logistics operations. It can contribute to sustainable production practices and promote more efficient resource utilization.

- **SDG 13 (Climate Action):**

SBM can aid in climate action by facilitating the monitoring and mitigation of greenhouse gas emissions from transportation activities. Accurate tracking and reporting of vehicle movements and fuel consumption can help identify areas for improvement, promote the adoption of cleaner technologies, and support climate change mitigation efforts.

- **SDG 17 (Partnerships for the Goals):**

SBM can foster partnerships and collaboration by providing a common framework for data sharing and cooperation among stakeholders involved in transportation and logistics. It enables the exchange of information, expertise, and resources, supporting the global partnership for sustainable development.

Overall, SBM's capabilities in tracking and monitoring transportation activities contribute to various SDGs by enhancing energy efficiency, supporting economic growth, promoting sustainable infrastructure, facilitating responsible consumption and production, advancing climate action, and fostering partnerships for sustainable development.